



P.M.A. de Jong

Continuous Descent Operations using Energy Principles

CONTINUOUS DESCENT OPERATIONS USING ENERGY PRINCIPLES

Paul de Jong

Cover photo by: Andres Meneses © 2007

Cover design by: GAW ontwerp en communicatie, Wageningen, The Netherlands

Printed by: GVO drukkers & vormgevers B.V. Ede, The Netherlands

Copyright © 2014 P. M. A. de Jong

All Rights Reserved. No part of the material protected by this copyright notice may be reproduced or utilized in any form or by any means, electronic or mechanical, including photocopying, recording or by any information storage and retrieval system, without the prior permission of the author.

Continuous Descent Operations using Energy Principles

Proefschrift

ter verkrijging van de graad van doctor
aan de Technische Universiteit Delft,
op gezag van de Rector Magnificus prof. ir. K.C.A.M. Luyben,
voorzitter van het College voor Promoties,
in het openbaar te verdedigen
op maandag 13 januari 2014 om 15.00 uur

door

Paul Mark Alexander DE JONG

ingenieur luchtvaart en ruimtevaart
geboren te Arnhem

Dit proefschrift is goedgekeurd door de promotor:

Prof. dr. ir. M. Mulder

Copromotor: Dr. ir. M.M. van Paassen

Samenstelling promotiecommissie:

Rector Magnificus

Prof. dr. ir. M. Mulder

Dr. ir. M.M. van Paassen

Prof. dr. -ing. habil. H. Fricke

Prof. J.-P.B. Clarke, Sc.D.

Prof. dr. ir. J.M. Hoekstra

Prof. dr. R. Curran

Ir. N. de Gelder

Prof. dr. ir. J.A. Mulder

voorzitter

Technische Universiteit Delft, promotor

Technische Universiteit Delft, copromotor

Technische Universität Dresden

Georgia Institute of Technology

Technische Universiteit Delft

Technische Universiteit Delft

Nationaal Lucht- en Ruimtevaartlaboratorium

Technische Universiteit Delft, reservelid

Dr. ir. C. Borst heeft als begeleider in belangrijke mate aan de totstandkoming van het proefschrift bijgedragen.



Dit proefschrift is mede mogelijk gemaakt door de financiële ondersteuning van het Europese zevende kaderprogramma (FP7/2007-2013) via het Clean Sky Joint Technology Initiative middels Grant Agreement no. CSJU-GAM-SGO-2008-001.

ISBN 978-94-6186-244-0

*“Als ik hard had willen werken, was ik geen vlieger geworden”
- Wim Huson*

*To Renske
for your love, support and encouragement*

SUMMARY

Continuous Descent Operations using Energy Principles

Paul M. A. de Jong

During today's aircraft descents, Air Traffic Control (ATC) commands aircraft to descend to specific altitudes and directions to maintain separation and spacing from other aircraft. When the aircraft is instructed to maintain an intermediate descent altitude, it requires engine thrust to maintain speed, leading to increased fuel burn and noise being produced. By eliminating these level flight segments, fuel consumption, noise and gaseous emissions can be reduced as aircraft can perform the descent at an engine-idle thrust setting. The aircraft will then fly a continuous descent, or Continuous Descent Operations (CDO), which at the same time raises the altitude profile, reducing the experienced noise levels at ground level.

Today, CDO's are operationally in use at various major airports, such as Amsterdam Airport Schiphol and London Heathrow. Due to difficulties in predicting aircraft trajectories and time of arrival when performing CDOs, ATC needs to add additional spacing buffers to assure proper spacing between aircraft. As a result, airport capacity is reduced, limiting the use of CDOs to hours of low capacity demand. Researchers investigated various concepts in an aim to improve the predictability of CDOs to maintain airport capacity during CDOs. However, many of these concepts require additional thrust to correct for deviations. Therefore, this research developed a new CDO concept, named Time and Energy Managed Operations (TEMO), that allows an aircraft to perform accurate 4D engine-idle descents using energy principles.

TEMO uses the principles of energy to correct deviations (replanning) without the need for additional thrust and simultaneously adhering to time constraints for spacing and sequencing. The concept uses an optimization algorithm to minimize thrust and speedbrake

use and to calculate accurate trajectories. The algorithm uses energy management by exchanging kinetic and potential energy by controlling the elevator to correct deviations. Sustained deviations are corrected for through either strategic replanning, when deviations exceed a predefined boundary, or using tactical replanning, which instantaneously corrects deviations. To improve flight accuracy and maintain acceptable workload levels, a TEMO descent is flown using the autopilot and auto-thrust systems. However, selection of flaps and gear, and commanding the autopilot are examples of actions that are still performed by the pilot.

The TEMO concept should be validated for different conditions to verify whether CDOs can be flown using energy management and whether the concept can cope with various disturbances. A study should verify whether environmental impact is reduced while the various replanning methods should be compared. Various errors could be artificially introduced to evaluate to what extent energy management alone can correct errors and in what scenarios thrust or speedbrakes are required. Moreover, the role of the human pilot in the TEMO concept should be evaluated. The human pilot introduces additional uncertainties that affect the flown descent. Another uncertainty during descent is wind and affects the trajectory accuracy greatly. Hence, can we improve wind estimation to enhance trajectory prediction? This thesis addresses these topics and questions.

A first experiment involved a fast-time batch simulation performed in MATLAB and aimed at identifying TEMO's environmental benefits and ability to correct deviations and errors using strategic replanning. Deviations result from modeling errors in the Trajectory Predictor (TP) and algorithm to simplify trajectory prediction. A comparison of baseline scenarios between TEMO descents and current step-down descents showed that TEMO reduces the 65 dB and 75 dB Sound Exposure Level (SEL) contour areas by 20% and 13%, respectively. Moreover, a reduction in fuel used was achieved between 11% and 20% for the descent. When considering fuel use per flight time, the reduction is slightly reduced to values between 9% and 16%. Gaseous emissions were effectively reduced by approximately 33–47%. The comparison also showed that without additional errors, no replanning was required to correct deviations that result from modeling errors.

Next, descents were simulated with introduced time, energy and wind estimation errors to evaluate how strategic replanning corrects such errors during descent. Without using additional thrust, a time error window of 8–16 seconds was achieved using energy management only. The actual dimensions of this time window depends on the wind estimation error. By allowing TEMO to command minimized amounts of thrust and speedbrakes, the algorithm was able to calculate a new trajectory that allowed the aircraft to arrive 30 seconds earlier and later than originally planned. In some extreme scenarios, the time deviation at the Initial Approach Fix (IAF) exceeded the 5 seconds required accuracy prescribed by the Required Time Performance (RTP). These larger time deviations primarily result from wind estimation errors that negatively affect time and energy performance. This continuous wind error resulted in multiple trajectory recalculations to correct for time and energy deviations.

This experiment also compared results of descents flown using strategic replanning with descents flown using hybrid replanning under wind conditions. This hybrid replanning method used a 4D-speed controller to continuously (tactically) correct for time deviations

and used a strategic replan before Terminal Maneuvering Area (TMA) entry to correct for energy deviations. The results showed that the 4D-controller effectively minimizes time deviations at the IAF with minimum cost to fuel use and noise contours, even when a wind estimation error is present. Hence, the tactical controller is efficient at correcting deviations resulting from a continuous disturbance. However, hybrid replanning showed larger energy deviations at localizer intercept which were not corrected using a replan but corrected upon glideslope intercept by the autopilot. Therefore, hybrid replanning should use stricter energy boundaries to reduce energy (and altitude) deviations when the aircraft approaches the localizer.

The fast-time simulations on TEMO performance included a zero-delay pilot response model that executed pilot tasks, such as configuration changes, perfectly. Hence, the question remained how variations in pilot response to manual actions affect TEMO performance. This question was addressed in a real-time experiment with pilots in the loop. This experiment also evaluated what information support pilots best to perform accurate TEMO descents and minimize variations in pilot response. Three Human-Machine Interface (HMI)'s were developed that provide support information during TEMO descents and differed in level of information displayed. Pilots preferred the HMI variant that included a timer to support accurate selection of flaps and gear, and responded that workload was acceptable. This configuration timer, however, did not significantly reduce time deviations at the runway threshold but reduced the variance in delay of setting configurations.

For comparison the pilot flown scenarios were also flown using a zero-delay pilot response model to investigate investigation of the effects of variations in pilot response on environmental impact and TEMO performance. A comparison of these simulations showed that human response had little effect on noise contour levels and Nitrogen Oxide emissions of a TEMO descent, while the difference in time deviation with respect to the automated runs was small. Consequently, pilots were sufficiently informed to perform their actions. The comparison also indicated that without delays in performing pilot actions, the aircraft did not arrive exactly on time either. This resulted from simplifications in modeling of aircraft dynamics in the TEMO algorithm and TP and guidance errors while following the prescribed speed-profile. In general, the aircraft arrived early and close to the early boundary of the RTP at the runway threshold for pilot flown scenarios. This raises the question whether an RTP of 2 seconds is achievable in real life. The guidance and planning functions should be improved to reduce this offset to be able to obtain similar time accuracies in less favorable wind conditions.

The analysis of all results showed that the energy deviation at the moment of intercepting the glideslope significantly influences the time of arrival for the automated runs, while for the human runs this effect was slightly smaller. This implies that to arrive exactly on time at the runway threshold, the energy deviation at glideslope intercept should be reduced and corrections during glideslope descent should be made possible.

The results from both experiments showed that TEMO is sensitive to disturbances and errors. The batch study showed that wind estimation errors contribute greatly to time and energy deviations. For this reason, it is expected that using accurate wind estimation data in the TEMO algorithm will reduce trajectory deviations. Today, aircraft primarily rely on

coarse and slowly updated wind estimates resulting in gross estimates of the prevailing wind when predicting the own trajectory. Therefore, a novel method for real-time estimation of a wind profile was developed, named Airborne Wind Estimation Algorithm (AWEA) that increases the temporal and spatial resolution of wind estimates. AWEA uses data transmitted by nearby aircraft to construct high resolution real-time wind profile estimates. The AWEA algorithm uses a Kalman filter to relate all received measurements to the own trajectory and reduce measurement noise. The wind estimation algorithm performance was evaluated using Mode-S derived meteorological data from Amsterdam Airport Schiphol. Using these wind observations, the AWEA algorithm showed an Root Mean Square (RMS) in the wind estimation error of 1.35 KTS along the own trajectory, which is lower than the observed RMS measurement error of 1.94 KTS. Relating the measurements to the own trajectory also proved beneficial in reducing wind estimation errors. In another experiment, estimated wind profiles along the own trajectory constructed by AWEA showed to improve spacing performance during approach.

The TEMO experiments showed promising results as clear benefits to the environment have been identified whilst the aircraft adheres to time constraints accurately. However, some issues require further investigation before TEMO could be used in real-life. TEMO was designed for the Airbus A320 flying straight-in descents and evaluated in a single aircraft environment. Future work should investigate TEMO's use in other aircraft types, include turn dynamics, and realistic wind and turbulence conditions. AWEA should be integrated with TEMO to reduce deviations resulting from wind. Next, an experiment should investigate capacity, and spacing and separation between multiple aircraft performing TEMO descents. To improve TEMO time performance at the runway, TEMO should be able to perform replans while on the glideslope. Since energy management cannot be performed while the aircraft descends down the glideslope, deviations could be corrected using flap-scheduling such that engine-thrust remains idle, or a tactical component could use thrust and speedbrakes to simultaneously control time and energy.

Trajectory prediction will always include modeling errors as we cannot model the world explicitly, hence, effort should be put into reducing these errors to a minimum. Since strategic replanning can be considered as an open-loop (or slow, intermittent) control system, modeling errors will always result in deviations from the planned trajectory. To improve time performance by minimizing time deviations due to modeling errors and unknown disturbances, a closed-loop system should be used. Hybrid replanning augments strategic replanning with a fast closed-loop speed controller. Hence, research should investigate how hybrid replanning can be further improved and evaluate the human factors aspects of hybrid replanning in a real-time experiment with pilots in control.

Contents

Summary	v
1 Introduction	1
1-1 Background	1
1-1-1 Aircraft Descents Today	2
1-1-2 Way Forward	4
1-2 Continuous Descent Operations	5
1-3 Problem Definition	7
1-4 Research Approach	8
1-5 Enablers for the TEMO CDO Concept	11
1-5-1 Flight Deck Automation	11
1-5-2 Onboard Wind Estimation	12
1-6 Research Scope	14
1-7 Thesis Outline	15
References	17
2 Continuous Descents using Time and Energy Management	29
2-1 Time and Energy Managed Operations: Concept of Operations . . .	30
2-1-1 Energy Management	31
2-1-2 Speed Profile	33
2-1-3 Time Management	35
2-2 Replanning and Guidance	37
2-2-1 Strategic Replanning	37
2-2-2 Tactical Replanning	46
2-3 Flight Operations	47
References	49

3	Batch Study into TEMO Performance	53
3-1	Introduction	54
3-2	Time and Energy Managed Operations	55
3-2-1	TEMO Trajectory Planning	57
3-2-2	TEMO Algorithm and Trajectory Predictor	59
3-3	Experimental Evaluation	63
3-3-1	Method	63
3-3-2	Dependent Measures	66
3-3-3	Experimental Hypotheses	66
3-4	Discussion of Results	66
3-4-1	Simulation Study 1: Baseline	67
3-4-2	Simulation Study 2: Combination of Errors	70
3-4-3	Simulation Study 3: Strategic vs. Hybrid Replanning	79
3-4-4	General Discussion	81
3-5	Conclusions	82
	References	83
4	Human in the Loop Study using TEMO	89
4-1	Introduction	90
4-2	Time and Energy Managed Operations	91
4-2-1	The TEMO Concept	91
4-2-2	TEMO Flight Procedures	93
4-2-3	TEMO Algorithm and Trajectory Predictor	94
4-3	Supporting Pilots in Strategic Replanning	95
4-4	HMI Variants	96
4-5	Experimental Evaluation	98
4-5-1	Method	99
4-5-2	Experimental Hypotheses	104
4-6	Experiment Results	105
4-6-1	TEMO Performance	105
4-6-2	Questionnaires	108
4-6-3	Human versus Autobot Comparison	111
4-7	Discussion	113
4-8	Conclusions	114
	References	115
5	Wind Profile Estimation using Airborne Sensors	119
5-1	Introduction	120
5-2	Background	121
5-2-1	Wind Estimation	121
5-2-2	Applications of Wind Estimation	122
5-2-3	Current Methods for Wind Estimation	123
5-2-4	Atmospheric Measurements using Airborne Aircraft	123

- 5-2-5 Future Needs 124
- 5-3 AWEA: Airborne Wind Estimation Algorithm 125
 - 5-3-1 AWEA Working Principles 125
 - 5-3-2 Implementation Methods 126
- 5-4 AWEA Algorithm Principles 127
 - 5-4-1 Main Steps of the Algorithm 128
 - 5-4-2 AWEA Kalman Filter 128
- 5-5 AWEA Performance Evaluation 132
 - 5-5-1 Case Study 1: Simulations using Mode-S Enhanced Data . . . 132
 - 5-5-2 Case Study 2: Aircraft Spacing and Wind Estimation 136
- 5-6 Conclusions 141
- References 141

6 Discussion and Recommendations 147

- 6-1 Discussion 148
 - 6-1-1 Energy Principles 149
 - 6-1-2 Flight Deck Automation 152
 - 6-1-3 Wind Estimation 156
- 6-2 Recommendations 157
 - 6-2-1 Realism 157
 - 6-2-2 Capacity 158
 - 6-2-3 Environmental Impact 159
 - 6-2-4 New Concept 160
- 6-3 Future Work 161
- References 161

7 Conclusions 167

A Energy Equations and the Dynamics of Flight 169

- A-1 Reference Frames 169
 - A-1-1 Earth-centered Inertial Reference Frame 169
 - A-1-2 Earth-centered, Earth-fixed Reference Frame 169
 - A-1-3 Vehicle-carried Normal Earth Reference Frame 170
 - A-1-4 Aerodynamic Reference Frame 170
 - A-1-5 Kinematic Reference Frame 172
- A-2 Kinematics of a Point-Mass 172
- A-3 Equations of Motion of a Point-Mass 175
- A-4 The Energy Equations of Motion 177
 - A-4-1 Energy Rate 179
 - A-4-2 Energy Rate Demand 179
 - A-4-3 Energy Share Factor 180
 - A-4-4 Definition of Energy Error 181
- A-5 The Influence of a Vertical Wind Gradient on the Equations of Motion 182

A-6 Time Deviation Resulting from a Speed Deviation	184
References	185
B TEMO HMI Variants	187
C Answers to Post-Experiment Questionnaire	191
D RSME Rating Scale	195
E CARS Rating Scale	197
Abbreviations	199
Symbols	203
Samenvatting	207
Acknowledgements	213
Curriculum Vitae	215

INTRODUCTION

1-1 Background

The expected growth in air traffic [1], combined with more public concern for the environment and high oil-prices [2], forces the aviation industry to revise today's air traffic system design. The current air traffic system operates at its capacity limits and is expected to lead to large delays if traffic levels rise even further [3]. Moreover, the increase in oil prices resulted in higher airline operating costs [4]. The European Emission Trading Scheme (ETS), launched in 2005, includes the airline industry since January 2012 [5]¹, will also lead to higher airline operating costs when airlines exceed their emission cap.

The air transport industry has a large interest in reducing the growing public concern for environmental issues such as air pollution and noise disturbance. Today, aircraft certification standards address noise and aircraft gaseous emissions [6, 7] as these negatively affect the quality of life for the residential areas near airports [8]. To support further growth within the current regulations, the environmental footprint of aircraft should be reduced to make room to increase capacity. The latest aircraft designs have a significantly reduced environmental footprint resulting from new engines with improved fuel efficiency [9] and these new engines produce less noise [10] by increasing the engine's bypass ratio (bypass ratio is the ratio of cold mass flow to the hot mass flow). Furthermore, new composite materials lead to reduced aircraft weight [11]. However, airline companies cannot afford to retire their current fleet of aircraft for greener aircraft all at once. For this reason, only a gradual transition towards green air travel will commence resulting from new designs and many older aircraft will remain in use.

In 2001, the International Civil Aviation Organization (ICAO) developed the 'ICAO Balanced Approach' [12, 13] to noise mitigation which identified areas for exploration of noise reduction. For example, measures can be taken at the source of noise through research aiming at reducing the amount of emissions and noise generated by aircraft engines.

¹The Emission Trading Scheme (ETS) is temporarily suspended for international flights into and out of Europe until the 2013 ICAO General Assembly adopts a worldwide emission scheme.

Furthermore, new wing designs are evaluated to reduce the use of high-lift devices which contribute to aerodynamic noise once deployed. The Balanced Approach also addresses today's aircraft operations which could be further improved using procedures specifically designed and optimized for noise abatement and are commonly referred to as Noise Abatement Procedures (NAPs).

The environmental footprint of current aircraft can be reduced through improvements in aircraft operations using optimized lateral procedures [14–17], land-use planning and management [12, 13] or by excluding noisy aircraft from operating at an airport [18, 19]. Other examples are, for example, reduced engine thrust during departure and approach procedures [20] and a preferential runway system to distribute noise disturbance [21].

1-1-1 Aircraft Descents Today

During today's descent and approach procedures, Air Traffic Controllers (ATCos) use altitude and speed instructions to maintain and acquire spacing and separation between aircraft departing from and arriving to an airport. These instructions reduce the behavior of all aircraft to a single type of aircraft behavior that is known to the controller which makes it easier for a controller to maintain separation between aircraft. This single behavior, or performance, is far from optimal for each individual aircraft. Moreover, these instructions often include level segments during which an aircraft has to maintain a constant speed. In order to maintain altitude and speed, an aircraft requires thrust. Thus, by eliminating these level, constant-speed segments, and allowing aircraft to fly closer to their optimal performance, an aircraft could maintain a more environmentally-friendly engine-idle setting for a longer period of time and reduce the amount of noise and emissions produced [22]. At the same time, fuel use is reduced, saving money for the airlines.

Arrival procedures that aim at reducing level flight segments and minimizing engine thrust are commonly referred to as Continuous Descent Operations (CDO) [23]². As a result of flying a continuous descent, the resulting altitude profile is considerably higher compared to conventional step-down descents as shown in Figure 1-1. Hence, besides reduced thrust and fuel consumption, the distance between the aircraft and residential areas on the ground is increased, reducing the noise levels experienced on the ground.

Today, CDOs are operationally used at various major airports around the world, such as Schiphol Amsterdam, London Heathrow and Los Angeles International. However, current CDOs often limit airport capacity due to uncertainties in predicting the arrival time, spacing and trajectory of the aircraft involved [25]. The accuracy of trajectories calculated by both onboard and ground-based Trajectory Predictors (TPs) is affected by uncertainties and errors in estimating the wind forecast [26–35], and aircraft performance [30, 34, 36–39]. Furthermore, variations in pilot response in commanding the autopilot or configuration

²The UK Air Navigation Service Provider (ANSP) NATS adheres to a slightly less restrictive definition according to the UK Aeronautical Information Publication (AIP) [24, p. 24]: “a descent will be deemed to have been continuous provided that no segment of level flight longer than 2.5 nautical miles (nm) occurs below 6,000 ft QNH and ‘level flight’ is interpreted as any segment of flight having a height change of not more than 50 ft over a track distance of 2 nm or more”. Consequently, an aircraft that descends while using a level segment for less than 2.5 NM is still considered to fly ‘continuous’ descent.

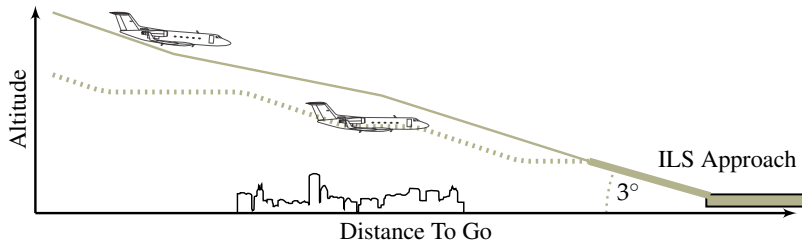


FIGURE 1-1: Altitude profile of a conventional, step-down descent (dashed) and an idle CDO (solid) descent.

changes, and Flight Management System (FMS) behavior [40] all affect the flown trajectory [29, 39, 41].

For these reasons, ATCos introduce additional spacing buffers [25, 42] such that the CDO can be performed without Air Traffic Control (ATC) interference. Interference from ATC would result in a less optimal execution of the CDO. The added spacing buffer reduces the runway throughput, and as a result reduces the usability of such procedures when airport capacity is vital. Therefore, CDOs are currently only used effectively during hours of low traffic demand when these buffers can easily be introduced without limiting capacity. In this thesis, the descent of an aircraft refers to the descent from Top of Descent (ToD) all the way down to the runway threshold.

A possible way to increase capacity is by including the time parameter to the definition of a trajectory to improve the temporal accuracy of current TPs. Time combined with the 3D path parameters yields a ‘4D trajectory’ that allows monitoring of flight progress and future intent and increases predictability and consistent arrival times at the runway [31, 43–46], resulting in a high and consistent runway throughput [47]. Using 4D trajectories for spacing of descents and approaches is expected to increase capacity [48, 49] and allows a trade-off between the efficiency of a single flight and the overall arrival sequence using Time-based Operations (TbO) or time management.

Another method to increase capacity during CDO operations is through controller support tools that support the ATCo in reducing the additional spacing buffers when performing CDOs. Examples of such tools are Tool for Analysis of Separation and Throughput (TASAT) [30, 39] and the Time Space Diagram (TSD) [50–52]. TASAT uses an improved TP for ground-based trajectory prediction to support ATCos in spacing of arrival aircraft and provides a probabilistic estimate of the target spacing between aircraft during procedure design. The TSD provides a graphical representation of predicted trajectories and Estimated-Time of Arrivals (ETAs). This representation allows ATCos to easily identify separation conflicts and intervene early on during descent. The display also provides hypothetical predictions of possible controller actions. The TSD proved to support ATCos and required less ATC instructions and acquire spacing earlier during descent allowing longer segments of a continuous descent.

Alternatively, the problem of spacing aircraft flying CDOs can be solved by delegating

the spacing task to the flight desk using airborne self-spacing [29, 47, 53–57]. Using airborne self-spacing, ATC uses a ground-based TP and/or intent information from arriving aircraft to sequence and space arrival traffic by providing a time-based or distance-based constraint. After successful receipt and acceptance of the clearance to commence the approach and spacing constraint, the separation task is transferred to the pilot, who uses the FMS's TP to adhere to the clearance and constraint.

1-1-2 Way Forward

Two high-level concepts for the next generation air traffic systems have been developed both in Europe [48], Single European Sky ATM Research (SESAR) and in the United States [49], NextGen. One of the key features of these concepts is the use of automation support systems for spacing of 4D trajectories using Time-based Operations. These 4D-trajectories serve as an intermediate concept until technology has sufficiently matured to implement Trajectory-based Operations (TBO) and ultimately, Performance-based Operations (PBO) [48].

The Initial 4D Concept [44, 58, 59], part of SESAR, uses an enhanced Required Time of Arrival (RTA) function to achieve accurate time control of up to 10 seconds at a single time constrained waypoint. Furthermore, SESAR and NextGen foresee the use of automated systems for conflict detection, ATC support tools and enhanced trajectory prediction. These tools support Air Traffic Management (ATM) development at bringing the current ATM system towards higher 'levels of automation' [60, 61].

Clean Sky, a public-private partnership between the European Commission and the aviation industry was established to reduce the environmental impact of aircraft. Clean Sky aims at developing new technologies that significantly contribute to reducing the environmental impact of aircraft. This is achieved by gaseous emission and noise reduction but also by improving the green life-cycle of aircraft. Part of Clean Sky is the System for Green Operations (SGO) Integrated Technology Demonstrator (ITD) [62] which aims at developing tools for optimizing aircraft trajectories that include environmental affects such as gaseous and noise emissions and developing aircraft systems towards a more electrical aircraft. The research described in this thesis was performed as part of SGO in collaboration with the National Aerospace Laboratory (NLR) and the German Aerospace Center (DLR).

Ideally, a new Continuous Descent Operations concept should allow accurate descents that reduce fuel burn, the amount of gaseous emissions and reduce the noise level experienced on the ground. This can all be accomplished by flying a continuous descent resulting in a higher vertical profile and the use of time management. Simultaneously, predictability, accuracy and consistency of such new descents and approaches should be high, such that ATCos are able to plan and control the arriving flow of traffic efficiently without sacrificing capacity. Furthermore, workload for the flight crew should not be negatively affected.

1-2 Continuous Descent Operations

The current Vertical Navigation (VNAV) function of a commercial-airliner FMS calculates a descent profile using backwards calculation [63, 64], starting at the runway threshold calculating back to ToD. The calculation routine takes all applicable and known constraints into account and connects constraints with a performance path or a geometric path. A performance path is an idle descent from ToD to the first constrained waypoint while a geometric path segment is defined as a path between two constrained waypoints or computed such to follow a prescribed vertical angle.

Geometric paths are flown using the elevator to control the aircraft's path and often require additional thrust. This control strategy of using the elevator to control the aircraft's path is referred to as Path-on-Elevator (POE). Hence, a VNAV descent cannot be flown using engine-idle power since idle thrust can only be guaranteed prior to the first constraint waypoint [63, 64]. Hence, approach designers should define constraints such that the FMS is able to construct a VNAV descent path with minimal or partial-idle thrust. Moreover, most FMSs are currently not able to include a time constraint in the descent.

Researchers have investigated new concepts that aimed at operating Continuous Descent Operations without the limitations of the procedures and technology in use today. Various projects have investigated concepts by defining a fixed trajectory [29, 32, 46, 65–70] while other concepts used aircraft-based [31, 71–74] or ground-based [27, 75–78] systems that calculated a specific trajectory for each individual aircraft. The most prominent concepts are briefly discussed in this section to provide their advantages and drawbacks.

Fixed Vertical Trajectories Back in 1990, retired-Captain Carl Vietor developed a calculation method that uses simple mathematical arithmetic to calculate a *Profile Descent* [65] for aircraft without a VNAV component. This Profile Descent allowed pilots to calculate a rather accurate descent profile using only simple rules of thumb to determine suitable rate of descents based on their distance to go and simple ATC constraints. By descending along this profile, the descent could be flown at a relatively low engine setting and without the use of speed brakes.

The Three-Degree Decelerating Approach (TDDA) [29, 32, 53, 67–69] and Advanced Continuous Descent Approach (ACDA) [66] defined a fixed 3° descending path and used flaps and gear to control the aircraft deceleration to allow self-spacing. Spacing is achieved by meeting a distance-based or time-based constraint and intercept the Instrument Landing System (ILS) safely. However, pilots commented that the use of flaps above nominal speeds would introduce an increased amount of flap wear and negatively affect passenger comfort.

Another project, named OPTIMAL [70, 79, 80], used a fixed 2° path that requires small amounts of thrust to fly less steep such that positive and negative speed changes can be made using thrust. As a consequence, the flown descent is less optimal as compared to a full idle descent. Both concepts suffer from the fact that they use a fixed vertical profile while certain aircraft cannot decelerate along a 2° or 3° descending path [69].

Low Noise Guidance Another CDO concept was developed by NASA and uses a new trajectory prediction algorithm, Low Noise Guidance (LNG), which calculates a “high-efficiency, low noise flight profile” [71] to improve the VNAV performance of the FMS. The primary goal of LNG is to fly as high as possible to maximize the distance between the noise-producing aircraft and the ground to reduce the actual noise experienced on the ground. Using this assumption, the resulting trajectory may consist of several constant flight-path angle segments and constant power setting segments. Hence, a larger variability of vertical trajectories is possible that suits the aircraft characteristics, current route and atmospheric conditions best to reduce noise. The algorithm would calculate a new profile if ATC directs the aircraft along a different route or issued a speed change. The pilot is in charge of managing the throttle to maintain the aircraft at a correct energy level. Even though the LNG concept proved to require more thrust than current-day, vectorized procedures, a reduction in noise experienced on the ground was achieved [71]. During the experiment, spacing or separation with other aircraft was not evaluated as the implementation of LNG did not include spacing and separation constraints. An updated version of LNG, named Energy Navigation (ENAV), has proven to respect spacing instructions from ATC and tactically follow the instructions using thrust or speedbrakes [73].

Continuous Descent Approach for Maximum Predictability The Continuous Descent Approach for Maximum Predictability (CDA-MP) concept developed by Boeing Research and Technology Europe (BRTE) uses a tactical control-law that corrects time deviations by guiding the aircraft along a groundspeed profile [81]. This profile is flown by using the elevator to control groundspeed and requires near-idle thrust. Using the elevator to control speed is referred to as Speed-on-Elevator (SOE). As a result of following a ground-speed profile, wind disturbances result in deviations from the predicted, near-idle descent path. When these deviations exceed prescribed altitude limits, an additional control-law uses the autopilot to increase or decrease thrust to correct the vertical deviation.

Optimum Profile Descent In the United States, some of the current Standard Arrival Routes (STARs) have been updated and improved by defining an Optimum Profile Descent (OPD) that optimizes the vertical path for a large variety of aircraft [23, 39, 49, 82, 83] to facilitate CDOs. These OPDs use altitude constraints to restrict the vertical profile to a near-optimal descent for many of the currently in use commercial aircraft which leads to different benefits per aircraft.

Tailored Arrivals Finally, the Tailored Arrivals (TA) concept developed by Boeing [76] aims at planning lateral and vertical trajectories, that are *tailored* to the current situation at hand on a per-aircraft basis. This concept uses a ground-based TP [75] and an onboard Future Aircraft Navigation System (FANS)-capable FMS to plan an idle-descent trajectory that contains a metering fix at the border of the Terminal Maneuvering Area (TMA). The ground-based TP provides aircraft with advisories containing appropriate descent speeds and constraints to reach the metering fix in time and continue a CDO towards the runway.

Most of the previously discussed research on CDOs actively control the altitude profile or speed profile. This often results in additional thrust variations to establish speed changes needed to maintain separation or to remain on path and on time. This additional use of thrust increases generated noise levels and fuel use. Therefore, the question remains, is there another method to define a CDO concept that allows an aircraft to perform accurate 4D descents and approaches whilst having the engines at idle?

1-3 Problem Definition

The goal of this research is to develop a new descent procedure that reduces environmental impact of aircraft without reducing airport capacity. The new procedure should aim at reducing the amount of thrust and speedbrakes compared to conventional descent operations and use an efficient mechanism to cope with disturbances compared to other developed CDO procedures by using *energy principles*:

Research Goal

Develop a new aircraft descent procedure, that uses energy principles to perform continuous descents that contain a time constraint, to reduce the environmental footprint of aircraft.

Using the elevator and SOE to follow a speed profile, an aircraft could use *energy management* to alter its descent to correct disturbances without using additional thrust or speedbrakes. Simultaneously setting the engines at idle, results in a variable vertical profile as potential energy and kinetic energy are exchanged. For example, an aircraft could gain speed by using these energy principles and descend steeper to exchange altitude for speed instead of using thrust. Alternatively, the aircraft could reduce speed by pitching up to decelerate instead of using additional drag devices.

Through the use of an onboard automated planning-system, an optimal trajectory can be generated by the FMS that incorporates all flight and safety constraints whilst simultaneously minimizing the use of engine thrust to provide benefits in terms of fuel, noise and gaseous emissions. This optimal trajectory consists of an airspeed profile and altitude profile which together define the energy profile. The autopilot is commanded to fly the planned speed profile using the elevator and no use of thrust. This results in deviations from the vertical trajectory due to unforeseen disturbances.

Instead of active control to correct deviations, small deviations are permitted which could eventually correct themselves later during descent. For example, this could result from a wind prediction error that could change direction due to a turn during descent. When the deviation exceeds a prescribed boundary, the deviation is corrected using energy principles by calculating new trajectories. The system initially uses energy exchange to calculate a new trajectory and only uses minimized amounts of thrust or speedbrakes when energy exchange does not suffice in correcting the deviations.

The question remains whether we can use energy principles to define an idle descent from ToD to the runway threshold. Additionally, can we introduce a time constraint into

these idle approaches to support ATCos to maintain runway capacity? These two questions combined define the problem definition of this thesis:

Problem Definition

How can we use energy principles to perform accurate, time-constrained, engine-idle descents and approaches?

Energy principles have been used to perform descents and approaches before but used near-idle thrust [81] or did not include a time constraint [84, 85]. Therefore, including time constraints into energy managed idle descents is a new endeavor.

This thesis presents a new Continuous Descent Operations concept named Time and Energy Managed Operations (TEMO). Time and Energy Managed Operations (TEMO) is a novel, automated and onboard, planning algorithm and guidance system that optimizes the descent using energy principles. The planning algorithm plans a full-idle descent, from ToD to the runway, including ATC constraints on the TMA boundary and/or runway. Based on energy principles, the algorithm and guidance system can exchange altitude for speed and speed for altitude to gain or lose time and energy. Different from other research projects, the TEMO algorithm calculates a nominal calibrated airspeed profile and uses the elevator to control the aircraft along this airspeed profile. As a result, the vertical trajectory will vary, depending on aircraft characteristics (i.e., weight and aerodynamics), atmospheric conditions, and the calculated airspeed profile.

The nominal calibrated airspeed profile is defined to satisfy any applicable speed constraint imposed by ATC, such as not to exceed 250 KIAS below 10,000 ft [86] and aircraft operational speeds. The constraints contained in the speed profile is similar for every type of aircraft flying a TEMO descent into a specific airport to establish a stable and homogeneous flow of incoming traffic and will vary due to differences in aerodynamic characteristics. To correct for disturbances during execution of the descent, limited deviations from the speed profile are allowed to reduce time and/or energy deviations.

Furthermore, the accuracy of calculated trajectories is sensitive to modeling simplifications and uncertainties in the TP. Wind estimation along the predicted trajectory is one such uncertainty parameter that affects the trajectory accuracy greatly. Hence, reducing this uncertainty of wind estimates is likely to improve trajectory prediction.

1-4 Research Approach

The energy principles, as defined in the problem definition, refer to the law of conservation of energy, see Appendix A. The law of conservation of energy states that the total amount of energy in a system remains constant over time. Energy can change form, through modulation, but it cannot be created or destroyed. Considering the aircraft as a system, an aircraft's *potential* energy is defined as:

$$E_{pot} = mgh$$

1-1

where g is the gravitational acceleration³ and h the altitude above a reference frame. Next, the *kinetic* energy of an aircraft relates to speed:

$$E_{kin} = \frac{1}{2}mV^2 \quad 1-2$$

where m is the aircraft mass, and V the aircraft speed relative to the same reference frame — often ground-level or moving air — as potential energy.

When these two forms of energy are combined together, the total energy, E_{tot} of an aircraft is obtained:

$$E_{tot} = mgh + \frac{1}{2}mV^2 \quad 1-3$$

The potential energy term relates to altitude, or position, of an aircraft whereas the kinetic energy term relates to the movement of an aircraft.

The law of conservation of energy leads to the conclusion that an aircraft can only reduce the total amount of energy through dissipation in the form of heat through aerodynamic forces. On the other hand, using the engine, the thrust force can add energy to the system. The rate of change of energy, or energy rate, is defined [87] as the difference between thrust and drag forces multiplied by the instantaneous true airspeed:

$$\dot{E}_{tot} = V(T - D) \quad 1-4$$

where \dot{E}_{tot} is the total energy rate, V the true airspeed, T the engine thrust and D the drag force. As a result of this relation, a pilot can only control the total energy rate through the throttle to control thrust, through speedbrakes, flaps or gear to control drag and elevator to control speed.

Now consider the descent of an aircraft towards the runway. At the start of the descent, an aircraft is at a high altitude and at high speed; hence, the aircraft has a large amount of total energy, whereas during landing, the aircraft is at a low altitude and low speed resulting in a low energy state. During an idle descent, thrust is close to zero, reducing the energy rate to a relation between drag and speed:

$$\dot{E}_{tot, idle} \approx -VD \quad 1-5$$

During descent, the aircraft has to reduce its total level of energy and, theoretically, does not require any thrust to accomplish this when using proper energy management.

When flying manually, a pilot is able to control the exchange of potential and kinetic energy using the elevator. According to Langewiesche, *altitude = speed* [88] (see Appendix A), meaning that if a pilot uses the elevator to gain altitude, as a consequence, speed will decrease. The opposite holds when the aircraft is commanded to go down which will increase the aircraft speed. This principle only holds if we assume that the elevator does not contribute significantly to the drag force, which is valid considering that the drag forces

³In this thesis, the gravitational acceleration is assumed constant and independent of altitude as at the altitudes under consideration in this thesis, the decrease of the gravitational acceleration is less than 2%.

introduced by the elevator are relatively small compared to the drag forces introduced by drag devices such as speedbrakes, gear and flaps. Moreover, the aircraft's induced drag could be affected by elevator control which could affect the aircraft energy. Fortunately, the maneuver rates for commercial aircraft are rather small for passenger comfort. In other words, controlling the elevator has a negligible effect on the total energy and energy rate of an aircraft, and as such is a perfect control device to exchange potential and kinetic energy.

Amelink describes these principles using his reservoir analogy [85], which contains two reservoirs, containing potential and kinetic energy. Together, these two reservoirs determine the total energy. Energy is added to the system using the aircraft's engines and energy can leave the reservoir system through drag dissipation. Drag dissipation can be controlled by the pilot by using drag-devices such as flaps and speedbrakes. The elevator controls the distribution of total energy between the two reservoirs. If no energy flow exists, the elevator exchanges the energy between the two reservoirs. Efficient control and exchange of energy is often referred to as *energy management*.

The TEMO concept uses energy management to correct deviations from the trajectory in contrast to most existing CDO concepts that use thrust to correct errors. The concept defines a speed profile and relaxes the vertical profile. These profiles are calculated by a new optimization algorithm and enhanced TP that plans (predicts) trajectories that use idle thrust only and do not require the use of additional drag devices. However, when such trajectories cannot satisfy all ATC imposed constraints, the TEMO algorithm minimizes the use of additional thrust or speedbrakes to comply with all constraints.

The TEMO concept should be validated under different conditions to verify TEMO's ability to cope with various disturbances using energy management. Various design options could be validated and verified whether environmental impact is reduced by comparing TEMO descents with current step-down descents. Various errors could be artificially introduced to evaluate to what extent energy management is able to correct these errors and in what cases thrust or speedbrakes are required.

TEMO uses automation as it allows for fast, consistent, repetitive and multi-objective optimization for calculating trajectories. However, given that modeling errors are present in the TP and algorithm, the accuracy of calculated trajectories should be investigated. During a TEMO descent, the pilot supervises the system and is actively involved with entering relevant descent data used by the TEMO algorithm and performs manual actions as demanded by the planned trajectory. This new role of the pilot should be evaluated and the cockpit displays should be enhanced to support the pilot in working with TEMO. How much (additional) and what sort of information is required to perform these new descents and approaches, could be evaluated using a human-in-the-loop experiment. Furthermore, the effects of variations in pilots response of manual actions on time performance should be evaluated. For comparison, the simulated descents flown by pilots with similar simulated descents using a zero-delay pilot response model should be performed.

1-5 Enablers for the TEMO CDO Concept

Based on these questions and the problem definition, this research is divided into three challenges. First, energy management is evaluated as a method for correcting deviations during time-constrained CDOs as defined by the research goal. Due to the multi-objective nature of the CDO trajectory, the TP is highly automated. Second, since TEMO relies heavily on automation but due to the unanticipated variability in ‘open’ systems [89] such as aircraft, there is always a role foreseen for the human operator to retain abilities such as inductive reasoning and complex pattern matching which still outperform automated systems. Therefore, automation should be designed with the human operator in mind. Third, the quality of predicted trajectories depends on the quality of the supplied data and applied modeling. An example of such data are wind estimates at locations along the own trajectory. Today, these wind estimates are often of low resolution and can be multiple hours old. Hence, improving the quality of wind estimates is expected to benefit trajectory prediction accuracy.

This section discusses enablers that support evaluation of these research challenges in the context of TEMO: the issues of automating the flight deck and how wind estimates could be improved to increase the accuracy of predicted trajectories.

1-5-1 Flight Deck Automation

Through the course of aviation history and the simultaneous advances made in development of new technologies, various manual and labor intensive tasks have been replaced by automated systems in an aim to reduce costs, improve safety and trajectory accuracy, and reduce pilot workload. Costs have been reduced by replacing the Flight Engineer (FE) by computerized systems. Through the introduction of the FMS in 1982, aircraft navigation was simplified reducing pilot workload, while flight trajectories could be flown more accurately, reducing fuel use [90]. Other examples of automated systems are Aircraft Collision Avoidance System (ACAS) [91] and Terrain Awareness and Warning System (TAWS) which provide warnings and evasive maneuvers to prevent mid-air collisions or Controlled Flight into Terrain (CFIT), respectively.

According to Fitts list [92], often referred to as MABA-MABA (‘Man are better at, Machines are better at’), humans and machines both excel at different tasks. For example, machines outperform humans in repetitive, precise and simultaneous tasks, while humans surpass machines at inductive reasoning making humans better suited for high-level decision making and unforeseen situations. Therefore, automated machines could be used for routine and repetitive tasks to reduce pilot boredom and workload. The list also suggests that we should not automate every manual task, taking advantage of human capabilities. Others suggest that problems in human-automation interaction could be solved by adding more automation to remove the human operator from the cockpit [93]. However, automated systems cannot be fully and explicitly modeled [94, Ch. 4] and automation cannot be designed for every possible scenario [95] as these automated systems are still designed and developed by humans.

Designers often assume that automation and humans can work independently and simply

shift tasks from humans to automation and backwards without considering the consequences of this shift [95] as proper understanding of human-machine interaction is lacking. For this reason, often cockpit displays provide less state information about the automated system to the human pilot. Thus, designers often automate complex tasks whilst excluding the human operator in the design process [96, 97], resulting in a loss of information to support the pilot in operating the new automated system or provide sufficient training to comprehend an automated system.

Due to these new automated systems, the role of humans in the cockpit shifted from an active, manual flying pilot towards a supervisory [94] monitoring pilot. In this new role, pilots supervise and monitor an automated system and intervene [98] or execute actions based on the presented information using automation management strategies [99]. In this supervisory role, pilots complement the automated system to account for scenarios that either cannot be modeled or were unforeseen during the design.

This new supervisory role of humans using automated systems potentially results in humans being taken out of the loop [100], over-trust or biased in automation [60, 97, 101, 102], and a loss of awareness [60, 103, 104]. As a result of reduced awareness, pilots could potentially make incorrect decisions. A human pilot can be surprised about what an automated system is doing [105] and affects mental workload [60] and become mode-confused [106]. Automation surprises occur as such systems seem to ‘always’ work as intended resulting in over-trust as failure cases are rare. As automated systems substitute the human pilot, the pilot’s skill at performing such tasks will deteriorate [60], which could prove catastrophic when the automation system fails and the human operator must take control. Due to these problems, the *irony of automation* [107] states that automation is often used to reduce workload and simplify operations, while it actually introduces additional workload and make life more difficult as humans often struggle with understanding automation.

A prerequisite to enable proper human-machine interaction is to properly inform the human operator about the rationale that drives the automated system [95]. Hence, the question remains, what and how much additional information should support a system, such as TEMO, to ensure proper human-machine coordination and maintain high levels of performance? This question is addressed in this thesis by developing three different Human-Machine Interface (HMI) variants that differ in amount of additional information provided.

In principle, TEMO is an enhanced descent predictor that improves the performance of current VNAV predictions. Therefore, TEMO aims at using existing avionics and guidance systems and prescribed only minimal changes to current flight procedures and cockpit displays. Therefore, during a TEMO descent, pilots supervise the automated TEMO system and are actively involved with entering relevant descent data and perform manual actions as planned by TEMO.

1-5-2 Onboard Wind Estimation

Wind affects the groundspeed of the aircraft and consequently the ETA of an aircraft [26–35, 69]. Wind also affects the flight-path angle of an aircraft during approach as shown in Figure 1-2. The acting horizontal tailwind, V_w , increases the aircraft groundspeed and

simultaneously decreases the flight-path angle relative to Earth, γ_k , provided the aircraft descends at a particular constant speed. This change in kinematic flight-path angle also adjusts the groundspeed. Due to the change in effective flight-path angle, an aircraft will require a longer distance to descend from the same altitude relative to a situation where the aircraft experiences no wind or a headwind. Moreover, the change of flight-path angle alters the aircraft's deceleration capability. When a windfield varies with altitude, the motion of the aircraft relative to the air varies as well [108, 109] affecting both the deceleration and flight-path angle due to this wind gradient, see Appendix A.

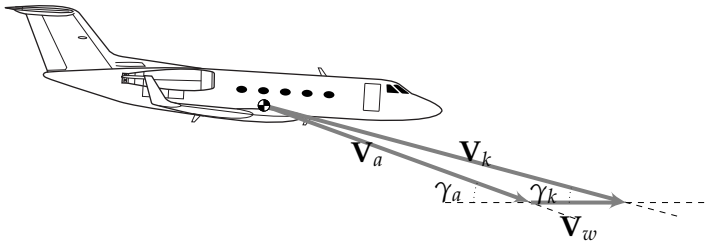


FIGURE 1-2: The effect of wind on an aircraft trajectory during descent.

The FMS uses wind information to predict trajectory parameters, such as ETAs and fuel calculations, and requires estimates of the wind data along the route towards the arrival airport [110]. Any error in estimating the wind will result in an error of the predicted groundspeed and flight-path angle. In turn, the flight-path angle error affects the predicted groundspeed and predicted vertical trajectory. Hence, the accuracy of the trajectory, both temporal and spatial, is greatly influenced by the wind estimation error [26, 27].

Today, wind data is extracted from meteorological wind charts and Automatic Terminal Information Service reports. These charts are updated slowly and provide wind information on coarse grid. Moreover, these charts are often only available prior to the start of a flight. For this reason, new systems have been developed to provide aircraft with improved wind estimates during flight execution. Examples of such systems are Boeing's 'Wind Updates' [111] and AVTECH's 'Aventus NowCast' [112]. Others have looked at using aircraft radar tracks [113, 114] and meteorological measurements from other aircraft [115]. Although these systems provide a definite improvement compared to current wind charts, there is further room for improvement in terms of temporal and spatial resolution.

A new wind estimation algorithm is developed in this thesis that aims at providing a high temporal and spatial resolution wind estimation profile. This is achieved by using wind data from nearby surrounding aircraft to improve the availability and coverage of the wind estimate. Inherent to these measurements is measurement noise [116, 117] which the algorithm addresses using stochastic principles. The algorithm is able to quickly generate and update the wind profile estimate in the FMS depending on the broadcast rate of other aircraft. It is expected that the availability of more and faster updated wind profile improves the performance of the TP [26–28, 30, 33, 118] and consequently the accuracy of CDOs.

1-6 Research Scope

In order to accomplish the goals of this thesis, the research is subject to several assumptions and limitations to reduce the overall scope.

Aircraft Validation of CDOs is done through simulations which require an aircraft model. When choosing an aircraft model there is a trade-off to be made between accuracy and relevance of the aircraft model. An aircraft model can be quite accurate but represent only a small percentage of the worldwide fleet of aircraft and; hence, be irrelevant. As such, this research uses aircraft models [119–121] based on the Airbus A320, as single-aisle aircraft represent the vast majority of worldwide commercial aircraft [122].

Furthermore, earlier in 2008, the Airbus A320 was selected as a viable option to serve as technology evaluator within the Clean Sky program and selected as reference aircraft within SGO [123]. In the future, however, TEMO should adapted to fit in other commercial aircraft types. Besides the use of Airbus A320 aircraft model, the Airbus A320 serves as a basis around which TEMO is developed and designed. This includes the current cockpit displays and systems.

Airspace system The airspace system used throughout this project is targeted for operation in 2018 as foreseen by SESAR [48]. This includes the assumption that aircraft communicate through System Wide Information Management (SWIM) using data-link systems to communicate trajectory changes and instructions. Moreover, wind is assumed to have only a horizontal component as the vertical component is relatively small during descent due to the small flight-path angle.

The time constraint provided by ATC is assumed to be provided by a ground-based Arrival Manager (AMAN) and is issued such to assure arrival sequencing and scheduling. This AMAN is assumed to be able to accurately sequence aircraft at the time-constrained waypoint using aircraft performance, forecast wind data, enhanced ground-based TPs and controller support tools. Prior to reaching ToD, aircraft are separated such that they are able to achieve their time constraint at the Initial Approach Fix (IAF) as required.

To reduce the complexity of the problem definition, ATC issues are beyond the scope of this research and the thesis focuses on the flight-deck and aircraft performance only. Therefore, spacing of aircraft pairs and spacing of arriving and departing aircraft is beyond the scope of this thesis as the principle aim of this research is to investigate how accurate aircraft can perform TEMO descents. It is assumed that sufficient spacing was achieved at ToD prior to start of the descent using an advanced AMAN or controller support tool, and the spacing compression effect resulting from in-trail decelerating aircraft.

Emergencies and non-nominal conditions Emergencies, such as loss of control or engine failures, are not considered and only normal operations are investigated. It is assumed that pilots will abort any TEMO operations when an emergency occurs and revert to current day emergency operations.

The TEMO algorithm is validated for several different disturbances which can be considered non-nominal conditions. During nominal conditions, the aircraft planning is assumed to know the parameters of the aircraft perfectly well, and with no planned energy or time error. The non-nominal conditions represent situations in real-life where errors in estimating position and velocity and aircraft mass estimation would be present.

Flaps Previous research [29, 32, 53, 66–69] used flaps and landing gear to control the aircraft's speed profile along a fixed vertical trajectory. The resulting negative effect on flap wear and aircraft maintenance lead to the requirement that in this research selection of flaps and landing gear extension should be performed at fixed nominal speeds. These nominal speeds are based on the aircraft minimum maneuvering speed for that aircraft configuration. Also, flaps and gear will not be retracted after having been extended. As such, these devices are not used as active drag devices to correct for disturbances even though this might be more energy efficient than deploying speedbrakes or using thrust.

Flight trajectory The flight trajectory throughout this thesis is defined as a trajectory from ToD to the stabilization point at 1,000 ft; here the aircraft must be stabilized and fully configured for landing. After reaching 1,000 ft, the aircraft performs a precision approach and no corrective actions can be applied to minimize deviations.

Moreover, it is assumed that all aircraft fly a fixed closed-path route from ToD to the runway threshold on a flat Earth surface. These routes are specifically designed to avoid populated residential areas and are fixed to improve predictability of the trajectory to be flown by restricting lateral variability. Theoretically, these arrival routes can also be designed such that lateral spacing from departing aircraft is assured. In the research described in this thesis, all descents follow a straight-in trajectory to simplify the dynamic equations.

Furthermore, it is assumed that the Calibrated Airspeed (CAS) equals the Indicated Airspeed (IAS) and, hence, position and instrument errors are discarded. However, compressibility effects are accounted for when converting CAS to True Airspeed (TAS) and TAS to CAS and, hence, no use is made of the Equivalent Airspeed (EAS) [109].

1-7 Thesis Outline

This thesis consists of eight chapters, each describing a different part of this research. Besides these chapters, the appendices contain background information related to this research. Two chapters are submitted papers and their contents have been revised, not to reiterate the same texts too extensively. At the start of these chapters, a short description is provided that explains the changes made to these papers. Besides these papers, the thesis contains other chapters in the order listed below. Figure 1-3 shows the structure of this thesis and how these chapters are related to each other.

Chapter 2 presents a new algorithm that uses energy principles and calculates trajectories to perform accurate, idle descents. The concept of Time and Energy Managed Operations is discussed by explaining the rationale of replanning. Moreover, the theory and

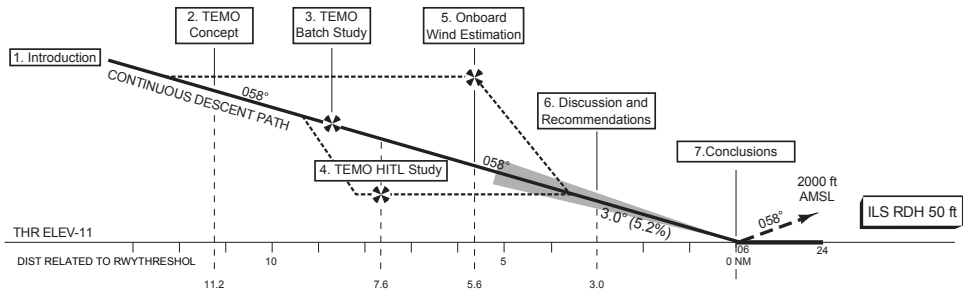


FIGURE 1-3: Visual structure of this thesis.

assumptions of strategic and tactical replanning are explained.

Chapter 3 discusses the results of a fast-time simulation study. Several time and energy errors are introduced to validate robustness of the TEMO algorithm. Moreover, an error in wind estimation is introduced to investigate the algorithm's ability to cope with wind errors. Both strategic and tactical replanning are compared for similar conditions. Furthermore, a comparison between TEMO descents and approaches and a current-day, step-down approach is performed in order to determine TEMO's environmental benefits.

In order to determine whether a pilot can operate an aircraft using the automated TEMO system, an experiment with pilots in the loop is discussed in **Chapter 4**. For this, a new iteration in TEMO development was performed to improve the TEMO algorithm for use in a real-time environment. Moreover, three different HMI displays were developed that differ in level of information provided which each aim at reducing variations in pilot response while providing efficient human-machine interaction. The effects of automation and the interaction between automation and the human pilot were investigated to evaluate whether pilots can work with such a high-demand automated system. Finally, a comparison between fully automation simulations and simulations with pilots is performed in order to investigate the effect of the human in the cockpit during TEMO descents.

Chapter 5 discusses a new wind estimation algorithm. During trajectory predictions, wind estimates are one of the larger contributors to errors and uncertainties in the predicted trajectory. A new algorithm has been developed that reduces the measurement noise of sensed wind observations and combines the observations of the own aircraft with observations communicated by other nearby aircraft. The algorithm gathers all received data and reduces the noise to improve the wind profile estimate along the own trajectory. This new approach yields rapid updates of the estimated wind forecasts compared to current wind-chart practices. This algorithm is evaluated using actual wind observations received from the Royal Netherlands Meteorological Institute (KNMI). Moreover, the algorithm is evaluated in a simulated environment used for aircraft spacing during approach.

The results of all experiments are combined to yield a discussion on the challenges of Continuous Descent Operations using energy principles in **Chapter 6**. This chapter also discusses the effect of improved onboard wind estimation for Continuous Descent Operations. This discussion reflects on the results and limitations, and contains recommendations

and implications for further research.

Finally, **Chapter 7** draws conclusions and identifies whether the research goals have been met.

References

- [1] **EUROCONTROL**. Long-Term Forecast: IFR Flight Movements 2010-2030. Tech. Rep. CND/STATFOR Doc415, EUROCONTROL, 2010.
- [2] **IATA**. Jet Fuel Price Development. <http://www.iata.org/publications/economics/fuel-monitor/>, 2013.
- [3] **SESAR**. Air Transport Framework: The Current Situation. Tech. Rep. SESAR TR DLM-0602-001-03-00, EUROCONTROL, 2006.
- [4] **IATA**. Financial Forecast. <http://www.iata.org/whatwedo/Documents/economics/Industry-Outlook-Dec2012.pdf>, 2012.
- [5] Directive 2008/101/EC of the European Parliament and of the Council. Official Journal of the European Union, 2008.
- [6] **ICAO**. *Annex 16 to the Convention on International Civil Aviation - Environmental Protection - Volume I, Aircraft Noise*. International Civil Aviation Organization, Montreal, Canada, 2011.
- [7] **ICAO**. *Annex 16 to the Convention on International Civil Aviation - Environmental Protection - Volume II, Aircraft Engine Emissions*. International Civil Aviation Organization, Montreal, Canada, 2008.
- [8] **D. Schreckenberger, M. Meis, C. Kahl, C. Peschel, and T. Eikmann**. Aircraft Noise and Quality of Life around Frankfurt Airport. *International Journal of Environmental Research and Public Health*, 7(9), 3382–3405, 2010. doi:10.3390/ijerph7093382.
- [9] **J. E. Penner, D. H. Lister, D. J. Griggs, D. J. Dokken, and M. McFarland**. Aviation and the Global Atmosphere. Special report, Intergovernmental Panel on Climate Change, Cambridge, England, 1999.
- [10] **S. Martens**. Jet Noise Reduction Technology Development at GE Aircraft Engines. In: **G. Masters**, ed., *Proceedings of the 23th Congress of the International Council of the Aeronautical Sciences, Toronto, Ontario Canada, September 8–13, ICAS 2002-8.4.2*, pp. 1–10, 2002.
- [11] **P. Smith**. Date with the Eight. *Flight International*, 182(5370), 26–35, 2012.
- [12] **ICAO**. *Guidance on the Balanced Approach to Aircraft Noise - Doc 9829 AN/451*. International Civil Aviation Organization, Montreal, Canada, second edition edn., 2008.

- [13] **ICAO.** *Guidance on the Balanced Approach to Aircraft Noise - Doc 9829 AN/451 - Amendment No. 1.* International Civil Aviation Organization, Montreal, Canada, second edition edn., 2010.
- [14] **H. G. Visser** and **R. A. A. Wijnen.** Optimization of Noise Abatement Arrival Trajectories. *The Aeronautical Journal*, 107(1076), 607–615, 2003.
- [15] **F. Vormer, M. Mulder, M. M. Van Paassen,** and **J. A. Mulder.** Optimization of Flexible Approach Trajectories Using a Genetic Algorithm. *Journal of Aircraft*, 43(4), 941–952, 2006. doi:10.2514/1.13609.
- [16] **S. Hartjes, H. G. Visser,** and **S. J. Hebly.** Optimization of RNAV Noise and Emission Abatement Departure Procedures. *The Aeronautical Journal*, 114(1162), 2010.
- [17] **M. L. Braakenburg, S. Hartjes, H. G. Visser,** and **S. J. Hebly.** Development of a Multi-Event Trajectory Optimization Tool for Noise-Optimized Approach Route Design. In: *Proceedings of the 11th AIAA Aviation Technology, Integration, and Operations (ATIO) Conference, Virginia Beach, Virginia, September 20–22, AIAA 2011-6929*, pp. 1–13. American Institute of Aeronautics and Astronautics, 2011.
- [18] Council Directive 92/14/EEC of 2 March 1992 on the limitation of the operation of aeroplanes covered by Part II, Chapter 2, Volume 1 of Annex 16 to the Convention on International Civil Aviation, second edition (1988), 1992.
- [19] Council Regulation 925/1999 of 29 April 1999 on the registration and operation within the Community of certain types of civil subsonic jet aeroplanes which have been modified and recertificated as meeting the standards of volume I, Part II, Chapter 3 of Annex 16 to the Convention on International Civil Aviation, third edition (July 1993), 1999.
- [20] **ICAO.** *Procedures for Air Navigation Services - Aircraft Operations - Volume I, Flight Procedures - Doc 8168, OPS/611.* International Civil Aviation Organization, Montreal, Canada, 2006.
- [21] **R. De Neufville** and **A. R. Odoni.** *Airport Systems: Planning, Design and Management.* McGraw-Hill Professional, 2002. Chapter 6, 10.
- [22] **E. P. Dinges.** Determining the Environmental Benefits of Implementing Continuous Descent Approach Procedures. In: *Proceedings of the 7th USA/Europe Air Traffic Management Research and Development Seminar, Barcelona, July 2–5*, pp. 1–10, 2007.
- [23] **ICAO.** *Continuous Descent Operations (CDO) Manual - Doc 9931 AN/476.* International Civil Aviation Organization, Montreal, Canada, 2010.
- [24] **NATS.** EGLL–LONDON HEATHROW: AD 2.EGLL-1. Aeronautical Information Publication, 2012.

- [25] **L. J. J. Erkelens.** Research into new noise abatement procedures for the 21st century. In: *Proceedings of the AIAA Guidance, Navigation and Control Conference and Exhibit, Denver, Colorado, August 14–17*, AIAA 2000-4474, pp. 1–10. American Institute of Aeronautics and Astronautics, 2000. doi:10.2514/6.2000-4474.
- [26] **R. E. Cole, S. Green, M. Jardin, B. E. Schwartz, and S. G. Benjamin.** Wind Prediction Accuracy for Air Traffic Management Decision Support Tools. In: *Proceedings of the 3rd USA/Europe Air Traffic Management Research and Development Seminar, Napoli, Italy, June 13–16*, pp. 1–9, 2000.
- [27] **S. M. Green, M. P. Grace, and D. H. Williams.** Flight Test Results: CTAS and FMS Cruise/Descent Trajectory Prediction Accuracy. In: *Proceedings of the 3rd USA/Europe Air Traffic Management Research and Development Seminar, Napoli, Italy, June 13–16*, pp. 1–11, 2000.
- [28] **N. T. Ho and J.-P. B. Clarke.** Methodology for Optimizing Parameters of Noise-Abatement Approach Procedures. *Journal of Aircraft*, 44(4), 1168–1176, 2007. doi:10.2514/1.22292.
- [29] **J. L. De Prins, K. F. M. Schippers, M. Mulder, M. M. Van Paassen, A. C. In 't Veld, and J.-P. B. Clarke.** Enhanced Self-Spacing Algorithm for Three-Degree Decelerating Approaches. *Journal of Guidance, Control and Dynamics*, 30(2), 576–590, 2007. doi:10.2514/1.24542.
- [30] **L. Ren and J.-P. B. Clarke.** Flight-Test Evaluation of the Tool for Analysis of Separation and Throughput. *Journal of Aircraft*, 45(1), 323–332, 2008. doi:10.2514/1.30198.
- [31] **J. K. Klooster, K. D. Wickman, and O. F. Bleeker.** 4D Trajectory and Time-of-Arrival Control to Enable Continuous Descent Arrivals. In: *Proceedings of the AIAA Guidance, Navigation and Control Conference and Exhibit, Honolulu, Hawaii, August 18–21*, AIAA 2008-7402, pp. 1–17. American Institute of Aeronautics and Astronautics, 2008. doi:10.2514/6.2008-7402.
- [32] **A. M. P. De Leege, A. C. In 't Veld, M. Mulder, and M. M. Van Paassen.** Three-Degree Decelerating Approaches in High Density Arrival Streams. *Journal of Aircraft*, 46(5), 1681–1691, 2009. doi:10.2514/1.42420.
- [33] **J. Bronsvort, G. McDonald, R. Potts, and E. Gutt.** Enhanced Descent Wind Forecast for Aircraft: Facilitation of Continuous Descent Arrivals with Improved Efficiency and Predictability by the use of Tailored Descent Wind Forecasts. In: *Proceedings of the 9th USA/Europe Air Traffic Management Research and Development Seminar, Berlin, Germany, June 14–17*, pp. 1–10, 2011.
- [34] **D. Garrido-López, R. Gomez Ledesma, G. R. Gershzohn, and S. Moore.** Analysis of Aircraft Descent Predictability: Implications for Continuous Four-Dimensional

- Navigation. In: *Proceedings of the AIAA Guidance, Navigation and Control Conference, Portland, Oregon, August 8–11*, AIAA 2011-6217, pp. 1–18. American Institute of Aeronautics and Astronautics, 2011. doi:10.2514/6.2011-6217.
- [35] **F. J. L. Bussink, J. J. Van der Laan, and P. M. A. De Jong.** Combining Flight-deck Interval Management with Continuous Descent Approaches in high density traffic and realistic wind conditions. In: *Proceedings of the AIAA Guidance, Navigation and Control Conference, Minneapolis, Minnesota, August 13–16*, AIAA 2012-4523, pp. 1–25. American Institute of Aeronautics and Astronautics, 2012. doi:10.2514/6.2012-4523.
- [36] **L. L. Stell.** Predictability of Top of Descent Location for Operational Idle-thrust Descents. In: *Proceedings of the 10th AIAA Aviation Technology, Integration, and Operations (ATIO) Conference, Fort Worth, Texas, September 13–15*, AIAA 2010-9116, pp. 1–12. American Institute of Aeronautics and Astronautics, 2010.
- [37] **D. Knorr, M. Rose, J. Guldung, R. Galaviz-Schomisch, P. Enaud, and H. Hegen-doerfer.** Estimating ATM Terminal Area Efficiency Gains Through Speed Changes in Cruise. In: *Proceedings of the 11th AIAA Aviation Technology, Integration, and Operations (ATIO) Conference, Virginia Beach, Virginia, September 20–22*, AIAA 2011-6876, pp. 1–17. American Institute of Aeronautics and Astronautics, 2011.
- [38] **Y. Glina, S. Troxel, T. Reynolds, and M. McPartland.** Wind Information Requirements to Support Four Dimensional Trajectory-Based Operations. In: *Proceedings of the 12th AIAA Aviation Technology, Integration, and Operations (ATIO) Conference and 14th AIAA/ISSM, Indianapolis, Indiana, September 17–19*, AIAA 2012-5702, pp. 1–14. American Institute of Aeronautics and Astronautics, 2012. doi:10.2514/6.2012-5702.
- [39] **J.-P. B. Clarke, J. Brooks, G. Nagle, A. Scacchioli, W. White, and S. R. Liu.** Optimized Profile Descent Arrivals at Los Angeles International Airport. *Journal of Aircraft*, 50(2), 360–369, 2013. doi:10.2514/1.C031529.
- [40] **A. Herndon, M. Cramer, K. Sprong, and R. Mayer.** Analysis of advanced flight management systems (FMS), flight management computer (FMC) field observations trials, vertical path. In: *Proceedings of the 26th Digital Avionics Systems Conference, Williamsburg, Virginia, October 21–25*, pp. 4.A.4–1–4.A.4–12. IEEE/AIAA, 2007. doi:10.1109/DASC.2007.4391899.
- [41] **J.-P. B. Clarke, N. T. Ho, L. Ren, J. A. Brown, K. R. Elmer, and K.-O. Tong.** Continuous Descent Approach: Design and Flight Test for Louisville International Airport. *Journal of Aircraft*, 41(5), 1054–1066, 2004. doi:10.2514/1.5572.
- [42] **L. J. J. Erkelens.** Advanced Noise Abatement Procedures for Approach and Departure. In: *Proceedings of the AIAA Guidance, Navigation, and Control Conference and Exhibit, Monterey, California, August 5–8*, AIAA 2002-4858, pp. 1–9. American Institute of Aeronautics and Astronautics, 2002.

- [43] **E. Freville, J.-P. Nicolaon, A. Vidal, and P. Crick.** Potential Benefits of a Time-based Separation Procedure to maintain the Arrival Capacity of an Airport in strong head-wind conditions. In: *Proceedings of the 5th USA/Europe Air Traffic Management Research and Development Seminar, Budapest, Hungary, June 23–27*, pp. 1–7, 2003.
- [44] **S. Muresean.** Initial 4D - 4D Trajectory Data Link (4DTRAD) - Concept of Operations. Tech. rep., EUROCONTROL, Brussels, Belgium, 2008.
- [45] **J. K. Klooster, A. Del Amo, and P. Manzi.** Controlled Time-of-Arrival Flight Trials Results and Analysis. In: *Proceedings of the 8th USA/Europe Air Traffic Management Research and Development Seminar, Napa, California, June 29–July 2*, pp. 1—11, 2009.
- [46] **P. M. A. De Jong, K. De Vos, C. Borst, M. M. Van Paassen, and M. Mulder.** Time-based Spacing for 4D Approaches using Speed-Profiles. In: *Proceedings of the AIAA Guidance, Navigation and Control Conference, Portland, Oregon, August 8–11*, AIAA 2011-6215, pp. 1–14. American Institute of Aeronautics and Astronautics, 2011. doi:10.2514/6.2011-6215.
- [47] **T. S. Abbot.** A Brief History of Airborne Self-Spacing Concepts. Contractor Report NASA/CR–2009-215695, National Aeronautics and Space Administration, Langley Research Center, Hampton, Virginia 23681-2199, 2009.
- [48] **SESAR.** European ATM Master Plan. Tech. Rep. Edition 2, EUROCONTROL, 2012. SESAR JU & SESAR Work Package C and Partners.
- [49] **NextGen Office.** FAA’s NextGen Implementation Plan 2012. Tech. rep., FAA, 800 Independence Avenue, Washington, DC, 2012.
- [50] **M. Tielrooij, A. C. in ’t Veld, M. M. van Paassen, and M. Mulder.** Development of a Time-Space Diagram to Assist ATC in Monitoring Continuous Descent Approaches. In: **M. Mulder**, ed., *Air Traffic Control*, pp. 135–147. InTech, Rijeka, Croatia, 2010. ISBN 978-953-307-103-9. doi:10.5772/9845.
- [51] **A. M. P. De Leege, A. C. In ’t Veld, M. Mulder, and M. M. Van Paassen.** A Time-Space Diagram as Controller Support Tool for Closed Path Continuous Descent Operations. In: *Proceedings of the AIAA Guidance, Navigation and Control Conference, Portland, Oregon, August 8–11*, AIAA 2011-6220, pp. 1–29. American Institute of Aeronautics and Astronautics, 2011. doi:10.2514/6.2011-6215.
- [52] **A. Van der Eijk, C. Borst, A. C. In ’t Veld, M. M. Van Paassen, and M. Mulder.** Assisting Air Traffic Controllers in Planning and Monitoring Continuous-Descent Approaches. *Journal of Aircraft*, 49(5), 1376–1390, 2012. doi:10.2514/1.C031686.
- [53] **A. C. In ’t Veld and J.-P. B. Clarke.** Trajectory Prediction for Self Separation during Decelerating Approaches in a DATA-LINK Environment. In: *Proceedings of the*

- 2nd AIAA Aircraft Technology, Integration, and Operations (ATIO) 2002 Technical Forum, Los Angeles, California, October 1–3, AIAA 2002-5887, pp. 1–6. American Institute of Aeronautics and Astronautics, 2002.*
- [54] **T. S. Abbot.** Speed Control Law for Precision Terminal Area In-Trail Self Spacing. Technical Memorandum NASA/TM-2002-211742, National Aeronautics and Space Administration, Langley Research Center, Hampton, Virginia 23681-2199, 2002.
 - [55] **M. Westerlaken.** *Conceptual Development of the Free-Degree Decelerating Approach, Achieving Noise Abatement and Time-Based Self-Spacing by Flight Path Changes during Idle-Thrust Descents.* Unpublished MSc. Thesis, Faculty of Aerospace Engineering, Delft University of Technology, 2009.
 - [56] **J. Ellerbroek, M. Visser, S. B. J. Van Dam, M. Mulder, and M. M. Van Paassen.** Design of an Airborne Three-Dimensional Separation Assistance Display. *IEEE Transactions on Systems, Man, and Cybernetics, part A: Systems and Humans*, 41(6), 863–875, 2011. ISSN 1083-4427. doi:10.1109/TSMCA.2010.2093890.
 - [57] **J. Ellerbroek, K. C. R. Brantegem, M. M. Van Paassen, and M. Mulder.** Experimental Evaluation of a Co-planar Airborne Separation Display. *IEEE Transactions on Human Machine Systems*, 1(3), 2013. In press.
 - [58] **P. Pellerin.** SESAR JU - Initial 4D “On Time”. Presentation at ATC Global 2012, Amsterdam, The Netherlands, 2012.
 - [59] **D. De Smedt.** Aircraft Systems and 4D Trajectory Management. Presentation at the 2nd Round of Military CNS Technical Implementation Information Days, 2012.
 - [60] **R. Parasuraman, T. B. Sheridan, and C. D. Wickens.** A Model for Types and Levels of Human Interaction with Automation. *IEEE Transactions on Systems, Man and Cybernetics, Part A*, 30(3), 286–297, 2000. doi:10.1109/3468.844354.
 - [61] **N. Suarez.** Higher Levels of Automation in ATM. White paper, HALA! SESAR Research Network, 2011.
 - [62] **Clean Sky JU.** Systems for Green Operations (SGO) Integrated Technology Demonstrator at a glance. http://www.cleansky.eu/sites/default/files/documents/fact_sheet_sgo_march_2011.pdf, 2011.
 - [63] **B. Bulfer and S. Gifford.** *Big Boeing FMC User’s Guide.* Leading Edge Publishing, 85 Macready Drive, Merced, California 95341, second edn., 1999.
 - [64] **B. Bulfer.** *737 FMC Users’ Guide.* Leading Edge Libraries, 2031 River Falls Drive Kingwood, Humble, Texas 77339-3113, fourth edn., 2003.
 - [65] **C. W. Vietor.** *Precision Three-Dimensional Flying for Jet Transport Aircraft - The Profile Descent.* Los Angeles, California, 1990.

- [66] **M. F. Koeslag**. Advanced Continuous Descent Approaches. Tech. Rep. NLR-TR-2001-359, Faculty of Aerospace Engineering, Delft University of Technology and National Aerospace Laboratory NLR, 2001.
- [67] **W. F. De Gaay Fortman, M. M. Van Paassen, M. Mulder, A. C. In 't Veld, and J.-P. B. Clarke**. Implementing Time-Based Spacing for Decelerating Approaches. *Journal of Aircraft*, 44(1), 106–118, 2007. doi:10.2514/1.22253.
- [68] **A. C. In 't Veld, M. Mulder, M. M. Van Paassen, and J.-P. B. Clarke**. Pilot Support Interface for Three-Degree Decelerating Approach Procedures. *The International Journal of Aviation Psychology*, Volume 19, Issue 3, 287–308, 2009. doi:10.1080/10508410902983938.
- [69] **P. M. A. De Jong, A. C. In 't Veld, A. M. P. De Leege, M. M. Van Paassen, and M. Mulder**. Control Space Analysis of Three-Degree Decelerating Approaches at Amsterdam Airport Schiphol. In: *Proceedings of the AIAA Guidance, Navigation and Control Conference, Toronto, Ontario Canada, August 2–5*, AIAA 2010-8454, pp. 1–20. American Institute of Aeronautics and Astronautics, 2010. doi:10.2514/6.2010-8454.
- [70] **R. P. M. Verhoeven and N. de Gelder**. Time-based navigation and ASAS interval managed CDA procedures. In: *CEAS Conference, Manchester, United Kingdom, 26–29 October*, pp. 1–10, 2009.
- [71] **D. H. Williams, R. M. Oseguera-Lohr, and E. T. Lewis**. Design and Testing of a Low Noise Flight Guidance Concept. Technical Memorandum NASA/TM-2004-213516, National Aeronautics and Space Administration, Langley Research Center, Hampton, Virginia 23681-2199, 2004.
- [72] **R. M. Oseguera-Lohr, D. H. Williams, and E. T. Lewis**. Crew Procedures for Continuous Descent Arrivals Using Conventional Guidance. Technical Memorandum NASA/TM-2007-214538, National Aeronautics and Space Administration, Langley Research Center, Hampton, Virginia 23681-2199, 2007.
- [73] **D. H. Williams, R. M. Oseguera-Lohr, and E. T. Lewis**. Energy Navigation: Simulation Evaluation and Benefit Analysis. Technical Publication NASA/TP-2011-217167, National Aeronautics and Space Administration, Langley Research Center, Hampton, Virginia 23681-2199, 2011.
- [74] **S. G. Park and J.-P. B. Clarke**. Vertical Trajectory Optimization for Continuous Descent Arrival Procedure. In: *Proceedings of the AIAA Guidance, Navigation and Control Conference, Minneapolis, Minnesota, August 13–16*, AIAA 2012-4757, pp. 1–19. American Institute of Aeronautics and Astronautics, 2012. doi:10.2514/6.2012-4757.
- [75] **R. A. Copenbarger, R. Lanier, D. N. Sweet, and S. Dorsky**. Design and Development of the En Route Descent Advisor (EDA) for Conflict-Free Arrival Metering. In:

- Proceedings of the AIAA Guidance, Navigation, and Control Conference and Exhibit, Providence, Rhode Island, August 16–19, AIAA 2004-4875, pp. 1–19. American Institute of Aeronautics and Astronautics, 2004. doi:10.2514/6.2004-4875.*
- [76] **R. A. Coppenbarger, R. W. Mead, and D. N. Sweet.** Field Evaluation of the Tailored Arrivals Concept for Datalink-Enabled Continuous Descent Approach. *Journal of Aircraft*, 46(4), 1200–1209, 2009. doi:10.2514/1.39795.
- [77] **T. Miquel, H. Manzoni, F. Legrand, D. Martin, and M. Millischer.** 4D Green Approach Trajectory: Illustrative Assessment On Toulouse Approach. In: *Proceedings of the AIAA Guidance, Navigation, and Control Conference, Toronto, Ontario, Canada, August 2–5, AIAA 2010-8456, pp. 1–15. American Institute of Aeronautics and Astronautics, 2010. doi:10.2514/6.2010-8456.*
- [78] **M. Kaiser, M. Schultz, and H. Fricke.** Automated 4D Descent Path Optimization using the Enhanced Trajectory Prediction Model (ETPM). In: *Proceedings of the 5th International Conference on Research in Air Transportation — ICRAAT 2012, Berkeley, California, May 22–25, pp. 1–8, 2012.*
- [79] **R. J. De Muynck, L. Verhoeff, R. P. M. Verhoeven, and N. De Gelder.** Enabling Technology Evaluation for Efficient Continuous Descent Approaches. In: **I. Grant**, ed., *Proceedings of the 26th Congress of the International Council of the Aeronautical Sciences including the 8th AIAA Aviation Technology, Integration, and Operations (ATIO) Conference, Anchorage, Alaska, 14–19 September, ICAS 2008-8.9.2, pp. 1–9, 2008.*
- [80] **H. Lenz and B. Korn.** Enabling Advanced Continuous Descent Approaches – Results of the European Project OPTIMAL. In: *Proceedings of the 28th Digital Avionics Systems Conference, Orlando, Florida, October 23–29, pp. 2.C.3–1–2.C.3–10. IEEE/AIAA, 2009. doi:10.1109/DASC.2009.5347546.*
- [81] **D. Garrido-López, L. D’Alto, and R. Gomez Ledesma.** A Novel Four-Dimensional Guidance for Continuous Descent Approaches. In: *Proceedings of the 28th Digital Avionics Systems Conference, Orlando, Florida, October 23–29, pp. 6.E.1–1–6.E.1–11. IEEE/AIAA, 2009. doi:10.1109/DASC.2009.5347433.*
- [82] **J. E. Robinson and M. Kamgarpour.** Benefits of Continuous Descent Operations in High-Density Terminal Airspace Under Scheduling Constraints. In: *Proceedings of the 10th AIAA Aviation Technology, Integration, and Operations (ATIO) Conference, Fort Worth, Texas, September 13–15, AIAA 2010-9115, pp. 1–21. American Institute of Aeronautics and Astronautics, 2010. doi:10.2514/6.2010-9115.*
- [83] **J.-P. B. Clarke, J. Brooks, G. Nagle, A. Scacchioli, W. White, and S. R. Liu.** Optimized Profile Descent Arrivals at Los Angeles International Airport. *Journal of Aircraft*, 50(2), 360–369, 2013. doi:10.2514/1.C031529.

- [84] **M. C. L. Van den Hoven, P. M. A. De Jong, C. Borst, M. Mulder, and M. M. Van Paassen.** Investigation of Energy Management during Approach - Evaluating the Total Energy-Based Perspective Flight-Path Display. In: *Proceedings of the AIAA Guidance, Navigation and Control Conference, Toronto, Ontario Canada, August 2–5*, AIAA 2010-8401, pp. 1–20. American Institute of Aeronautics and Astronautics, 2010. doi:10.2514/6.2010-8401.
- [85] **M. H. J. Amelink.** *Ecological Automation Design, Extending Work Domain Analysis*. Ph.D. thesis, Faculty of Aerospace Engineering, Delft University of Technology, 2010.
- [86] **Federal Aviation Administration.** Federal Aviation Regulations Part 91 - General Operating and Flight Rules, 2013. Sec. 91.117 — Aircraft speed.
- [87] **M. Asselin.** *An Introduction to Aircraft Performance*. AIAA Educational Series. American Institute of Aeronautics and Astronautics, Reston, Virginia, 1997.
- [88] **W. Langewiesche.** *Stick and Rudder: An Explanation of the Art of Flying*. McGraw-Hill Inc., 1944.
- [89] **K. J. Vicente and J. Rasmussen.** Ecological Interface Design: Theoretical Foundations. *IEEE Transactions on Systems, Man, and Cybernetics*, 22(4), 589–606, 1992. doi:10.1109/21.156574.
- [90] **S. B. Fishbein.** *Flight Management Systems: The Evolution of Avionics and Navigation Technology*. Praeger, 1995.
- [91] **M. Kayton and W. R. Fried,** eds. *Avionics Navigation Systems*. John Wiley & Sons, Inc., second edn., 1997.
- [92] **P. M. Fitts.** Human Engineering for an Effective Air Navigation and Traffic Control System. Tech. Rep. ATI 133 954, Ohio State University Research Foundation, Columbus, Ohio, 1951.
- [93] **A. R. Pritchett.** Aviation Automation: General Perspectives and Specific Guidance for the Design of Modes and Alerts. *Reviews of Human Factors and ergonomics*, 5(1), 82–113, 2009. doi:10.1518/155723409X448026.
- [94] **T. B. Sheridan.** *Telerobotics, Automation, and Human Supervisory Control*. MIT Press, Cambridge, Massachusetts, 1992.
- [95] **K. Christoffersen and D. D. Woods.** How to Make Automated Teams Team Players. In: **E. Salas**, ed., *Advances in Human Performance and Cognitive Engineering Research*, vol. 2, pp. 1–12. JAI Press/Elsevier, 2002.
- [96] **S. W. A. Dekker.** On the other side of promise: what should we automate today? In: **D. Harris**, ed., *Human Factors for Civil Flight Deck Design*, chap. 8, pp. 183–198. Ashgate Publishing Limited, 2004.

- [97] **M. L. Cummings.** Automation Bias in Intelligent Time Critical Decision Support Systems. In: *Proceedings of the AIAA 1st Intelligent Systems Technical Conference, Chicago, Illinois, 20–22 September*, AIAA 2004-6313, pp. 1–6. American Institute of Aeronautics and Astronautics, 2004. doi:10.2514/6.2004-6313.
- [98] **S. W. A. Dekker** and **D. D. Woods.** To Intervene or not to Intervene: The Dilemma of Management by Exception. *Cognition, Technology & Work*, 1(2), 86–96, 1999.
- [99] **W. A. Olson** and **N. B. Sarter.** Automation Management Strategies: Pilot Preferences and Operational Experiences. *The International Journal of Aviation Psychology*, 10(4), 327–341, 2000. doi:10.1207/S15327108IJAP1004_2.
- [100] **D. B. Kaber** and **M. R. Endsley.** Out-of-the-Loop Performance Problems and the Use of Intermediate Levels of Automation for Improved Control System Functioning and Safety. *Progress Saftey Progress*, 16(3), 126–131, 1997. doi:10.1002/prs.680160304.
- [101] **E. L. Wiener.** Complacency: Is the term useful for air safety? In: *Proceedings of the 26th Corporate Aviation Safety Seminar, Denver, Colorado*, pp. 116–125, 1981.
- [102] **R. Parasuraman, R. Molloy,** and **I. L. Singh.** Performance Consequences of Automation-Induced ‘Complacency’. *The International Journal of Aviation Psychology*, 3(1), 1–23, 1993. doi:10.1207/s15327108ijap0301_1.
- [103] **M. R. Endsley.** Automation and Situation Awareness. In: **R. Parasuraman** and **M. Mouloua**, eds., *Automation and Human Performance: Theory and Applications*, pp. 163–181. Lawrence Erlbaum Associates, Inc., Mahway, New Jersey, 1996.
- [104] **C. E. Billings.** *Aviation Automation: The Search for a Human-Centered Approach.* Lawrence Erlbaum Associates, Inc., Mahway, New Jersey, 1997.
- [105] **N. B. Sarter** and **D. D. Woods.** Team Play with a Powerful and Independent Agent: Operational Experiences and Automation Surprises on the Airbus A-320. *Human Factors*, 39(4), 553–569, 1997.
- [106] **A. Joshi, S. P. Miller,** and **P. E. H. Mats.** Mode Confusion Analysis of a Flight Guidance System using Formal Methods. In: *Proceedings of the 22nd Digital Avionics Systems Conference, Indianapolis, Indiana, October 12–16*, vol. 1, pp. 2.D.1—21–12. IEEE/AIAA, 2003. doi:10.1109/DASC.2003.1245813.
- [107] **L. Bainbridge.** Ironies of Automation. *Automatica*, 19(6), 775–779, 1983. doi:10.1016/0005-1098(83)90046-8.
- [108] **W. A. Mair.** The Effect of a Wind Gradient on the Rate of Climb of an Aircraft. A.R.C. Technical Report Reports end Memoranda No. 2 9 5 3, Cambridge university Aeronautics Laboratory, 1954.
- [109] **G. J. J. Ruijgrok.** *Elements of Airplane Performance.* Delft University Press, 1996.

- [110] **R. Walter.** *The Aviation Handbook*, chap. 15, Flight Management Systems. CRC Press LLC, 2000.
- [111] **M. Durham.** inFlight optimization Services offers Airlines more Fuel-efficient en-route operations. *AERO Magazine*, 42(Quarter 2), 21–23, 2011.
- [112] **AVTECH Sweden AB.** Aventus NowCast: Great fuel savings by accurate wind information. Product sheet, 2012.
- [113] **D. Delahaye, S. Puechmorel, and P. Vacher.** Windfield Estimation by Radar Track Kalman Filtering and Vector Spline Extrapolation. In: *Proceedings of the 22nd Digital Avionics Systems Conference, Indianapolis, Indiana, October 12–16*, vol. 1, pp. 5.E.2–1–5.E.2–11. IEEE/AIAA, 2003. doi:10.1109/DASC.2003.1245869.
- [114] **A. M. P. De Leege, M. Mulder, and M. M. Van Paassen.** Using Automatic Dependent Surveillance-Broadcast for Meteorological Monitoring. *Journal of Aircraft*, 50(21), 249–261, 2013. doi:10.2514/1.55833.
- [115] **N. Bienert and H. Fricke.** Real-time Wind Uplinks for Prediction of the Arrival Time and Optimization of the Descent Profile. In: *Proceedings of the 3rd ENRI International Workshop on ATM/CNS, Tokyo, Japan, February 19–22*, EN-045, pp. 1–6. ENRI, 2013.
- [116] **D. J. Painting.** Aircraft Meteorological Data Relay (AMDAR) Reference Manual. Tech. Rep. WMO-No. 958, World Meteorological Organization, 2003.
- [117] **EUROCAE.** *Minimum Operational Performance Standards for 1090 MHz Extended Squitter Automatic Dependent Surveillance – Broadcast (ADS-B) and Traffic Information Services – Broadcast (TIS-B) - ED-102A*. EUROCAE, 92240 Malakoff, France, 2012. Appendix V.3.2.
- [118] **J. Wat, J. Follet, R. Mead, J. Brown, R. Kok, F. Dijkstra, and J. Vermeij.** In Service Demonstration of Advanced Arrival Techniques at Schiphol Airport. In: *Proceedings of the 6th AIAA Aviation Technology, Integration, and Operations Conference (ATIO), Wichita, Kansas, September 25–27*, AIAA 2006-7753, pp. 1–20. American Institute of Aeronautics and Astronautics, 2006.
- [119] **P. J. Van der Geest.** Validation of aircraft simulation models for the analysis of in-trail following dynamics - Deliverable D1 of the AMAAI project. Contract Report NLR-CR-2002-044, National Aerospace Laboratory, Amsterdam, The Netherlands, 2002.
- [120] **P. J. Van der Geest.** The AMAAI modelling toolset for the analysis of in-trail following dynamics - Deliverable D2: Description and User Guide. Contract Report NLR-CR-2002-112, National Aerospace Laboratory, Amsterdam, The Netherlands, 2002.

- [121] **H. Smaili, M. Laban, and J. Dominicus.** New Integrated Modeling and Simulation Techniques for Research and Training Applications. In: *Proceedings of the AIAA Modeling and Simulation Technologies Conference and Exhibit, San Francisco, California, 15–18 August*, AIAA 2005-6294, pp. 1–17. American Institute of Aeronautics and Astronautics, 2005. doi:10.2514/6.2005-6294.
- [122] **AIRBUS.** Global Market Forecast 2012–2031 - Navigating the Future, 2012.
- [123] **J.-P. Huynh, J. Chaptal, S. Le Moing, S. Vial, C. Cros, B. Morizet, D. Duturc., C. Marizy, and J.-C. Mere.** Mission Data Package. Deliverable SGO-WP 1.1-A-F-SPEC-0016-B_D_1.1.1_5, Airbus France, 2009. WP1-Technology Studies and Concept Validation, System for Green Operations ITD.

CONTINUOUS DESCENTS USING TIME AND ENERGY MANAGEMENT

The previous chapter discussed several concepts of Continuous Descent Operations (CDO) that each use different techniques to perform a CDO. Each of these techniques has its specific advantages and disadvantages but most of the concepts still require small amounts of engine thrust to cope with uncertainties and disturbances along the descent. A new concept has been developed that aims at minimizing the use of thrust throughout the entire descent by using the law of conservation of energy: Time and Energy Managed Operations. This chapter discusses the design of this new concept and the various components that comprise the system such as the planning algorithm, guidance and spacing techniques. Two design options that have been developed are discussed as well.

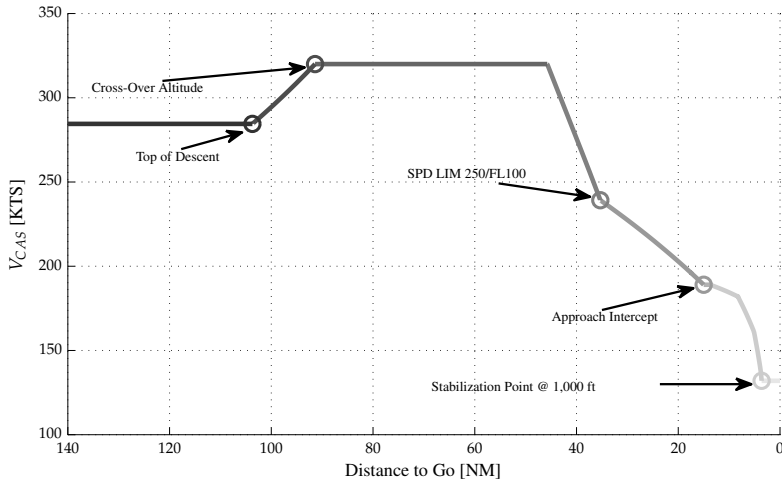


FIGURE 2-1: A nominal TEMO calibrated airspeed profile (CAS vs. Distance to Go) indicating TEMO characteristic phase transitions. The trajectory shows the phases from Top of Descent (≈ 105 NM) to the runway threshold (0 NM).

2-1 Time and Energy Managed Operations: Concept of Operations

Time and Energy Managed Operations (TEMO) is a new Continuous Descent Operations (CDO) concept that minimizes fuel use, gaseous and noise emissions whilst conforming to absolute or relative time constraints imposed by Air Traffic Control (ATC). The TEMO system enhances the current vertical guidance of the aircraft using an optimization algorithm to calculate *energy-neutral* trajectories and an improved guidance function. An energy-neutral trajectory requires only engine idle thrust and uses no additional drag devices during descent from Top of Descent (ToD) to the stabilization point at 1,000 ft above ground level. At the stabilization point the aircraft is stabilized, configured and ready for landing following a precision approach. To improve predictability, the calculated trajectories adhere to the definition of a closed-path trajectory as defined by ICAO [1].

The TEMO concept uses the principles of energy exchange to control the aircraft to a given point in space and time. The trajectory consists of a nominal airspeed profile, see Figure 2-1, that complies with applicable speed constraints. This airspeed profile is similar at lower altitudes for all aircraft to achieve a stable and predictable arrival flow. To arrive earlier or later than originally planned, TEMO allows the aircraft to deviation from this nominal profile but only within prescribed speed margins. The speed profile is flown by the guidance system using Speed-on-Elevator (SOE) control and with thrust set to idle. This implies that the aircraft does not follow a fixed vertical profile and the actual flown vertical profile depends on aircraft characteristics and disturbances.

Due to disturbances, such as wind estimation errors, the aircraft could deviate from the planned trajectory in terms of time and energy (altitude and velocity). These deviations could be corrected instantaneously, using control-laws, resulting in a *tactical* approach. Another method is a *strategic* approach that allows small deviations from the planned trajectory and calculates a new trajectory when these deviations exceed a predefined boundary.

The current time deviation is defined as the difference between the actual time and planned time at current position and is negative when the aircraft arrives too early and positive when the aircraft arrives too late. The energy deviation is defined as the difference between the actual energy state and planned energy state at the current position.

The trajectories are calculated by the novel TEMO algorithm that aims at finding an energy-neutral trajectory using *energy management*. Proper energy management allows an aircraft to exchange kinetic and potential energy, resulting in an energy-neutral trajectory, which implies that no additional energy is added or dissipated. However, situations could occur where the TEMO algorithm cannot find a trajectory without using thrust or drag devices. In these cases, the algorithm minimizes thrust and drag device use resulting in an *energy-optimal* trajectory. In extreme cases, the TEMO algorithm is unable to find a valid trajectory that satisfies all constraints, which is referred to as a *reject*. In these cases, pilots notify ATC to negotiate new constraints, new route or revert to a vector-based arrival. The TEMO algorithm could, theoretically, include other parameters in the cost function such as noise, fuel use and emissions.

TEMO is 4D capable by using time constraints. This constraint can be an absolute time constraint, using a Controlled-Time of Arrival (CTA), at a location along the trajectory [2], or a relative time interval to a leading aircraft using Interval Management (IM) [3]. The time constraints commanded by ATC include a Required Time Performance (RTP) which prescribes the time accuracy that the aircraft is required to meet at constrained locations for at least 95% of all operations. During hours of low-demand, the RTP can be less restrictive and set to a high value to achieve more environmentally friendly descents, whereas during hours of high-demand, the RTP can be set to a low value to ensure tight inter-aircraft spacing accuracy to satisfy runway throughput requirements.

TEMO uses an automated optimization algorithm and enhanced Trajectory Predictor (TP) to quickly and repeatedly calculate trajectories with high precision. To reduce uncertainty caused by variations in pilot responses during execution of the descent, the descent is flown using the autopilot and the aircraft cockpit displays are enhanced to support pilots in flying TEMO descents.

The TEMO concept is developed and evaluated for the Airbus A320 aircraft. However, TEMO should be adapted to allow CDOs with other modern, commercial aircraft in the future.

2-1-1 Energy Management

At cruise level, an aircraft flies high and maintains a high speed while prior to touchdown, the aircraft flies low and slowly. Both situations can be expressed using *energy* (see Appendix A) which is defined as the capacity of a system to do *work*. Work is defined as a

force acting on an object, or system, that causes movement of this object. The total energy, E_{tot} , is the sum of potential energy (altitude) and kinetic energy (velocity), given by:

$$E_{tot} = mgh + \frac{1}{2}mV^2 \quad 2-1$$

In this equation m is the aircraft mass, g the gravitational acceleration, h the altitude with respect to sea-level and V the true airspeed. Hence, energy is considered with respect to the moving air around the aircraft.

The law of conservation of energy prescribes that the level of total energy in a closed system remains constant over time. Hence, energy cannot be destroyed or created but can change form or location within the system. Regarding the aircraft as a closed system, the total energy level can be adjusted by applying external forces. External forces acting on an aircraft are for example the engine thrust, which transforms chemical energy into kinetic energy, and drag forces through heat transfer.

The external forces working on an aircraft in longitudinal direction are engine thrust, T , and aerodynamics drag, D . By assuming that these forces act along the flight-path, the difference between these forces and the true airspeed form the energy rate of change, i.e.,

$$\dot{E}_{tot} = V(T - D) \quad 2-2$$

This equation can also be derived by considering the aircraft longitudinal equation of motion:

$$m \frac{dV}{dt} = T - D + mg \sin \gamma_a \quad 2-3$$

where γ_a is the aerodynamic flight-path angle. By differentiating Eq. (2-1) and rearranging and inserting Eq. (2-3), the energy rate of change (Eq. (2-2)) is obtained.

A popular analogy for the principles of energy exchange is a roller coaster ride. A winch pulls the roller coaster cart to the top of the track, resulting in an increase of potential energy by adding energy to the cart in the form of work. Once the winch rests and the cart is released, the design of the track prescribes the potential energy profile of the cart and consequently the kinetic energy profile. Throughout the ride, no additional energy is added and friction and drag forces perform work and dissipate energy to put the cart to a stop at the end of the ride.

The roller coaster analogy can also be applied to an aircraft. An aircraft performs energy exchange through the elevator by directly controlling the altitude of the aircraft, while aerodynamic forces dissipate energy to reduce the total energy level. When the minimum maneuvering speed of the aircraft in the current configuration is nearly reached, flaps are used to remain airborne and decelerate further until the aircraft reaches a fully configured configuration to land the aircraft at a low speed.

Using energy management, the TEMO algorithm can select different energy strategies to correct disturbances or satisfy (updated) ATC constraints. For example, when the aircraft is estimated to arrive late with respect to the time constraint, it can gain speed by pitching down, resulting in a decrease of potential energy and equal increase of kinetic energy [4].

This process of exchanging energy is referred to as energy management. A parameter which prescribes the balance of potential and kinetic energy rate is the *energy share factor*, k see Appendix A. The goal of TEMO is to use energy management to correct deviations and only use thrust or speedbrakes if energy management alone does not suffice.

During the descent, an aircraft reduces its high energy state to a lower energy state at the runway threshold. Energy is reduced when Eq. (2-2) is negative and, as a result, the drag force should be larger than the thrust force. Thus, theoretically, during descent the aircraft requires no thrust to descent when the energy state is reduced in a controlled manner. However, for safety reasons, the engines are set to idle and to assure that the aircraft remains airborne and respects operational speeds, a speed profile is commanded that adheres to these operating limitations.

With the engines set to idle, the amount of fuel consumption during descent is minimized. Consequently, the engines generate less noise, reducing the experienced noise levels on the ground. With the engines set to idle and no additional use of drag devices (flaps, speedbrakes, etc.), the aircraft can only adjust its airspeed profile through energy management and reduce the total energy level simultaneously through drag dissipation, see Eq. (2-2). In other words, if the aircraft requires a higher velocity, the aircraft will have to descend.

2-1-2 Speed Profile

To stabilize the flow of arriving aircraft below FL 100, a nominal calibrated airspeed profile is defined which most modern commercial aircraft are capable of flying by using typical speeds during descent and approach, as seen in Figure 2-1. This nominal Calibrated Airspeed profile is primarily based on today's operating procedures [5] of an Airbus A320. Above FL 100, typical Mach and CAS descent speeds are flown. The definition of the various phases are summarized in Table 2-1.

The speed profile serves as an initial profile to provide a continuous descending and engine-idle descent to the runway. To gain or loose time, the aircraft is allowed to deviate from this nominal speed profile. The maximum allowed speed deviation depends on the phase of the aircraft and ranges between ≈ 10 KCAS and ≈ 50 KCAS. These speed limits respect aircraft operational limits and anticipates airborne spacing to create a stable flow of arriving aircraft. Furthermore, the trajectory definition does not allow climbing segments. This assures a relatively high vertical trajectory compared to current-day, step-down approaches, and reduces the noise exposure at ground level and provides a consistent trajectory to both pilots and ATC.

The initial descent, starts at ToD with a phase where the aircraft flies a constant Mach number until it reaches the crossover altitude where it starts to fly a constant Calibrated Airspeed (CAS) speed. When an aircraft descends while flying a constant Mach number, the True Airspeed (TAS) and CAS increase. Once the CAS equals the planned CAS descent speed, the aircraft continuous descending using this constant CAS speed. As the aircraft is descending simultaneously, the aircraft's TAS will reduce due to the increase of air density at lower altitudes.

TABLE 2-1: Definition of flight phases in TEMO concept.

Phase	Name	Phase entry-trigger	Path Constraint(s)	Operational Constraints
0	Cruise	Start of Run	$\dot{M} = 0$	$M_{green\ dot} \leq M \leq M_{MO}$
1	Mach	Descent Top of Descent	$\dot{M} = 0$	$M_{green\ dot} \leq M \leq M_{MO}$
2	CAS	Crossover Altitude	$\dot{V}_{CAS} = 0$	$V_{green\ dot} \leq V_{CAS} \leq V_{MO}$
3	Fast Deceleration		$\dot{k} = 0$	$230 \leq V_{CAS} \leq V_{MO}$
4	Slow Deceleration	FL 100	$\dot{V}_{CAS} = 0$	$V_{Flaps\ 1} < V_{CAS} \leq 250$
5	Approach	Localizer Intercept	$\dot{V}_{CAS} = 0$	
6	Decelerate on ILS	Glideslope Intercept	$\dot{V}_{CAS} < 0$	
7	ILS-stabilized	1,000 ft, $V_{CAS} = FAS$	$\dot{\gamma}_a = 0, \dot{V}_{CAS} = 0$	

The next constraint in the speed profile is based on the common speed restriction of not exceeding 250 KIAS/KCAS below FL 100 [6, 7]. The TEMO algorithm will calculate the start of this decelerating segment by calculating a constant energy share factor, k , that allows a fast deceleration to the nominal approach speed of 240 KCAS at FL 100. This constraint is 10 KCAS below the restriction of 250 KCAS to allow for some control space when the aircraft has to gain speed in order to arrive earlier. By decelerating rapidly, the average speed of the aircraft is relatively high which allows for shorter arrivals and increased throughput.

Once the approach speed is reached, the aircraft pitches up to maintain the approach speed approximately 15 NM from the runway threshold. At a certain point located prior to Instrument Landing System (ILS) intercept, the aircraft will decelerate to the nominal localizer intercept speed of 190 KCAS. Again, a margin of 10 KCAS is used to allow a maximum localizer intercept speed of 200 KCAS. During this deceleration phase, the first flap configuration will be selected as the aircraft will decelerate below its typical minimum maneuvering speed for clean configuration.

The aircraft intercepts the localizer at this constant speed. Once the aircraft is established on the localizer, it will decelerate further and intercept the glideslope. This will often lead to a relatively late selection of the second flap configuration compared to current operations. While on the glideslope, the speed will continuously decrease as the engines remain idle and increased drag due to flap selection and gear deployment.

While on the glideslope, the aircraft will reach a point where gear will be selected and later the third and fourth flap configurations. Gear deployment does not depend on the aircraft altitude but is defined on a speed in the middle of the second and third flap selection speeds. This assures that flap and gear selection will never occur at the exact same time.

Selection of the fourth configuration occurs just before descending through 1,000 ft at which the aircraft shall be fully configured, stable and engines set to maintain Final Approach Speed (FAS). The last segment is flown as a stabilized approach [8] where the aircraft continues the descent along the ILS and passes the runway threshold at an altitude of approximately 50 ft. To ensure a stable final approach and landing, TEMO is disabled during this final flight phase and hence no corrective actions will occur. The full nominal speed profile is shown in Figure 2-1.

The speeds at which configuration changes (flaps and gear) shall be performed are fixed

and based on the minimum maneuvering airspeed of the current configuration and depend on the current aircraft weight. Selection of the landing gear is defined as the midpoint between the second and third flap configuration. These fixed speeds provide a consistent cue for the pilot to perform configuration changes as opposed to several other CDO concepts [9, 10] where flap selections were performed at varying speeds to control the aircraft's deceleration. Once a configuration has been selected, the TEMO system will not command the pilot to retract that configuration.

2-1-3 Time Management

To improve predictability and to reduce inter-arrival time of arrival aircraft, TEMO uses time management. Time management can be categorized as absolute time management or relative time management. The TEMO implementations used in this thesis all use absolute time management using CTAs. By consecutively assigning a CTA at the Initial Approach Fix (IAF) and runway threshold, ATC has two control points for flow management and arrival spacing.

Prior to ToD, ATC provides aircraft that fly a TEMO descent with a CTA at the IAF. This CTA is used by ATC to *control* spacing of arriving aircraft from different directions and can be used as an initial measure to create a stable incoming flow of traffic. Onboard an aircraft, the CTA is used as a Required Time of Arrival (RTA) in the Flight Management System (FMS) as it represents a *required* constraint for the aircraft to adhere to.

Before the aircraft reaches the IAF — the aircraft is still expected to arrive at the IAF on time — ATC will command a CTA for the runway threshold to establish the final sequence of landing aircraft. As soon as this new CTA is entered into the FMS, the previous RTA is deleted as the aircraft is no longer required to satisfy this constraint. Therefore, TEMO only includes the new time constraint at the runway threshold. For this reason, an aircraft might not arrive exactly at the previously assigned CTA at the IAF when the new trajectory that includes the CTA at the runway threshold commands the aircraft to deviate from the old trajectory in order to satisfy the new CTA at the runway threshold.

The TEMO algorithm calculates earliest and latest Estimated-Time of Arrivals (ETAs) at the active time-constrained waypoint and broadcasts these ETAs to ATC through Automatic Dependent Surveillance - Broadcast (ADS-B). These ETAs provide ATC with information for sequencing and spacing of aircraft.

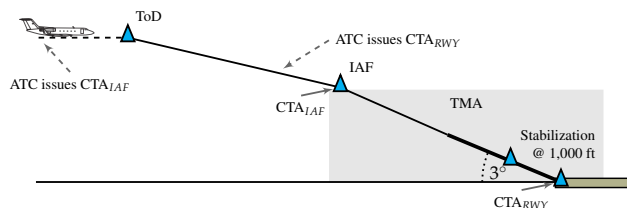


FIGURE 2-2: Absolute time management using a CTA at the IAF and runway threshold.

The CTA clearance at the IAF and at the runway threshold consists of a specific absolute time and RTP, that prescribes the required time accuracy of the CTA. The actual value of the RTP is defined by ATC and can be set to a value to meet ATC demands. During hours of low demand, the RTP can be increased to achieve more environmental benefits whereas during hours of high demand, the RTP can be set to a lower value to ensure high runway throughput at the cost of additional thrust or drag devices use.

In this concept, the time deviation at the constrained waypoints should remain within the RTP in order to satisfy the time constraint. The values of the RTP require a higher accuracy than the values defined in the current Required Navigation Performance (RNP) Specification [11]. Furthermore, the Initial 4D Concept [12–14] of Single European Sky ATM Research (SESAR), which is supported by the 4D Navigation Working Group EURO-CAE WG-85 / RTCA SC-227, requires an RTA tolerance of 30 seconds in en-route airspace and 10 seconds within the Terminal Maneuvering Area (TMA) [12–14] for 95% of all operations. The initial values for the RTP at the constrained waypoints in the TEMO experiments require stricter accuracies such that both near-term time tolerances can be easily met and future, mid-term, stricter tolerances will be within the capabilities of TEMO.

Relative time management can be applied using IM, where an aircraft spaces in time with respect to an aircraft ahead of the own aircraft, referred to as the lead aircraft. This lead aircraft broadcasts its own ETA at a metering point, using ADS-B, and ATC commands the own aircraft to achieve spacing with a time interval at that metering point from the lead aircraft. The own 'required' arrival time is computed using the ETA of the lead aircraft and time interval from ATC. These principles are shown in Figure 2-3. Relative time management could increase inter-arrival time which will increase runway throughput and provides a more stable arrival stream [2, 15].

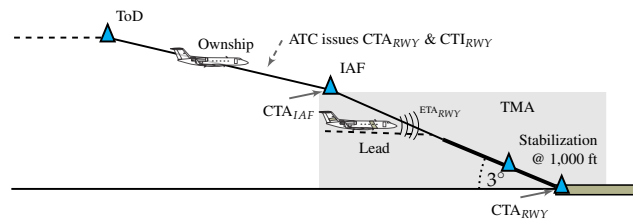


FIGURE 2-3: Relative time management within the TMA once ADS-B message received successfully from Lead aircraft.

Relative time spacing can be applied in the TMA where the distance between the lead and own aircraft is sufficiently small such that ADS-B broadcasts can be received. Aircraft on a TEMO descent will initially fly towards the IAF using a CTA for initial spacing. Before reaching the TMA, aircraft receive clearance from ATC to space behind the lead aircraft using a time interval. This ATC clearance also includes a CTA at the runway threshold which is active while no ADS-B information from the lead aircraft is received. When the aircraft successfully receives ADS-B information from the lead aircraft, it will transition from absolute spacing to relative spacing.

In this concept, the time deviation is calculated as the difference between the own ETA and the lead aircraft ETA with time interval added. The goal of this concept is to reduce the deviation to within the RTP such that spacing remains within the time interval.

The work described in this thesis uses absolute time spacing only with typical values for the RTP as shown in Table 2-2. An implementation of relative time spacing in the TMA while flying a TEMO approach will be investigated in a later experiment of the Clean Sky Project.

2-2 Replanning and Guidance

The TEMO algorithm generates an initial trajectory based on aircraft dynamics, assigned CTA, nominal speed profile and current position. This plan is stored in the FMS as the *current plan*. From this current plan the calibrated airspeed at a given distance from runway threshold is derived and fed to the guidance system and autopilot, which uses SOE to control calibrated airspeed. Once the TEMO system detects time and/or energy deviations, TEMO uses replanning to correct the deviations.

The next subsections describe two different implementations of replanning: *strategic* replanning and *tactical* replanning. Strategic replanning allows small time and energy deviations and replans only when these deviations exceed a preset boundary. Alternatively, tactical replanning continuously corrects a detected deviation using a control system. As such, strategic replanning can be considered as an open-loop control system (or slow, closed-loop system) whereas tactical replanning performs as a closed-loop control system. Furthermore, strategic replanning takes the entire trajectory into account when correcting deviations through replanning and optimizes the location of corrective actions, whereas tactical replanning takes immediate action at the location of the detected deviation, which might not be optimal.

2-2-1 Strategic Replanning

TEMO can use strategic replanning to meet the environmental and time goals of CDOs. During strategic replanning, the FMS monitors the aircraft time progress and energy state at the current position and compares this with the planned state to detect deviations. When a deviation exceeds an allowable, predefined boundary, a new trajectory will be calculated by the TEMO algorithm to correct the deviation. This process of calculating a new trajectory is referred to as strategic replanning. A schematic overview of strategic replanning is found in Figure 2-4.

The boundaries are defined as a positive and negative value at ToD, the IAF and runway threshold. The boundaries are linearly interpolated between these locations and reduce in value as the control space reduces while the aircraft approaches the time constrained waypoint. Typical values for these boundaries and the RTP values used in the human-in-the-loop experiment are found in Table 2-2. The time boundary is expressed in seconds whereas the energy boundary is expressed in specific energy, or energy height, by dividing

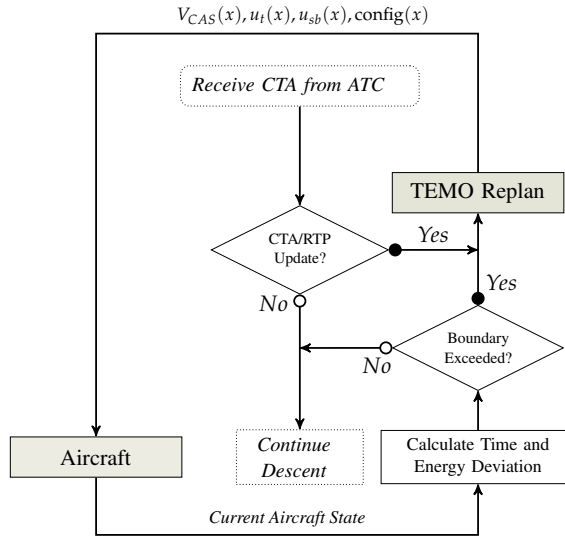


FIGURE 2-4: Schematic overview of strategic replanning.

Eq. (2-1) by the weight (mg) of the aircraft. Energy height does not represent a ‘physical’ altitude but is the altitude the aircraft would, theoretically, reach if all kinetic energy would be transformed to potential energy in a climb.

TABLE 2-2: TEMO deviation boundaries and Required Time Performance (RTP).

Active CTA	RTP [s]	Deviation Boundary					
		Top of Descent		IAF		Runway Threshold	
		Time [s]	Energy [ft]	Time [s]	Energy [ft]	Time [s]	Energy [ft]
IAF	5	± 10	± 400	± 5	± 200	-	-
Runway	2	-	-	± 4	± 200	± 2	± 100

As the final segment of a TEMO descent is flown on the ILS, the energy boundary merely represents a speed boundary of $\approx 10\text{KCAS}$ as the altitude is fixed to the glideslope descent path. Moreover, from the stabilization point at 1,000 ft, the aircraft maintains its FAS and TEMO replanning is disabled to maintain a stable descent.

The boundaries are set such that strategic replanning does not take immediate action when a (small) deviation is detected. This allows a deviation to evolve in time which could also mean that the deviation reduces to zero or change sign. For example, the aircraft could estimate to arrive a little early due to an unforeseen tailwind. However, due to 180° turn later in the trajectory, this same wind could lead to a headwind which could restore the estimated arrival time. These boundaries thus prevent instantaneous actions to present a stable descent to the cockpit crew.

The FMS uses a simplified aircraft performance model such as lift and drag characteristics, aircraft and engine dynamics and aircraft mass, hence, modeling errors [16, 17] during

TABLE 2-3: Definition of flight phases in initial TEMO algorithm.

Phase	Name	Phase entry-trigger	Configuration	Path Constraint(s)	Operational Constraints
0	Cruise	Start of Run	Clean	$\dot{M} = 0$	$M_0 \leq M \leq M_{MO}$
1	Mach	Top of Descent	Clean	$\dot{M} = 0$	$M_0 \leq M \leq M_{MO}$
2	CAS	Crossover Altitude	Clean	$\dot{V}_{CAS} = 0$	$V_0 \leq V_{CAS} \leq V_{MO}$
3	CAS		Clean	$\dot{V}_{CAS} = 0$	$V_0 \leq V_{CAS} \leq V_{MO}$
4	Fast Deceleration		Clean	$\dot{k} = 0$	$230 \leq V_{CAS} \leq V_{MO}$
5	Slow Deceleration	FL 100	Clean	$\dot{V}_{CAS} = 0$	$V_{F1} < V_{CAS} \leq 250$
6	Slow Deceleration	V_{F1}	F1	$\dot{V}_{CAS} = 0$	$V_{F2} < V_{CAS} \leq V_{F1}$
7	Approach	V_{LOC} , 15 NM	F1	$\dot{V}_{CAS} = 0$	$V_{F2} < V_{CAS} \leq V_{F1}$
8	Approach	Glideslope intercept	F1	$\dot{\gamma}_a = 0, \dot{V}_{CAS} < 0$	$V_{F2} < V_{CAS} \leq V_{F1}$
9	Decelerate on ILS	V_{F2}	F2	$\dot{\gamma}_a = 0, \dot{V}_{CAS} < 0$	$V_G < V_{CAS} \leq V_{F2}$
10	Decelerate on ILS	V_G	F2 & Gear	$\dot{\gamma}_a = 0, \dot{V}_{CAS} < 0$	$V_{F3} < V_{CAS} \leq V_G$
11	Decelerate on ILS	V_{F3}	F3 & Gear	$\dot{\gamma}_a = 0, \dot{V}_{CAS} < 0$	$V_{F4} < V_{CAS} \leq V_{F3}$
12	Decelerate on ILS	V_{F4}	F4 & Gear	$\dot{\gamma}_a = 0, \dot{V}_{CAS} < 0$	$V_{FAS} < V_{CAS} \leq V_{F4}$
13	Final Approach	1,000 ft, $V_{CAS} = FAS$	F4 & Gear	$\dot{\gamma}_a = 0, \dot{V}_{CAS} = 0$	$V_{CAS} = V_{FAS}$

aircraft trajectory prediction could cause the aircraft to arrive at a different time or energy state than originally planned. These modeling errors could be minimized by using a perfect aircraft model, if available. However, such a model would introduce additional complexity and hence increase calculation times significantly. Other sources of trajectory prediction errors are inaccurate wind estimates [9, 10, 18–20] or erroneous sensor measurements [21].

If the deviation or time update is too large to satisfy all constraints, the algorithm calculates an energy-optimal trajectory that uses minimized amounts of thrust and drag devices. However, situations could occur that an energy-optimal solution cannot be achieved as well, resulting in a replan being rejected. This can be due to the definition of a TEMO descent or too limiting constraints. In these cases, pilots will notify ATC that an optimized descent is not feasible whilst satisfying all active constraints and negotiate new constraints, new route or revert to a vector-based arrival.

The first implementation of the TEMO algorithm was developed in MATLAB and is based on the optimal control toolbox General Pseudospectral Optimal Control Software (GPOPS) [22, 23]. To improve calculation times, the revised version of the algorithm was developed in C/C++ and FORTRAN using the open source software package PSOPT [24].

Replanning using GPOPS

The TEMO algorithm calculates optimized speed profiles that satisfy ATC constraints and meet an absolute time constraint at a waypoint. A typical example that indicates the different flight phases and velocity strategies is shown in Figure 2-5. In this figure, the outer dashed-lines represent the airspeed limits that are set as operational constraints as listed in Table 2-3. The corresponding vertical profile is shown in Figure 2-6. A baseline scenario consisting of conventional, step-down approach is also shown in Figure 2-6.

The objective of TEMO is to minimize the use of thrust and speedbrakes whilst adhering to aircraft, operational, and time constraints. This is formulated as an optimal control problem using an objective function given by:

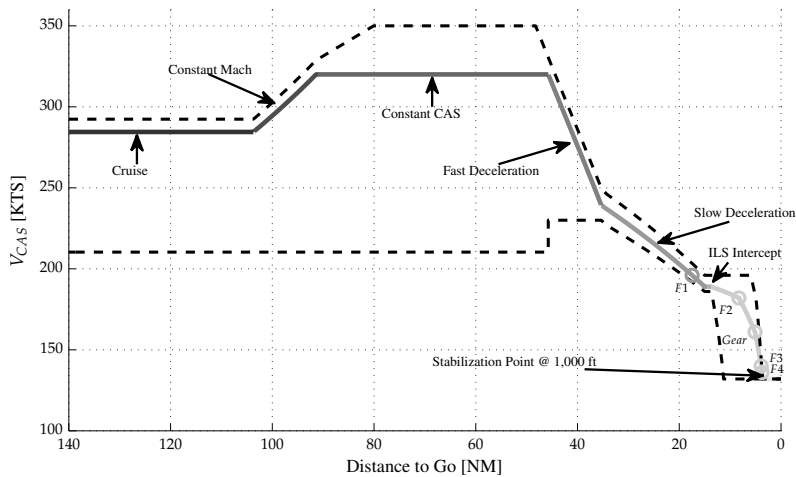


FIGURE 2-5: A typical TEMO calibrated airspeed profile (CAS vs. Distance to Go) indicating the different flight phases from Top of Descent (~105 NM) to the runway threshold (0 NM). Included are the operational velocity boundaries (dashed lines).

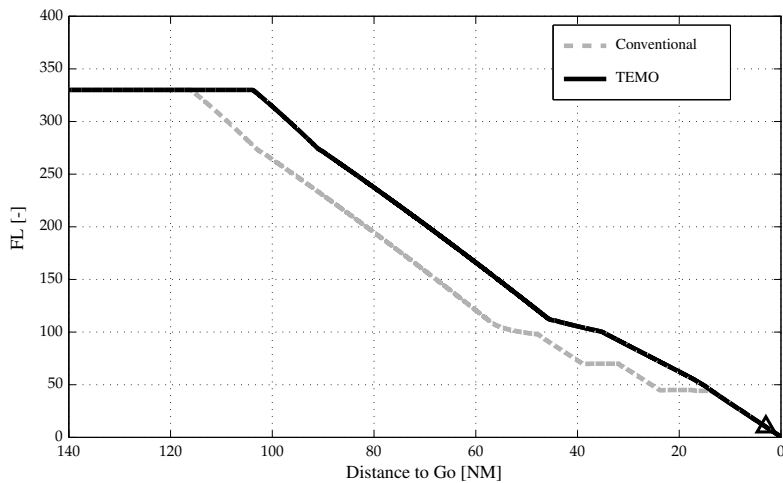


FIGURE 2-6: Vertical profiles for TEMO and conventional descent and approach.

$$J = \int_{t_{now}}^{t_f} [K_{THR}u(t)_{THR}]^2 + [K_{SB}u(t)_{SB}]^2 dt \quad 2-4$$

The objective function is defined as a *minimum control problem*, with K_{THR} and K_{SB} the scaling parameters for the throttle, $u(t)_{THR}$ and speedbrake control, $u(t)_{SB}$.

The optimal control problem is subject to the dynamic constraints:

$$\begin{aligned} \dot{V} &= g \left[\frac{T(V, h, u_{THR}) - D(V, h, u_{SB}, config)}{mg} - \sin \gamma_a \right] \\ \dot{x} &= V \cos \gamma_a \\ \dot{h} &= V \sin \gamma_a \\ \dot{m} &= -ff(V, h, u_{THR}) \end{aligned} \quad 2-5$$

In Eq. (2-5), the engine thrust, T , depends on true airspeed, altitude and throttle position, while the aircraft drag, D , depends on true airspeed, altitude, speedbrakes and aircraft configuration, i.e., flaps and gear. The aircraft mass, m , decreases with fuel-flow, ff , which is a function of airspeed, altitude and throttle position. The aircraft's vertical motion is described by the flight-path angle relative to the air, γ_a .

A time constraint at the IAF — located 50 NM from the runway — is included in the optimization problem as one of the following boundary conditions:

$$\begin{aligned} t(x_{IAF}) &= CTA_{IAF} + \Delta t \\ t(x_{RWY}) &= \text{free} \end{aligned} \quad 2-6$$

The time constraint at the IAF is defined by the combination of the inserted CTA and a Δt . This Δt defines a time window during which the trajectory should pass the IAF and is set to four seconds. By allowing a time window, the algorithm gains additional control space to find an energy-neutral trajectory that satisfies the CTA and RTP. In contrast, setting this margin to zero, could yield an energy-optimal trajectory that exactly satisfies the CTA. The one second time difference between the RTP and Δt is reserved for unanticipated deviations. Through this time-constrained window, time accuracy is reduced in favor of a more environmental trajectory.

The arrival time at the runway is free in this initial implementation of the TEMO algorithm. This implies that a time deviation within the TMA will not be corrected using a TEMO replan.

The optimal control problem is also subject to the operational path constraints listed in Table 2-3. Moreover, configuration changes, such as flaps and gear deployment, are based on the A320 minimum maneuvering airspeed [25] of the preceding configuration as listed in Table 2-4 or FAS. The minimum maneuvering airspeed depends on the current aircraft weight while any dependency on speedbrakes is neglected.

The optimal control problem defined by Eq. (2-4) is solved by the TEMO algorithm using General Pseudospectral Optimal Control Software (GPOPS) [22, 23]¹. GPOPS approximates the state and control of the optimal control problem through discretization of continuous time using collocation. This reduces the optimal control problem into a finite set

¹GPOPS is freely available for academic purposes and can be obtained from <http://www.gpops.org/>

TABLE 2-4: TEMO configuration change speeds in GPOPS.

Configuration	F1	F2	Gear	F3	F4
TEMO Speed	V_{F1}	V_{F2}	V_G	V_{F3}	V_{F4}
Definition	V_0	V_S	$\frac{V_S + V_F}{2}$	V_F	$\frac{V_{APP} + V_F}{2}$

of algebraic equations. GPOPS uses the *hp*-adaptive Radau pseudospectral method [26, 27] with collocation points at the Legendre-Gauss-Radau points [28] and allows for mesh refinement. The toolbox also allows automatic scaling of the optimization problem, and GPOPS translates the high-level optimal control problem to the input definitions required by the Nonlinear Program (NLP) optimizer SNOPT [29]. First and second order derivatives of all equations in the optimization problem can be computed using numerical, complex-step [30], analytical and automatic differentiation [31] techniques. From these differentiation methods, automatic differentiation using a third-party software package INTLAB [32] provided the fastest and most accurate results with minimum user effort and flexibility.

As a TEMO replan require time to calculate a full trajectory, the aircraft location, time and energy state is predicted and used as initial position of the replan. The location of this predicted point is located between 15 and 30 seconds ahead of the current position along the active plan depending on the distance relative to the runway. During the calculation process, the aircraft will continue flying the active plan and intercept the new trajectory at the initial position of the new trajectory.

Replanning to correct a time deviation is disabled when the aircraft is close to a time-constrained waypoint as the initial position will be located too close to the constrained waypoint resulting in a limited space to resolve the time deviation. In real-life operations, this should not occur as ATC would have commanded a new CTA at the runway threshold way ahead of the TMA entry.

Once the aircraft is established on the localizer and close to intercepting the glideslope, replan calculation times are extremely long and often did not yield valid trajectories as energy exchange is not possible on the glideslope. Moreover, while intercepting the glideslope – transitioning from SOE to Path-on-Elevator (POE) — the autopilot could command thrust or speedbrakes to correct altitude deviations whilst maintaining the TEMO commanded speed. Therefore, replanning is not used to correct deviations after intercepting the localizer as this could counteract the glideslope intercept and often does not obtain a valid result. Consequently, the time and energy boundaries are deactivated at the localizer intercept. Unfortunately, the autopilot corrections to intercept the glideslope correct the energy deviation but can also introduce undesired time deviations. However, these time deviations can be neglected since no CTA is active at the runway threshold.

The phases in Table 2-3 prescribe strict path constraints that, for example, do not permit the aircraft to accelerate or decelerate with respect to their Mach number or CAS descent throughout phase 1 and 2 respectively. Consequently, this means that a newly calculated trajectory could require an instantaneous speed change at the initial position of this new tra-

jectory². Unfortunately, this instantaneous speed change cannot be followed by an autopilot causing the aircraft to deviate substantially from the commanded speed profile which will result in a new time deviation. So, in stead of correcting deviations, a replan could thus introduce deviations.

To overcome this issue, a *transition* phase is inserted in the speed profile that provides a gentle transition from the initial position of the new trajectory to the next phase the aircraft will enter according to the definition of the speed profile. The boundaries of the transition phase are similar to the values of the current phase but the transition phase has no path constraints in order to allow accelerations or decelerations. To assure that the transition phase does not extend to the entire trajectory, the maximum duration of this phase is set to 20 seconds.

Replanning using PSOPT

The initial implementation of replanning used MATLAB and required a minimum of 30 seconds to successfully calculate a new trajectory. For the human-in-the-loop experiment, discussed in Chapter 4, a faster calculation routine was required and TEMO had to be included in existing experimental FMS software.

Therefore, a new and improved implementation of the algorithm was developed [33] in C++ using PSOPT [24]. PSOPT³ is a state-of-the-art, open-source package that uses direct collocation methods, such as local and pseudospectral discretization to approximate optimal control problems. PSOPT uses Legendre or Chebyshev polynomials for global discretization using pseudospectral methods and trapezoidal and Hermite-Simpson transcriptions for local discretization methods.

The new TEMO algorithm uses PSOPT's automatic scaling, IPOPT [34] optimizer, and a trapezoidal collocation method for discretization. To calculate first and second order derivatives, PSOPT uses ADOL-C [35], a C/C++ package that allows automatic differentiation.

The definition of phases in the new algorithm has been revised to reduce the complexity of the optimization problem, see Table 2-5. Several phases use minimum and maximum speeds as defined by $V_{LOC}^- = \max(V_{F2} + 2, V_0 - 10)$, $V_{LOC}^+ = V_0 - 2$, and $V_{LOC} = \frac{V_{F1} + V_{F2}}{2}$. In these equations, V_0 is the green-dot speed and V_{F1} and V_{F2} the maneuvering speeds for Flaps 1 and Flaps 2, receptively. The resulting calibrated airspeed profile for a typical descent starting at FL 250 and hence without a constant Mach phase is shown in Figure 2-7.

In addition to the phases defined in Table 2-5, a transition phase is implemented to allow for a gradual speed change between the initial position of the new trajectory and the first, path-constrained phase. This transition phase is implemented similar to the implementation in GPOPS.

The results from the batch study showed that calculating new trajectories while close to

²True airspeed is not restricted to be constant at the predicted initial position as this would prevent the aircraft from adjusting airspeed in this 'free' phase.

³PSOPT is freely available under the GNU Lesser GPL v2.1 from <http://www.psopt.org/>

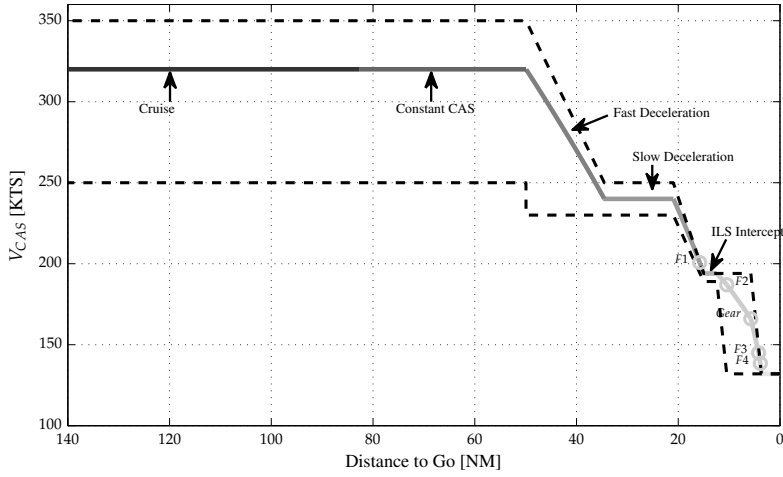


FIGURE 2-7: A calibrated airspeed profile (CAS vs. Distance to Go) calculated using PSOPT indicating the different flight phases from Top of Descent (≈ 83 NM) to the runway threshold (0 NM). Included are the operational velocity boundaries (dot-dashed lines).

and on the glideslope required extensive calculation times due to the limited control space when established on the glideslope. In this segment, the aircraft cannot use energy exchange and can only use thrust or speedbrakes to control the aircraft speed. For these reasons, phases 8–13 (Table 2-5) are not included in the optimization algorithm. Consequently, the TEMO algorithm only optimizes the trajectory from ToD (or current position) down to the glideslope intercept point and uses a predefined trajectory and speed profile from glideslope intercept to the runway. As a result, any disturbance that occurs whilst transitioning towards and descending on the glideslope will not be corrected for using replanning nor will the TEMO algorithm command additional thrust or speedbrake use while the aircraft descends down the glideslope. This last limitation differs from the GPOPS implementation where the TEMO algorithm could command additional thrust or speedbrakes in these phases.

The objective of TEMO is to minimize thrust and speedbrakes whilst complying with aircraft, operational, and time constraints, and is formulated as a *minimum control problem* with the objective function given by:

$$J = \int_{t_{now}}^{t_f} [K_{th} u_{\widehat{N1}}(t)]^2 + u_{sb}^2(t) dt \quad 2-7$$

With $u(t)_{\widehat{N1}}$, the normalized engine fan speed, $\widehat{N1}$ control and, $u(t)_{sb}$, the speedbrake control. K_{THR} is a scaling parameter to balance throttle and speedbrake control.

To reduce complexity and further reduce calculation times, the aircraft mass has been removed as a state variable from the optimization problem and is considered being constant throughout the descent. This assumption can be easily justified as fuel consumption is rather

TABLE 2-5: Definition of flight phases in revised TEMO algorithm.

Phase	Name	Phase entry-trigger	Configuration	Path Constraint(s)	Operational Constraints
0	Cruise	Start of Run	Clean	$\dot{M} = 0, \dot{h} = 0$	$M_{250} \leq M \leq M_{MO}$
1	Mach	Top of Descent	Clean	$\dot{M} = 0$	$M_{250} \leq M \leq M_{MO}$
2	CAS	Crossover Altitude	Clean	$\dot{V}_{CAS} = 0$	$250 \leq V_{CAS} \leq V_{MO}$
3	Decelerate		Clean	$\dot{V}_{CAS} = 0$	$230 \leq V_{CAS} \leq V_{MO}$
4	Intermediate Speed	FL 100	Clean	$\dot{V}_{CAS} = 0$	$230 \leq V_{CAS} \leq 250$
5	Decelerate to F1	V_{F1}	Clean	$\dot{V}_{CAS} = 0$	$V_{F1} < V_{CAS} \leq 250$
6	Decelerate to LOC	V_{LOC}	F1	$\dot{V}_{CAS} = 0$	$V_{LOC} < V_{CAS} \leq 250$
7	LOC Intercept	15 NM from Runway	F1	$\dot{V}_{CAS} = 0$	$V_{LOC}^- \leq V_{CAS} \leq V_{LOC}^+$
8	Decelerate to F2/GS		F1	$\dot{V}_{CAS} = 0$	$V_{F2} < V_{CAS} \leq V_{LOC}^+$
9	Decelerate to Gear	V_{F2}	F2	$\dot{\gamma}_a = 0$	$V_G < V_{CAS} \leq V_{F2}$
10	Decelerate to F3 ^a	V_G	F2 & Gear	$\dot{\gamma}_a = 0$	$V_{F3} < V_{CAS} \leq V_G$
11	Decelerate to F4	V_{F3}	F3/F4 ^a & Gear	$\dot{\gamma}_a = 0$	$V_{F4} < V_{CAS} \leq V_{F3}$
12	Decelerate to 1,000ft	V_{F4}	F4 & Gear	$\dot{\gamma}_a = 0$	$V_{FAS} < V_{CAS} \leq V_{F4}$
13	Final Approach	1,000 ft	F4 & Gear	$\dot{\gamma}_a = 0, \dot{V}_{CAS} = 0$	$V_{CAS} = V_{FAS}$

^a To reduce the number of pilot actions, the HMI commands pilots to select Flaps 4 at the location of Flaps 3 since Flaps 4 succeeds Flaps 3 almost instantly at that particular deceleration rate.

low (less than 1% of Maximum Landing Weight (MLW)) when flying an idle approach [36]. Hence, the optimization problem is subject to the following dynamic constraints:

$$\begin{aligned}
 \dot{V} &= g \left[\frac{T(V, h, u_{\widehat{N1}}) - D(V, h, u_{sb}, config)}{mg} - \sin \gamma_a \right] \\
 \dot{x} &= V \cos \gamma_a \\
 \dot{h} &= V \sin \gamma_a
 \end{aligned}
 \tag{2-8}$$

Where in Eq. (2-8), thrust depends on true airspeed, altitude and the normalized fan speed, $\widehat{N1}$, and drag depends on true airspeed, altitude, speedbrakes and aircraft configuration, i.e., flaps and gear. The normalized fan speed ranges between idle and maximum thrust and is converted to the engine fan speed, $N1$ and fed to the auto-thrust system.

Also, the optimization problem is subject to the operational path constraints listed in Table 2-5. Moreover, configuration changes are based on the minimum maneuvering airspeed (see Table 2-4) incremented with an offset of 5 KCAS. This offset is added to the minimum maneuvering speed to prevent the auto-thrust system from applying thrust to avoid decelerating below the minimum maneuvering speed.

Finally, the PSOPT implementation can calculate trajectories that include a CTA at the IAF, runway threshold or at both points. Only one single time constraint is active and time deviation within the TMA will be corrected when the CTA at the runway threshold is active. The revised algorithm is required to calculate trajectories that satisfy the active CTA exactly to allow more maneuvering space for the autopilot. The optimization problem is thus subject to one of the following boundary conditions:

$$\begin{aligned}
 t(x_{IAF}) &= CTA_{IAF} \\
 t(x_{RWY}) &= CTA_{RWY}
 \end{aligned}
 \tag{2-9}$$

The revised algorithm could theoretically include both constraints simultaneously, however, the TEMO concept assumes only one active time constraint. Additional to trajectories

including these time constraints, the updated algorithm can calculate trajectories that include earliest and latest ETAs at the IAF and runway threshold. These earliest and latest arrival estimates are displayed in the Control and Display Unit (CDU) RTA page of the waypoint as an indication to the pilot of acceptable CTAs from ATC and are broadcast to ATC through ADS-B.

Similar to the implementation based on GPOPS, the revised algorithm predicts the aircraft states ahead of the current position along the active plan. Since PSOPT requires significantly less time to calculate a new trajectory, this location has been reduced from 30 seconds to 20 seconds. The maximum allowed computation time for the TEMO algorithm is set to 18 seconds to allow for a minimum buffer of 2 seconds between a successful replan and start of the new trajectory. By reducing this prediction location, the aircraft follows the old, *active* plan for a shorter duration such that deviations are corrected faster and have less time to accumulate. When the algorithm is finished, the FMS appends the new trajectory to the old trajectory at the location of the predicted location. Finally, no replan is started if this prediction location ahead is located behind the time-constrained waypoint.

The PSOPT implementation of TEMO only replans when the time or energy boundary remains out-of-bounds for at least 10 seconds, not to trigger a replan due to a temporary deviation caused by, for example, a sudden wind gust. Furthermore, replanning is disabled when the aircraft is close too a time-constrained waypoint or close to intercepting the glideslope since these last phases are not included in the optimization algorithm.

2-2-2 Tactical Replanning

Sustained deviations can also be minimized using a tactical control-law that adjusts the speed profile to minimize time and uses thrust or speedbrakes to maintain the vertical profile and updated speed profile. Using this tactical approach, the deviation boundaries are disabled and a (strategic) replan is only activated to correct large time deviations or a new CTA/Controlled-Time Interval (CTI) update. In case the tactical controller approaches aircraft operational limits, a strategic replan could be used to correct further deviations. This tactical implementation is likely to use more thrust and, hence, consume more fuel. For these reasons, this implementation has not been investigated as TEMO aims at minimizing fuel.

However, a hybrid solution corrects time and energy deviations using different replanning methods: time deviations are corrected using tactical replanning and energy deviation are corrected using strategic replanning, see Figure 2-8. Different from full strategic replanning, see Figure 2-4, the deviation boundaries are checked separately such that time deviations are reduced using a controller that commands calibrated airspeed changes [37]. These speed changes are flown using SOE resulting in an altitude deviation from the planned vertical trajectory as no additional thrust is used. When the altitude (or energy deviation) exceeds a boundary, the deviation is corrected using a TEMO strategic replan. The Continuous Descent Approach for Maximum Predictability (CDA-MP) [38–40], developed by Boeing Research and Technology Europe (BRTE), uses a similar, tactical approach by using a groundspeed control-law to reduce accumulated errors during an idle descent.

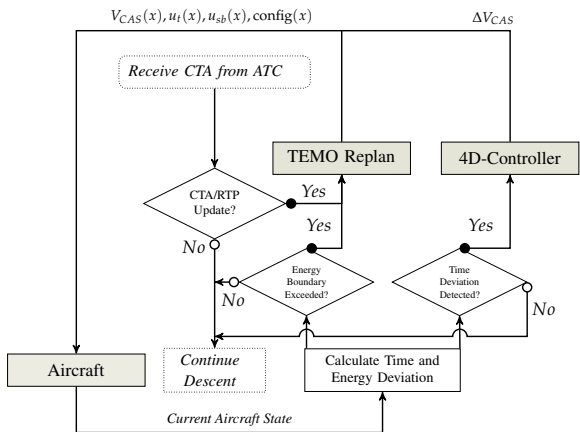



FIGURE 2-8: Schematic overview of hybrid replanning.

Using hybrid-replanning, the TEMO algorithm calculates an initial trajectory and corresponding speed profile. The TEMO guidance continuously calculates time and energy deviations separately and corrects time deviations using a novel, closed-loop, 4D-controller (Figure 2-8), developed by German Aerospace Center (DLR). The controller determines the time deviation and calculates a ΔV_{CAS} to reduce the time deviation using SOE control. The controller respects operational speed constraints and uses anti-windup to prevent controller saturation. Also, in case ATC issues a large time update, or the broadcast ETA from the lead aircraft differs significantly from previous broadcasts, TEMO uses strategic replanning to correct the time update and reinitialize the 4D-controller.

Because the controller continuously adjusts the speed profile, the actual altitude profile will deviate from the planned altitude profile through energy management as the aircraft uses the elevator to control speed. Hence, the controller actions result in a different energy strategy compared with the originally planned trajectory. Therefore, these altitude deviations and speed offsets could result in an energy deviation which is corrected using a replan.

2-3 Flight Operations

During cruise, pilots receive a descent clearance that includes a CTA for the IAF from ATC through data-link. Pilots review the clearance and insert the clearance information , such as Standard Arrival Route (STAR), runway, descent altitude, CTA and RTP into the FMS through CDU and Flight Control Unit (FCU). The CTA is now internally used by the FMS as a RTA. All pilot actions are depicted in Figure 2-9.

The data-link interface allows pilots to automatically load CTA information from the data-link window into the CDU, while the clearance altitude — typically FL 130 — is entered manually into the FCU. Using the clearance details, the TEMO algorithm optimizes the descent trajectory that complies with the received clearance. Once successful, the pilots

accept the clearance and notify ATC using data-link. Next, pilots prepare the autopilot and FMS to fly the calculated trajectory and perform the descent checklist.

10 NM prior to passing ToD, the aircraft warns the flight deck when auto-speedbrakes ^(SB) — a new TEMO-specific function that automatically deploys speedbrakes when demanded by TEMO — are not activated by displaying a Special Message on the Flight Mode Annunciator (FMA) of the Primary Flight Display (PFD). Once engaged, the FMA message disappears. At ToD, the aircraft automatically intercepts the descent trajectory similar to current Boeing aircraft and pilots monitor flight progress. By monitoring differences between commanded speed and actual speed, possible time deviations can be induced by the pilots.

Prior to reaching the TMA, ATC sends an updated clearance to descend to the runway containing routing information, lower descent altitude, QNH, and CTA and RTP at the runway threshold. Pilots, again, insert the new clearance details ^(C) into the FMS which removes the RTA information from the IAF and adjust the FCU altitude window. When the RTA_{RWY} is different from the current ETA_{RWY} , the TEMO algorithm will calculate a new trajectory to arrive on time.

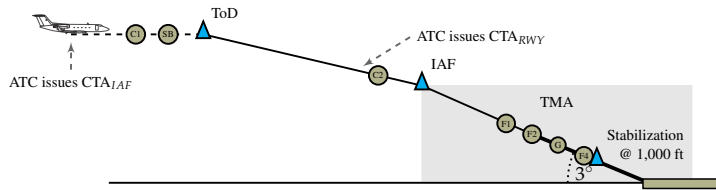


FIGURE 2-9: Overview of pilot actions during a TEMO descent.

Before intercepting the localizer, pilots set the first flap configuration ^(F1). After setting Flaps 1, the ILS display markers and QNH for descent are set and thereafter the localizer intercept mode is armed. At this stage, the aircraft decelerates slowly towards ILS approach speed and the pilots perform the approach checklist and set Flaps 2 when demanded by TEMO ^(F2). When Flaps 2 are fully deployed, the pilots select Approach mode on the FCU to intercept the glideslope. Once established on the ILS, the pilots engage the second autopilot to perform a full CAT III landing. From this point onwards, TEMO is automatically disengaged and does not calculate new trajectories to correct deviations resulting in an open-loop system.

The next pilot action is to lower the landing gear ^(G) to increase the deceleration performance and subsequently set the go-around altitude in the FCU window. Finally, Flaps 4 ^(F4) are selected prior to reaching FAS. Once Flaps 4 are fully deployed, the pilot arms the ground spoilers and performs the landing check-list.

In the PSOPT implementation, selection of Flaps 3 was skipped. Due to the rapid deceleration after selecting Flaps 3, the next flap selection (Flaps 4) succeeds instantly after selecting Flaps 3. To reduce the amount of pilot actions and workload, selection of Flaps 3 is skipped and Flaps 4 selection is executed at the speed at which normally Flaps 3 would be selected.

During the batch study, which used an automated pilot response model, Flaps 3 and later Flaps 4 were both selected by the pilot response model. The results of this study showed little time between Flaps 3 and Flaps 4 selection and formed the basis of removing Flaps 3 selection from the flight procedures

The TEMO concept can be used in mixed operations, where some aircraft perform TEMO while other aircraft perform conventional approaches, by increasing the spacing between mixed-mode aircraft. Either the interval between CTAs or the actual CTI can be increased to provide sufficient spacing and account for the uncertainty of non-TEMO aircraft performance. Additional research is required to investigate what adjustments are required in order to operate safely in mixed-mode arrivals.

References

- [1] **ICAO.** *Continuous Descent Operations (CDO) Manual - Doc 9931 AN/476.* International Civil Aviation Organization, Montreal, Canada, 2010.
- [2] **T. S. Abbot.** A Brief History of Airborne Self-Spacing Concepts. Contractor Report NASA/CR-2009-215695, National Aeronautics and Space Administration, Langley Research Center, Hampton, Virginia 23681-2199, 2009.
- [3] **EUROCAE.** *Safety, Performance and Interoperability Requirements Document for Airborne Spacing - Flight Deck Interval Management (ASPA-FIM) - ED-195.* EUROCAE, 92240 Malakoff, France, 2011.
- [4] **W. Langewiesche.** *Stick and Rudder: An Explanation of the Art of Flying.* McGraw-Hill Inc., 1944.
- [5] **N. De Gelder, F. J. L. Bussink, and R. P. M. Verhoeven.** Multi-Parameter Guidance: Time and Energy Managed Operations - Concept of Operation. Deliverable SGO-WP 3.3.1-NLR-DEL-0040, National Aerospace Laboratory, Amsterdam, The Netherlands, 2010. WP3.3-Technology Studies and Concept Validation, System for Green Operations ITD.
- [6] **Air Traffic Control the Netherlands.** Aeronautical Information Publication, 2013.
- [7] **Federal Aviation Administration.** Federal Aviation Regulations Part 91 - General Operating and Flight Rules, 2013. Sec. 91.117 — Aircraft speed.
- [8] **ICAO.** *Procedures for Air Navigation Services - Aircraft Operations - Volume I, Flight Procedures - Doc 8168, OPS/611.* International Civil Aviation Organization, Montreal, Canada, 2006.
- [9] **J. L. De Prins, K. F. M. Schippers, M. Mulder, M. M. Van Paassen, A. C. In 't Veld, and J.-P. B. Clarke.** Enhanced Self-Spacing Algorithm for Three-Degree Decelerating Approaches. *Journal of Guidance, Control and Dynamics*, 30(2), 576–590, 2007. doi:10.2514/1.24542.

- [10] **A. M. P. De Leege, A. C. In 't Veld, M. Mulder, and M. M. Van Paassen.** Three-Degree Decelerating Approaches in High Density Arrival Streams. *Journal of Aircraft*, 46(5), 1681–1691, 2009. doi:10.2514/1.42420.
- [11] **EUROCAE.** *Minimum Aviation System Performance Specification: Required Navigation Performance for Area Navigation - ED-75B*. EUROCAE, 92240 Malakoff, France, 2003.
- [12] **S. Muresean.** Initial 4D - 4D Trajectory Data Link (4DTRAD) - Concept of Operations. Tech. rep., EUROCONTROL, Brussels, Belgium, 2008.
- [13] **P. Pellerin.** SESAR JU - Initial 4D “On Time”. Presentation at ATC Global 2012, Amsterdam, The Netherlands, 2012.
- [14] **D. De Smedt.** Aircraft Systems and 4D Trajectory Management. Presentation at the 2nd Round of Military CNS Technical Implementation Information Days, 2012.
- [15] **T. S. Abbot.** Speed Control Law for Precision Terminal Area In-Trail Self Spacing. Technical Memorandum NASA/TM-2002-211742, National Aeronautics and Space Administration, Langley Research Center, Hampton, Virginia 23681-2199, 2002.
- [16] **R. A. Coppenbarger, R. W. Mead, and D. N. Sweet.** Field Evaluation of the Tailored Arrivals Concept for Datalink-Enabled Continuous Descent Approach. *Journal of Aircraft*, 46(4), 1200–1209, 2009. doi:10.2514/1.39795.
- [17] **S. Torres, J. K. Klooster, L. Ren, and M. Castillo-Effen.** Trajectory Synchronization between Air and Ground Trajectory Predictors. In: *Proceedings of the 30th Digital Avionics Systems Conference, Seattle, Washington, October 16–20t*, pp. 1E3–1–1E3–14. IEEE/AIAA, 2011. doi:10.1109/DASC.2011.6096175.
- [18] **N. T. Ho and J.-P. B. Clarke.** Methodology for Optimizing Parameters of Noise-Abatement Approach Procedures. *Journal of Aircraft*, 44(4), 1168–1176, 2007. doi:10.2514/1.22292.
- [19] **J. K. Klooster, A. Del Amo, and P. Manzi.** Controlled Time-of-Arrival Flight Trials Results and Analysis. In: *Proceedings of the 8th USA/Europe Air Traffic Management Research and Development Seminar, Napa, California, June 29–July 2*, pp. 1–11, 2009.
- [20] **F. J. L. Bussink, J. J. Van der Laan, and P. M. A. De Jong.** Combining Flight-deck Interval Management with Continuous Descent Approaches in high density traffic and realistic wind conditions. In: *Proceedings of the AIAA Guidance, Navigation and Control Conference, Minneapolis, Minnesota, August 13–16*, AIAA 2012-4523, pp. 1–25. American Institute of Aeronautics and Astronautics, 2012. doi:10.2514/6.2012-4523.
- [21] **Y. Glina, S. Troxel, T. Reynolds, and M. McPartland.** Wind Information Requirements to Support Four Dimensional Trajectory-Based Operations. In: *Proceedings*

- of the 12th AIAA Aviation Technology, Integration, and Operations (ATIO) Conference and 14th AIAA/ISSM, Indianapolis, Indiana, September 17–19, AIAA 2012-5702, pp. 1–14. American Institute of Aeronautics and Astronautics, 2012. doi:10.2514/6.2012-5702.
- [22] **A. V. Rao, D. A. Benson, C. L. Darby, M. A. Patterson, C. Francolin, and G. T. Huntington.** Algorithm 902: GPOPS, A MATLAB Software for Solving Multiple-Phase Optimal Control Problems Using the Gauss Pseudospectral Method. *ACM Transactions on Mathematical Software*, 37(2), 39, 2009. doi:10.1145/1731022.1731032. Article 22.
- [23] **A. V. Rao, D. A. Benson, C. L. Darby, C. Francolin, M. A. Patterson, I. Sanders, and G. T. Huntington.** *User Manual for GPOPS Version 3.3: A MATLAB Software for Solving Optimal Control Problems Using Pseudospectral Methods*. University of Florida, Gainesville, Florida, 2010.
- [24] **V. M. Becerra.** Solving complex optimal control problems at no cost with PSOPT. In: *Proceedings of the IEEE International Symposium on Computer-Aided Control System Design (CACSD), Yokohama, Japan, 8–10 September*, pp. 1391–1396, 2010. doi:10.1109/CACSD.2010.5612676.
- [25] **Airbus.** *Flight Crew Operations Manual (Vol. 3)*, rev. 14 edn., 2002.
- [26] **D. Garg, M. A. Patterson, C. L. Darby, C. Francolin, G. T. Huntington, W. W. Hager, and A. V. Rao.** Direct Trajectory Optimization and Costate Estimation of Finite-Horizon and Infinite-Horizon Optimal Control Problems via a Radau Pseudospectral Method. *Computational Optimization and Applications*, 49(2), 335–358, 2009. doi:10.1007/s10589-009-9291-0.
- [27] **D. Garg, M. A. Patterson, W. W. Hager, A. V. Rao, D. A. Benson, and G. T. Huntington.** Unified Framework for the Numerical Solution of Optimal Control Problems Using Pseudospectral Methods. *Automatica*, 46(11), 1843–1851, 2010. doi:10.1016/j.automatica.2010.06.048.
- [28] **M. Abramowitz and I. A. Stegun,** eds. *Handbook of Mathematical Functions with Formulas, Graphs, and Mathematical Tables*. Dover Publications, New York, New York, 1964. U.S. Department of Commerce, National Bureau of Standards.
- [29] **P. E. Gill, W. Murray, and M. A. Saunders.** *User's Guide for SNOPT Version 7: Software for Large-Scale nonlinear Programming*. Department of Mathematics, University of California, San Diego, La Jolla, California 92093-0112, 2008.
- [30] **J. R. R. Martins, P. Sturdza, and J. J. Alonso.** The Complex-Step Derivative Approximation. *ACM Transactions on Mathematical Software*, 29(3), 245–262, 2003. doi:10.1145/838250.838251.

- [31] **L. B. Rall.** *Automatic Differentiation: Techniques and Applications*, vol. 120. Springer, 1981. Lecture Notes in Computer Science.
- [32] **S. Rump.** *INTLAB - INTerval LABoratory*. Kluwer Academic Publishers, Dordrecht, 1999.
- [33] **R. P. M. Verhoeven.** Pseudospectral aircraft descent trajectory optimization: An initial implementation. Contract Report NLR-CR-2012-378, National Aerospace Laboratory, Amsterdam, The Netherlands, 2012.
- [34] IPOPT, Interior Point OPTimizer, 2012. <https://projects.coin-or.org/Ipopt/wiki>.
- [35] ADOL-C, Automatic Differentiation by Overloading C++, 2012. <https://projects.coinor.org/ADOL-C>.
- [36] **P. M. A. De Jong, F. J. L. Bussink, N. De Gelder, R. P. M. Verhoeven, and M. Mulder.** Time and Energy Management during Descent and Approach for Aircraft. In: **D. Young and S. Saunders-Hodge**, eds., *Proceedings of the 5th International Conference on Research in Air Transportation — ICRAT 2012, Berkeley, California, May 22–25*, pp. 1–6. FAA and EUROCONTROL, 2012.
- [37] **P. M. A. De Jong, K. De Vos, C. Borst, M. M. Van Paassen, and M. Mulder.** Time-based Spacing for 4D Approaches using Speed-Profiles. In: *Proceedings of the AIAA Guidance, Navigation and Control Conference, Portland, Oregon, August 8–11*, AIAA 2011-6215, pp. 1–14. American Institute of Aeronautics and Astronautics, 2011. doi:10.2514/6.2011-6215.
- [38] **D. Garrido-López, L. D’Alto, and R. Gomez Ledesma.** A Novel Four-Dimensional Guidance for Continuous Descent Approaches. In: *Proceedings of the 28th Digital Avionics Systems Conference, Orlando, Florida, October 23–29*, pp. 6.E.1–1–6.E.1–11. IEEE/AIAA, 2009. doi:10.1109/DASC.2009.5347433.
- [39] **D. Garrido-López, R. Gomez Ledesma, G. R. Gershohn, and S. Moore.** Analysis of Aircraft Descent Predictability: Implications for Continuous Four-Dimensional Navigation. In: *Proceedings of the AIAA Guidance, Navigation and Control Conference, Portland, Oregon, August 8–11*, AIAA 2011-6217, pp. 1–18. American Institute of Aeronautics and Astronautics, 2011. doi:10.2514/6.2011-6217.
- [40] **J. L. De Prins and R. Gomez Ledesma.** Towards Time-based Continuous Descent Operations with Mixed 4D FMS Equipage. In: *Proceedings of the 11th AIAA Aviation Technology, Integration, and Operations (ATIO) Conference, Virginia Beach, Virginia, September 20–22*, AIAA 2011-7018, pp. 1–18. American Institute of Aeronautics and Astronautics, 2011. doi:10.2514/6.2011-7018.

BATCH STUDY INTO TEMO PERFORMANCE

The previous chapter presented the Time and Energy Managed Operations (TEMO) concept. This chapter evaluates the TEMO concept using a Fast-Time Batch Study. Several time and energy errors are introduced to validate TEMO's robustness. Moreover, a wind estimation error is introduced in the planning algorithm to investigate TEMO's ability to cope with such errors. Both strategic and tactical replanning are compared for similar conditions. Furthermore, TEMO descents and approaches are compared with present step-down approaches to determine TEMO's environmental benefits.

Paper title Time and Energy Management during Descent and Approach: A Fast-Time Simulation Study

Authors P.M.A. de Jong, N. de Gelder, R.P.M. Verhoeven, F.J.L. Bussink, R. Kohrs, M.M. van Paassen and M. Mulder

Published in Submitted to Journal of Aircraft 2013

ABSTRACT

A novel integrated planning and guidance concept has been developed that optimizes aircraft trajectories from Top of Descent to the runway threshold to achieve a continuous engine-idle descent. The new concept, named Time and Energy Managed Operations (TEMO), aims at reducing noise, gaseous emissions and fuel burn while maintaining airport landing capacity by means of time management. TEMO uses an optimization algorithm to minimize thrust and speedbrake use through energy management by exchanging kinetic and potential energy. Sustained deviations during descent are corrected using a strategic or tactical approach. TEMO is evaluated in a batch simulation study and compared with conventional step-down descents in terms of environmental impact. Various disturbances are introduced to test TEMO's robustness to disturbances and time constraints. Moreover, the two different methods of correcting deviations are compared. The results show that TEMO allows idle descents whilst adhering to time constraints and reduces the environmental impact of aircraft. Moreover, TEMO can cope with disturbances and updated time constraints. However, large wind estimation errors degrade TEMO performance.

3-1 Introduction

European [1] and American [2] legislators have established research projects to develop the future Air Transportation System (ATS) and address the capacity, environmental, safety and financial issues of the current ATS. With the expected growth in air traffic [3], the current ATS operates at its capacity limits and is expected to experience increased delays if traffic levels increase further [4]. Combined with an increased public concern for the environment and increased oil prices, this has forced the aviation industry to investigate green technologies to reduce the environmental footprint of aircraft and enable capacity growth. To allow capacity growth within the current regulations, the environmental footprint of aircraft should be reduced to accommodate further capacity growth. This is achieved by improving aircraft operations [5] to reduce fuel, emissions and noise mitigation of residential areas [6].

Today, Air Traffic Controllers (ATCos) use level flight segments to maintain separation between departing and arriving aircraft. While flying level, an aircraft requires thrust to maintain speed, burning fuel. These level segments also force aircraft to fly relatively low compared with a continuous descent. By eliminating these level segments, aircraft could maintain a more environmentally friendly engine-idle setting for a longer period of time and consequently reduce the amount of noise and pollutants emitted [7]. Consequently, these descents reduce fuel use and operating costs for airlines. Arrival procedures that reduce these level segments and aim at flying an engine-idle descent are referred to as Continuous Descent Operations (CDO) [8].

Various airports already have CDOs in operation, but only during hours of low-traffic demand due to inaccuracies in predicting the arrival time and trajectory of aircraft that perform such procedures. Therefore, ATCos introduce additional spacing buffers such that a CDO can be performed without Air Traffic Control (ATC) interference. The added spacing buffer reduces the runway throughput, and as a result reduces the usability of such procedures.

Researchers have investigated new CDO concepts in an attempt to improve predictabil-

ity. Examples are concepts that use a fixed vertical trajectory [9–15], such as the Three-Degree Decelerating Approach. Using engines or employing drag devices, the deceleration of the aircraft could be controlled. However, certain aircraft cannot decelerate along 3° descent with engines (near-)idle. Other CDO concepts generally make use of ground-based [16–19] or aircraft-based [20–26] Trajectory Predictors (TPs).

Most of the discussed CDO concepts actively control the altitude or speed profile. This often results in additional thrust variations to control speed changes to maintain spacing or to remain on path, which has a negative effect on noise nuisance and fuel use. In the following, a new CDO concept named Time and Energy Managed Operations (TEMO), developed within Clean Sky, uses the law of conservation of energy to couple altitude and speed profiles, allowing exchange of kinetic and potential energy to correct deviations without using thrust or speedbrakes.

The TEMO algorithm plans a full-idle descent, from Top of Descent (ToD) to the stabilization point at 1,000 ft above ground level, including ATC (time-)constraints. Using energy principles, the algorithm can decide to exchange altitude for speed and vice versa to gain or lose time and energy. Different from other research projects is that TEMO calculates a calibrated airspeed profile and uses Speed-on-Elevator (SOE) control to guide the aircraft along this airspeed profile. As a result, the vertical trajectory will vary depending on aircraft characteristics (i.e., weight and aerodynamics), atmospheric conditions, and the calculated airspeed profile.

This paper reports on the results of a fast-time batch simulation study simulating TEMO descents for different initial conditions to evaluate deviations. The robustness of the algorithm to disturbances was tested by introducing time, energy and wind estimation errors to evaluate methods for correcting deviations and resulting effects on environmental impact. Furthermore, TEMO's environmental impact is compared with results from conventional step-down descents.

This paper is organized as follows. It starts with a discussion of the TEMO concept in Section 3-2. Section 3-2-2 reports on the algorithm developed to calculate TEMO trajectories, used in this experiment. The experimental setup of the fast-time simulations is discussed in Section 3-3, with results of the simulations reported in Section 3-4 and conclusions in Section 3-5.

3-2 Time and Energy Managed Operations

TEMO is a new CDO concept that aims at reducing fuel use, gaseous and noise emissions whilst conforming to absolute or relative time constraints imposed by ATC. TEMO enhances the current vertical guidance of the aircraft using an optimization algorithm and improved TP to calculate *energy-neutral* trajectories and an improved guidance function. An energy-neutral trajectory requires only engine idle thrust and uses no additional drag devices during descent from ToD to the stabilization point at 1,000 ft above ground level. At the stabilization point the aircraft is stabilized, configured and ready for landing following a precision approach. To improve predictability, the calculated trajectories adhere to the definition of a

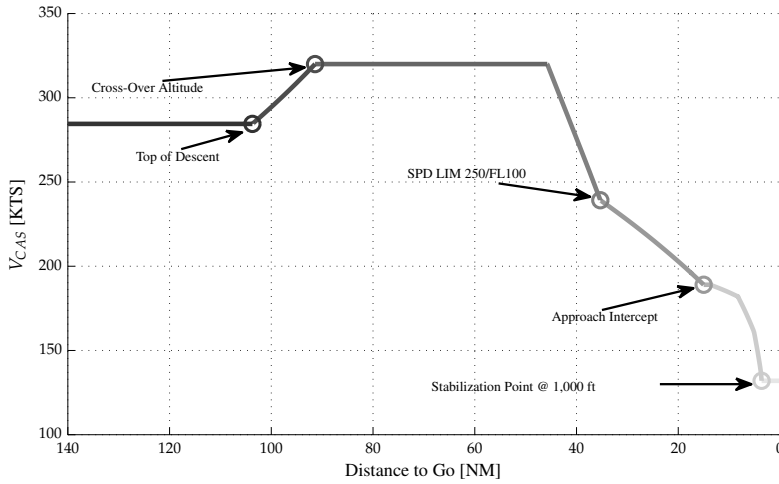


FIGURE 3-1: A nominal TEMO calibrated airspeed profile (CAS vs. Distance to Go) indicating TEMO characteristic phase transitions. The trajectory shows the phases from Top of Descent (≈ 105 NM) to the runway threshold (0 NM).

closed-path trajectory [8].

The TEMO concept uses the principles of energy exchange to control the aircraft to a given point in space and time. The trajectory consists of a nominal airspeed profile, see Figure 3-1, that complies with applicable speed constraints. This airspeed profile is similar at lower altitudes for all aircraft to achieve a stable and predictable arrival flow. To arrive earlier or later than originally planned, TEMO commands deviations from the nominal profile but only within prescribed speed margins. The speed profile is flown by the guidance system using SOE control and thrust set to idle. This implies that the aircraft does not follow a fixed vertical profile. The actual flown vertical profile depends on aircraft characteristics and disturbances.

Due to disturbances, such as wind estimation errors, an aircraft could deviate from the planned trajectory in terms of time and energy (altitude and velocity). These deviations could be corrected instantaneously using control-laws, resulting in a *tactical* approach. Another method is a *strategic* approach that allows small deviations from the planned trajectory and only calculates a new trajectory when these deviations exceed a predefined boundary.

The time deviation is defined as the difference between the actual time and planned time at current position and is negative when the aircraft arrives too early and positive when the aircraft arrives too late. The energy deviation is defined as the difference between the actual energy state and planned energy state at the current position.

The trajectories are calculated by the novel TEMO algorithm that aims at finding an energy-neutral trajectory using *energy management*. Proper energy management allows an aircraft to exchange kinetic and potential energy, resulting in an energy-neutral trajectory,

which implies that no additional energy is added or dissipated. However, situations could occur in which TEMO cannot find a trajectory without using thrust or drag devices. In these cases, TEMO minimizes thrust and drag device use resulting in an *energy-optimal* trajectory. In extreme cases, TEMO is unable to find a valid trajectory that satisfies all constraints, which is referred to as a *reject*. In these cases, pilots notify ATC to negotiate new constraints, new route or revert to a vector-based arrival.

TEMO is 4D capable by using time constraints. A time constraint can be an absolute time constraint, using a Controlled-Time of Arrival (CTA), at a location along the trajectory [27], or a relative time interval to a leading aircraft using Interval Management (IM) [28]. The time constraints commanded by ATC include a Required Time Performance (RTP), which prescribes the accuracy at which the aircraft is required to meet the time constraints for at least 95% of all operations. During hours of low-demand, the RTP can be less restrictive and set to a high value to achieve more environmentally friendly descents, whereas during hours of high-demand, the RTP can be set to a low value to ensure tight inter-aircraft spacing accuracy to satisfy runway throughput requirements.

TEMO uses an automated optimization algorithm to quickly and repeatedly calculate trajectories with high precision. To reduce uncertainty caused by variations in pilot responses during execution of the descent, the descent is flown using the autopilot and the aircraft cockpit displays are enhanced to support pilots in flying TEMO descents.

The TEMO concept is developed and evaluated for the Airbus A320 aircraft. However, TEMO should be adapted to allow CDOs with other modern, commercial aircraft in the future.

3-2-1 TEMO Trajectory Planning

To simplify trajectory prediction, an aircraft Flight Management System (FMS) uses a simplified aircraft performance model containing lift and drag characteristics, aircraft and engine dynamics. Therefore, modeling errors [17, 29], due to this simplification, could cause an error in prediction of the planned trajectory resulting in the aircraft to arrive at a different time or energy state than originally planned. Other sources of trajectory prediction errors are inaccurate wind estimates [10, 11, 30–32] or erroneous sensor measurements [33].

The TEMO concept defines two different implementations for correcting deviations: *strategic* replanning and *tactical* replanning. Strategic replanning allows small time and energy deviations and replans only when these deviations exceed a preset boundary, see Table 3-1. This allows a deviation to evolve in time which could also result in the error dissolving or changing sign. For example, the aircraft could estimate to arrive slightly early due to an unforeseen tailwind. However, due to a 180° turn later in the trajectory, this same wind could lead to a headwind which could restore the estimated arrival time.

Alternatively, tactical replanning continuously corrects a detected deviation using a control system. As such, strategic replanning can be considered as an open-loop control system (or slow, intermittent control system) whereas tactical replanning acts as a continuous closed-loop control system. Furthermore, strategic replanning takes the entire trajectory into account when correcting deviations through replanning and optimizes the location of

corrective actions, whereas tactical replanning takes immediate action at the location of the detected deviation, which might not be optimal.

Strategic Replanning

Using strategic replanning, the FMS monitors the aircraft time progress and energy state at the current position and compares this with the planned state to detect deviations. When a deviation exceeds an allowable boundary, a new trajectory will be calculated by the TEMO algorithm to correct the deviation. This process of calculating a new trajectory is referred to as strategic replanning. A schematic overview of strategic replanning is found in Figure 3.2(a).

The boundaries are defined as a positive and a negative value at ToD, Initial Approach Fix (IAF) and runway threshold. The boundaries are linearly interpolated between these locations and reduce in value as the control space reduces while the aircraft approaches a time constrained waypoint. Typical values for these boundaries and the RTP values used in this simulation study are found in Table 3-1. The values for the RTPs are well within the 10 seconds prescribed Terminal Maneuvering Area (TMA) time accuracy used in the Initial 4D project [34] of Single European Sky ATM Research (SESAR). The energy boundary is expressed in specific energy, or energy height, by dividing total energy by the weight (mg) of the aircraft.

TABLE 3-1: TEMO deviation boundaries and Required Time Performance (RTP).

Active Waypoint	RTP [s]	Error Boundary					
		Top of Descent		IAF		Runway Threshold	
		Time [s]	Energy [ft]	Time [s]	Energy [ft]	Time [s]	Energy [ft]
IAF	5	± 5	± 500	± 0	± 200	-	-
Runway	-	-	-	-	± 200	-	± 100

As the final segment of a TEMO descent is flown on the Instrument Landing System (ILS), the energy boundary merely represents a speed boundary of $\approx 10\text{KCAS}$ as the altitude profile is fixed to the glideslope. Moreover, from the stabilization point at 1,000 ft, the aircraft maintains Final Approach Speed (FAS) and TEMO replanning is disabled to maintain a stable approach.

Tactical Replanning

Sustained deviations can also be corrected using a tactical control-law that adjusts the speed profile to minimize time and uses thrust or speedbrakes to maintain the vertical profile and updated speed profile. Using this tactical approach, the deviation boundaries are disabled and a (strategic) replan is only activated to correct large time deviations or a new CTA/Controlled-Time Interval (CTI) update. When the tactical controller reaches aircraft operational limits, a strategic replan could also be used to correct further deviations. This tactical implementation is likely to use more thrust and, hence, consume more fuel. For these reasons, this implementation has not been investigated as TEMO aims at minimizing

TABLE 3-2: Definition of flight phases in GPOPS algorithm.

Phase	Name	Phase entry-trigger	Configuration	Path Constraint(s)	Operational Constraints
0	Cruise	Start of Run	Clean	$\dot{M} = 0$	$M_0 \leq M \leq M_{MO}$
1	Mach	Top of Descent	Clean	$\dot{M} = 0$	$M_0 \leq M \leq M_{MO}$
2	CAS	Crossover Altitude	Clean	$\dot{V}_{CAS} = 0$	$V_0 \leq V_{CAS} \leq V_{MO}$
3	CAS		Clean	$\dot{V}_{CAS} = 0$	$V_0 \leq V_{CAS} \leq V_{MO}$
4	Fast Deceleration		Clean	$\dot{k} = 0$	$230 \leq V_{CAS} \leq V_{MO}$
5	Slow Deceleration	FL 100	Clean	$\dot{V}_{CAS} = 0$	$V_{F1} < V_{CAS} \leq 250$
6	Slow Deceleration	V_{F1}	F1	$\dot{V}_{CAS} = 0$	$V_{F2} < V_{CAS} \leq V_{F1}$
7	Approach	V_{LOC} , 15 NM	F1	$\dot{V}_{CAS} = 0$	$V_{F2} < V_{CAS} \leq V_{F1}$
8	Approach	Glideslope intercept	F1	$\dot{\gamma}_a = 0, \dot{V}_{CAS} < 0$	$V_{F2} < V_{CAS} \leq V_{F1}$
9	Decelerate on ILS	V_{F2}	F2	$\dot{\gamma}_a = 0, \dot{V}_{CAS} < 0$	$V_G < V_{CAS} \leq V_{F2}$
10	Decelerate on ILS	V_G	F2 & Gear	$\dot{\gamma}_a = 0, \dot{V}_{CAS} < 0$	$V_{F3} < V_{CAS} \leq V_G$
11	Decelerate on ILS	V_{F3}	F3 & Gear	$\dot{\gamma}_a = 0, \dot{V}_{CAS} < 0$	$V_{F4} < V_{CAS} \leq V_{F3}$
12	Decelerate on ILS	V_{F4}	F4 & Gear	$\dot{\gamma}_a = 0, \dot{V}_{CAS} < 0$	$V_{FAS} < V_{CAS} \leq V_{F4}$
13	Final Approach	1,000 ft, $V_{CAS} = FAS$	F4 & Gear	$\dot{\gamma}_a = 0, \dot{V}_{CAS} = 0$	$V_{CAS} = V_{FAS}$

fuel.

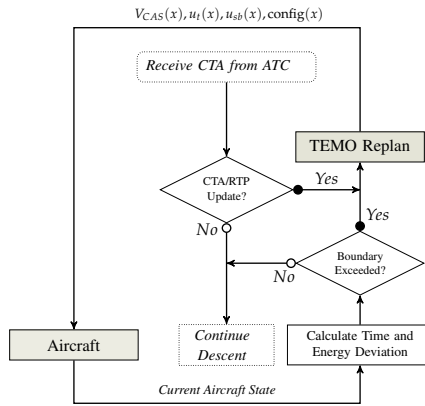
However, hybrid replanning, uses both tactical replanning and strategic replanning to correct deviations. In this replan method, deviations are corrected using different replan approaches: time deviations are corrected using a novel, closed-loop, 4D-controller (Figure 3.2(b)), developed by German Aerospace Center (DLR), while energy deviations are corrected using a TEMO replan. The controller controls the aircraft speed by calculating a ΔV_{CAS} to correct the time deviation using SOE control. Because the controller continuously adjusts the speed profile, the flown altitude profile will deviate from the planned altitude profile through energy management as the aircraft uses the elevator to control speed. Hence, the controller actions result in a different energy strategy compared to the original trajectory. Therefore, altitude deviations and speed offsets could result in an energy deviation which is corrected using a replan.

The 4D-controller respects operational speed constraints and uses anti-windup to prevent controller saturation. Also, when ATC issues a large time update, TEMO uses strategic replanning to calculate a new trajectory and the 4D-controller is reinitialized.

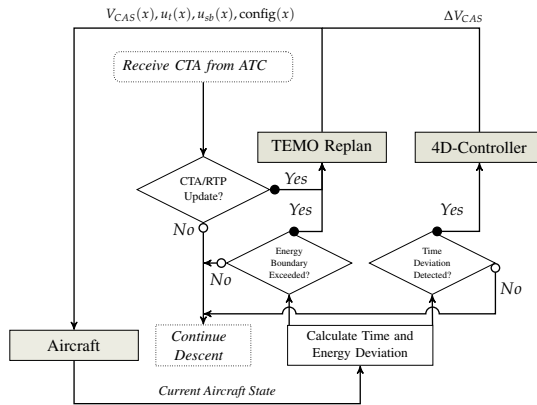
3-2-2 TEMO Algorithm and Trajectory Predictor

A nominal TEMO speed profile, indicating the different flight phases and velocity strategies is shown in Figure 3.3(a). In this figure, the dashed lines represent the airspeed limits that are set as operational constraints as listed in Table 3-2. The corresponding vertical profile is shown in Figure 3.3(b). For comparison, a baseline scenario consisting of a conventional, step-down approach is also shown in Figure 3.3(b).

The objective of TEMO is to minimize the use of thrust and speedbrakes whilst adhering to aircraft, operational, and time constraints, which is formulated as an optimal control problem by the objective function:

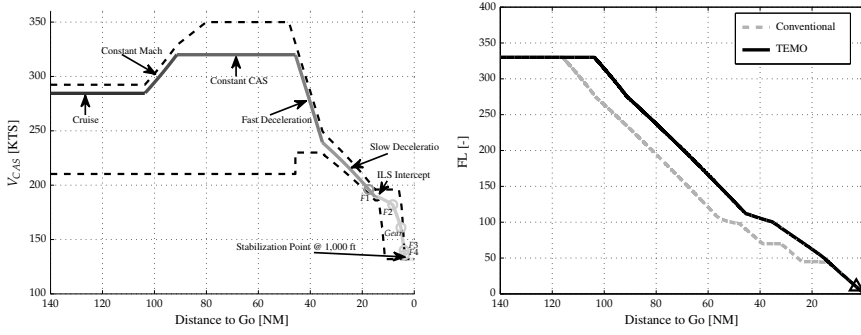


(a) Strategic replanning.



(b) Hybrid replanning.

FIGURE 3-2: Replanning implementation defined by the TEMO concept.



(a) Speed profile including the operational velocity constraints (dashed lines) and TEMO flight phases. (b) Vertical profiles for a TEMO and conventional constraints (dashed lines) and TEMO descent.

FIGURE 3-3: A typical TEMO calibrated airspeed profile (CAS vs. Distance to Go) from Top of Descent (≈ 105 NM) to the runway threshold (0 NM).

$$J = \int_{t_{now}}^{t_f} [K_{THR}u(t)_{THR}]^2 + [K_{SB}u(t)_{SB}]^2 dt \quad 3-1$$

The objective function is defined as a *minimum control problem*, with K_{THR} and K_{SB} , scaling parameters for throttle, $u(t)_{THR}$ and speedbrake control, $u(t)_{SB}$.

The optimal control problem is subject to the dynamic constraints:

$$\begin{aligned} \dot{V} &= g \left[\frac{T(V, h, u_{THR}) - D(V, h, u_{SB}, config)}{mg} - \sin \gamma_a \right] \\ \dot{x} &= V \cos \gamma_a \\ \dot{h} &= V \sin \gamma_a \\ \dot{m} &= -f_f(V, h, u_{THR}) \end{aligned} \quad 3-2$$

In Eq. (3-2), the engine thrust, T , depends on true airspeed, altitude and throttle position, while the aircraft drag, D , depends on true airspeed, altitude, speedbrakes and aircraft configuration, i.e., flaps and gear. The aircraft mass, m , decreases with fuel-flow, f_f , which is a function of airspeed, altitude and throttle position. The aircraft's vertical motion is described by the flight-path angle relative to the air, γ_a , hence, any effects of wind are ignored.

In this simulation study, an absolute time constraint at the IAF — located 50 NM from the runway — is included while the arrival time at the runway is free. These constraints are included in the optimization problem as boundary conditions, shown in Eq. (3-3):

$$\begin{aligned} t(x_{IAF}) &= CTA_{IAF} + \Delta t \\ t(x_{RWY}) &= \text{free} \end{aligned} \quad 3-3$$

The time constraint at the IAF is defined by a combination of the assigned CTA and a Δt . This Δt defines a planning time window which the algorithm can use to deviate from the CTA at the IAF to find a trajectory. By allowing a planning time window, the algorithm

has more solution space to find an energy-neutral trajectory that satisfies the CTA within the RTP. In contrast, without this window, the algorithm could find an energy-optimal trajectory that exactly satisfies the CTA at the expense of thrust or speedbrake use. Through this time window, time accuracy is reduced in favor of a more environmental trajectory. To allow a margin for unanticipated deviations, the window is slightly smaller — 4 seconds — than the RTP.

The optimal control problem is also subject to the operational path constraints listed in Table 3-2. As a result, the algorithm plans selection of configuration changes, such as flaps and gear deployment. These selections are based on the A320 minimum maneuvering speeds (Green-dot, Slat and Flap speed [35]) as listed in Table 3-3 or final approach speed. The location of selecting configurations is prescribed by the planned location where the aircraft obtains these speeds.

TABLE 3-3: TEMO configuration selection speeds in GPOPS.

Configuration	F1	F2	Gear	F3	F4
TEMO Speed Definition	V_0	V_S	$\frac{V_S + V_F}{2}$	V_F	$\frac{V_{FAS} + V_F}{2}$

The optimal control problem defined by Eq. (3-1) is solved by the TEMO algorithm using General Pseudospectral Optimal Control Software (GPOPS) [36, 37]. GPOPS approximates states and controls of the optimal control problem through discretization of continuous time using collocation. This reduces the optimal control problem into a finite set of algebraic equations.

Since a TEMO replan requires time to calculate a full trajectory, the aircraft location, time and energy state is predicted ahead of the aircraft and used as initial position of the replan. Depending on the distance to the runway, this predicted point is located between 15 and 30 seconds ahead. During the calculation process, the aircraft will continue on the active plan and intercept the new trajectory at the initial position of the new trajectory. An unconstrained transition is included to provide a smooth transition from this initial position to the next constrained phase according to Table 3-2.

Replanning to correct a time deviation is disabled when the aircraft is near a time-constrained waypoint as the initial position will be located too close to the constrained waypoint resulting in a limited space to resolve the time deviation. In real-life operations, this should not occur as ATC would have commanded a new CTA at the runway threshold way ahead of the TMA entry. Similarly, TEMO does not replan when the aircraft is close to the glideslope as energy exchange is not possible on the glideslope and hence only a limited distance is available to correct any deviations at this point. As a result, during these segments of no replanning, time and energy deviations can grow in excess of the set boundaries.

3-3 Experimental Evaluation

To evaluate the TEMO concept, a fast-time simulation tool was developed in MATLAB and Simulink that simulated a flight from cruise to the runway threshold while flying a TEMO descent. The TEMO algorithm, as discussed in the previous section, was implemented in this simulation tool.

3-3-1 Method

Simulation Models

The simulation tool uses an aircraft model based on the Airbus A320 [38, 39]. The TEMO algorithm uses a derived and simplified point-mass model based upon the same aircraft model. Pilot actions were modeled using a zero-delay nominal pilot response model.

Disturbances

Disturbances during a TEMO descent can be divided into two categories: *a*) instantaneous errors, and *b*) steady-state errors. Instantaneous errors occur on a single basis and disrupt flight only for a short while. Typical instantaneous errors that were applied in this experiment are an update of the CTA or an energy error due to a single guidance/autopilot or sensor error. Steady state errors occur due to modeling and prediction errors. Modeling errors occur due to differences in modeling of aircraft dynamics and performance due to simplifications. Prediction errors, due to wind estimation errors and incorrect mass estimation, continuously affect the energy state of the aircraft.

Time and energy deviations due to instantaneous errors can be corrected for using a strategic replan, while a steady-state error would continuously trigger a strategic replan when the resulting deviation advances and exceeds a boundary. Tactical replanning corrects instantaneous errors but requires either excessive control actions or an extended duration to correct such errors. However, tactical control is expected to be an efficient method to correct for steady-state errors as it continuously calculates time and energy errors and provides control inputs to correct the steady-state errors.

Both categories of disturbances were investigated in this experiment by introducing errors when the aircraft starts the descent at ToD.

Scenarios

The batch study comprised three simulation studies. A first study used TEMO reference scenarios and compared these descents to a conventional, step-down descent for different initial conditions. The second study introduced a combination of time and energy errors as instantaneous errors, and a wind estimation error as a steady-state error which were corrected using strategic replanning. Finally, the third study compared strategic replanning descents with descents that use hybrid replanning to correct time deviations, for various wind estimation errors.

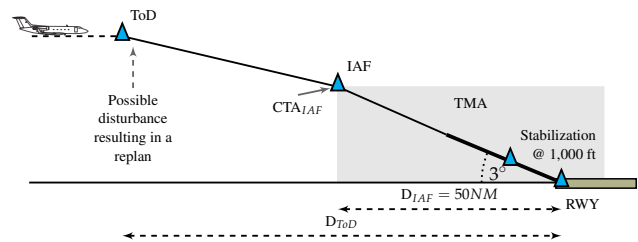


FIGURE 3-4: Overview of a typical TEMO simulation scenario.

All scenarios were defined as straight-in descents in an International Standard Atmosphere without turbulence. Scenarios flown using TEMO had a Controlled-Time of Arrival (CTA) located at the IAF and associated time and energy boundaries according to Table 3-1. A schematic overview of these scenarios is illustrated in Figure 3-4.

Simulation Study 1: Baseline This baseline study identified whether the modeling errors in the algorithm were sufficiently small to not trigger replans. The scenarios consisted of 27 descents that differ in initial conditions, and depend on aircraft mass, cruise altitude and speed schedule (Descent Mach and CAS speed) and started approximately 150 NM from the runway threshold. The three parameters were varied to explore the effects of these conditions based on three levels of each of these parameters, see Table 3-4.

TABLE 3-4: Variation of initial conditions for baseline scenarios.

	Aircraft Mass [% MLW ^a]	Speed schedule [Mach/KCAS]	Cruise Altitude [ft]
Low	70%	0.76/280	33,000
Medium	80%	0.78/300	35,000
High	90%	0.80/320	37,000

^a MLW is 64,500 kg.

The environmental impact of TEMO descents were compared with conventional, step-down descents that are typical for today’s approaches. Typical vertical profiles of a TEMO descent and a conventional descent are shown in Figure 3.3(b).

The results reported in this paper are the result of new simulations and differ from results reported earlier [40]. These new simulations have been flown with a revised aircraft model that was also used in the simulations of the combined errors and hybrid replanning scenarios reported in this paper. The conventional scenarios have also been simulated again, as an error in modeling of the glideslope intercept in these scenarios was found.

Simulation Study 2: Combination of Errors In these scenarios, errors were introduced to investigate the control space of strategic replanning. TEMO replanning was disabled at cruise level such that the algorithm cannot change the location of ToD to correct an error and, hence, must resort to energy management. All scenarios in this study started

at an aircraft mass of 70% MLW at 35,000 ft, used a speed schedule of Mach 0.80 and 320 KCAS and started approximately 130 NM from the runway threshold.

A CTA update was simulated using a time error by issuing a CTA offset at the IAF just after passing ToD. Energy errors were introduced at cruise level and consisted of an altitude and true airspeed error that jointly determine the specific energy error, expressed in units of feet. These energy errors simulate guidance and sensor errors. Wind estimation errors were introduced by applying a constant horizontal windfield which the current TEMO algorithm discards, see Eq. (3-2). A positive value of the windfield represents a headwind. Consequently, wind will continuously alter the aircraft's groundspeed and flight-path angle resulting in time and energy deviations from the planned trajectory.

This study was further split into two sets; a first set where the TEMO system *cannot* use thrust and speedbrakes and another set where thrust and speedbrakes could be used to correct errors. The first set introduced errors as listed below:

Time Error	-18 [s] to +18 [s], steps of 2 [s]
Energy Error	-500 [ft] to + 500 [ft], steps of 250 [ft]
Wind Estimation Error	-5 [KTS], -3 [KTS], 0 [KTS], +3 [KTS], +5 [KTS]

These scenarios allow us to find the control space of energy-neutral trajectories. Hence, the induced errors were rather limited as the control space was expected to be relatively small. When a replan at ToD was unsuccessful, the simulation was stopped and considered a failure.

The errors were extended for the scenarios where the TEMO system can use thrust or speedbrakes, as the available control space is larger. In these scenarios, the TEMO algorithm was still able to calculate energy-neutral trajectories but also calculated energy-optimal trajectories for larger errors. However, the combination of errors could result in TEMO rejecting a trajectory.

Time Error	-30 [s] to +30 [s], steps of 5 [s]
Energy Error	-500 [ft] to + 500 [ft], steps of 250 [ft]
Wind Estimation Error	-10 [KTS], +10 [KTS], steps of 5 [KTS]

In case a combination of errors did not yield a valid trajectory after the first replan, the simulation was stopped and the scenario was considered a failure. If further down the descent a replan rejected the trajectory, the simulation continued while flying the latest valid trajectory including the sustained time and/or energy errors whilst the TEMO algorithm performed new replans to find a valid trajectory. Even if no attempt was successful, the autopilot will correct any energy error when it transitions from SOE to Path-on-Elevator (POE) at glideslope intercept.

Simulation Study 3: Strategic versus Hybrid Replanning The full strategic replanning implementation was compared with an implementation that uses tactical replanning to

correct the time error for three different scenarios: a) no wind; b) 5 KTS headwind; c) 5 KTS tailwind.

3-3-2 Dependent Measures

TEMO performance The performance of the TEMO system was assessed by analyzing the maximum time, energy and wind estimation errors the TEMO algorithm can successfully correct using strategic replanning. Other performance indicators were the actual time and energy deviations of the aircraft when passing the IAF. The aircraft's altitude at the IAF was also analyzed to verify the variability of the vertical profile at this location. Furthermore, the energy deviation at ILS intercept was analyzed to assess the amount of energy exchange required to intercept the glideslope. Finally, the analysis verified whether the simulated approaches were stabilized at 1,000 ft.

When a replan required thrust or speedbrakes to correct deviations, the replan performance is expressed as the cumulative amount of additional throttle setting and/or speedbrakes required between ToD and glideslope intercept.

Environmental impact To assess the environmental benefits of TEMO and investigate the differences between energy-neutral and energy-optimal trajectories, fuel, noise and gaseous emissions have been calculated.

Noise levels were calculated using a noise model [41] based on the ECAC/CEAC Doc. 29 specification [42]. The noise model calculates values for Sound Exposure Level (SEL) and Maximum A-weighted Noise Level (LA_{MAX}) on a user-defined grid, which were used to calculate the surface area of the 65 dB and 75 dB SEL contours.

Nitrogen Oxide (NO_x) emissions were calculated using the Boeing Method 2 (BM2) [43] emission model. The BM2 model uses the ICAO Emission Databank for reference engine values and compensates for off-test conditions, such as different throttle settings and atmospheric conditions. The total amount of Carbon Dioxide (CO_2) emissions was determined by multiplying the amount of fuel burned with a factor of 3.15 kg CO_2 /kg fuel [44]. The analysis reported in this paper only investigated emissions that were emitted below the mixing height of 3,000 ft which directly affect quality of life of residential areas.

The amount of fuel used was determined as the difference in fuel weight between a point at cruise level and the runway threshold.

3-3-3 Experimental Hypotheses

It was hypothesized that TEMO is able to correct for all time and energy errors, whilst adhering to ATC time constraints, using strategic replanning and energy management.

3-4 Discussion of Results

This section presents the results of the analysis of all simulations. Correlation results reported in this section have been performed using Kendall's τ rank correlation test (two-

tailed) as most data was not normally distributed. The first subsection covers the 27 baseline scenarios and compares the environmental impact with conventional step-down descents. The second subsection discusses results of the simulations run with additional time, energy or wind estimation errors. This section concludes with a comparison between a full strategic replanning method and a method that employs tactical replanning for time errors.

3-4-1 Simulation Study 1: Baseline

All 27 scenarios showed that TEMO guidance and planning systems are capable of guiding the aircraft along a planned TEMO trajectory with minimal time deviation at the IAF.

TEMO performance During all simulations, the time and energy deviations remained within the allowable deviation boundaries and, hence, did not trigger a trajectory replan. Consequently, the modeling errors in the algorithm are sufficiently small to execute a nominal approach without replanning. All descents were stabilized at 1,000 ft.

Interestingly, the results indicated that the descent speeds (speed schedule) between ToD and the IAF affects the time deviation at the IAF, which was confirmed by a rank correlation analysis, indicating a strong negative correlation ($\tau = -0.668, p < 0.001$). A thorough investigation of these runs showed that the deviations from the calibrated airspeed profile increased when the autopilot guides the aircraft at higher speeds which resulted in increased speed deviations and altitude deviations.

The altitude at which the aircraft passed the IAF varied between FL 128 and FL 142, depending on the initial mass and speed schedule. Fast ($\tau = -0.586, p < 0.001$) and/or heavy ($\tau = -0.524, p < 0.001$) aircraft passed the IAF relatively low due to the effects of mass inertia and airspeed on the flight-path angle and corresponding distance required to descend to the runway.

Environmental impact The TEMO simulations are compared with conventional step-down descents using the same initial conditions and aircraft characteristics, however, without any time constraints. The total surface area of the 65 dB SEL noise contours and 75 dB SEL noise contours for these 27 TEMO and conventional simulations are shown in Figure 3-5. For a TEMO descent, the 65 dB SEL area extend to approximately 30 NM from the runway and the 75 dB SEL area extends to only 8 NM out from the runway threshold.

The comparisons for both noise level contours showed that descents flown using a TEMO descent reduce the experienced noise levels on the ground significantly, ranging between 22.1% and 28.2% for the 65 dB SEL contour and between 13.5% and 20% for the 75 dB SEL contour. Hence, noise reduction is achieved both close to — represented by higher SEL values — and farther away from the airport. The 65 dB area extends farther away from the airport than the 75 dB area, which is mostly affected by the final 10 NM of the trajectory. As both the TEMO descent and the conventional descent trajectory fly a typical 3° ILS approach, smaller differences in this area were to be expected.

The aircraft mass was the only parameter that influenced the noise contour areas on the ground. For both the 65 dB and 75 dB contour areas, a significant correlation

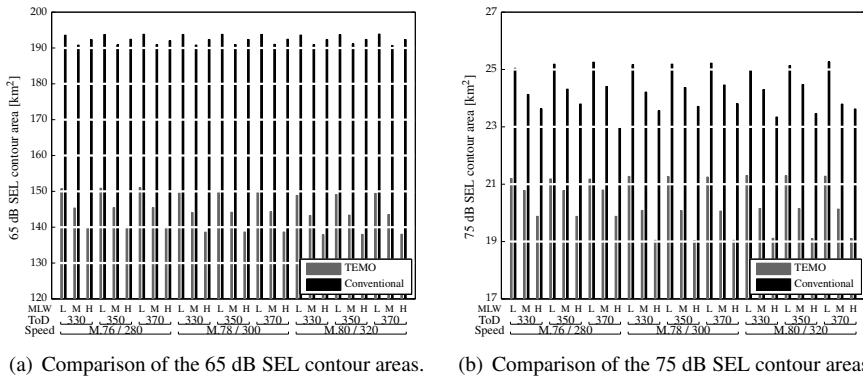


FIGURE 3-5: Sound Exposure Level (SEL) contour areas comparison for TEMO and conventional descents.

($\tau = -0.832, p < 0.001$) was found for the TEMO descents, while the conventional approaches only showed an affect on the 75 dB area ($\tau = -0.818, p < 0.001$). Aircraft mass determines the final approach speed which in turn determines the duration of the final segment and consequently the SEL which integrates Instantaneous A-weighted Noise Level (LA) over time. The speed schedules of both TEMO and conventional descents are rather similar during the final 10 NM whereas differences exist prior to glideslope intercept. These speed schedule differences lead to the differences found in 65 dB and 75 dB contour correlations. Comparing contour areas per flight time, the reduction of the 65 dB contour was between 8.8% and 11% while the 75 dB contour reduction is negligible (0.5%–0.9% reduction).

Fuel use between 140 NM from the runway at cruise level and the runway threshold was determined for all scenarios. Aircraft flying at a lower cruise level require less distance to descend and consequently fly relatively longer at cruise level than aircraft starting at a higher flight level. This effect is clearly visible in Figure 3.6(a) where fuel consumption shows a negative correlation ($\tau = -0.812, p < 0.001$) with cruise level for both TEMO and conventional simulations ($\tau = -0.791, p < 0.001$). The comparison of fuel used show a reduction in fuel use between 11% and 19.5% in favor of TEMO. However, when considering fuel use per flight time, the reduction decreases to values between 9% and 15.7%, see Figure 3.6(b).

CO_2 and NO_x emissions below the mixing height are shown in Figure 3-7. TEMO proves to reduce CO_2 emissions between 33.2% and 39.6% depending on the aircraft mass. NO_x emissions also show major reductions between 42.1% and 47.2%. Both reductions of emissions were to be expected as CO_2 and NO_x are proportional to fuel consumption [45].

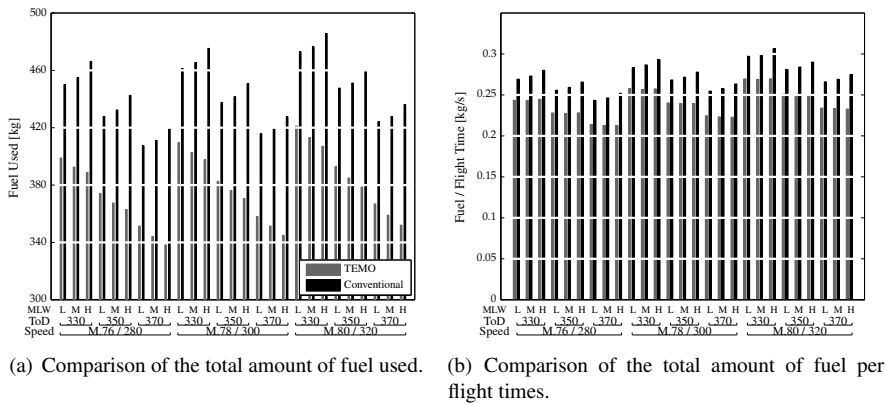


FIGURE 3-6: Comparison of total amount of fuel burned for TEMO and conventional approaches.

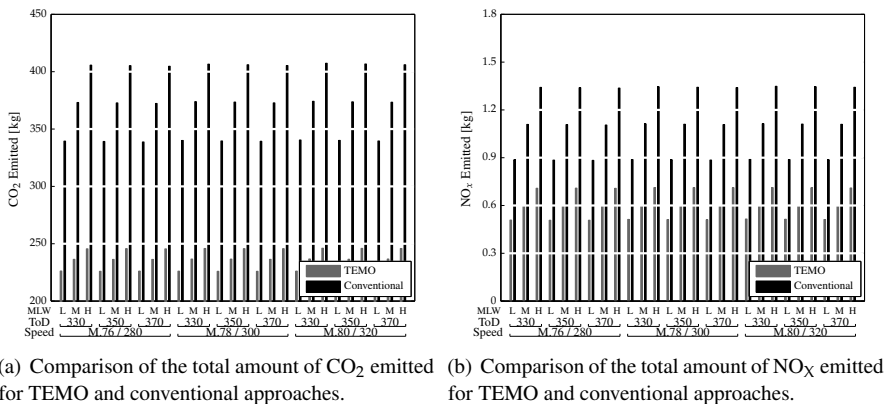


FIGURE 3-7: Comparison of total amount of CO₂ and NO_x emitted below 3,000 ft.

3-4-2 Simulation Study 2: Combination of Errors

Scenarios with no thrust and speedbrakes

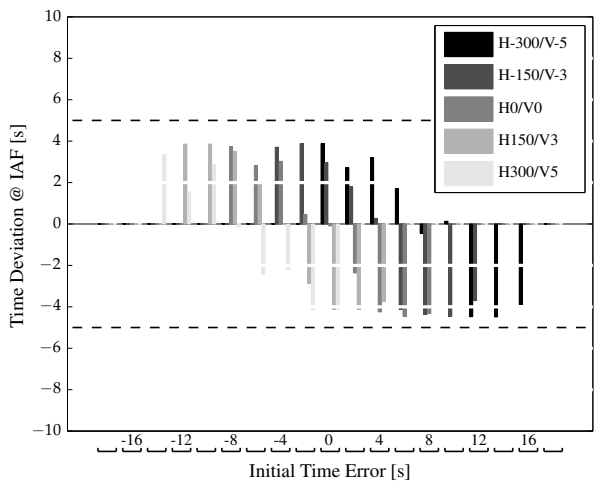
In this simulation TEMO was restricted to find energy-neutral trajectories only. The combination of errors resulted in 475 scenarios of which only 217 yielded successful replans after passing ToD. The results of these energy-neutral trajectories are analyzed in this section and are categorized by the wind estimation errors. All 217 simulations were stabilized at 1,000 ft.

TEMO performance The time deviation at the IAF for the various scenarios is shown in Figure 3-8. The time deviations remain within the 5 seconds RTP for the scenarios where no wind error was present. The scenarios with a head- or tailwind of 3 KTS exceeded the 5 seconds RTP in certain scenarios, and remained within a 7 seconds accuracy. The most stressing conditions of 5 KTS headwind or tailwind remained within a 9 seconds accuracy. This effect of wind on time performance was expected as the TEMO algorithm does not use wind information when calculating the trajectories. Hence, the acting wind affects the aircraft ground speed and flight-path angle resulting in the observed time and energy deviations. The results showed that an increasing wind estimation error reduces the time accuracy. This conclusion was confirmed by a rank correlation analysis for the time deviation at the IAF and the wind estimation error ($\tau = 0.497, p < 0.001$). The introduced time error has only a minor negative correlation with the time deviation ($\tau = -0.177, p < 0.001$).

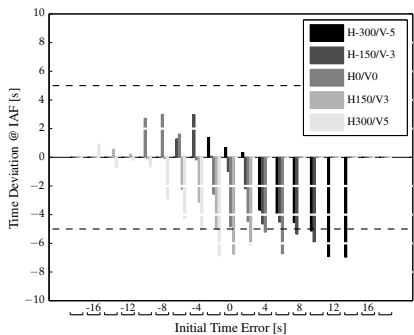
The scenarios exceeding the 5 second RTP result from early replans that absorbed the planning time window, Δt , to obtain an energy-neutral trajectory. Therefore, only a relatively small time deviation from this trajectory results in a total time deviation at the IAF in excess of 5 seconds. In combination with this, the algorithm often performed an unsuccessful energy-neutral replan while the aircraft was close to the IAF, while in other scenarios the time boundary was exceeded while the aircraft was too close to the IAF and thus did not trigger a replan. In these cases the aircraft continued flying the old energy-neutral trajectory resulting an increased time error until the aircraft passed the IAF.

The time control space of energy-neutral trajectories is shown in Table 3-5. This table indicates which time errors resulted in energy-neutral trajectories for a combination of energy and wind estimation errors. Overall, the control space was approximately 16 seconds for the 'no wind' scenarios. Furthermore, the initial energy error and wind error shift the time control space as a negative time error causes the aircraft to find only valid trajectories that arrive later at the IAF and a headwind, as to be expected, causes the aircraft to arrive later as well.

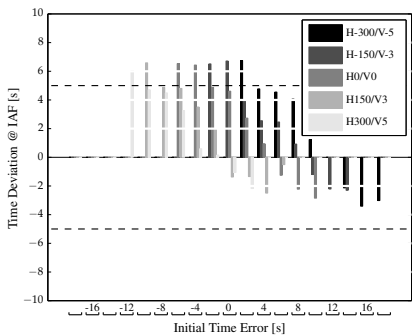
The aircraft passed the IAF at an altitude of FL 135 in the scenario without errors. The errors required replanning of the nominal trajectory which resulted in the aircraft passing the IAF between FL 123 and FL 147. As to be expected, a tailwind caused a relatively high crossing at the IAF ($\tau = -0.454, p < 0.001$) while arriving early (negative time error) caused a rather low altitude at the IAF ($\tau = 0.209, p < 0.001$) as the aircraft pitches down to gain speed.



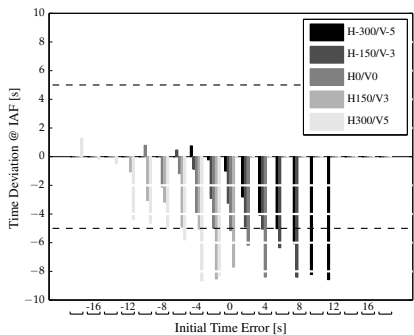
(a) Wind Estimation Error = 0 KTS.



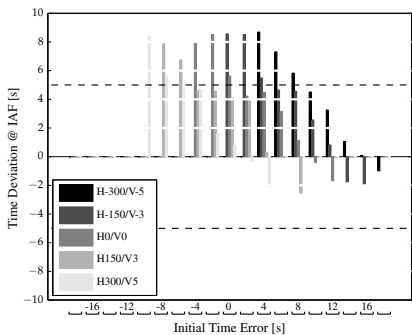
(b) Wind Estimation Error = -3 KTS.



(c) Wind Estimation Error = +3 KTS.



(d) Wind Estimation Error = -5 KTS.



(e) Wind Estimation Error = +5 KTS.

FIGURE 3-8: Time deviation at the IAF for various error scenarios and additional thrust and speedbrakes restricted.

TABLE 3-5: Combination of errors that yield valid energy-neutral trajectories at ToD and pass the IAF within the RTP.

	H-300/V-5	H-150/V-3	H0/V0	H150/V3	H300/V5
W+5	+10 to +18 (range 8 [s])	+6 to +16 (range 10 [s])	+2 to +12 (range 10 [s])	-4 to +8 (range 12 [s])	-6 to +4 (range 10 [s])
W+3	+4 to +18 (range 14 [s])	+2 to +14 (range 12 [s])	-2 to +10 (range 12 [s])	-8 to +6 (range 14 [s])	-10 to +2 (range 12 [s])
W0	0 to +16 (range 16 [s])	-4 to +12 (range 16 [s])	-8 to +8 (range 16 [s])	-12 to +4 (range 16 [s])	-14 to 0 (range 14 [s])
W-3	-2 to +8 (range 10 [s])	-6 to +6 (range 12 [s])	-10 to +2 (range 12 [s])	-14 to -2 (range 12 [s])	-16 to -6 (range 10 [s])
W-5	-4 to +6 (range 10 [s])	-6 to +2 (range 8 [s])	-2 to -10 (range 8 [s])	-12 to -4 (range 8 [s])	-18 to -8 (range 10 [s])

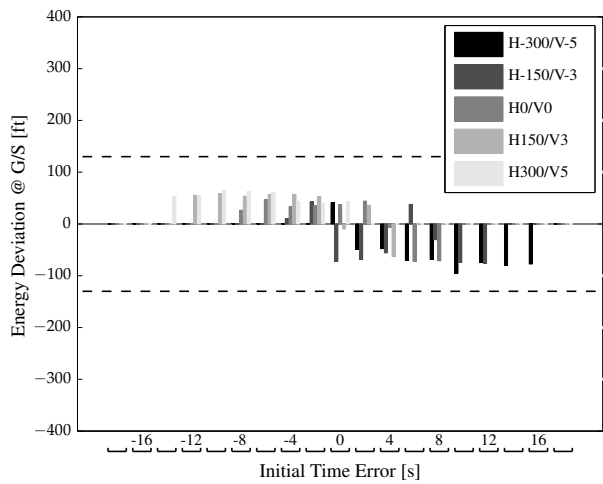
When the aircraft guidance starts to intercept the glideslope, the autopilot switches from SOE to POE control. During this transition, any sustained energy deviation is automatically corrected for using thrust or speedbrakes to remain flying the calibrated airspeed profile whilst correcting the energy deviation and intercepting the glideslope. The amount of energy deviation that needed to be corrected at glideslope intercept is shown in Figure 3-9. Replanning occurs only up to the localizer intercept point, at which the energy boundary is ± 130 ft, see Table 3-1. Hence, after localizer intercept, the energy deviation could continue to grow until the glideslope is intercepted using thrust or speedbrakes.

Due to the introduced errors, the aircraft starts to intercept the glideslope between 2,300 ft and 4,640 ft and 8.8 and 13.4 NM from the runway threshold, while without errors the aircraft would intercept the glideslope at 3,500 ft and 10.7 NM from the runway. Similar to the altitude at which the IAF was crossed, the energy deviation is primarily related to the wind estimation error ($\tau = -0.810, p < 0.001$), causing larger decelerations for stronger headwinds resulting from different speeds. The time error ($\tau = 0.222, p < 0.01$) also affects the energy deviation at glideslope intercept.

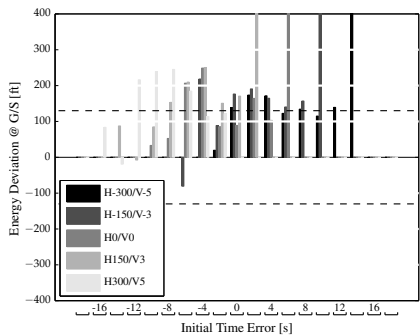
Figure 3-9 shows that many scenarios exceed the 130 ft allowable energy deviation, active at localizer intercept, resulting from rejected replans. Furthermore, replanning was disabled after passing the localizer intercept point and the energy deviation is corrected while the autopilot guides the aircraft towards the glideslope. Hence, between localizer and glideslope intercept, no action was performed to correct time or energy deviations. If thrust or speedbrakes use would have been available during this replan, the energy deviation at this point would likely be corrected. In this case, a replan could find a trajectory that would potentially be more environmentally-friendly using thrust and speedbrakes at higher altitudes during descent than at this last moment at glideslope intercept, close to the ground.

The energy error at ToD had no effect on any of the previously discussed metrics as these errors were corrected using a first replan after passing ToD and were too small to cause significant effects farther along the trajectory.

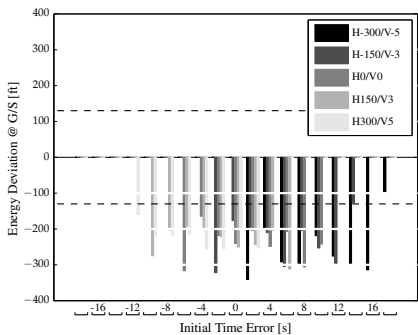
Environmental impact Fuel use between 110 NM from the runway at cruise level and the runway threshold was determined for all 217 successful simulations. Since in these



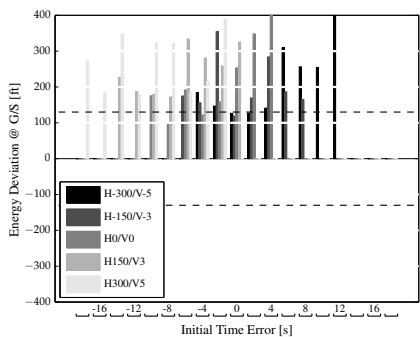
(a) Wind Estimation Error = 0 KTS.



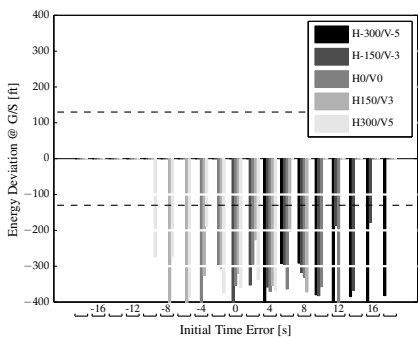
(b) Wind Estimation Error = -3 KTS.



(c) Wind Estimation Error = +3 KTS.



(d) Wind Estimation Error = -5 KTS.



(e) Wind Estimation Error = +5 KTS.

FIGURE 3-9: Energy deviation at glideslope intercept for various error scenarios and additional thrust and speedbrakes restricted.

simulations a time constraint was only active at the IAF, the time error shows to have only a minor positive correlation ($\tau = 0.169, p < 0.001$) with the amount of fuel used. As to be expected, the wind estimation error has a large positive correlation ($\tau = 0.793, p < 0.001$) on the amount of fuel used. As thrust could not be used down to the glideslope, flight duration ($\tau = 0.859, p < 0.001$) shows a major effect on fuel used.

Although the aircraft flies energy-neutral trajectories in all 217 simulations, the sustained deviations and energy-management strategies affect noise and emissions. The 65 dB contour area ranges from 133 km² to 163 km² while the 75 dB area varies between 18.7 km² and 24.7 km². The wind estimation error shows a correlation with the 65 dB SEL noise contour area ($\tau = 0.558, p < 0.001$) and 75 dB area ($\tau = 0.526, p < 0.001$) while the time error shows only a minor correlation for the 65 dB area ($\tau = 0.235, p < 0.001$) and 75 dB area ($\tau = 0.191, p < 0.001$). Both wind estimation and time errors lead to an energy deviation at glideslope intercept which was corrected using thrust when the aircraft was below path. The wind estimation error affected this location of planned glideslope intercept ($\tau = -0.321, p < 0.001$). This additional thrust also lead to larger noise contour areas, as indicated by the rank correlation analysis of additional thrust from glideslope intercept down to the runway and the 75 dB area ($\tau = 0.497, p < 0.001$). Furthermore, the acting wind affects the aircraft groundspeed and hence the duration of the final segment as discussed earlier.

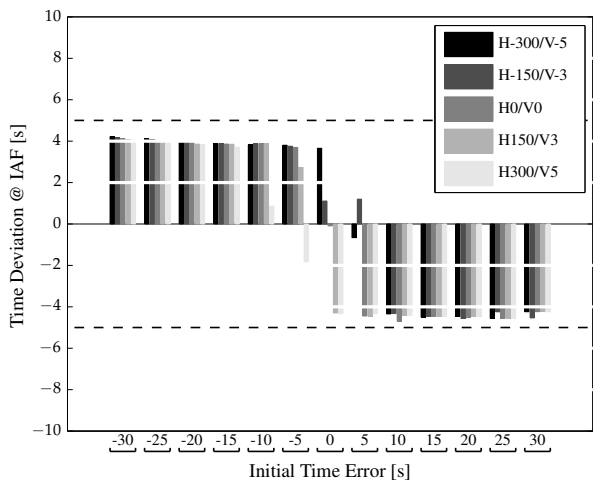
Similar results are found for the NO_x emissions, which are also affected by the introduced wind estimation error ($\tau = 0.883, p < 0.001$) and time error ($\tau = 0.195, p < 0.001$). The wind estimation error ($\tau = 0.849, p < 0.001$) and time error ($\tau = 0.191, p < 0.001$) both affect the amount of CO₂ emitted below 3,000 ft.

Scenarios with minimum thrust and speedbrakes

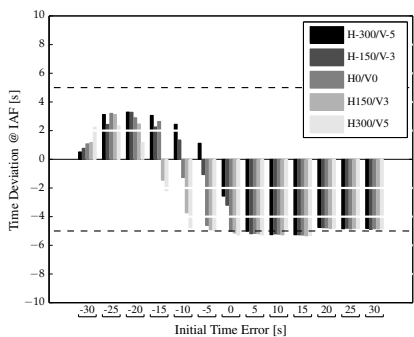
In total, 325 scenarios were simulated with equal initial conditions and errors introduced at ToD. During these simulations, the TEMO algorithm could plan the use of thrust or speedbrakes to correct these errors. The results of these trajectories are analyzed in this section and are categorized by the wind estimation errors. All 325 simulations were stabilized at 1,000 ft.

TEMO performance The time deviations at the IAF for the scenarios that could use thrust or speedbrakes are shown in Figure 3-10. All scenarios were successful and the time deviations remained within the 5 seconds RTP for the scenarios where no wind error was present. Some scenarios with a headwind or tailwind of 5 KTS exceeded the 5 seconds RTP slightly, but showed improved time performance compared with similar restricted use of thrust and speedbrake scenarios. The most stressing conditions of 10 KTS head- or tailwind achieved an 8 and 7 seconds accuracy, respectively.

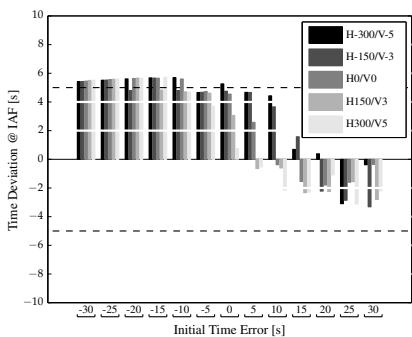
The wind estimation error ($\tau = 0.638, p < 0.001$) and time error ($\tau = -0.361, p < 0.001$) both affect the time deviation at the IAF. The negative correlation of the time error and time deviation of the IAF shows that for earlier CTAs, the actual deviation at the IAF was often slightly later. This shows that the TEMO algorithm uses the planning time window



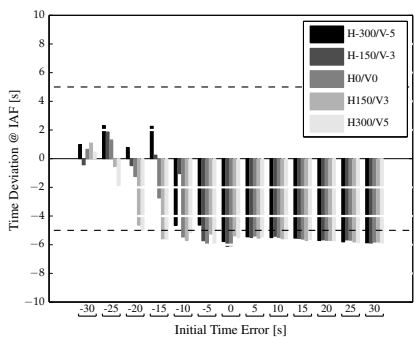
(a) Wind Estimation Error = 0 KTS.



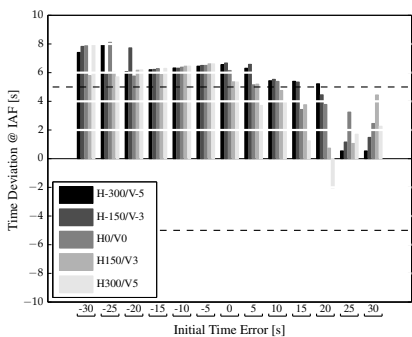
(b) Wind Estimation Error = -5 KTS.



(c) Wind Estimation Error = +5 KTS.



(d) Wind Estimation Error = -10 KTS.



(e) Wind Estimation Error = +10 KTS.

FIGURE 3-10: Time deviation at the IAF for various error scenarios using thrust and speed-brakes.

(Eq. (3-3)) to reduce the actual time offset in favor of minimizing thrust and speedbrake use.

Note that the largest time deviations at the IAF (+8 seconds, i.e., arriving too late) occur for headwind estimation errors in combination with large, negative time errors (i.e., arrive earlier). Both the headwind and introduced time error lead to an increased speed schedule, which is often limited by aircraft maximum operational speeds during the descent towards the IAF. Also, the calculated trajectories contain shallow segments — to maximize true airspeed — which is limited by the no-climb constraint. The combination of these factors caused that a sustained time deviation could not be corrected close to the IAF.

Other scenarios, where the time deviation at the IAF typically remained within ± 6.7 seconds, are the result of replans that absorb the planning time window, leaving too little room for additional deviations. Particularly, since replanning is not initiated when the aircraft is near the IAF, the wind estimation error will cause additional deviations. These results show that the planning time window should not exceed 2.3 seconds to allow for a 2.7 seconds of time deviations due to a wind estimation error. Alternatively, the RTP could be relaxed to 10 seconds to allow for a planning time window of 7.3 seconds.

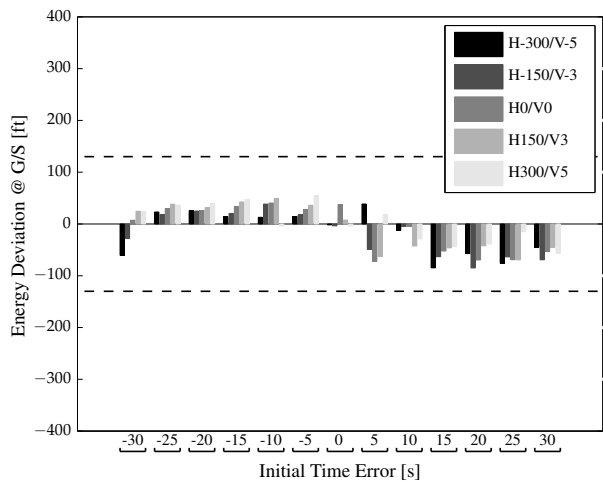
The aircraft passed the IAF at a minimum altitude of FL 111 and at a maximum altitude of FL 240. The time ($\tau = 0.169, p < 0.001$) and wind error ($\tau = -0.178, p < 0.001$) show a minor correlation with the altitude at the IAF. The maximum altitude at the IAF is relatively high and is a result of the aircraft flying level for an extended period to maintain a high True Airspeed (TAS) to arrive earlier whilst experiencing a strong headwind.

The energy deviations at glideslope intercept are shown in Figure 3-11. Compared to the earlier runs where thrust or speedbrakes were restricted, the deviations for the scenarios with thrust and speedbrakes are smaller as they have been corrected earlier during the descent by an energy-optimal replan.

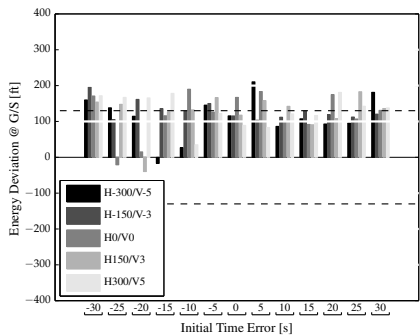
However, for the scenarios with a wind estimation error, certain scenarios still exceed the 130 ft energy boundary that is active at the moment of localizer intercept. This happens for two reasons: First, the error was below the energy boundary at localizer intercept but continued to grow until the glideslope was intercepted as during this segment replanning is disabled. Second, the last replan that was executed before the localizer was intercepted, was unsuccessful due to the limited remaining control space.

Eight scenarios of the 10 KTS tailwind simulations showed energy deviations at glideslope intercept in excess of 300 ft. In these simulations, the combination of introduced errors resulted in rejected trajectories after passing the IAF when the aircraft decelerates towards the localizer intercept speed, phase 4 and 5 of Table 3-2. The deceleration is restricted by an energy share factor which proved to be limiting the aircraft's deceleration in these tailwind cases.

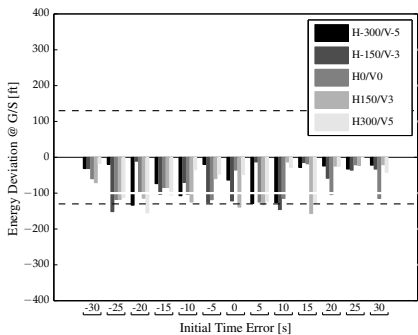
Also, in these simulations the wind estimation error affects the energy deviation at glideslope intercept ($\tau = -0.747, p < 0.001$), while the time error shows no significant correlation with the energy deviation at glideslope intercept. This is the result of successful replans that yield energy-optimal trajectories after passing the IAF. Additional thrust ($\tau = -0.667, p < 0.001$) was used to reduce a negative energy deviation and speedbrakes were used to reduce a positive energy deviation ($\tau = 0.685, p < 0.001$) at glideslope intercept.



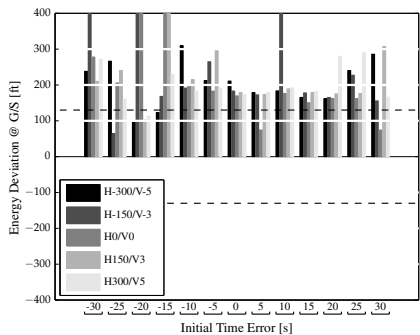
(a) Wind Estimation Error = 0 KTS.



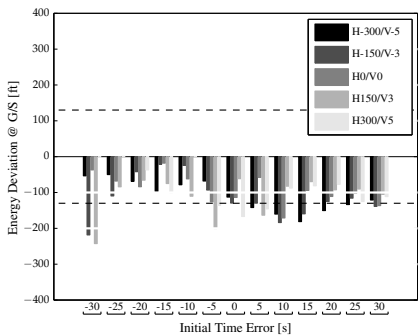
(b) Wind Estimation Error = -5 KTS.



(c) Wind Estimation Error = +5 KTS.



(d) Wind Estimation Error = -10 KTS.



(e) Wind Estimation Error = +10 KTS.

FIGURE 3-11: Energy deviation at glideslope intercept for various error scenarios using thrust and speedbrakes.

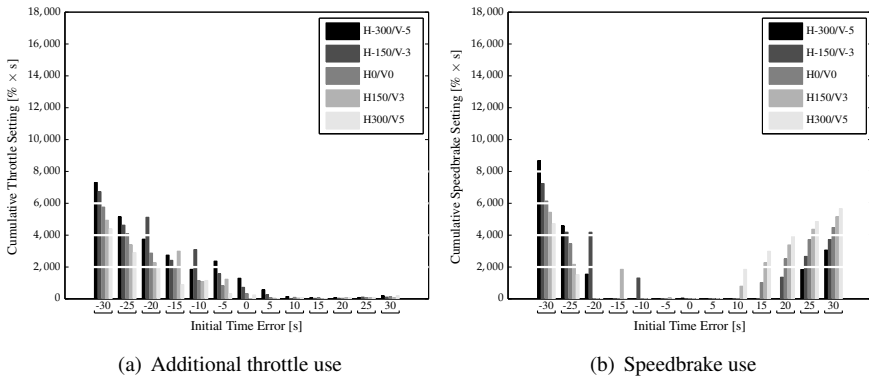


FIGURE 3-12: Cumulative additional throttle and speedbrakes use from ToD till glideslope intercept for 5 KTS headwind estimation errors.

Figure 3-12 indicates the cumulative use of additional throttle (above idle) and use of speedbrakes between ToD and the glideslope intercept. As can be expected, earlier CTAs at the IAF result in the use of thrust ($\tau = -0.459, p < 0.001$) and later CTAs result in the use of speedbrakes ($\tau = 0.298, p < 0.001$). To arrive earlier, the aircraft requires a higher speed which results in increased drag and hence a lower energy state. Hence, thrust is required to correct this lower energy state.

Interestingly, speedbrakes are also required for earlier CTAs. In these runs, the aircraft initially accelerates using thrust but requires speedbrakes to decelerate rapidly to satisfy the constraint of 250 KTS below FL 100. As expected, thrust and speedbrakes are not used simultaneously but occurs as speedbrakes are required to decelerate — and reduce the higher energy state — after the CTA at the IAF is reached at a high speed to adhere to the speed-constraint at FL 100. This reduces the correlation between speedbrakes and time error.

Environmental impact In these scenarios, the time error shows a slight negative correlation with fuel use ($\tau = -0.127, p < 0.001$), resulting from energy-optimal replans that used thrust to correct the time error. The wind estimation error showed a strong positive correlation with the amount of fuel used ($\tau = 0.829, p < 0.001$) as energy was added to compensate for prevailing headwinds.

The wind estimation error affects the size of 65 dB ($\tau = 0.373, p < 0.001$) and 75 dB SEL ($\tau = 0.484, p < 0.001$) contour areas. In these energy-optimal scenarios, the time error showed only a significant, though minor, correlation ($\tau = 0.217, p < 0.001$) with the 65 dB noise contour area. This minor correlation of the time error on the noise contours is not surprising as no CTA was active at the runway and thus no replans were initiated to correct time deviations.

The dimensions of the contour areas have slightly changed compared to the energy restricted scenarios as the 65 dB contour area ranges between 139 km² and 166 km² and the

75 dB area ranges between 19.1 km² and 22.7 km². The change of area dimensions are the result of thrust or speedbrake use earlier during descent to correct energy deviations. Consequently, the energy deviation at the glideslope intercept is reduced and hence less additional thrust is required to intercept the glideslope.

Gaseous emissions were primarily affected by the introduced wind estimation error for NO_x ($\tau = 0.896, p < 0.001$) and CO₂ ($\tau = 0.896, p < 0.001$). Contrary to the restricted thrust and speedbrakes simulations, these energy-optimal simulations show no significant correlation between NO_x or CO₂ and the time error. Since in these last scenarios, deviations can be corrected using thrust and speedbrakes, more replan calculations between IAF and localizer were successful. As these replans are independent of the time error, the minor correlation found for the energy-neutral scenarios have disappeared.

3-4-3 Simulation Study 3: Strategic vs. Hybrid Replanning

As shown above, a wind estimation error causes multiple replans when only strategic replanning is used. For this reason, a tactical controller is implemented that actively minimizes time deviations. Results of hybrid replanning and strategic replanning simulations were compared for three wind scenarios (tailwind, headwind, no wind).

In these three scenarios, the aircraft receives a CTA at the IAF *and* runway threshold. These constraints assure that both replan methods minimize time errors throughout the entire descent. However, the TEMO algorithm often did not find a valid trajectory between IAF and runway. For this reason, the deviation boundaries and RTP values have been relaxed as seen in Table 3-6.

TABLE 3-6: TEMO deviation boundaries and Required Time Performance (RTP).

Active Waypoint	RTP [s]	Error Boundary					
		Top of Descent		IAF		Runway Threshold	
		Time [s]	Energy [ft]	Time [s]	Energy [ft]	Time [s]	Energy [ft]
IAF	10	±5	±1,000	±4	±500	-	-
Runway	4	-	-	-	±500	±2	±50

Hybrid replanning actively uses energy management to correct time deviations by exchanging potential energy for kinetic energy through Speed-on-Elevator (SOE). Moreover, a replan is performed 10 NM prior to the IAF to correct sustained energy deviations in excess of ± 100 ft. Both replanning and the tactical controller are disabled once the aircraft intercepts the localizer at 15 NM from the runway. After this point, the aircraft flies the latest calculated trajectory and uses guidance logic to intercept the glideslope.

As a result, the tactical controller is expected to improve time accuracy as it continuously nullifies the time deviations while strategic replanning allows deviations to evolve within boundaries. However, the question remains whether this approach increases the environmental footprint.

Table 3-7 provides a detailed comparison of the performance and environmental metrics between the two replanning methods.

TABLE 3-7: Comparison of performance metrics for strategic and hybrid replanning.

		Wind Estimation Error					
		Wind = 0 KTS		Wind = -5 KTS		Wind = 5 KTS	
		Strategic	Hybrid	Strategic	Hybrid	Strategic	Hybrid
IAF	Time Deviation [s]	-0.0906	-0.0276	-8.4019	-0.7640	6.8996	2.9414
	Energy Deviation [ft]	45.48	47.15	322.14	150.92	-252.23	-130.67
	Altitude [FL]	135.00	135.06	137.00	145.56	129.66	135.44
	Added Throttle [% \times s]	14.92	15.24	15.63	35.18	14.14	38.66
	Added Speedbrakes [% \times s]	0	0	0	0	0	0
	Number of replans	0	0	1	1	2	1
	Number of rejects	0	0	0	0	0	0
Localizer	Time Deviation [s]	-0.3286	0.0768	-6.2344	-0.4681	5.2587	0.4773
	Energy Deviation [ft]	37.16	52.52	110.93	424.32	-104.25	-647.19
	Altitude [FL]	49.47	49.61	50.74	53.72	47.28	42.09
	Added Throttle [% \times s]	14.92	15.24	15.63	35.18	756.92	38.66
	Added Speedbrakes [% \times s]	0	0	0.09	0	9.43	0
	Number of replans	0	0	11	1	11	1
	Number of rejects	0	0	8	0	8	0
Glideslope	Time Deviation [s]	-0.3681	-0.0543	-10.1598	-3.7221	5.3187	0.5586
	Energy Deviation [ft]	37.41	52.16	170.06	12.01	-102.82	-642.58
	Distance to RWY [NM]	10.73	10.73	8.83	8.83	14.91	14.91
	Altitude [FL]	35.04	35.20	30.33	28.98	47.11	42.03
Runway	Time Deviation [s]	-0.4764	-0.1600	-18.8339	-12.7876	18.1712	13.4925
	Added Throttle [% \times s \times 100]	21.60	21.65	20.13	21.17	35.16	33.56
	Added Speedbrakes [% \times s \times 100]	49.04	50.75	59.01	28.15	2.24	2.11
Environment	65 dB Area [km ²]	150.59	150.17	145.90	134.59	158.90	167.21
	75 dB Area [km ²]	21.22	21.17	21.09	21.57	21.53	21.50
	Fuel Used [kg]	262.48	262.57	256.69	256.62	269.41	278.79
	NO _x [kg]	0.5063	0.5084	0.4531	0.4583	0.5608	0.5604
	CO ₂ [kg]	225.55	225.69	207.55	208.20	241.97	242.26

The results show that the hybrid approach achieved smaller time deviations at the IAF compared to the strategic replanning approach. The tactical controller showed improved time accuracy at the IAF when a wind estimation error is present. The time deviation at the IAF for the hybrid scenario in headwind is the result of the replan prior to the IAF that absorbed part of the replan time window. In both wind scenarios and strategic replanning, the time deviation boundary was exceeded near the IAF when replanning is disabled and no corrective replan was performed. However, since the time boundary was stricter than the RTP, the aircraft still adhered to the RTP.

When a wind estimation error was present, the tactical controller corrects time deviations at cruise level using thrust, while strategic replanning did not correct the error until the descent was started. Hence, the increased added throttle use before the IAF for hybrid replanning resulted from the engines spooling down after ToD. Trajectories flown with hybrid replanning required less speedbrakes compared to strategic replanning since the controller does not use speedbrakes. The large energy deviations for strategic replanning were the result of rejected replans – resulting from excessive time deviations — and relaxed energy boundaries between ToD and IAF compared with scenarios in the previous discussed studies. The observed energy deviations for hybrid replanning were the result of SOE control to correct time deviations.

The time deviation at the runway exceeded the RTP value of 4 seconds for all scenarios with a wind present. This results from disabled replanning (either tactical, or strategic) after intercepting the localizer. However, hybrid replanning showed smallest deviations since strategic replanning often did not find trajectories (rejects) prior to the glideslope and hence was less effective in minimizing time deviations.

Interestingly, the energy deviation for the tailwind scenario using hybrid replanning reduces between localizer and glideslope intercept. This results from the aircraft reverting from tactical speeds to planned speeds. The aircraft was flying slower than planned to counteract the tailwind resulting in excess potential energy (higher altitude). Moreover, the lower speed causes earlier selection of flaps, which increases the aircraft drag and energy rate. Furthermore, at the localizer intercept point, the aircraft transitions to the (higher) planned speed exchanging potential energy for kinetic energy which reduces the altitude deviation. The reverse does not occur in the headwind scenario since the aircraft would select flaps later due to higher speeds and intercepts the glideslope almost instantly after intercepting the localizer to reduce speed along the glideslope.

The largest difference in environmental affect was found for the 65 dB SEL contour. Since hybrid replanning uses SOE to correct time deviations, the flown vertical profile deviated from the planned profile. In case of a headwind, descents using hybrid replanning flew a relatively low trajectory because the aircraft pitched down to gain speed. This resulted in an increased 65 dB area compared with strategic replanning. On the other hand, for a tailwind error, the 65 dB area was smaller due to pitch-up commands to reduce speed. Moreover, hybrid replanning required more fuel for the headwind scenario as it arrived lower than planned when intercepting the glideslope. Consequently, the aircraft required more thrust to correct this deviation. During glideslope intercept, the guidance also commanded an undesired short climb resulting in increased fuel use.

3-4-4 General Discussion

The combined errors simulations show that under the most stressing initial conditions and given a moderate wind estimation error (3–5 KTS), time errors at the IAF in the range of 8–10 seconds can be corrected with energy management only. This time window improves to 16 seconds for no wind estimation errors. When thrust and speedbrakes are allowed, the TEMO system was successful for all time errors, with the exception of some strong headwind conditions in which the headwind errors in combination with large negative time errors result in time deviations in excess of the 5 seconds RTP. From these runs it was also concluded that the combination of the planning time window (4 s) and deviation boundary (0 sec at the IAF) should be set to a of maximum of 2.3 seconds instead of the currently chosen 4 seconds. This ensures that the actual time error will not exceed the 5 seconds RTP when the aircraft approaches the IAF and replanning is disabled.

Energy-neutral trajectories are only found down to the glideslope intercept where often thrust or speedbrakes are required to intercept the glideslope and correct an energy error. When a wind estimation error is present, more energy is added or removed than expected which potentially leads to situations where the TEMO algorithm cannot find an energy-neutral trajectory. When thrust and speedbrakes are allowed, the energy deviation at glideslope intercept is reduced at the cost of thrust or speedbrakes use earlier during descents.

In strong tailwind runs, the unanticipated wind in combination with unfavorable conditions (already high on energy to meet an early time constraint) resulted in rejected replans as trajectory constrains during deceleration after passing the IAF were limiting. These rejects

allowed the energy deviations to grow until a replan was successful. The energy deviations at glideslope intercept could be reduced by extending the replan activation area from localizer to glideslope intercept and redefining the trajectory constraints. Alternatively, use could be made of a speed-controller between localizer intercept and glideslope intercept to minimize the errors in this short segment. Furthermore, using estimated wind data [46] during strategic replanning could reduce the wind estimation error and consequently reduce path deviations.

The results of this experiment show that wind estimation errors were the primary cause of time and energy deviations while time deviations show causality but to a lesser extent. Energy errors at ToD were corrected through a single replan and causes no further disturbance once the replan was successful. The study also shows that the wind estimation error results in multiple replans as the error continues to grow after each successful replan as it remains present as a steady-state error. A tactical controller, such as the speed-controller in the hybrid replanning approach, reduces the number of replans caused by a wind estimation error.

The tactical controller proved to achieve improved time accuracy at the IAF, even when a wind estimation error was present. When no wind estimation error is present, the differences in TEMO performance and environmental impact are small. The tactical controller thus serves as a good method to correct steady-state errors. Furthermore, hybrid replanning required less replans compared to full strategic replanning but showed large energy deviations upon localizer intercept. By defining stricter energy boundaries for hybrid replanning or using full tactical replanning, these large energy deviations could be minimized. The results of these simulations also show that defining a stricter time deviation boundary than the actual RTP assures that the aircraft adheres to the RTP since more room is available for deviations when replanning is disabled.

When a time constraint is active at the runway, the required time accuracy was not achieved by either replan method in the presence of wind estimation errors. These deviations resulted from disabled replanning after intercepting the localizer. Hence, effort should be put in reducing wind estimation errors. Additionally, the required accuracy at the runway could be relaxed while relative time constraints using IM could provide increased robustness to wind estimation errors [47]. Alternatively, a new degree of freedom, e.g., thrust, speed-brakes or flap-scheduling [12], could be used during descent down the glideslope.

In this experiment, pilot actions were modeled using a zero-delay response model, however, in real-life, this assumption is no longer valid and the effect of variations in pilot response is investigated in a next experiment. This experiment evaluates the role and effects of the human pilot during TEMO descents.

3-5 Conclusions

Time and Energy Managed Operations (TEMO) is a new concept that allows engine-idle descents from Top of Descent (ToD) down to the stabilization altitude using energy management. The results show that TEMO satisfies required time accuracies and respects current

operational restrictions when external disturbances are not present. Compared to conventional step-down descents, TEMO reduces the 65 dB and 75 dB Sound Exposure Level (SEL) contour areas and fuel use during descent. Combined errors simulations show that under the most stressing initial conditions and a moderate wind estimation error (3–5 KTS), time errors at the Initial Approach Fix (IAF) in the range of 8–10 seconds can be corrected using energy management only. Furthermore, this experiment showed that wind estimation errors primarily affect time and energy deviations while introduced time errors cause deviations but to a lesser extent. The effects of wind estimation errors were effectively minimized using a tactical controller, reducing time deviations with minimum impact to the environmental. Disabling corrective actions after intercepting the localizer lead to excessive time deviations at the runway when wind estimation errors are present.

Acknowledgments

The research leading to these results received funding from the European Union's Seventh Framework Programme (FP7/2007-2013) through the Clean Sky Joint Technology Initiative under Grant Agreement no. CSJU-GAM-SGO-2008-001.

References

- [1] **SESAR**. European ATM Master Plan. Tech. Rep. Edition 2, EUROCONTROL, 2012. SESAR JU & SESAR Work Package C and Partners.
- [2] **NextGen Office**. FAA's NextGen Implementation Plan 2012. Tech. rep., FAA, 800 Independence Avenue, Washington, DC, 2012.
- [3] **EUROCONTROL**. Long-Term Forecast: IFR Flight Movements 2010-2030. Tech. Rep. CND/STATFOR Doc415, EUROCONTROL, 2010.
- [4] **SESAR**. Air Transport Framework: The Current Situation. Tech. Rep. SESAR TR DLM-0602-001-03-00, EUROCONTROL, 2006.
- [5] **ICAO**. *Guidance on the Balanced Approach to Aircraft Noise - Doc 9829 AN/451*. International Civil Aviation Organization, Montreal, Canada, second edition edn., 2008.
- [6] **S. Hartjes, H. G. Visser, and S. J. Hebly**. Optimization of RNAV Noise and Emission Abatement Departure Procedures. *The Aeronautical Journal*, 114(1162), 2010.
- [7] **E. P. Dinges**. Determining the Environmental Benefits of Implementing Continuous Descent Approach Procedures. In: *Proceedings of the 7th USA/Europe Air Traffic Management Research and Development Seminar, Barcelona, July 2–5*, pp. 1–10, 2007.
- [8] **ICAO**. *Continuous Descent Operations (CDO) Manual - Doc 9931 AN/476*. International Civil Aviation Organization, Montreal, Canada, 2010.

- [9] **J.-P. B. Clarke, N. T. Ho, L. Ren, J. A. Brown, K. R. Elmer, and K.-O. Tong.** Continuous Descent Approach: Design and Flight Test for Louisville International Airport. *Journal of Aircraft*, 41(5), 1054–1066, 2004. doi:10.2514/1.5572.
- [10] **J. L. De Prins, K. F. M. Schippers, M. Mulder, M. M. Van Paassen, A. C. In 't Veld, and J.-P. B. Clarke.** Enhanced Self-Spacing Algorithm for Three-Degree Decelerating Approaches. *Journal of Guidance, Control and Dynamics*, 30(2), 576–590, 2007. doi:10.2514/1.24542.
- [11] **A. M. P. De Leege, A. C. In 't Veld, M. Mulder, and M. M. Van Paassen.** Three-Degree Decelerating Approaches in High Density Arrival Streams. *Journal of Aircraft*, 46(5), 1681–1691, 2009. doi:10.2514/1.42420.
- [12] **P. M. A. De Jong, A. C. In 't Veld, A. M. P. De Leege, M. M. Van Paassen, and M. Mulder.** Control Space Analysis of Three-Degree Decelerating Approaches at Amsterdam Airport Schiphol. In: *Proceedings of the AIAA Guidance, Navigation and Control Conference, Toronto, Ontario Canada, August 2–5*, AIAA 2010-8454, pp. 1–20. American Institute of Aeronautics and Astronautics, 2010. doi:10.2514/6.2010-8454.
- [13] **P. M. A. De Jong, K. De Vos, C. Borst, M. M. Van Paassen, and M. Mulder.** Time-based Spacing for 4D Approaches using Speed-Profiles. In: *Proceedings of the AIAA Guidance, Navigation and Control Conference, Portland, Oregon, August 8–11*, AIAA 2011-6215, pp. 1–14. American Institute of Aeronautics and Astronautics, 2011. doi:10.2514/6.2011-6215.
- [14] **R. J. De Muynck, L. Verhoeff, R. P. M. Verhoeven, and N. De Gelder.** Enabling Technology Evaluation for Efficient Continuous Descent Approaches. In: **I. Grant**, ed., *Proceedings of the 26th Congress of the International Council of the Aeronautical Sciences including the 8th AIAA Aviation Technology, Integration, and Operations (ATIO) Conference, Anchorage, Alaska, 14–19 September*, ICAS 2008-8.9.2, pp. 1–9, 2008.
- [15] **H. Lenz and B. Korn.** Enabling Advanced Continuous Descent Approaches – Results of the European Project OPTIMAL. In: *Proceedings of the 28th Digital Avionics Systems Conference, Orlando, Florida, October 23–29*, pp. 2.C.3–1–2.C.3–10. IEEE/AIAA, 2009. doi:10.1109/DASC.2009.5347546.
- [16] **R. A. Coppensbarger, R. Lanier, D. N. Sweet, and S. Dorsky.** Design and Development of the En Route Descent Advisor (EDA) for Conflict-Free Arrival Metering. In: *Proceedings of the AIAA Guidance, Navigation, and Control Conference and Exhibit, Providence, Rhode Island, August 16–19*, AIAA 2004-4875, pp. 1–19. American Institute of Aeronautics and Astronautics, 2004. doi:10.2514/6.2004-4875.
- [17] **R. A. Coppensbarger, R. W. Mead, and D. N. Sweet.** Field Evaluation of the Tailored Arrivals Concept for Datalink-Enabled Continuous Descent Approach. *Journal of Aircraft*, 46(4), 1200–1209, 2009. doi:10.2514/1.39795.

- [18] **T. Miquel, H. Manzoni, F. Legrand, D. Martin, and M. Millischer.** 4D Green Approach Trajectory: Illustrative Assessment On Toulouse Approach. In: *Proceedings of the AIAA Guidance, Navigation, and Control Conference, Toronto, Ontario, Canada, August 2–5*, AIAA 2010-8456, pp. 1—15. American Institute of Aeronautics and Astronautics, 2010. doi:10.2514/6.2010-8456.
- [19] **M. Kaiser, M. Schultz, and H. Fricke.** Automated 4D Descent Path Optimization using the Enhanced Trajectory Prediction Model (ETPM). In: *Proceedings of the 5th International Conference on Research in Air Transportation — ICRAT 2012, Berkeley, California, May 22–25*, pp. 1–8, 2012.
- [20] **D. H. Williams, R. M. Oseguera-Lohr, and E. T. Lewis.** Design and Testing of a Low Noise Flight Guidance Concept. Technical Memorandum NASA/TM-2004-213516, National Aeronautics and Space Administration, Langley Research Center, Hampton, Virginia 23681-2199, 2004.
- [21] **R. M. Oseguera-Lohr, D. H. Williams, and E. T. Lewis.** Crew Procedures for Continuous Descent Arrivals Using Conventional Guidance. Technical Memorandum NASA/TM-2007-214538, National Aeronautics and Space Administration, Langley Research Center, Hampton, Virginia 23681-2199, 2007.
- [22] **J. K. Klooster, K. D. Wickman, and O. F. Bleeker.** 4D Trajectory and Time-of-Arrival Control to Enable Continuous Descent Arrivals. In: *Proceedings of the AIAA Guidance, Navigation and Control Conference and Exhibit, Honolulu, Hawaii, August 18–21*, AIAA 2008-7402, pp. 1—17. American Institute of Aeronautics and Astronautics, 2008. doi:10.2514/6.2008-7402.
- [23] **D. Garrido-López, L. D’Alto, and R. Gomez Ledesma.** A Novel Four-Dimensional Guidance for Continuous Descent Approaches. In: *Proceedings of the 28th Digital Avionics Systems Conference, Orlando, Florida, October 23–29*, pp. 6.E.1–1–6.E.1–11. IEEE/AIAA, 2009. doi:10.1109/DASC.2009.5347433.
- [24] **J. L. De Prins and R. Gomez Ledesma.** Towards Time-based Continuous Descent Operations with Mixed 4D FMS Equipage. In: *Proceedings of the 11th AIAA Aviation Technology, Integration, and Operations (ATIO) Conference, Virginia Beach, Virginia, September 20–22*, AIAA 2011-7018, pp. 1–18. American Institute of Aeronautics and Astronautics, 2011. doi:10.2514/6.2011-7018.
- [25] **D. H. Williams, R. M. Oseguera-Lohr, and E. T. Lewis.** Energy Navigation: Simulation Evaluation and Benefit Analysis. Technical Publication NASA/TP-2011-217167, National Aeronautics and Space Administration, Langley Research Center, Hampton, Virginia 23681-2199, 2011.
- [26] **S. G. Park and J.-P. B. Clarke.** Vertical Trajectory Optimization for Continuous Descent Arrival Procedure. In: *Proceedings of the AIAA Guidance, Navigation and Control Conference, Minneapolis, Minnesota, August 13–16*, AIAA 2012-4757, pp. 1–19. American Institute of Aeronautics and Astronautics, 2012. doi:10.2514/6.2012-4757.

- [27] **T. S. Abbot.** A Brief History of Airborne Self-Spacing Concepts. Contractor Report NASA/CR-2009-215695, National Aeronautics and Space Administration, Langley Research Center, Hampton, Virginia 23681-2199, 2009.
- [28] **EUROCAE.** *Safety, Performance and Interoperability Requirements Document for Airborne Spacing - Flight Deck Interval Management (ASPA-FIM) - ED-195.* EUROCAE, 92240 Malakoff, France, 2011.
- [29] **S. Torres, J. K. Klooster, L. Ren, and M. Castillo-Effen.** Trajectory Synchronization between Air and Ground Trajectory Predictors. In: *Proceedings of the 30th Digital Avionics Systems Conference, Seattle, Washington, October 16-20t*, pp. 1E3-1-1E3-14. IEEE/AIAA, 2011. doi:10.1109/DASC.2011.6096175.
- [30] **N. T. Ho and J.-P. B. Clarke.** Methodology for Optimizing Parameters of Noise-Abatement Approach Procedures. *Journal of Aircraft*, 44(4), 1168-1176, 2007. doi: 10.2514/1.22292.
- [31] **J. K. Klooster, A. Del Amo, and P. Manzi.** Controlled Time-of-Arrival Flight Trials Results and Analysis. In: *Proceedings of the 8th USA/Europe Air Traffic Management Research and Development Seminar, Napa, California, June 29-July 2*, pp. 1-11, 2009.
- [32] **F. J. L. Bussink, J. J. Van der Laan, and P. M. A. De Jong.** Combining Flight-deck Interval Management with Continuous Descent Approaches in high density traffic and realistic wind conditions. In: *Proceedings of the AIAA Guidance, Navigation and Control Conference, Minneapolis, Minnesota, August 13-16*, AIAA 2012-4523, pp. 1-25. American Institute of Aeronautics and Astronautics, 2012. doi:10.2514/6.2012-4523.
- [33] **Y. Glina, S. Troxel, T. Reynolds, and M. McPartland.** Wind Information Requirements to Support Four Dimensional Trajectory-Based Operations. In: *Proceedings of the 12th AIAA Aviation Technology, Integration, and Operations (ATIO) Conference and 14th AIAA/ISSM, Indianapolis, Indiana, September 17-19*, AIAA 2012-5702, pp. 1-14. American Institute of Aeronautics and Astronautics, 2012. doi: 10.2514/6.2012-5702.
- [34] **S. Muresean.** Initial 4D - 4D Trajectory Data Link (4DTRAD) - Concept of Operations. Tech. rep., EUROCONTROL, Brussels, Belgium, 2008.
- [35] **Airbus.** *Flight Crew Operations Manual (Vol. 3)*, rev. 14 edn., 2002.
- [36] **A. V. Rao, D. A. Benson, C. L. Darby, M. A. Patterson, C. Francolin, and G. T. Huntington.** Algorithm 902: GPOPS, A MATLAB Software for Solving Multiple-Phase Optimal Control Problems Using the Gauss Pseudospectral Method. *ACM Transactions on Mathematical Software*, 37(2), 39, 2009. doi:10.1145/1731022.1731032. Article 22.

- [37] **A. V. Rao, D. A. Benson, C. L. Darby, C. Francolin, M. A. Patterson, I. Sanders, and G. T. Huntington.** *User Manual for GPOPS Version 3.3: A MATLAB Software for Solving Optimal Control Problems Using Pseudospectral Methods.* University of Florida, Gainesville, Florida, 2010.
- [38] **P. J. Van der Geest.** Validation of aircraft simulation models for the analysis of in-trail following dynamics - Deliverable D1 of the AMAAI project. Contract Report NLR-CR-2002-044, National Aerospace Laboratory, Amsterdam, The Netherlands, 2002.
- [39] **P. J. Van der Geest.** The AMAAI modelling toolset for the analysis of in-trail following dynamics - Deliverable D2: Description and User Guide. Contract Report NLR-CR-2002-112, National Aerospace Laboratory, Amsterdam, The Netherlands, 2002.
- [40] **P. M. A. De Jong, F. J. L. Bussink, N. De Gelder, R. P. M. Verhoeven, and M. Mulder.** Time and Energy Management during Descent and Approach for Aircraft. In: **D. Young and S. Saunders-Hodge,** eds., *Proceedings of the 5th International Conference on Research in Air Transportation — ICRAAT 2012, Berkeley, California, May 22–25*, pp. 1–6. FAA and EUROCONTROL, 2012.
- [41] **S. Hebly and E. Bloem.** Specification and Verification of the Cycle-2 NLR Noise Tool. Deliverable SGO-WP 3.1.2-NLR-SPEC-0153-C, National Aerospace Laboratory, Amsterdam, The Netherlands, 2011. WP 3.1.2-Models for the Optimization Framework (GATAC), System for Green Operations ITD.
- [42] Standard Method of Computing Noise Contours around Civil Airports. Tech. Rep. Document 29, ECAC/CEAC, 2005. 3rd Edition, Volume 1.
- [43] **R. L. Martin, C. A. Oncina, and J. P. Zeeben.** A simplified method for estimating aircraft engine emissions. In: **S. L. Baughcum, T. G. Tritz, S. C. Henderson, and D. C. Pickett,** eds., *Scheduled Civil Aircraft Emission Inventories for 1992: Database Development and Analysis - NASA Contractor Report 4700, April 1996*, pp. D1–D11. National Aeronautics and Space Administration, 1995. Reported as “Boeing Method 2” fuel flow methodology description in appendix D.
- [44] **M. Winther and K. Rypdal.** EMEP/EEA Air Pollutant Emission Inventory Guidebook. Tech. Rep. 1.A.3.a, 1.A.5.b, European Environment Agency, 2009. Updated December 2010.
- [45] **G. J. J. Ruijgrok and D. M. Van Paassen.** *Elements of Aircraft Pollution.* Delft University Press, P.O. Box 98 2600 MG Delft, The Netherlands, 2005.
- [46] **P. M. A. De Jong, J. J. Van der Laan, A. C. In ’t Veld, M. M. Van Paassen, and M. Mulder.** Wind Profile Estimation using Airborne Sensors. *Journal of Aircraft*, pp. 1–18, 2013. Submitted for publication.

- [47] **V. E. Houston** and **B. Barmore**. An Exploratory Study of Runway Arrival Procedures: Time-Based Arrival and Self-Spacing. In: *Proceedings of the 9th AIAA Aviation Technology, Integration, and Operations Conference (ATIO), Hilton Head, South Carolina, September 21–23*, AIAA 2009-7005, pp. 1–14. American Institute of Aeronautics and Astronautics, 2009.

HUMAN IN THE LOOP STUDY USING TEMO

In the previous chapter, Time and Energy Managed Operations (TEMO) was evaluated in a fully automated, fast-time study for different initial conditions and disturbances. One important factor in flying Continuous Descent Operations (CDO) was left out of this study and is the primary focus of this chapter: the human pilot. To evaluate the role of the human pilot when flying TEMO, a real-time experiment was performed on NLR's APERO simulator. This study focuses on the influence of the human pilot on the performance of the flown descents by comparing simulation runs flown with the pilot in the loop and simulation runs flown using an automated pilot. Furthermore, the experiment evaluated three different Human-Machine Interface (HMI) variants that support the pilots in flying TEMO descents. These three variants differed in the amount of information presented to the pilot in order to establish what information the pilot requires during TEMO operations.

Paper title Time and Energy Management during Descent and Approach: A Human-in-the-Loop Study

Authors P.M.A. de Jong, F.J.L. Bussink, R.P.M. Verhoeven, N. de Gelder, M.M. van Paassen and M. Mulder

Published in Submitted to Journal of Aircraft 2013

ABSTRACT

A new integrated planning and guidance concept has been developed that optimizes the vertical trajectory to achieve a continuous engine-idle descent whilst satisfying time constraints. The new concept, named Time and Energy Managed Operations (TEMO), reduces noise, gaseous emissions and fuel consumption, while adhering to time constraints yielding control points for spacing and sequencing. TEMO uses an optimization algorithm to minimize thrust and speedbrake use through energy management by exchanging kinetic and potential energy. Sustained deviations are only corrected when a predefined boundary is exceeded. TEMO was evaluated in a real-time environment involving nine pilots to receive feedback and to investigate what information supports pilots best to perform accurate TEMO descents. Three Human-Machine Interfaces (HMIs) have been developed that aim at reducing variations due to pilot response and vary in level of information displayed to evaluate what information is required to meet all TEMO objectives. In addition, simulations flown using a zero-delay pilot response model were compared with piloted simulation in terms of TEMO performance and environmental impact. Results show that the influence of human response is limited and the automation response showed only small improvements in time performance, noise levels and NO_x emissions. However, in certain simulations, pilot response resulted in too early arrivals. Pilots preferred the HMI variant that included a timer to support accurate selection of flaps and gear. The timer, however, did not significantly reduce time deviations but did reduce variance in pilot response. The results also showed that modifications to the TEMO concept could potentially improve time performance.

4-1 Introduction

The expected growth in air traffic [1], combined with an increased public concern for the environment and increased oil-prices, have forced legislators to rethink the current air traffic system design. Both in the United States [2] and Europe [3], research projects have been initiated to develop the future Air Transportation System (ATS) to address capacity, and environmental, safety and economic issues.

To address the environmental issues during descent and approach, a novel Continuous Descent Operations (CDO) concept [4], named Time and Energy Managed Operations (TEMO) [5], has been developed. It uses energy principles to reduce fuel burn, gaseous emissions and noise nuisance whilst maintaining runway capacity. Different from other CDO concepts [6–12], TEMO optimizes the descent by using energy management to achieve a continuous engine-idle descent while satisfying time constraints at the Initial Approach Fix (IAF) and the runway threshold. As such, TEMO enables two control points for flow management and arrival spacing.

Although TEMO, integrated in a capable Flight Management System (FMS) and autopilot, could be useful in full authority automation during the descent phase of flight, research in flight deck automation has shown that incorrect use of automation could lead to severe human performance problems [13–16], especially during unanticipated events that require human intervention [17]. Due to the unanticipated variability in ‘open’ systems [18] such as aircraft, there is always a role foreseen for the human operator to retain abilities, such as inductive reasoning and complex pattern matching, which still outperform computer design.

However, a prerequisite for enabling such behavior is to properly inform the human operator about the rationale that drives the automated system [19]. Hence, the question remains, what and how much information should be displayed to support pilots operating TEMO, to ensure proper human-machine coordination and maintain high levels of performance?

This paper reports on the results of a human-in-the-loop study that assessed TEMO operations with increased realism. The study evaluated what information pilots require to perform TEMO descents using the new, automated TEMO system. Three Human-Machine Interfaces (HMIs) were designed that provide efficient human-machine interaction, reduce variations in pilot response and differ in level of information displayed. Moreover, by comparing the experiment results with simulations using a zero-delay pilot-response model, the experiment investigated whether variations in pilot response introduce additional disturbances that could reduce the accuracy of TEMO descents.

The outline of this paper is as follows: the next section discusses the Time and Energy Managed Operations (TEMO) concept and Trajectory Predictor (TP). To support the pilot in performing TEMO descents, display elements have been designed that support the pilot during TEMO operations. The role and responsibility of the human pilot during TEMO operations and the three HMI variants are discussed in Section 4-3. The paper continues with a description of the set-up of the human-in-the-loop experiment. Section 4-6 discusses the results of the experiment by evaluating the objective flight performance and response to questionnaires, followed by a general discussion in Section 4-7. The final section draws conclusions and provides recommendations for future research.

4-2 Time and Energy Managed Operations

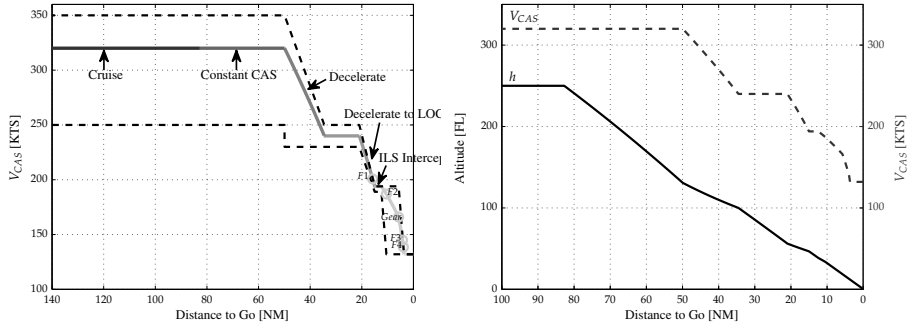
TEMO is a new CDO concept that aims at reducing fuel use, gaseous and noise emissions whilst conforming to time constraints imposed by Air Traffic Control (ATC). This section discusses the TEMO concept and the various parts it comprises.

4-2-1 The TEMO Concept

TEMO enhances the current vertical guidance of the aircraft using an optimization algorithm to calculate *energy-neutral* trajectories and employs an improved guidance function to fly these trajectories. An energy-neutral trajectory requires only engine idle thrust and uses no additional drag devices during descent from Top of Descent (ToD) to the stabilization point at 1,000 ft above ground level. At the stabilization point the aircraft is stabilized, configured and ready for landing following a conventional Instrument Landing System (ILS) procedure. To improve predictability, calculated trajectories adhere to the definition of a closed-path trajectory as defined by ICAO [4].

The TEMO concept uses the principles of energy exchange to control the aircraft to a given point in space and time. By following a nominal calibrated airspeed profile, see Figure 4-1, aircraft comply with applicable speed constraints. This profile is defined similar for arriving aircraft at lower altitudes to obtain a stable and predictable arrival flow. To

arrive earlier or later, the TEMO algorithm can deviate from the nominal profile but only within prescribed speed margins. The speed profile is flown by the guidance system using Speed-on-Elevator (SOE) control and with thrust set to idle. This implies that the aircraft does not follow a fixed vertical profile. The actual flown vertical profile depends on aircraft characteristics and disturbances.



(a) TEMO characteristic phases (excluding Mach descent) from Top of Descent at FL 250 to the runway threshold (0 NM). (b) Nominal TEMO altitude profile and calibrated airspeed profile (CAS vs. Distance to Go).

FIGURE 4-1: Nominal TEMO calibrated airspeed profiles and altitude profile.

Due to disturbances, such as wind estimation errors, the aircraft could deviate from the planned trajectory in terms of time and energy (altitude and velocity). These deviations could be corrected instantaneously, using control-laws, resulting in *tactical replanning*. Another method is a *strategic replanning* approach that permits small deviations from the planned trajectory but calculates a new trajectory when these deviations exceed a predefined boundary. In the experiment discussed in this paper, TEMO used strategic replanning to correct deviations.

The trajectories are calculated by the novel TEMO algorithm that aims at finding an energy-neutral trajectory using *energy management*. Proper energy management allows an aircraft to exchange kinetic and potential energy, resulting in an energy-neutral trajectory, which implies that no additional energy is added or dissipated. However, situations could occur where the TEMO algorithm cannot find a trajectory without using thrust or drag devices. In these cases, the algorithm minimizes thrust and drag device use resulting in an *energy-optimal* trajectory. In extreme cases, the TEMO algorithm is unable to find a valid trajectory that satisfies all constraints, which is referred to as a *reject*. In case of a reject, pilots notify ATC to negotiate new constraints or revert to a vector-based arrival.

TEMO uses time constraints to enable 4D flight trajectories. A time constraint can be an absolute time constraint, using a Controlled-Time of Arrival (CTA), at a location along the trajectory [20], or a relative time interval to a leading aircraft using airborne spacing [20]. The time constraints commanded by ATC includes a Required Time Performance (RTP) that prescribes the required accuracy to meet time constraints for 95% of all operations. During

hours of low-demand, the RTP could be set less restrictive to achieve more environmental benefits, whereas during hours of high-demand, the RTP can be set to a low value to ensure a high inter-aircraft spacing accuracy to satisfy runway throughput requirements. This experiment used CTAs at the IAF and runway threshold for time management.

TEMO uses an automated optimization algorithm and enhanced TP for rapid, accurate and consistent calculations. However, pilots still manage the system through the Control and Display Unit (CDU) and Flight Control Unit (FCU) and set configuration changes as planned by the TEMO algorithm. To reduce uncertainty caused by variations in pilot response during execution of the idle descent, the descent is flown using the autopilot and the aircraft cockpit displays are enhanced to support pilots in performing actions during TEMO descents. The TEMO flight procedures are discussed in the next section.

The TEMO concept is developed and tested for the Airbus A320 aircraft. However, TEMO could be adapted to allow CDOs with other modern, commercial aircraft in the future.

4-2-2 TEMO Flight Procedures

During cruise, pilots receive a descent clearance that includes a CTA for the IAF from ATC through data-link. Pilots review the clearance and activate the clearance information ^(C1), such as Standard Arrival Route (STAR), runway, descent altitude, CTA and RTP into the FMS through CDU and FCU. The CTA is now internally used by the FMS as a Required Time of Arrival (RTA). All required pilot actions are illustrated in Figure 4-2.

Using the clearance details, the TEMO algorithm optimizes the descent trajectory that complies with the received clearance. Once successful, the pilots accept the clearance and notify ATC using data-link. Next, pilots prepare the autopilot and FMS to fly the calculated trajectory and perform the descent checklist.

At ToD, the aircraft automatically intercepts the descent trajectory similar to current Boeing aircraft and pilots monitor flight progress. By monitoring differences between commanded speed and actual speed, possible time deviations can be anticipated.

Prior to Terminal Maneuvering Area (TMA) entry, ATC sends an updated clearance to descend to the runway with associated CTA and RTP at the runway. Pilots, again, insert the clearance details ^(C2) into the FMS, which automatically removes the RTA information from the IAF and adjust the FCU altitude window accordingly. When the RTA_{RWY} is different from the current Estimated-Time of Arrival $(ETA)_{RWY}$, the TEMO algorithm calculates a new trajectory to arrive on time.

Within the TMA, pilots perform approach and landing checklists and execute configuration changes at planned locations as demanded by the trajectory. Delays in selection of configurations results in deviations from the planned trajectory and consequently, pilots are expected to set the configurations accurately and timely.

In general, Flaps 1 ^(F1) is set prior to intercepting the localizer, followed by Flaps 2 ^(F2) after which the glideslope is intercepted. Hereafter, pilots lower the landing gear ^(G) to

increase deceleration and set the go-around altitude. Finally, Flaps 4¹ (E4) is selected prior to reaching Final Approach Speed (FAS).

Upon glideslope intercept TEMO is automatically disengaged and no longer calculates new trajectories to correct deviations. From this point onwards, the descent is an open-loop system and hence accurate selection of configuration changes is required to limit deviations from the planned trajectory.

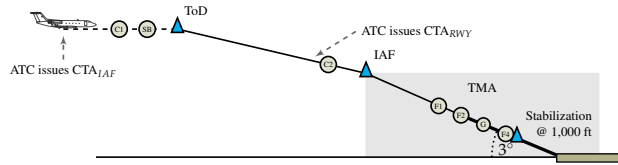


FIGURE 4-2: Overview of pilot actions during a TEMO descent.

4-2-3 TEMO Algorithm and Trajectory Predictor

In a preceding batch-study [5] that investigated TEMO performance, used a MATLAB implementation of the TEMO algorithm that required a minimum of 30 seconds to calculate a new trajectory. For this real-time, human-in-the-loop experiment, a faster calculation routine was required that could be integrated into existing simulation software. Therefore, a new algorithm was developed [21] in C++ using PSOPT [22]. PSOPT is a state-of-the-art, open-source tool that uses direct collocation methods, such as local and pseudospectral discretizations to rapidly solve optimal control problems.

To improve calculation time, the glideslope is not included in the optimization algorithm. Consequently, the algorithm only optimizes the trajectory from ToD (or current position) down to the glideslope intercept point. As a result, the deviation boundaries are deactivated upon intercepting the glideslope and any disturbance that occurs while descending down the glideslope will not be corrected for (open-loop), nor can the TEMO algorithm command additional thrust or speedbrakes while the aircraft descends down the glideslope.

TABLE 4-1: TEMO deviation thresholds and Required Time Performance (RTP).

Active CTA	RTP [s]	Deviation Boundary					
		Top of Descent		IAF		Runway Threshold	
		Time [s]	Energy [ft]	Time [s]	Energy [ft]	Time [s]	Energy [ft]
IAF	5	±10	±400	±5	±200	-	-
Runway	2	-	-	±4	±200	±2	±100

The algorithm calculates earliest and latest achievable ETAs at the time-constrained waypoint to inform pilots of the achievable time window. These ETAs are broadcast to ATC through datalink to provide ATC with information for sequencing and spacing of aircraft.

¹To reduce the number of pilot actions, the HMI commands pilots to select Flaps 4 at the location of Flaps 3 since Flaps 4 succeeds Flaps 3 almost instantly at that particular deceleration rate.

Once a deviation exceeds a boundary and remains out of bounds for 10 seconds, the algorithm calculates a new, optimized plan that returns the aircraft to the center of the boundaries upon automatic plan activation. The boundaries (Table 4-1) are defined as a positive and negative value and reduce in value as the control space reduces while approaching the time constrained waypoint. The RTP values are smaller than the prescribed 10 seconds accuracy used in the Initial 4D project [23] of SESAR in an aim to increase runway capacity.

Replanning is disabled when the aircraft is too close to a time-constrained waypoint or the glideslope as both the calculation process requires time and the available distance to correct a deviation is limited. Before replanning, a position and altitude constraint is *predicted* serving as initial position for replanning. This constraint is located 20 seconds in front of the current position along the active plan. However, a replan must be calculated within 18 seconds to provide a 2 second window to transition to the new trajectory. If the replan was not successful within 18 seconds, the FMS reports a reject.

4-3 Supporting Pilots in Strategic Replanning

Research showed that new and advanced automated systems in the cockpit often lead to less information being displayed to the pilot as display designers assume that automation and humans can work independently [19] and tasks can simply be shifted from humans to automation and backwards. Also, designers often automate complex tasks while excluding the human operator in the design process [16], resulting in a loss of information to support the pilot in operating the automation. As a result, the human operator is placed out-of-the-loop [24] or loses awareness [13–15]. The reduced awareness could potentially result in the pilot not performing or incorrectly performing an action in situations where the pilot was expected to intervene [25].

For these reasons, the role of new automated systems should be carefully evaluated to ensure that the automation system and the human operator work as team-players [19]. According to Christoffersen and Woods, this is achieved by providing (more) information about what the automation system is doing and what it will be doing in the future. Moreover, the human operator should be supported sufficiently in recognizing situations where they should intervene and be able to reprogram the automated system accordingly.

TEMO relies on automation as it allows for consistent, reliable and fast multi-objective optimization. However, pilots are still required to perform manual actions as present cockpits are not completely automated since automated aircraft systems cannot be fully and explicitly modeled [26]. Hence, pilots complement and supervise an automated system for cases that cannot be modeled or were unforeseen during design.

The research in this paper investigated how much and what information is required to perform TEMO descents using strategic replanning. Therefore, three HMI variants that differed in amount of information displayed were designed. The displays provide efficient human-machine interaction and have been designed in an aim to minimize variations in pilots response. The TEMO-specific elements were designed using a constraint-based approach [27, 28], inspired by Ecological Interface Design (EID) [18], to provide more

transparency by visualizing the automation constraints required by the TEMO algorithm to calculate a new trajectory through strategic replanning. The role of the pilot in the TEMO concept is graphically shown in Figure 4-3. This figure also shows the different elements added to the cockpit displays in support of TEMO to each HMI variant. The working principles and design of these elements are discussed in the next section.

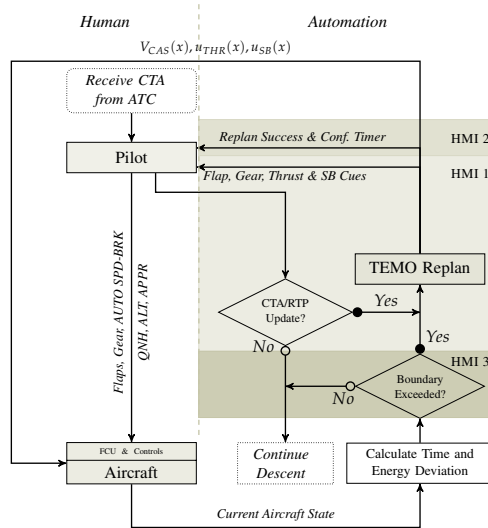


FIGURE 4-3: Schematic of the pilots' role in TEMO and the information displayed by the HMI variants.

4-4 HMI Variants

This section discusses the new HMI variants and automation features to support pilots in operating descents using TEMO. Each subsequent HMI variant contains the elements of its predecessors and has new functions (more information) displayed. Besides these specific features, the RTA page of each waypoint on the CDU has been adapted to present earliest and latest achievable ETAs and RTP information. All elements were designed for the Airbus A320 cockpit, since the A320 represents a large percentage of the worldwide aircraft fleet.

HMI Variant 1

The basic HMI variant includes only new elements that are required for TEMO operations. The new features added to the Airbus displays are listed below.

Auto-Speedbrakes TEMO uses a newly developed flight control system referred to as auto-speedbrakes, inspired by Airbus' A318 steep-approach [29] system to perform steep ILS approaches into London City Airport. Boeing also developed an auto-drag function [30]

for the Boeing 787 that controls speedbrakes to increase the aircraft's descent rate when above path. This system is especially useful when intercepting the ILS glideslope from above.

The TEMO auto-speedbrakes function controls speedbrakes as demanded by a planned trajectory to reduce pilot workload. The pilot operates the system by enabling the auto-speedbrake function on the overhead panel and by setting the speedbrake lever. The lever position limits the maximum deflection allowed by the planning and guidance functions, similar to the use of auto-thrust on Airbus aircraft.

Flap and Gear Cues The TEMO algorithm plans the position where configurations must be set, based upon a fixed calibrated airspeed that depends on the minimum maneuvering speed [5]. The configuration change speed is shown on the the Primary Flight Display (PFD) speed-tape and a flap 'hook', left of the speed-tape, shows the second next flap speed.

The speed-tape also shows the commanded Calibrated Airspeed (CAS), commanded speed-trend (extended from the bullet) and speed target (magenta triangle). If the commanded speed and target speed are equal, the speed will remain constant until a change in flight-path angle as drawn on the Vertical Situation Display (VSD).

The predicted locations where configuration speeds are obtained are visualized on the Navigation Display (ND) and VSD as a pseudo-waypoint to improve observability. These pseudo-waypoints are the primary cue for selecting configurations as this provides a self-correcting mechanism for deviations. Although TEMO commands a speed profile, small time deviations could still occur. For example, when the aircraft is ahead of schedule the configuration change location is reached earlier, such that a selected configuration generates additional drag. To avoid decelerating below the minimum maneuvering speed an offset of 5 KTS is added to obtain the configuration speeds.

Thrust and Speedbrake Cues Thrust and speedbrakes are in principle undesired since these actions are not energy-neutral and sub-optimal in terms of environmental impact. These control actions can also cause engine spooling and vibrations due to aerodynamic drag. Therefore, the planned locations of additional thrust or speedbrake use in excess of 5% and 2.5%, respectively, are drawn on the ND and VSD to inform pilots of these undesired actions.

HMI Variant 2

To improve pilot awareness, a configuration timer and notifications of successful replans have been added to the basic variant to obtain HMI variant 2.

Configuration Timer To support pilots in selecting the next configuration, a timer is added to the right of the PFD speed-tape as shown in Figure 4-5. The timer is visible 20 seconds prior to reaching the predicted location of the configuration change and starts to count down 10 seconds later. Once the timer is visible any disturbances occurring between this point and the actual configuration change do not change the countdown time or countdown

speed. Therefore, speed deviations during this time window could cause the timer to finish too early or late.

Replan Notifications In all HMI variants, the display informs pilots of an active replan calculation by removing all FMS predicted values from the CDU, ND and VSD. Hence, all fuel and time predictions are displayed as dashes when the system is replanning. To improve directability, the TEMO algorithm informs pilots of a rejected replan through messages on the Flight Mode Annunciator (FMA) and CDU. In this case, the aircraft remains flying the old plan until pilots select a different flight mode or remove constraints to activate a new replan. Optionally, when a replan was successful, a message shows PLAN CHANGE on the ND in variants 2 and 3.

HMI Variant 3

Variant 3 includes a Time and Energy Indicator (TEI) for awareness of sustained deviations.

Time and Energy Indicator Time and energy deviations are shown on the new TEI, see Figure 4-4. The current thresholds, given by the current position and values of Table 4-1 and reduce in size during descent (③). The TEI follows the inside-out design as a magenta marker represents the *planned* time and energy position (②) and the cross in the center (①) indicates the *actual* positions. The situation depicted in Figure 4-5 shows an aircraft slightly late (behind schedule) and low on energy. The boundary (③) changes color when the planned indicator exceeds a boundary and a replan will commence when the indicator remains 10 seconds outside the boundaries.

The TEI provides an indication of possible replan solutions as a low energy state or expected late arrival can be resolved using thrust while speedbrakes can be assigned to a high energy state or too early arrival (light-gray areas). Conversely, when the aircraft is rather early and low on energy, correct energy exchange could resolve the deviation (white areas). Since an aircraft flying fast and low could have an equal level of total energy as an aircraft flying slow and high, pilots should monitor speed and altitude indicators to deduce the cause of energy deviations. Hence, the TEI is primarily designed to anticipate replans and improve TEMO's observability and directability [19].

4-5 Experimental Evaluation

This experiment evaluates the human role in operational use of TEMO and to compare the three different HMI variants that support the pilot in performing TEMO operations using strategic replanning. Variations have been restricted to controlled disturbances such that observed variations were limited to pilot response. The metrics that are evaluated are, among others, mental workload and TEMO performance expressed as time deviation from the CTA at the runway threshold.

The primary objective of the piloted experiment was to receive feedback regarding the HMI variants and TEMO procedures. The results were evaluated qualitatively and when pos-

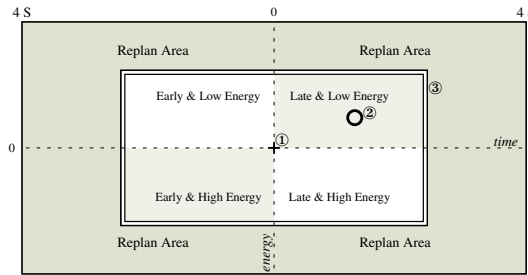


FIGURE 4-4: Working principles of the Time and Energy Indicator (TEI): 1. Current Time and Energy position; 2. Planned Time and Energy position; 3. Current Time and Energy boundaries.

sible, statistical tests have been performed to determine significance of the results. Besides these runs flown with pilots, several scenarios have been flown using an automated pilot response model, referred to as Autobot, to identify whether pilots have been sufficiently informed to reduce variations in pilot response.

4-5-1 Method

Pilot Subjects

Nine professional airline pilots participated in the experiment as Pilot Flying (PF). Their total flight hours ranged between 1,050 hours and 18,200 hours ($\bar{X} = 8,200$ hours, $\sigma_X = 5,988$ hours) and pilot age ranged between 32 and 78 years old ($\bar{X} = 50.33$, $\sigma_X = 13.63$). Five pilots had previous datalink experience, two pilots had experience with using a VSD, six pilots had experience with CTAs, and seven pilots had experience with flying Continuous Descent Approaches (CDAs). Table 4-2 lists a summary of pilots' experience.

The pilots received an extensive briefing guide, informing the pilots about the TEMO concept, the new cockpit-display elements and the experiment set-up before the experiment date. Pilots were instructed to adhere to Standard Operating Procedure (SOP) and the newly defined TEMO procedures of Section 4-2-2 as much as possible. Pilots were also told to adhere to these procedures in case pilots' expected not to meet the CTA or reach the stabilization requirements before passing 1,000 ft.

The subject pilots acted as PF and were accompanied by a host-pilot² as Pilot Not Flying (PNF).

Apparatus

The experiment was performed at NLR's Avionics Prototyping Environment for Research and Operations (APEROP), a fixed-base research flight simulator providing flexible avionics prototyping. APEROP has a modular cockpit and comprises five high-resolution touchscreen

²All host-pilots are, or were, licensed test pilots and also supported the TEMO developers during set-up of the experiment and design of the new cockpit-displays.

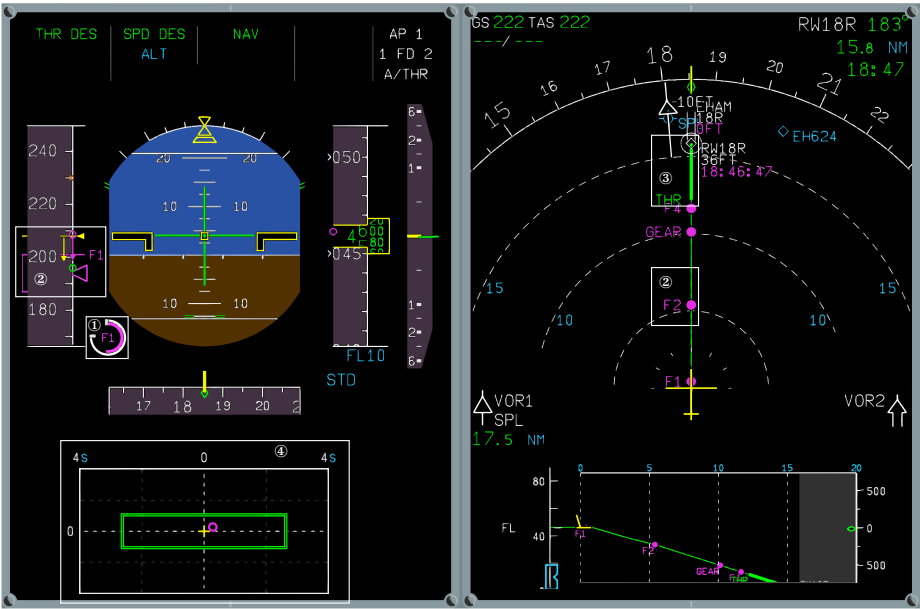


FIGURE 4-5: Overview of the HMI variants with the various TEMO functions; ① Configuration Timer; ② Configuration Cues and Commanded Speed; ③ Additional Thrust (THR) Cue; ④ Time and Energy Indicator.

TABLE 4-2: Characteristics of pilot participants in the experiment.

Pilot	Age	Flight Hours	CDA Experience	Aircraft Types
1	51	13,820	yes	B737, B747, B777, MD-11, C500
2	36	2,700	yes	Cessna Citation C550, PA31, DA42, BE18
3	58	14,000	yes	DC-9/10, A310-200, MD-11, B747, A320, B737
4	32	4,000	yes	B737, A319
5	47	6,630	yes	MD-11, B747, A330
6	78	9,500	no	Fokker 27, Fokker 50, Fokker 28, Fokker 70/100, F104, F16
7	54	3,900	no	Fokker 70/100, various Cessna and Gulfstream business jets
8	42	1,050	yes	Cessna Citation 550, Fairchild Metroliner II
9	53	18,200	yes	Fokker 27, B747, A310, MD-11, B777

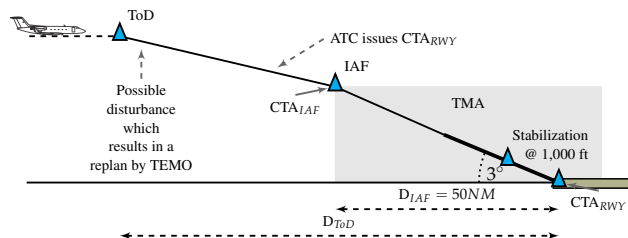


FIGURE 4-6: Overview of a typical TEMO experimental scenario.

LCDs that simulate cockpit displays. A High Definition LCD-TV displays the outside visual using Microsoft Flight Simulator X.

Pilots controlled the aircraft using the FCU and CDU by setting the correct FCU altitude, lateral and vertical autopilot modes. Manual flying was possible but pilots were instructed to fly the aircraft using the autopilot system. The CDU was used to enter and review CTA information and trajectory data and the Data Communications Display Unit (DCDU) was used to send and receive datalink messages.

Independent Variables

In this experiment, two independent variables were manipulated. First, three different *HMI variants* were designed (see Section 4-3 for a more detailed explanation). The three HMI variants vary in amount of additional information displayed. The minimal differences between the variants allow for the validation of the individual items that are added or removed from each subsequent variant.

The second independent variable is an *error disturbance*, consisting of four levels. The first level is used as a baseline and contained no disturbance throughout the entire descent.

The second level of disturbance introduced an energy error by commanding the autopilot to intercept the descent 10 seconds early, resulting in a continuously growing altitude deviation and consequently in a total energy deviation (both potential and kinetic energy are affected) with respect to the planned trajectory.

The third level introduced an offset time constraint at the runway. By issuing a CTA_{RWY} at the runway threshold that significantly differs from the current ETA_{RWY} at the threshold, an instantaneous time deviation occurs exceeding the current time boundary to force a replan. Depending on the size of this time deviation, an energy-neutral or energy-optimal plan is found by the TEMO algorithm. The commanded CTA_{RWY} value was such that a replan would result in an energy-optimal plan requiring thrust and/or speedbrakes.

The fourth disturbance level introduced both a growing energy error and an instantaneous time error. Figure 4-6 shows a schematic overview of a typical experiment scenario and the location of disturbances shown using dashed arrows.

Scenarios

The measurement runs consisted of twelve scenarios, see Table 4-3. The first half was designed as a within-subjects repeated-measures design defining six scenarios consisting of the three HMI variants and the first two disturbances. This allows a full comparison between the three HMI variants for these disturbances and a comparison between disturbances for each HMI variant,

The second half of all scenarios contained the third and fourth disturbances. The CTAs differed per scenario so pilots would experience both earlier and later arrivals. For the same reason, the energy disturbance, a combination of a time and energy error, is also different.

For a full factorial design, two additional levels in the disturbance variable should have been introduced, resulting in six additional runs and approximately three hours of additional simulation time. With a total experiment time of one and a half day per pilot, it was decided not to fully include these conditions and hence combine the earlier and later arrivals into a single variable level. As a consequence, these scenarios were not used in statistical analyses.

The objective of the experiment was to test nominal TEMO operations and procedures using absolute time management; therefore, no other traffic or emergency situations (such as engine failures) were modeled that could disrupt TEMO operations.

The twelve scenarios are depicted in the experiment matrix shown in Table 4-3. This matrix also shows the scenario number and type and/or amount of disturbance introduced in that scenario. The second number in the scenario number reflects the disturbance variable while the last number reflects the HMI variant. Scenarios 111–123 have been used in the statistical analysis discussed in the next section.

TABLE 4-3: Experiment Matrix of the human-in-the-loop experiment.

	Scenario											
	111	112	113	121	122	123	131	132	133	141	142	143
HMI Variant	1	2	3	1	2	3	1	2	3	1	2	3
Disturbance												
CTA Offset [s]	0	0	0	0	0	0	+25	-20	+25	-35	+15	-35
Energy Error	-	-	-	ToD	ToD	ToD	-	-	-	ToD	ToD	ToD

All pilots flew the scenarios in a randomized order to counteract learning effects using a mixed random-balanced Latin Square design. As only nine pilots could participate in the experiment, a full Latin Square design was not possible. Therefore, nine rows out of a 12×12 Latin Square were randomly assigned to each of the nine pilots.

Approach Conditions and Aircraft Characteristics

Each scenario started at FL 250 in cruise phase and 18 NM from ToD and located 120 NM from Amsterdam Airport Schiphol runway 18R. The aircraft was trimmed at 320 KIAS, in clean flaps configuration with the landing gear retracted and at 90% Maximum Landing Weight (MLW). The trajectory was a straight-in descent and pre-programmed in the FMS. The lateral trajectory was fixed and the IAF was located 50 NM from the runway threshold. The vertical profile was optimized by the TEMO algorithm up to glideslope intercept and

continued as a 3° path to the runway.

The simulation used a high-fidelity non-linear aircraft model of the Airbus A320 [31]. From this model, a simplified point-mass model was derived for use by the TEMO algorithm. The autopilot included modes for lateral and vertical navigation (Lateral Navigation (LNAV)/Vertical Navigation (VNAV)), localizer and glideslope intercept and used a non-moving auto-thrust system.

The atmosphere was modeled using the International Standard Atmosphere (ISA) while no wind or turbulence were modeled to reduce variations.

Procedure

The experiment began with training runs and continued with measurement runs. The training started with a briefing and a Q & A session, and continued in the APERO simulator to introduce the three HMI variants. The training runs allowed pilots to familiarize with aircraft controls and dynamics, and operation of Controller Pilot Data Link Communications (CPDLC) and new FMS functions.

In total, the experiment required one and a half day per pilot to fly all training and measurement runs. A single simulation scenario required approximately 25 minutes to complete.

After every simulation pilots were asked to fill out a post-run questionnaire, containing questions about the flown simulation. Pilots indicated their Rating Scale Mental Effort (RSME) [32] on a single analog scale, which makes it easier and simpler to use than for instance the NASA-TLX that uses multiple scales [33]. Moreover, pilots rated their trust in the automated system using a modified version of the Controller Acceptance Rating Scale (CARS) [34] rating scale for automated systems in ATC. Open-ended questions related to the concept and procedures served as explanatory answers to the rating scales. The questionnaire concluded with three open-ended questions asking pilots whether they met the time-constraints within the allowed RTP, and whether the final approach was stabilized at 1,000 ft.

At the end of the experiment, pilots filled out the final post-experiment questionnaire about the TEMO concept. Pilots indicated their agreement with statements concerning safety, acceptance, thrust and speedbrake use, situational awareness, configuration changes on a 5-point Likert scale ranging from strongly disagree to strongly agree. Moreover, pilots were asked to rate their preference about the HMI variants and TEMO features.

Dependent Measures

The dependent measures were grouped into objective and subjective measures. The objective measures were,

Pilot performance The performance of the pilot is measured by calculating the delay in selecting configurations. Any delay, either negative or positive, from the planned position will result in a deviation from the planned trajectory, which could lead to time and/or energy deviations. The time deviation could eventually result in a time offset at the threshold that

exceeds the RTP. The deviation from the assigned CTA_{RWY} at the runway threshold and the time deviation at the IAF were also determined to establish how well the time goals were met. These time deviations for pilot runs are compared with the results from Autobot to analyze effects of pilot response.

Environmental impact Environmental impact is compared between the human flown runs and the Autobot runs to investigate the effect of pilot variations on environmental impact. The noise impact of each run is evaluated using the total area of the 75 dB Sound Exposure Level (SEL) noise contour. A noise model, based on the ECAC/CEAC Document 29 specification [35] is used to calculate the 75 dB SEL contour. Moreover, the amount of Nitrogen Oxide (NO_x) emissions below the mixing height of 3,000 ft is calculated using the Boeing Method 2 [36] model. Finally, the amount of fuel burned is analyzed.

By filling out the post-run and post-experiment questionnaires, the pilots were asked to provide their subjective assessments regarding workload, TEMO procedures and system, safety and perception of their performance. The subjective measures that follow from these questionnaires are,

Workload Pilots were asked to rate their RSME per scenario as a metric for workload. The absolute scores provided by the pilots are subjective and one pilot might rate all scenarios relatively high on the RSME scale whereas another pilot might rate all approaches low on the RSME scale. Since we are only interested in relative performance per display and per disturbance, the RSME scores are transformed into z-scores per pilot to remove this variability.

TEMO In the post-experiment questionnaire, pilots were asked to express their preference for one of the three HMI variants and the specific TEMO display details in terms of usefulness and representation. These answers were used to understand their preference for a particular HMI variant and are, as such, not a metric itself.

Safety The stabilization criteria have been objectively set to the criteria listed below. At 1,000 ft, the aircraft should be a) $FAS \leq V_{IAS} \leq FAS+20$; b) flaps are set for landing; c) landing gear is down; d) thrust is stabilized to maintain Final Approach Speed; e) less than 1 dot deviation from the localizer and glideslope; f) all checklists and briefings are completed.

After each simulation, pilots were asked to rate on a 5-point Likert scale their judgment concerning the safety of the flown approach. Additionally, the pilots were asked whether they thought to have been stabilized when descending through 1,000 ft. This was verified with objective results

4-5-2 Experimental Hypotheses

Based on the objective of this experiment, the following hypotheses have been formulated:

Hypothesis 4.1. *Pilots will be able to meet assigned time and stabilization requirements with all HMI variants. This makes HMI variant 1 the required variant and HMI variant 2 the preferred variant.*

Hypothesis 4.2. *Pilots accept the arrivals that are flown and find the TEMO procedures acceptable, but they will find the configuration changes very stringent.*

Hypothesis 4.3. *There will be no substantial difference in environmental impact between the Autobot and human runs.*

4-6 Experiment Results

This section discusses the results obtained from the human-in-the-loop experiment, starting with TEMO performance in terms of time deviations and pilot acceptance. The next part discusses the subjective responses from pilots on the questionnaire. This section ends with a comparison of time performance and environmental impact between all scenarios flown with pilots and scenarios flown with the Autobot.

4-6-1 TEMO Performance

Time of Arrival Performance

Figure 4.7(a) shows the time deviation when the aircraft passes the IAF for scenarios including the two disturbances (no disturbance, energy disturbance at ToD) under consideration for each HMI variant. The HMI shows no effect on the time deviation at this location as up to the IAF the influence of the pilot (and hence, the display) is limited as no configurations have to be selected prior to passing the IAF. The only ‘variation’ up to this point is how quickly the pilot enters the received CTA_{RWY} data into the CDU, which determines the initial position of a replan. Hence, this ‘disturbance’ has no significant effect on the time deviation at the IAF.

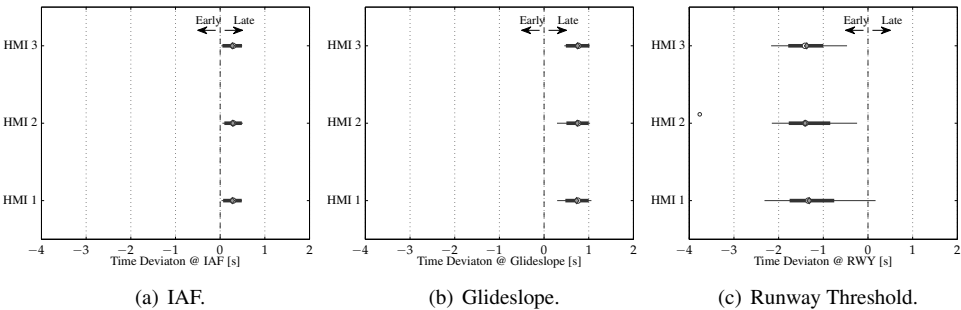


FIGURE 4-7: Time Deviation at the IAF, glideslope and runway threshold for each HMI variant ($N = 18$).

The moment at which TEMO replanning is disabled, the time deviation has grown slightly, see Figure 4.7(b), but remained within a 1 second accuracy. Interestingly, the time deviation at the runway threshold, see Figure 4.7(c), shows a bias to arrive early with respect to the assigned CTA_{RWY} and the time deviation has shifted sign and increased in magnitude. These results show that the aircraft gained approximately 1.9 seconds between glideslope intercept and runway. Analysis showed that the aircraft typically had excess energy upon glideslope intercept ($\tau = -0.747, p < 0.001$, Kendall's tau two-tailed). Consequently, the aircraft exchanges potential energy for kinetic energy to follow the glideslope. This results in an increased airspeed and an earlier arrival as TEMO descents are open-loop after intercepting the glideslope.

Twelve of the 108 simulation runs flown with pilots did not meet the required RTP at the runway threshold of ± 2 seconds ($\bar{X} = 1.246$ seconds *early*, $\sigma_X = 0.668$ seconds, $N = 108$). The earliest arrival was 3.766 seconds early while the latest arrival was 0.367 seconds late. In all cases of RTP violations, the aircraft was planned to arrive on time when TEMO replanning was disabled and deviations while on the glideslope were not corrected.

The time deviation at the runway, $t_{e_{RWY}}$ deviated from a normal distribution due to a single outlier in scenario 112 ($D(9) = 0.297, p = 0.021$). Since the Analysis of Variance (ANOVA) test is relatively robust to non-normality when sample sizes are equal [37], a two-way, repeated-measures ANOVA was performed on the time deviation at the runway. Due to the small sample size, the statistical analysis should be considered merely as an indication of possible effects. The results of all ANOVA tests are summarized in Table 4-4.

Mauchly's test showed that sphericity was not violated for the display variable while sphericity was not considered for the disturbance variable, consisting of only two degrees of freedom. For the three HMI variants, the time deviations are rather equal as shown in Figure 4.7(c) and confirmed by the result of the two-way ANOVA.

For validation, a two-way Friedman test that adjusts for possible row effects [38] but does not test interaction effects, was performed to verify the assumption of ANOVA's robustness. The results indicate that there was indeed no significant effect ($\chi_F^2(2) = 0.408, p = 0.816$) for the HMI variable.

The results of the ANOVA showed a significant main effect caused by the disturbance variable. This introduced disturbance requires a replan to correct the disturbance after passing ToD. Analysis showed that this new trajectory extended flight duration as the time constraint at the runway is inactive and leads to a significantly reduced energy deviation, $E_{e_{GS}}$, at the glideslope intercept point. The energy deviation at the glideslope violated normality for scenarios 111 ($D(9) = 0.289, p = 0.029$) and 112 ($D(9) = 0.315, p = 0.011$). This difference in energy deviation resulted from smaller deviations between planned and actual trajectory. The smaller energy deviation reduces the amount of energy exchange during the transition towards the glideslope resulting in reduced speed deviations and hence time deviations. The results of the ANOVA test also showed no significant interaction between the display and disturbance variables.

TABLE 4-4: Results of two-way Repeated Measures ANOVA tests.

Metric	Variable	ANOVA	Significance	Mauchly's Test	Greenhouse-Geisser Correction
$t_{\epsilon_{RVY}}$	HMI	$F(2, 16) = 0.268$	$p = 0.769$	$\chi^2(2) = 5.964$	$p = 0.051$
	Disturbance	$F(1, 8) = 59.299$	$p < 0.001^{***}$		
	Interaction	$F(2, 16) = 0.681$	$p = 0.520$	$\chi^2(2) = 0.859$	$p = 0.651$
$E_{\epsilon_{GS}}$	HMI	$F(2, 16) = 1.264$	$p = 0.309$	$\chi^2(2) = 1.850$	$p = 0.396$
	Disturbance	$F(1, 8) = 21.062$	$p < 0.010^{**}$		
	Interaction	$F(2, 16) = 1.072$	$p = 0.366$	$\chi^2(2) = 2.250$	$p = 0.325$
τ_{F1}	HMI	$F(2, 16) = 2.924$	$p = 0.083$	$\chi^2(2) = 3.895$	$p = 0.143$
	Disturbance	$F(1, 8) = 2.473$	$p = 0.154$		
	Interaction	$F(2, 16) = 0.199$	$p = 0.822$	$\chi^2(2) = 9.818$	$p = 0.007^{**}$ $F(1.140, 9.122) = 0.199$ $p = 0.698$
τ_{F2}	HMI	$F(2, 16) = 6.646$	$p = 0.008^{**}$	$\chi^2(2) = 1.236$	$p = 0.539$
	Disturbance	$F(1, 8) = 11.133$	$p = 0.010^{**}$		
	Interaction	$F(2, 16) = 2.278$	$p = 0.135$	$\chi^2(2) = 3.378$	$p = 0.185$
τ_G	HMI	$F(2, 16) = 0.284$	$p = 0.757$	$\chi^2(2) = 6.237$	$p = 0.044^*$ $F(1.258, 10.064) = 0.284$ $p = 0.658$
	Disturbance	$F(1, 8) = 11.891$	$p = 0.009^{**}$		
	Interaction	$F(2, 16) = 1.246$	$p = 0.314$	$\chi^2(2) = 7.665$	$p = 0.022^*$ $F(1.201, 9.607) = 1.246$ $p = 0.303$
τ_{F4}	HMI	$F(2, 16) = 0.648$	$p = 0.536$	$\chi^2(2) = 9.729$	$p = 0.008^{**}$ $F(1.142, 9.138) = 0.648$ $p = 0.461$
	Disturbance	$F(1, 8) = 4.219$	$p = 0.074$		
	Interaction	$F(2, 16) = 0.940$	$p = 0.411$	$\chi^2(2) = 26.114$	$p < 0.001^{***}$ $F(1.012, 8.097) = 0.940$ $p = 0.362$

*, Significant at the 0.05 level; **, Significant at the 0.01 level; ***, Significant at the 0.001 level.

Configuration Delays

Pilots were requested to perform configuration changes, see Figure 4-2, when the aircraft passes a pseudo-waypoint located along route. Since the configuration timer is not present in all HMI variants, the deviation between selection of a configuration and the moment of passing the pseudo-waypoint is determined to evaluate the effect of the timer.

In the first configuration, normality ($D(9) = 0.327, p = 0.006$) was violated for Flaps 1, τ_{F1} , due to a single outlier in scenario 123 where the pilot was distracted and selected Flaps 1 rather late. A two-way repeated measures ANOVA was performed and the results are shown in Table 4-4. Sphericity was not violated and the result of the ANOVA showed no significant effect for the HMI variant, disturbance or interaction between both independent variables.

The delays in selection of Flaps 2, τ_{F2} , were all normally distributed. Sphericity was valid and the resulting ANOVA showed a significant effect of the HMI variant on the selection delay. A post-hoc pairwise comparison, adjusted with a Bonferroni correction, showed that HMI variant 1 performed worse than HMI variant 2 and 3. The disturbance variable also showed a significant effect, with earlier selections for the no disturbance scenarios and relatively later selections during energy disturbance scenarios. Finally, the ANOVA showed no significant effect for interaction between the two variables.

The data for Gear extension also followed a normal distribution. Sphericity, however, was violated and consequently a Greenhouse-Geisser correction was applied. The effect of HMI variant was not significant while the effect of a disturbance was significant. The effect of interaction between variables was not significant.

The last configuration, Flaps 4, violated normality ($D(9) = 0.330, p = 0.005$) due to two outliers in scenario 121. In both cases, pilots were distracted and selected full flaps too late. Mauchly's test indicated that sphericity was violated and none of the results proved significant.

Interestingly, the energy disturbance at ToD causes a significantly smaller selection de-

lay for Flaps 2 and Gear. Similar to the time deviation at the runway, this is the result of the new trajectory resulting from a replan to correct the energy disturbance. Analysis showed that differences between actual flown trajectory and planned trajectory, resulting from modeling errors, were smaller for these scenarios. These smaller deviations improved the prediction of the timer start location. As the selection delay of Flaps 2 and Gear was affected by the disturbance this suggests that pilots often relied on the timer for configuration selections.

Although the delays in selecting configurations were similar for all HMI variants and configurations, the timer does have an effect on the selection delay. Levene's test of homogeneity of variance showed that the variance of selection delay for HMI variant 1 (without a configuration timer) is different from the other two variants. Table 4-5 shows the results of Levene's test and indicates equal variances if the test was not significant. The configuration timer supports pilots in selecting flaps and gear effectively by reducing the variance in the selection delay.

A non-parametric rank correlation analysis was performed between the time deviation at the runway threshold and the configuration delays to investigate whether these delays affected time performance at the runway threshold. The results, shown in Table 4-6, reveal that only the last flap configuration shows limited correlation with the accuracy of arrival time. Since this flap configuration increases the aircraft's drag and lift considerably, the effect on the speed profile is large. Since the aircraft is close to the runway, there is only little time to correct a deviation. In this final phase aircraft speed is low and a small speed deviation will result in a relatively large time deviation caused by the inverse relation between time deviation and planned speed.

4-6-2 Questionnaires

Figure 4-8 shows the average RSME ratings and z-scores for each of the three HMI variants and all scenarios. RSME serves as a measure for workload. From this figure, no differences in RSME rating between each of three HMI variants can be identified. A two-way repeated measures ANOVA on the transformed RSME z-scores of scenarios (111–123) showed no significant differences for the display and disturbance variables. However, a marginally significant effect was found for the interaction between display and disturbance

TABLE 4-5: Results of Levene's test of homogeneity of variance for the configuration delays.

	Conditions Tested					
	HMI 1 & HMI 2		HMI 1 & HMI 3		HMI 2 & HMI 3	
	<i>F</i>	<i>p</i>	<i>F</i>	<i>p</i>	<i>F</i>	<i>p</i>
Flaps (1, 106)	10.028	< 0.01**	12.463	< 0.001***	0.669	0.415
Gear (1, 34)	3.665	0.064	5.181	< 0.05*	0.454	0.505
σ^2_{flaps}	7.739	1.104	7.739	0.888	1.104	0.888
σ^2_{gear}	5.918	0.961	5.918	0.486	0.961	0.486

*, Significant at the 0.05 level; **, Significant at the 0.01 level; ***, Significant at the 0.001 level.

TABLE 4-6: Kendall tau correlation coefficients for the configuration delays versus time deviation at the runway threshold.

Configuration	Correlation Coefficient	Significance
Flaps 1	$\tau = -0.010$	$p = 0.923$
Flaps 2	$\tau = 0.049$	$p = 0.607$
Gear	$\tau = 0.089$	$p = 0.347$
Flaps 4	$\tau = 0.214$	$p = 0.023^*$

*, Significant at the 0.05 level.

$(F(2, 14))^3 = 5.297, p = 0.019$). Over all questionnaires, one can conclude that the average RSME remained well below 30, which corresponds to less than ‘Little Effort’ [32].

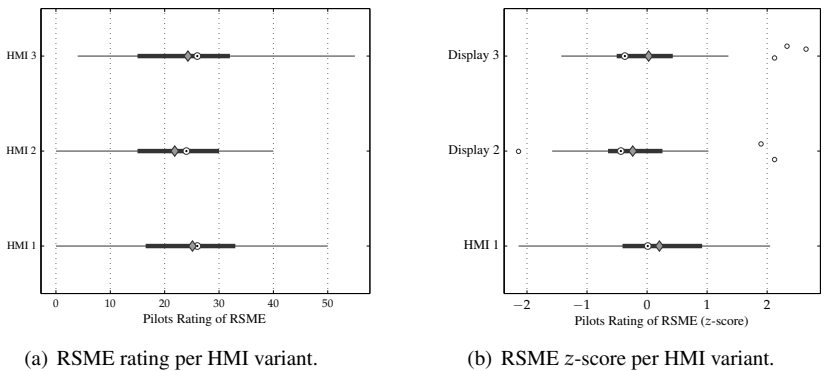


FIGURE 4-8: RSME ratings and z-scores per HMI variant ($N = 105^4$) including mean (diamond) and median (circle).

Pilots also rated their trust in the automated TEMO system using the CARS rating scale while considering all scenarios and the limited scope of the experiment. Their scores ranged between 6 (some improvement) and 9 (quite acceptable), ($\bar{X} = 7.44, \sigma_X = 1.13$).

TEMO Feedback All pilots indicated that the configuration changes were manageable and that they were “in the loop” throughout the entire experiment. Pilots indicated that the TEMO procedures were clear and acceptable. 67% of pilots found the procedures complete but some answered that during a CTA negotiation, communication could be time consuming, requiring improved procedures.

Some pilots argued that the required time accuracy at the runway threshold could be too strict in real-life operations with wind and turbulence. They also argued that using fixed speeds where configuration changed must be performed, disables the ability to correct deviations. Note that these deviations could even result from their own delayed actions.

³One questionnaire was lost through the course of the experiment. Hence, all scores from this pilot were removed in this analysis.

⁴One questionnaire was lost and two questionnaires did not contain RSME scores.

Therefore, pilots opted to remove this restriction to be able to correct deviations since they often use configuration changes to control the speed of the aircraft today.

One pilot argued that defining the time and energy boundaries up to the runway threshold does not make sense as replanning is deactivated once the aircraft is established on the glideslope. Hence, it would be more intuitive to define the boundaries from ToD to the IAF and finally to the glideslope intercept point.

Many pilots requested system improvements regarding occasional segments of fast decelerations that required level segments. The autopilot often climbed to decelerate sufficiently as a result of SOE control. This climb was sometimes very abrupt and pilots questioned whether passenger comfort would be affected. This control behavior was not intended in the design and the autopilot should be improved in future work.

The objective results showed that in seven out of 108 flown simulations pilots were not fully stabilized at 1,000 ft as they did not complete the landing checklist before descending through 1,000 ft, but performed the checklist later. Pilots responded that their airline procedures allow completion of the landing checklist at 500 ft. This relaxed prerequisite was met in all 108 simulations. All pilots agreed or strongly agreed that each flown scenario was safe.

HMI Feedback After all simulations, pilots were asked which HMI variant they preferred and the majority of the pilots preferred HMI variant 2 (5 out of 9). The pilots that preferred HMI variant 2 commented that they preferred this variant due to the added configuration timer. However, some pilots found the timer duration too long and requested to add an aural or flashing warning to inform pilots of short-term configuration actions. Moreover, since the timer estimates the start location of timer countdown, it could introduce a disturbance when this estimate is incorrect while the pilots trust the timer to be correct. Hence, removing the timer and adding an aural or flashing cue could avoid distraction and loss of attention.

One pilot indicated that to prefer HMI variant 1. In his opinion, all HMI variants lack a useful representation of the speed profile. Therefore, the pilot preferred HMI variant 1 as it was the most 'uncluttered' variant. The indication of upcoming speed changes on the VSD and target speed on the PFD speed-tape were insufficient in providing proper speed profile information.

All pilots appreciated the configuration cues on the ND and VSD visualized as pseudo-waypoints. This helped pilots in inferring time and distance intervals between configurations and plan their actions accordingly. Only few pilots preferred to have the configurations cues present on the speed-tape as well, others favored to remove these cues to reduce clutter. One pilot commented that the next flap 'hook' was not required or not even used.

Pilots preferring HMI variant 3 responded that they require the HMI variant 2 but liked the TEI as it supports them in gaining 'situation and automation awareness'. This HMI variant provided the most information and keeps the pilot in-the-loop. Other pilots argued that the TEI is unnecessary and could be distracting with the limited energy and time deviations seen during this experiment. However, they commented that the TEI could be useful

in real-life operations when larger deviations are expected due to wind estimation errors or turbulence.

Seven out of nine pilots indicated that they prefer to have an indication of every new TEMO replan. One pilot answered not to indicate every new TEMO replan, provided the algorithm successfully calculated a new plan. Another pilot indicated to be notified only of ‘considerable’ replans, that is, solving time deviations in excess of 2 seconds.

Pilots commented that the use of auto-speedbrakes is required for correct TEMO operations as manual selection of speedbrakes would be too labor intensive in the busy TMA. However, some pilots wondered what the effect on passenger comfort and load factor would be as they could not experience this themselves in the fixed-base simulator.

The thrust and speedbrake cues were considered a nice additional feature but was sometimes confusing as the text indication of thrust or speedbrakes actions was only visible for short period. One pilot argued that these cues are not required as he/she trusts the auto-thrust and auto-speedbrake functions to work as intended.

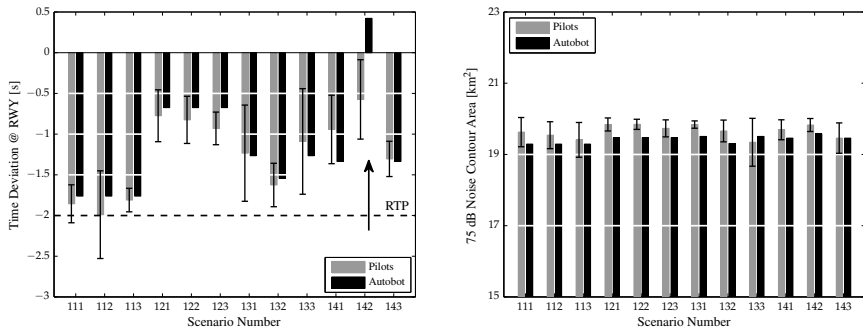
4-6-3 Human versus Autobot Comparison

The time deviations at the runway threshold are compared between human and Autobot runs, see Figure 4.9(a). The differences were the result of slightly earlier selection of configurations by pilots compared to the Autobot. However, the runs flown with the Autobot do not arrive exactly on time either and show a consistent offset. This offset results from deviations between planned and flown trajectory due to modeling errors and simplifications in the TEMO algorithm. Moreover, using strategic replanning, deviations are allowed within boundaries and, hence, deviations are not absolutely minimized. However, the results show that with a perfect pilot model, often most of the allowed time deviation is already consumed by modeling simplifications and errors. This leaves little room for additional disturbances, such as pilot response.

As seen with the piloted runs in Section 4-6-1, Figure 4.9(a), confirms that the introduced energy deviation (scenarios 121–123) at ToD and new trajectory leads to smaller time deviations at the threshold. Generally, pilots arrived slightly early compared to Autobot runs resulting from delayed selection of configurations.

Analysis of the Autobot runs showed that a strong negative correlation ($\tau = -1, p < 0.001$, Kendall’s tau two-tailed) exists between the time deviation ($D(12) = 0.247, p < 0.05$) at the runway and energy deviation ($D(12) = 0.309, p < 0.05$) at glideslope intercept. Hence, without variations in selecting configurations, the time deviation is fully correlated with the energy deviation at glideslope intercept.

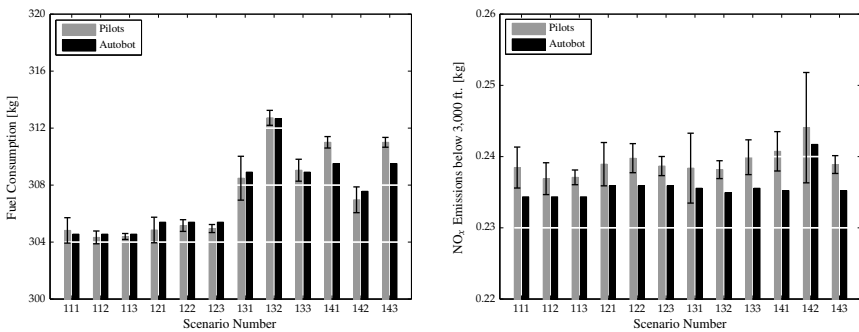
Scenario 142 shows that the Autobot arrived late while pilots, on average, arrived rather early in this scenario. Investigation of these runs showed that pilots require 15 seconds to enter the CTA into the FMS. Due to this delay, the aircraft predicts a different initial position for the TEMO replan. This leads to different trajectories and strategies resulting in different arrival times. For the conditions of scenario 142, the differences in trajectories were quite large whereas this effect was smaller for other scenarios. Moving towards real-life operations will increase uncertainties during prediction of this initial position. Hence,



(a) Comparison of time deviation at the runway threshold per scenario between Human vs. Autobot runs. (b) Comparison of the 75 dB Noise Contour Area per scenario between Human vs. Autobot runs.

FIGURE 4-9: Time deviation and 75 dB SEL comparison between Autobot and Human simulations including the 95% confidence interval for the Human simulations.

it remains to be seen what the effect of these uncertainties will be on the accuracy of the calculated trajectories. Trajectory calculation times also proved longer for scenario 142 compared to the other scenarios. Hence, scenario 142 proved to be a difficult optimization problem and sensitive to the supplied initial conditions.



(a) Comparison of fuel consumption per scenario between Human vs. Autobot runs. (b) Comparison of NO_x emitted below the mixing height between Human vs. Autobot runs.

FIGURE 4-10: Fuel and NO_x comparison between Autobot and Human simulations including the 95% confidence interval for the Human simulations.

Figure 4.9(b) shows a noise comparison between the human and Autobot runs. Results show that on average, the human runs generate slightly (2%) larger 75 dB SEL contour areas. The data in Figure 4.9(b) also shows that the energy disturbance at ToD results in a slightly larger 75 dB SEL contour. Interestingly, a negative CTA offset (arriving early) yields a

slightly smaller contour even though more thrust is required and more fuel is burned as shown in Figure 4.10(a). This additional engine use is compensated by the reduced flight duration, which counteracts these effects and reduces the noise contour area.

Figure 4.10(a) shows only small differences in fuel consumption of less than 0.5%. In certain scenarios the human runs consumed slightly less fuel, compared to automated response, which is the result of different solutions found after replanning. This holds in particular for the computationally difficult scenario 142 that found quite different trajectories due to late entering of CTA data into the FMS. Evident from this figure is the effect of flight duration on fuel use since arriving early costs more fuel.

Overall, automated response reduced NO_x emissions below 3,000 ft by only 2.3% compared to piloted runs.

4-7 Discussion

The performance data suggests that none of the three HMI's enabled pilots to perform actions more accurate, although the configuration timer showed to reduce the variance in configuration selection. However, this had only a minor effect on the actual time of arrival at the runway threshold. Hence, HMI variant 1 provides sufficient information to support pilots in flying TEMO descents. Pilots argued, however, that they prefer to have the configuration timer present as it supports them in selecting configurations on time. However, they opted to replace the timer by an aural cue to avoid distraction. Consequently, HMI 2 is the preferred HMI. Although the TEI (HMI 3) was designed to improve human-machine coordination, pilots responded that in the limited scope of this experiment, the TEI is not required for successful TEMO operations, but would be useful in real-life operations.

TEMO requires configuration changes to be performed at fixed nominal speeds as research [39] indicated the risk of increased wear if flaps are used to control aircraft speed. Although pilots found the configuration changes manageable but strict, they would prefer the ability to deviate from the commanded configuration changes to correct time deviations when descending on the glideslope. This yields a degree of freedom on the glideslope without using thrust or speedbrakes as pilots could add drag to reduce airspeed when flying faster than originally planned. Conversely, postponing selections could help the aircraft to gain time.

Pilots responded that the strict and accurate selection of configurations can not be achieved in real-life operations. Therefore, the TEMO concept should be revised to allow dynamic configuration changes for closed-loop control during descent down the glideslope. This reduces the need for strict selection of configurations as such variations can be corrected using the next configuration selection. For pilot-support, a flap-scheduling algorithm [39, 40] could use reduced maximum configuration extension speeds to reduce flap wear. Furthermore, flap-scheduling reduces the need for a configuration timer as data showed that the accuracy of the timer in estimating the timer start location is limited, due to speed and energy deviations during timer countdown.

The performance data also showed that the energy deviation at the glideslope intercept

point significantly affects the time of arrival for the Autobot runs, while for the human runs this effect was smaller due to variations in pilot response. Time deviations occur due to modeling errors in the planned trajectory and are inherent to strategic replanning, which allows deviations from the planned trajectory within boundaries. Reducing these deviations by enhanced modeling is limited to what we know of our environment [26] and is likely to extend replan calculation times. Therefore, the deviation boundaries could be constricted to reduce the allowed deviations while the glideslope intercept guidance could be enhanced to simultaneously intercept the glideslope whilst following the speed profile using thrust or speedbrakes.

Since replanning is disabled after glideslope intercept, the aircraft descends for an extended period during which deviations can occur and grow that are not corrected. Moving TEMO towards real-life operations will introduce more uncertainties than currently modeled. Aircraft mass, engine dynamics and wind will continuously disturb a TEMO descent. Hence, if strict time accuracies are required, sustained deviations and errors should be minimized, even on the glideslope. However, replans were often unsuccessful on the glideslope and close to the runway. For this reason, a different strategy is required to correct deviations during final descent to ‘close-the-loop’. The TEMO system could be closed using automation or the human pilot. Using a tactical control-law, automation supports the system to minimize deviations by continuously correcting deviations. This can be achieved by continuously changing the speed profile [5] or through flap-scheduling [39, 40]. Alternatively, the role of the supervising pilot could be increased by using flaps to control aircraft speed and by monitoring deviations to negotiate new constraints with ATC when required and possible. However, both solutions introduce new human-machine coordination issues that require further investigation.

4-8 Conclusions

Time and Energy Managed Operations (TEMO) was evaluated in a human-in-the-loop simulation study to evaluate the conceptual procedures and display support required by pilots to perform TEMO operations. Pilots responded that the procedures were clear and the pilots preferred HMI variant 2 that included the configuration timer. Analysis of objective data showed that there were no observed differences in performance using any of the three displays. Pilots responded that the requirement of accurate selection of configuration changes is too strict and would appreciate the ability to deviate from planned selection points. A comparison between human response and automated zero-delay response showed little effect of response variations on the environmental impact of a Time and Energy Managed Operations (TEMO) descent. However, TEMO performance is affected by human response as in some cases pilots do not arrive at the runway threshold within the Required Time Performance. However, the difference in time deviation with respect to the Autobot runs is small, suggesting that TEMO planning and guidance need improvement to reduce time deviation. Consequently, pilots were accurately informed to perform their actions. When the required accuracy of 2 seconds is necessary, the final segment where configuration changes

are executed requires further research since in this phase the largest time deviations occur while replanning is currently disabled.

Acknowledgments

The research leading to these results received funding from the European Union's Seventh Framework Programme (FP7/2007-2013) through the Clean Sky Joint Technology Initiative under Grant Agreement no. CSJU-GAM-SGO-2008-001.

The authors acknowledge the contributions of Monique Heiligers, Gerard Temme, Wim Huson, Vincent Steinmetz and Jon Ertzgaard of the NOCONDES consortium during preparation and execution of this experiment. Furthermore, Jaap Groeneweg, Bart Heesbeen, Adri Marsman and Michiel Valens (all NLR) and Clark Borst (TU Delft) are acknowledged. Much appreciation goes out to all pilots that participated in the experiment.

References

- [1] **EUROCONTROL**. Long-Term Forecast: IFR Flight Movements 2010-2030. Tech. Rep. CND/STATFOR Doc415, EUROCONTROL, 2010.
- [2] **NextGen Office**. FAA's NextGen Implementation Plan 2012. Tech. rep., FAA, 800 Independence Avenue, Washington, DC, 2012.
- [3] **SESAR**. European ATM Master Plan. Tech. Rep. Edition 2, EUROCONTROL, 2012. SESAR JU & SESAR Work Package C and Partners.
- [4] **ICAO**. *Continuous Descent Operations (CDO) Manual - Doc 9931 AN/476*. International Civil Aviation Organization, Montreal, Canada, 2010.
- [5] **P. M. A. De Jong, N. De Gelder, F. J. L. Bussink, R. P. M. Verhoeven, R. Kohrs, M. M. Van Paassen, and M. Mulder**. Time and Energy Management during Descent and Approach for Aircraft: A Batch-Simulation Study. *Journal of Aircraft*, 2013. Submitted for publication.
- [6] **D. H. Williams, R. M. Oseguera-Lohr, and E. T. Lewis**. Design and Testing of a Low Noise Flight Guidance Concept. Technical Memorandum NASA/TM-2004-213516, National Aeronautics and Space Administration, Langley Research Center, Hampton, Virginia 23681-2199, 2004.
- [7] **R. M. Oseguera-Lohr, D. H. Williams, and E. T. Lewis**. Crew Procedures for Continuous Descent Arrivals Using Conventional Guidance. Technical Memorandum NASA/TM-2007-214538, National Aeronautics and Space Administration, Langley Research Center, Hampton, Virginia 23681-2199, 2007.

- [8] **J. K. Klooster, K. D. Wickman, and O. F. Bleeker.** 4D Trajectory and Time-of-Arrival Control to Enable Continuous Descent Arrivals. In: *Proceedings of the AIAA Guidance, Navigation and Control Conference and Exhibit, Honolulu, Hawaii, August 18–21*, AIAA 2008-7402, pp. 1–17. American Institute of Aeronautics and Astronautics, 2008. doi:10.2514/6.2008-7402.
- [9] **D. Garrido-López, L. D’Alto, and R. Gomez Ledesma.** A Novel Four-Dimensional Guidance for Continuous Descent Approaches. In: *Proceedings of the 28th Digital Avionics Systems Conference, Orlando, Florida, October 23–29*, pp. 6.E.1–1–6.E.1–11. IEEE/AIAA, 2009. doi:10.1109/DASC.2009.5347433.
- [10] **J. L. De Prins and R. Gomez Ledesma.** Towards Time-based Continuous Descent Operations with Mixed 4D FMS Equipage. In: *Proceedings of the 11th AIAA Aviation Technology, Integration, and Operations (ATIO) Conference, Virginia Beach, Virginia, September 20–22*, AIAA 2011-7018, pp. 1–18. American Institute of Aeronautics and Astronautics, 2011. doi:10.2514/6.2011-7018.
- [11] **D. H. Williams, R. M. Oseguera-Lohr, and E. T. Lewis.** Energy Navigation: Simulation Evaluation and Benefit Analysis. Technical Publication NASA/TP-2011-217167, National Aeronautics and Space Administration, Langley Research Center, Hampton, Virginia 23681-2199, 2011.
- [12] **S. G. Park and J.-P. B. Clarke.** Vertical Trajectory Optimization for Continuous Descent Arrival Procedure. In: *Proceedings of the AIAA Guidance, Navigation and Control Conference, Minneapolis, Minnesota, August 13–16*, AIAA 2012-4757, pp. 1–19. American Institute of Aeronautics and Astronautics, 2012. doi:10.2514/6.2012-4757.
- [13] **M. R. Endsley.** Automation and Situation Awareness. In: **R. Parasuraman and M. Mouloua**, eds., *Automation and Human Performance: Theory and Applications*, pp. 163–181. Lawrence Erlbaum Associates, Inc., Mahway, New Jersey, 1996.
- [14] **C. E. Billings.** *Aviation Automation: The Search for a Human-Centered Approach*. Lawrence Erlbaum Associates, Inc., Mahway, New Jersey, 1997.
- [15] **R. Parasuraman, T. B. Sheridan, and C. D. Wickens.** A Model for Types and Levels of Human Interaction with Automation. *IEEE Transactions on Systems, Man and Cybernetics, Part A*, 30(3), 286–297, 2000. doi:10.1109/3468.844354.
- [16] **S. W. A. Dekker.** On the other side of promise: what should we automate today? In: **D. Harris**, ed., *Human Factors for Civil Flight Deck Design*, chap. 8, pp. 183–198. Ashgate Publishing Limited, 2004.
- [17] **L. Bainbridge.** Ironies of Automation. *Automatica*, 19(6), 775–779, 1983. doi:10.1016/0005-1098(83)90046-8.
- [18] **K. J. Vicente and J. Rasmussen.** Ecological Interface Design: Theoretical Foundations. *IEEE Transactions on Systems, Man, and Cybernetics*, 22(4), 589–606, 1992. doi:10.1109/21.156574.

- [19] **K. Christoffersen** and **D. D. Woods**. How to Make Automated Teams Team Players. In: **E. Salas**, ed., *Advances in Human Performance and Cognitive Engineering Research*, vol. 2, pp. 1–12. JAI Press/Elsevier, 2002.
- [20] **T. S. Abbot**. A Brief History of Airborne Self-Spacing Concepts. Contractor Report NASA/CR–2009-215695, National Aeronautics and Space Administration, Langley Research Center, Hampton, Virginia 23681-2199, 2009.
- [21] **R. P. M. Verhoeven**. Pseudospectral aircraft descent trajectory optimization: An initial implementation. Contract Report NLR-CR-2012-378, National Aerospace Laboratory, Amsterdam, The Netherlands, 2012.
- [22] **V. M. Becerra**. Solving complex optimal control problems at no cost with PSOPT. In: *Proceedings of the IEEE International Symposium on Computer-Aided Control System Design (CACSD), Yokohama, Japan, 8–10 September*, pp. 1391–1396, 2010. doi:10.1109/CACSD.2010.5612676.
- [23] **S. Muresean**. Initial 4D - 4D Trajectory Data Link (4DTRAD) - Concept of Operations. Tech. rep., EUROCONTROL, Brussels, Belgium, 2008.
- [24] **D. B. Kaber** and **M. R. Endsley**. Out-of-the-Loop Performance Problems and the Use of Intermediate Levels of Automation for Improved Control System Functioning and Safety. *Progress Saftey Progress*, 16(3), 126–131, 1997. doi:10.1002/prs.680160304.
- [25] **N. B. Sarter** and **D. D. Woods**. Team Play with a Powerful and Independent Agent: Operational Experiences and Automation Surprises on the Airbus A-320. *Human Factors*, 39(4), 553–569, 1997.
- [26] **T. B. Sheridan**. *Telerobotics, Automation, and Human Supervisory Control*. MIT Press, Cambridge, Massachusetts, 1992.
- [27] **C. Borst**, **M. Mulder**, and **M. M. Van Paassen**. Design and Simulator Evaluation of an Ecological Synthetic Vision Display. *Journal of Guidance, Control and Dynamics*, 33(5), 1577–1591, 2010. doi:10.2514/1.47832.
- [28] **J. Ellerbroek**, **M. Visser**, **S. B. J. Van Dam**, **M. Mulder**, and **M. M. Van Paassen**. Design of an Airborne Three-Dimensional Separation Assistance Display. *IEEE Transactions on Systems, Man, and Cybernetics, part A: Systems and Humans*, 41(6), 863–875, 2011. ISSN 1083-4427. doi:10.1109/TSMCA.2010.2093890.
- [29] **S. Vèque**. A318 - Steep Approach Operation. Presentation at OLM FBW 2006, Toulouse, France, 2006.
- [30] **P. Smith**. Date with the Eight. *Flight International*, 182(5370), 26–35, 2012.
- [31] **H. Smaili**, **M. Laban**, and **J. Dominicus**. New Integrated Modeling and Simulation Techniques for Research and Training Applications. In: *Proceedings of the*

- AIAA Modeling and Simulation Technologies Conference and Exhibit, San Francisco, California, 15–18 August*, AIAA 2005-6294, pp. 1–17. American Institute of Aeronautics and Astronautics, 2005. doi:10.2514/6.2005-6294.
- [32] **F. R. H. Zijlstra**. *Efficiency in Work Behaviour: A Design Approach for Modern Tools*. Ph.D. thesis, Delft University of Technology, 1993.
- [33] **S. G. Hart** and **L. E. Staveland**. Development of NASA-TLX (Task Load Index): Results of Empirical and Theoretical Research. *Human Mental Workload (Advances in Psychology)*, 52, 139–183, 1988. doi:10.1016/S0166-4115(08)62386-9.
- [34] **K. K. Lee** and **T. J. Davis**. The Development of the Final Approach Spacing Tool (FAST): A Cooperative Controller-Engineer Design Approach. Tech. Rep. NASA Technical Memorandum 110359, National Aeronautics and Space Administration, 1995.
- [35] Standard Method of Computing Noise Contours around Civil Airports. Tech. Rep. Document 29, ECAC/CEAC, 2005. 3rd Edition, Volume 1.
- [36] **R. L. Martin**, **C. A. Oncina**, and **J. P. Zeeben**. A simplified method for estimating aircraft engine emissions. In: **S. L. Baughcum**, **T. G. Tritz**, **S. C. Henderson**, and **D. C. Pickett**, eds., *Scheduled Civil Aircraft Emission Inventories for 1992: Database Development and Analysis - NASA Contractor Report 4700, April 1996*, pp. D1–D11. National Aeronautics and Space Administration, 1995. Reported as “Boeing Method 2” fuel flow methodology description in appendix D.
- [37] **A. Field**. *Discovering Statistics using SPSS*. SAGE Publications Ltd, 1 Oliver’s Yard, 55 City Road, London EC1Y 1SP, 2009.
- [38] **J. H. Zar**. *Biostatistical Analysis*. Prentice Hall, Inc., Upper Saddle River, New Jersey, fifth edn., 2010.
- [39] **A. M. P. De Leege**, **A. C. In ’t Veld**, **M. Mulder**, and **M. M. Van Paassen**. Three-Degree Decelerating Approaches in High Density Arrival Streams. *Journal of Aircraft*, 46(5), 1681–1691, 2009. doi:10.2514/1.42420.
- [40] **P. M. A. De Jong**, **A. C. In ’t Veld**, **A. M. P. De Leege**, **M. M. Van Paassen**, and **M. Mulder**. Control Space Analysis of Three-Degree Decelerating Approaches at Amsterdam Airport Schiphol. In: *Proceedings of the AIAA Guidance, Navigation and Control Conference, Toronto, Ontario Canada, August 2–5*, AIAA 2010-8454, pp. 1–20. American Institute of Aeronautics and Astronautics, 2010. doi:10.2514/6.2010-8454.

WIND PROFILE ESTIMATION USING AIRBORNE SENSORS

As discussed in Chapter 1, the accuracy of trajectory predictors depend on the quality of the data inputs. One of these input is wind data which contributes largely to the accuracy of the trajectory predictor. To reduce the uncertainty of wind data, this chapter presents the Airborne Wind Estimation Algorithm (AWEA). This algorithm reduces the noise in wind observations that serve as input to the Trajectory Predictor. This chapter starts with background theory and implementation, and results will show the advantages of onboard wind estimation for trajectory prediction and airborne spacing.

Paper title Wind Profile Estimation using Airborne Sensors

Authors P.M.A. de Jong, J.J. van der Laan, A.C. in 't Veld, M.M. van Paassen and M. Mulder

Published in Submitted to Journal of Aircraft 2013

ABSTRACT

Wind is one of the major contributors to uncertainties while flying Continuous Descent Operations. When aircraft are issued a required time of arrival over the runway threshold, as is foreseen in some of the future Air Transportation System concepts, the onboard availability of both dependable and accurate wind estimates becomes a necessity for spacing. This paper presents a method for real-time estimation of a wind profile in the terminal maneuvering area, based on data transmitted by nearby aircraft. The algorithm produces high resolution and real-time wind profile estimates, usable for accurate trajectory prediction to improve Continuous Descent Operations and spacing performance. The wind estimation algorithm is tested with Mode-S derived meteorological data from Amsterdam Airport Schiphol. It combines multiple measurements from different aircraft to estimate the current wind profile using a Kalman filter. Using these wind observations data, the algorithm showed a Root Mean Square in the estimation error of 1.35 KTS, which is lower than the observed Root Mean Square measurement error Root Mean Square of 1.94 KTS. The algorithm proved to be capable of accurate wind prediction along the own trajectory which significantly improves spacing performance during approach.

5-1 Introduction

Studies on new approach procedures, such as Boeing's Tailored Arrivals (TA) [1], Optimum Profile Descent (OPD) [2, 3] into San Francisco International Airport and Los Angeles International Airport, and Time and Energy Managed Operations (TEMO) [4, 5] have shown that a sufficiently accurate wind estimate is required for accurate descent profile prediction. Other studies investigated the effect of wind on, for example, time-of-arrival control [6, 7], predicting Top of Descent (ToD) [8] for idle descents and self-spacing [9] and concluded that for accurate trajectory predictions, an accurate knowledge of the prevailing winds is required [10–15].

Today, pilots mostly rely on Automatic Terminal Information Service reports and meteorological wind-charts which are slowly updated and of low resolution. These charts are used to update the onboard Flight Management System (FMS) with winds aloft information used by the Trajectory Predictor (TP) to perform fuel and time predictions. Different studies have turned to different solutions to improve wind information in the FMS, ranging from a simple profile [16] based on the wind measured onboard the aircraft and the wind reported at the runway [6], to up-linking high resolution wind grids [1, 17–19]. Mondoloni used statistical data and Kalman filtering techniques [20] to predict wind for use in trajectory prediction. Others have used aircraft radar tracks [21, 22] to estimate the windfield at an aircraft's position and use Kalman filtering to reduce the effects of measurement noise. Some solutions offer a high-resolution profile but do not provide a high update rate [1, 17–19] or only provide an estimate for a certain area [22].

To construct high resolution and real-time updated wind profile estimates for use during trajectory prediction, a novel wind estimation algorithm, referred to as Airborne Wind Estimation Algorithm (AWEA), has been developed [9, 23–25]. The rationale of AWEA is to take advantage of the fact that in the near future aircraft will be equipped with a data-link system, such as Automatic Dependent Surveillance - Broadcast (ADS-B), that could

broadcast measured atmospheric data. This allows aircraft to gather reliable atmospheric information from nearby aircraft at short time intervals.

AWEA constructs tailor-made wind estimation profiles using Kalman filtering. This allows to reduce noise from these measurements and to relate the various received measurements to the own trajectory. The benefit of this approach is that all aircraft produce information of the wind close to the own aircraft and, as such, act as airborne sensors, increasing the resolution and update rate of wind estimates significantly. This allows trajectory predictors to use the latest available and accurate wind estimates when predicting trajectories.

The paper is structured as follows: Section 5-2 covers background information regarding wind estimation, trajectory prediction and atmospheric measurements. Section 5-3 gives an overview of the concept of operation and principles used in this research. Section 5-4 contains the mathematical description of the new wind estimator algorithm. Section 5-5 presents results of two case-studies based on either derived real-life wind data or simulated wind data to review the performance of the new wind estimator. Finally, conclusions are drawn in Section 5-6 and the paper ends with a set of recommendations for further research.

5-2 Background

This section discusses how wind is estimated onboard aircraft and how wind estimates affect trajectory predictions. The section continues with today's approach to wind estimation used for trajectory prediction and possible ways for improvement.

5-2-1 Wind Estimation

Figure 5-1 shows an overview of the kinematics of an aircraft in horizontal flight and with a horizontal wind acting upon the aircraft. In this figure, the a -subscript denotes the air reference frame, the g -subscript denotes the Earth reference frame and the k -subscript denotes the aircraft kinematic reference frame.

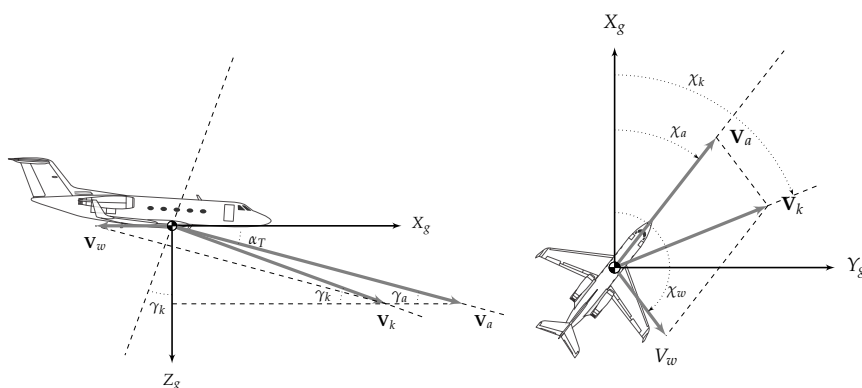


FIGURE 5-1: The effect of wind on an aircraft's trajectory during descent.

The aircraft groundspeed \mathbf{V}_g equals the horizontal component of the \mathbf{V}_k relative to the Earth. The wind speed vector \mathbf{V}_w is calculated onboard the aircraft by resolving the speed vectors \mathbf{V}_a , the True Airspeed (TAS), and groundspeed \mathbf{V}_g , see Figure 5-1. The TAS is determined using the Air Data Computer (ADC) and pitot-static system for input of impact pressure, static pressure and total air temperature. The groundspeed is calculated by the Inertial Reference Unit (IRU) and Global Positioning System (GPS). The vector calculation to obtain the wind speed is given by:

$$\mathbf{V}_w = \mathbf{V}_g - \mathbf{V}_a \quad \text{5-1}$$

Figure 5-1 shows that a horizontal headwind, \mathbf{V}_w , decreases the horizontal component of \mathbf{V}_k or aircraft groundspeed. When the aircraft is descending, the same windfield increases the flight-path angle relative to the Earth, γ_k , provided the aircraft descends at a given speed. Thus an aircraft will require a shorter distance to descend from the same altitude relative to a situation where the aircraft experiences no wind or a tailwind. When the windfield varies with altitude, the motion of the aircraft relative to the air varies as well [26, 27] affecting both the acceleration and descent angle change due to this wind gradient.

All velocity vectors must be measured with sufficient accuracy to accurately determine the wind since horizontal winds are relatively small compared to the true airspeed and groundspeed. It also requires measurements of the aircraft body angles and angle of attack. However, during descent the aircraft flight-path angle is relatively small, causing the aircraft's velocity component to be largest in horizontal direction. For this reason, the calculations can be simplified to include only TAS, groundspeed and heading and track angles by neglecting any vertical wind components [28]. From this point onward, wind is only considered in horizontal direction in this paper.

5-2-2 Applications of Wind Estimation

The FMS predicts trajectory parameters, such as Estimated-Time of Arrivals (ETAs) and fuel estimates, by performing calculations that require estimates of the windfield along the trajectory towards the arrival airport to improve the accuracy of these calculations. An error in estimating the windfield will result in an error of the predicted groundspeed, deceleration and flight-path angle. In turn, the flight-path angle error affects the predicted groundspeed and predicted vertical trajectory. Hence, the accuracy of the trajectory, both temporal and spatial, is greatly influenced by the wind estimation error [10, 11].

Today's FMSs are able to store wind and temperature information at waypoints contained in the flightplan during cruise. For climb and descent, the FMS has typically five altitude points available that can contain wind information, and linearly interpolates between these altitudes [29] and extrapolates beyond the altitude limits. Due to the low resolution of available data points (both horizontal and vertical), the FMS introduces an interpolation uncertainty additional to the wind prediction error. The FMS uses the sensed wind to correct the predicted winds by calculating a correction from the difference between the sensed and predicted wind [30].

5-2-3 Current Methods for Wind Estimation

The winds aloft data can be entered manually from paper or automatically through Aircraft Communication and Reporting System (ACARS) to simplify operations. The data is generally provided by airline dispatch who uses winds aloft data from weather sources, such as National Oceanic and Atmospheric Administration (NOAA)'s Aviation Weather Center. These forecast winds (and temperature) aloft data are generated four times a day for various worldwide locations at several altitudes. The winds aloft data are generated using complex numerical weather models that use observational data from radiosondes, satellites and aircraft as input. The predicted data are valid until 6, 12 or 24 hours beyond their issued time and thus the spatial and temporal resolution is low. However, for longer flights, it could be beneficial to update the winds aloft data when new data is available through a data-link.

To address the low update rate, Boeing developed *Wind Updates* [17] in an aim to reduce fuel. This service sends specifically tailored and updated wind information to each individual aircraft subscribed to the service. Pilots can accept the received data set through the ACARS control panel which automatically updates the wind data in the FMS. However, the system does not include additional altitude intervals at which wind data can be stored and thus primarily increases the temporal resolution of the wind estimates. AVTECH's Aventus NowCast [18] works in a similar way.

5-2-4 Atmospheric Measurements using Airborne Aircraft

Onboard aircraft, atmospheric parameters are calculated by the ADC. This data can be retrieved by other aircraft or ground-stations using various techniques, detailed in this section.

AMDAR

To increase the accuracy of numerical weather prediction, the World Meteorological Organization (WMO) in the 1970s proposed the Aircraft Meteorological Data Relay (AMDAR) [31] project to use aircraft sensory data to improve the number of observations used in (global) weather forecast models. The sensory data is transmitted automatically through ACARS or a satellite-based equivalent and has been active since the late 1990s [31]. The AMDAR panel foresees the use of Automatic Dependent Surveillance (ADS) for broadcasting of meteorological data in the future.

The observed atmospheric data is combined into a single AMDAR report [31] that contains position (latitude and longitude), altitude, time, temperature, (horizontal) wind direction and speed, turbulence (vertical acceleration), humidity and icing, phase of flight, a number of aircraft state variables such as roll and pitch angles, and an aircraft identifier.

Mode-S

A novel method uses aircraft transponder data to increase the number of atmospheric observations for estimating windfields [32, 33]. The Secondary Surveillance Radar (SSR) radars at major airports receive Mode-S Elementary Surveillance (Mode-S ELS) data from all air-

craft within range containing velocity and position data. These Mode-S ELS data messages are different from AMDAR data since these do not include direct wind and temperature measurements. However, aircraft transponders featuring Mode-S Enhanced Surveillance (Mode-S EHS) are able to relay additional information containing various Downlink Aircraft Parameters (DAP) integrated in Comm-B Data Selector (BDS) registers upon request that can be used to derive temperature and wind estimates.

These additional BDS registers contain flight level, Mach number, roll, heading and track angles, and TAS. The tracking radar complements the received messages with ground-speed, track and position information. The combined information is then used to derive the wind vector from TAS and groundspeed whereas temperature information is derived from TAS and Mach number as temperature measurements are not included in the Mode-S message [32].

Automatic Dependent Surveillance (ADS)

Using ADS, aircraft broadcast parameters at specified time intervals using a data-link system such as Mode-S Extended Squitter (Mode-S ES), Universal Access Transceiver (UAT) or VHF Data Link (VDL). The specification of Automatic Dependent Surveillance - Broadcast (ADS-B) prescribes the Air Referenced Velocity (ARV) report which contains TAS and heading information, while groundspeed and ground track are available from the State Vector (SV) report [28]. Using the data from these reports, the wind vector [28] can be resolved. However, according to de Leege [22], only few aircraft currently broadcast the ARV report resulting in a low availability of wind-derived data using ADS-B. Furthermore, as SV and ARV reports are broadcast at different rates (respectively 1 s and 30 s) [28], which will result in additional wind error.

Additionally, Automatic Dependent Surveillance - Contract (ADS-C) messages contain meteorological data upon request as agreed upon in a 'contract' between a ground-station and aircraft. ADS-C reports consist of several aircraft data blocks [34, 35], including a meteorological data block and air vector and ground vector blocks. The contract specifies sampling rate and content of the ADS-C reports. The meteorological data block contains wind speed and direction, temperature, humidity and turbulence data. Combined with the basic data block that contains spatial information, a full meteorological report is received. ADS-C messages without meteorological data can still be useful when only the ground and air vector blocks are received by deriving the wind vector from remaining data [33].

5-2-5 Future Needs

Aircraft primarily use rather coarse wind charts as input in the FMS which does not offer sufficient accuracy for today and tomorrow's demand for accurate flying of 4D RNP trajectories [36]. System Wide Information Management (SWIM) [36] is also expected to share meteorological data between users. By using the received meteorological observations from aircraft within range, an improved estimate of the prevailing winds can be constructed and frequently updated when new observations are received.

Combining this estimate with knowledge of the own trajectory, an aircraft specific wind estimate can be constructed along this profile. When the trajectory is unknown, for example on the ground, a wind profile or 3D grid for an entire area could be estimated.

5-3 AWEA: Airborne Wind Estimation Algorithm

This section discusses the basic principles of the new wind estimation algorithm, AWEA. AWEA is specifically developed for use onboard aircraft to improve onboard trajectory prediction but can also be used on the ground for estimation of an entire windfield.

5-3-1 AWEA Working Principles

AWEA uses airborne measurements from the own aircraft and other nearby aircraft to construct a wind profile along the own trajectory. The wind profile is modeled using a stochastic model. The advantage of such a model is that it does not rely on the modeling of physical processes that govern wind behavior but instead uses observations and stochastic principles to estimate any profile shape.

AWEA uses all incoming wind observation data from other aircraft within its range of reception. These observations are grouped together into equal altitude intervals. Measurements could be received through ADS, using a capable ADS-B-IN receiver or ADS-C through a relay station, as long as sufficient data is transmitted to derive a wind measurement. Next, the noise in the received data is filtered using a Kalman filter [37]. The purpose of the filter is to reduce the noise components from the measured wind data and to assign smaller weights to measurements that were taken at a larger distance from the own trajectory. The Kalman filter state vector consists of estimates at these altitude intervals. The smoothed data is used to construct a wind estimation for every altitude interval over a short time interval. These estimated wind speeds and directions are then combined to form the estimated wind profile using linear interpolation. The complete process is repeated at every time step including newly collected data. Every step of this iterative process will be discussed in more detail in the following sections.

AWEA runs separately for all meteorological variables for simplicity and to avoid non-linear state and observation dynamics of an Extended Kalman Filter (EKF) and multiplication effects of noise in speed and direction. For all variables, the state vector would be equal in size but the noise matrices contain different values to account for the differences in accuracy of the respective sensors. Running the algorithm for wind speed and direction separately, yields wind speed and wind direction profile estimates along the own 2-dimensional (altitude, along-track-distance) trajectory. For the remainder of this paper, only wind speed observations are discussed but the same algorithm principles hold for other meteorological sensory data, such as temperature or pressure.

The benefit of using aircraft data is that the observed meteorological data is spatially and temporally concentrated around the busiest routes at cruise altitudes and in the Terminal Maneuvering Areas (TMAs) around major airports, where aircraft typically follow the same

arrival and departure routes based on Area Navigation (RNAV) or Air Traffic Control (ATC) vectoring. Inevitably, the accuracy in the wind estimation at less crowded airports or during low traffic hours will be lower. This is not expected to cause major issues since in these situations the demanded runway capacity is usually substantially less than the maximum available capacity and lower trajectory prediction accuracy is acceptable.

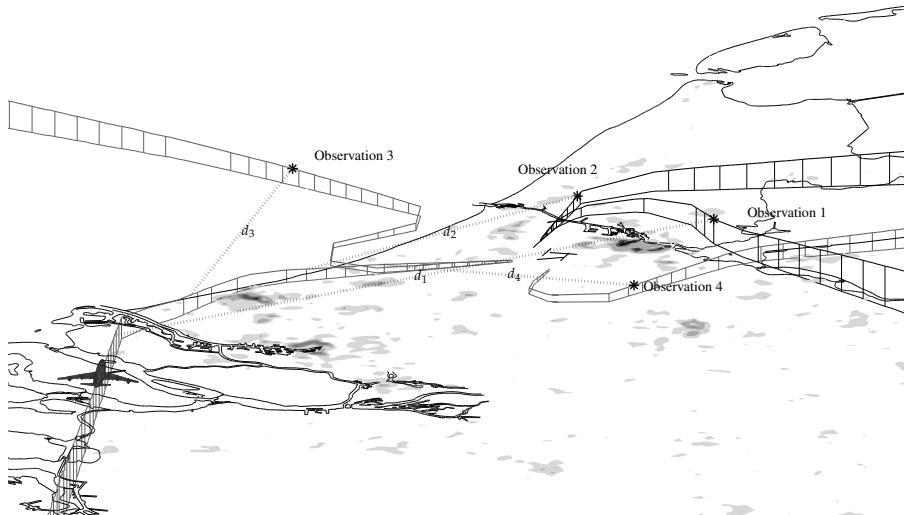


FIGURE 5-2: Own track of an aircraft (with aircraft symbol). The tracks of two departing aircraft (Observations 1 & 2) and two arriving aircraft (Observations 3 & 4) are also displayed. The asterisks indicate observations from other aircraft and their projections upon the own trajectory.

To account for the distance between the location of the measurement and the own trajectory (or grid-point in case of a ground-based station), the Kalman filter optionally uses this distance to adjust the influence of the observation on the new estimate by adding distance-based uncertainty to the measurement. This distance d is calculated by the shortest distance between the measurement and the planned position of the aircraft where it reaches the measurement altitude. An arbitrary 3-dimensional approach path of the own aircraft and tracks of other aircraft within the Amsterdam Airport Schiphol TMA is illustrated in Figure 5-2. Also shown in this figure are trajectories and observations from other arriving and departing aircraft. The relative distance d between the observation and the projection upon the own trajectory are indicated with dotted-lines. This relative distance is included in the Kalman filter as explained in Section 5-4.

5-3-2 Implementation Methods

AWEA can be run onboard the aircraft, where data are processed by the FMS, or run on ground, as seen in Figure 5-3. AWEA as an aircraft-based implementation, see Figure 5.3(a), uses observations from the own and surrounding aircraft, and optionally complemented

with a profile received from a ground station. The airborne observations contain distance information and are used to alter the current estimate based upon the aircraft's trajectory to the runway. This allows for tailored wind profile estimation and increases the update rate of the estimation as the algorithm receives frequent updates from other aircraft.

A ground-based implementation, as seen in Figure 5.3(b), could work as follows: a ground station uses AWEA and receives meteorological observations to continuously estimate a wind profile representative for the entire TMA. When aircraft enter the TMA, they receive the latest estimated wind profile to update planning of the final segment of the descent. Updated wind profiles could be sent more frequently but this will require significant bandwidth.

The ground station could estimate the wind along 3D grid-points using distant information between a grid-point and an aircraft. An intelligent algorithm, using aircraft intent, could create a tailored wind profile for each aircraft entering the TMA. Alternatively, to simplify the implementation, distance information can be ignored to obtain a wind profile representative of the entire TMA. Hence, all aircraft entering the TMA at the same time will receive the same profile.

A ground-based implementation of AWEA provides ATC with an estimated wind profile to support accurate vectoring of aircraft. Moreover, aircraft without ADS-C capabilities or with insufficient FMS computational power to use AWEA could receive an estimated profile constructed by a ground station [9]. The update rate and accuracy will be lower compared to an onboard estimator but at least wind data will be available with an improved resolution. This way, more aircraft benefit from the airborne 'sensors' nearby.

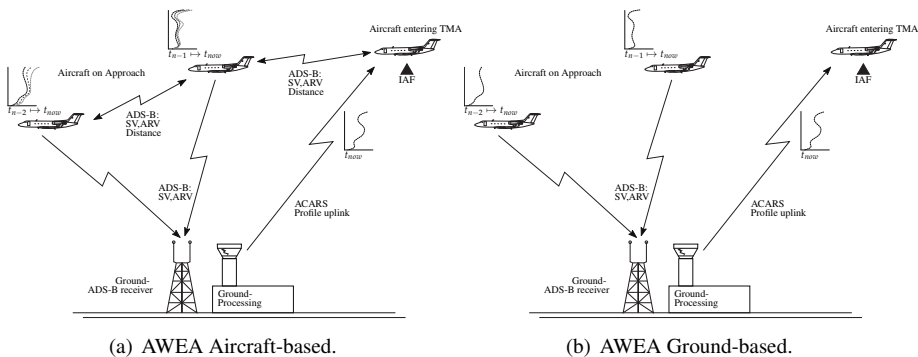


FIGURE 5-3: Various methods of implementing AWEA.

5-4 AWEA Algorithm Principles

This section discusses the principles of the estimation algorithm running onboard an aircraft to estimate wind speed and resides inside the FMS. However, the derivations are similar for use in a ground station that would construct the wind profile for an entire area or 3D grid.

5-4-1 Main Steps of the Algorithm

The algorithm consists of the following steps to construct a wind profile estimation:

- Step 1: Determine the nominal flight profile of the own aircraft. This profile is the intended route as currently planned. Along this profile, the wind profile will be estimated. The altitude resolution of the state vector is chosen to provide the desired altitude resolution; here set to 500 ft. It is noted that the accuracy of the estimation depends on the number of measurements and the spatial and temporal spread of the incoming data. Using smaller intervals increases the accuracy of the estimates slightly but increases algorithm calculation times.
- Step 2: Generate an initial estimate. This initial estimate can be based upon a nominal profile provided by a ground station, or constructed using a wind measurement from the own aircraft. Based on this own measurement, a standard logarithmic wind profile is constructed according to the power-law [38]:

$$V_w(h) = V_{w_0} \left(\frac{h}{h_0} \right)^p \quad 5-2$$

In this equation, V_w varies with altitude and depends on the wind velocity V_{w_0} at a reference altitude h . The exponent p is an empirically derived constant and has a value of $1/7$ [38].

- Step 3: Update the Kalman filter. Although all aircraft broadcast data at the same rate, they do so at different times. Moreover, the Kalman filter considers measurements at each update step to be broadcast at the same moment in time. Therefore, the Kalman filter is updated at 1 Hz intervals to allow for a fast update of the estimates. This final step is discussed in more detail in the next section.

5-4-2 AWEA Kalman Filter

AWEA uses a Kalman filter to reduce measurement noise and relate the incoming measurements to the own trajectory. The result of the filter is an estimated wind profile at arbitrary altitude intervals along the own trajectory.

The general state and measurement equations are given by:

$$\begin{aligned} x(k) &= A(k|k-1)x(k-1) + w(k-1) \\ y(k) &= C(k)x(k) + v(k) \end{aligned} \quad 5-3$$

In the state equation, $x(k)$ is the wind speed vector at time k including all observations up to time $k-1$. $A(k|k-1)$ is the transition matrix and $w(k-1)$ is the process noise. In the measurement equation, $y(k)$ is the measured wind speed vector at time k , $C(k)$ is the measurement matrix and $v(k)$ the measurement noise. AWEA does not include system (wind) dynamics in the estimation model, such that only filtering is applied. Therefore, the

transition matrix A reduces to the identity matrix, $A(k|k-1) = I(n \times n)$, where n is the number of altitude intervals (states) to be filtered.

The random variables w and v are process and measurement noise, respectively. Both noise sources are assumed to be constant, white, zero mean noise signals with,

$$\begin{aligned} Q &= \mathbb{E} \{ww^T\} \\ R &= \mathbb{E} \{vv^T\} \end{aligned} \quad \text{5-4}$$

The elements of the Kalman filter comprise of five consecutive steps, at each time instant k in the following fashion,

1. The filter starts to *predict* the state estimate \hat{x} and estimate covariance P . The estimated state vector \hat{x} is an $n \times 1$ vector, where n is the number of altitudes, depending on the chosen resolution (in this case, the resolution is set at 500 ft, depicted as Flight Levels). The state estimate, $\hat{x}(k|k-1)$, initially equals the previous estimate and is:

$$\hat{x}(k|k-1) = \begin{pmatrix} v_w^0 & v_w^{05} & v_w^{10} & v_w^{15} & \dots & v_w^{100} \end{pmatrix}^T \quad \text{5-5}$$

The prediction error covariance matrix, $P(n \times n)$, is predicted using the process noise covariance matrix $Q(n \times n)$ and no model dynamics:

$$P(k|k-1) = P(k-1|k-1) + Q(k-1) \quad \text{5-6}$$

In this equation $P(k|k-1)$ denotes the covariance of the state estimate at time k using all observations up to time $k-1$. The initial values of the P matrix are set high to assign more weight to incoming measurements as the accuracy of the initial wind estimate is uncertain.

2. When a new observation comes in, the wind speed or direction are stored, along with the altitude and position at which the observation was recorded (for example at 1,700 ft, N52° 14' 36.96" E4° 37' 8.76", indicates as $v_w^{1,700}$), and processed at the new *update* cycle of the filter:

$$y(k) = \begin{pmatrix} v_w^{1,700} \end{pmatrix} \quad \text{5-7}$$

The observations are used to construct the observation model matrix $C(m \times n)$, where m indicates the number of received observations. The C matrix determines which elements of the state vector can be updated when a measurement comes in, corresponding to the two points that are closest to the altitude of the measurement. The weights in the matrix are determined based on the altitude difference between the states of interest and the measurement and are linearly interpolated. In this example, with a

sample observation recorded at 1,700 ft (hence, between 1,500 ft and 2,000 ft), the C matrix is filled as:

$$C(k) = \begin{pmatrix} 0 & 0 & 0 & 0.6 & 0.4 & \dots & 0 \end{pmatrix} \quad 5-8$$

The observations also determine the measurement noise covariance matrix $R(m \times m)$. R depends on the shortest, horizontal, distance between the location of the measurement and the own track d in nautical miles (see Figure 5-2),

$$R(k) = \begin{pmatrix} R_0^{alt} + K_w \cdot d(k) & 0 & 0 & \dots & 0 \\ 0 & R_0^{alt} + K_w \cdot d(k) & 0 & \dots & 0 \\ \vdots & \vdots & \vdots & \ddots & \vdots \\ 0 & 0 & 0 & \dots & R_0^{alt} + K_w \cdot d(k) \end{pmatrix} \quad 5-9$$

where K_w is a scaling parameter, varying between 0 and 1, that determines the influence of an observation based upon the horizontal distance between the measurement and the own trajectory at the same altitude. For our example of a single measurement at 1,700 ft, the R matrix is:

$$R(k) = \begin{pmatrix} R_0^{1,700} + K_w \cdot d(k) \end{pmatrix} \quad 5-10$$

3. With the observation matrix, C , the current estimate for the altitude of the observation can be calculated, and its value can be compared to the measured value to determine the innovation, $e(m \times 1)$:

$$\hat{y}(k|k-1) = C(k)\hat{x}(k|k-1) \quad 5-11$$

$$e(k) = y(k) - \hat{y}(k|k-1) \quad 5-12$$

This approach assures that an incoming measurement influences only the states in its (vertical) vicinity as shown in Figure 5-4.

Using the C and R matrices, the innovation covariance matrix, $S(m \times m)$, is calculated:

$$S(k) = C(k)P(k|k-1)C(k)^T + R(k) \quad 5-13$$

where $P(k|k-1)$ is the prediction error covariance matrix calculated in Eq. (5-6).

4. The next step determines the Kalman gain, $K(n \times m)$, by using the observation model, state covariance and innovation covariance matrices. The Kalman gain is based on the relative magnitudes of the uncertainties in the current estimate and the new measurement:

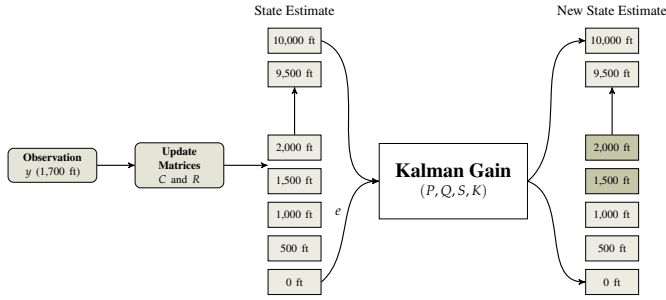


FIGURE 5-4: Schematic of a state update in which the darker elements of the new state vector were updated.

$$K(k) = \frac{P(k|k-1)C(k)^T}{S(k)} = \frac{P(k|k-1)C(k)^T}{C(k)P(k|k-1)C(k)^T + R(k)} \quad 5-14$$

5. In the final step, the innovation is multiplied by the Kalman gain yielding the updated state estimate $\hat{x}(k|k)$:

$$\hat{x}(k|k) = \hat{x}(k|k-1) + K(k) \cdot e(k) \quad 5-15$$

The prediction error covariance matrix P is updated using the Kalman gain and observation model:

$$P(k|k) = (I - K(k)C(k)) P(k|k-1) \quad 5-16$$

A high uncertainty in the current estimate (high P) and much confidence in the accuracy of the measurement (low S) yields a high value of the Kalman gain, which in turn assigns a large weight to the incoming observation in updating the state estimate through the innovation:

The opposite holds for a low uncertainty in the current estimate (low P), and little confidence in the accuracy of the measurement (high S) which yields a low value of the Kalman gain. This results in a small weight for the incoming observation when updating the state estimate.

When no new observation data are received, there will be no innovation, and the loop is reduced to updating the prediction error covariance P . In this way, the uncertainty about an estimate increases when time passes without new incoming measurements. This ensures that more weight is assigned to newly received observations to alter the estimate. A schematic of the algorithm loop is shown in Figure 5-5, illustrating that a prediction step is driven by a new time step and an update step is driven by a newly received measurement.

The output of the algorithm are estimates at the given altitude intervals along the planned trajectory which represent the evolution of the wind speed or direction, starting from the

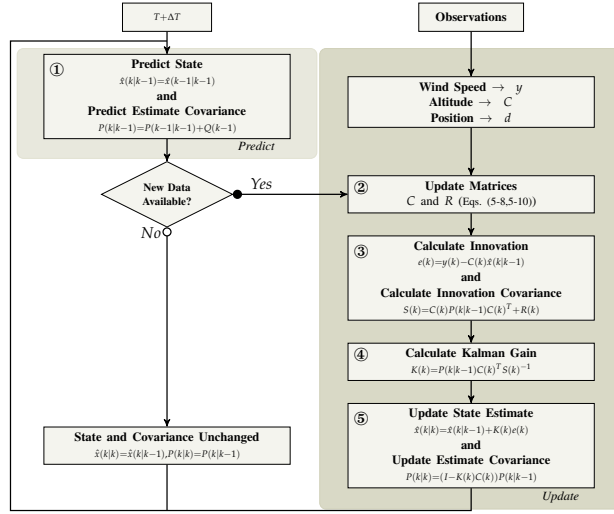


FIGURE 5-5: AWEA Kalman Filter schematic containing all five steps.

current position until the time T minutes ahead at the end of trajectory. After each estimation step, the complete wind profile is constructed through linear interpolation of the estimates per altitude interval.

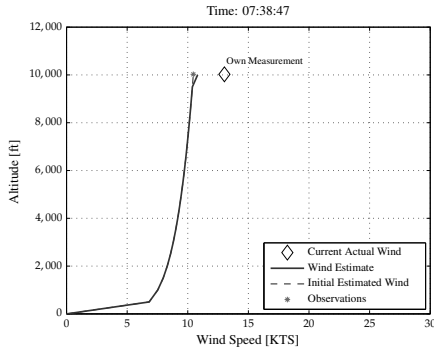
5-5 AWEA Performance Evaluation

This section discusses the performance of the AWEA algorithm using two case studies. First, the wind estimator performance in an off-line simulation is analyzed. For these simulations, measurement data from aircraft based upon actual Mode-S EHS radar soundings — courtesy of the Royal Netherlands Meteorological Institute — in the vicinity of Amsterdam Airport Schiphol were used. The data set was calibrated and corrected using methods described by de Haan [32].

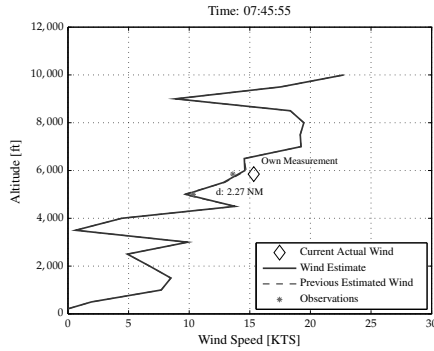
Second, results of a fast-time simulation study into aircraft spacing [9] in a varying wind-field are analyzed to investigate the effect of improved wind profile estimation on trajectory predictions.

5-5-1 Case Study 1: Simulations using Mode-S Enhanced Data

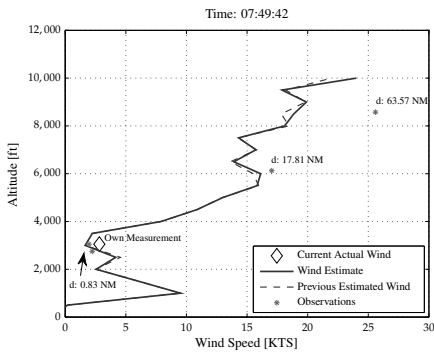
For this analysis, the available observations, consisting of over 305,000 radar soundings, were considered to be the true wind speed. One aircraft was selected to represent the own aircraft which estimates a wind profile using AWEA. The algorithm estimates the wind from TMA entry at 10,000 ft down to the runway and estimated an initial profile using the power-law of Eq. (5-2).



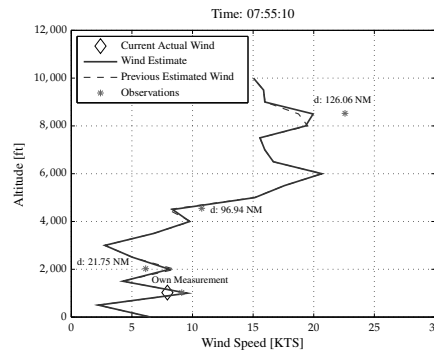
(a) Wind speed update process, $h = 10,025$ ft.



(b) Wind speed update process, $h = 5,775$ ft.



(c) Wind speed update process, $h = 3,050$ ft.



(d) Wind speed update process, $h = 1,025$ ft.

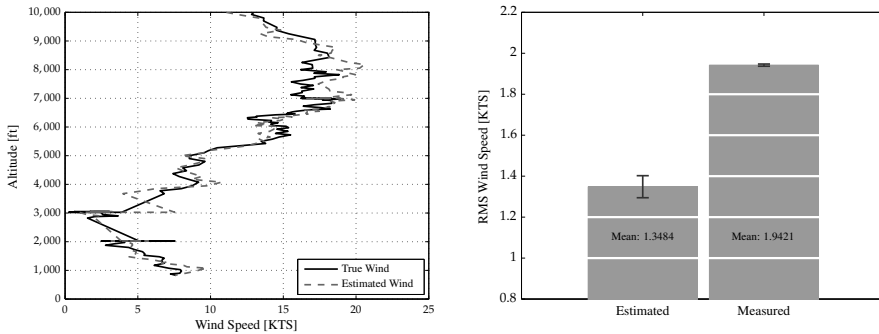
FIGURE 5-6: Estimated wind profile evolving throughout the descent ($R_0=10$, $K_w=0.4$).

A normally distributed noise (mean: 0, std: 1.94 KTS, such that measurement errors are within a 3σ value of ± 5.83 KTS, which corresponds to a typical measurement error [31] of 3 m/s) was added to the data set, to represent noisy incoming measurements. These simulated measurements form the input for the AWEA algorithm onboard the aircraft.

Figure 5.6(a) shows that the initial estimate (solid line) when the aircraft descends through 10,000 ft, based on the single first incoming measurement, equals the logarithmic profile discussed in Section 5-4. For this estimate, the initial prediction error matrix P is set high as no observations had been received yet. This yields a high Kalman gain, giving a high weight to the first set of observed data. Figure 5.6(b), Figure 5.6(c) and Figure 5.6(d) show profiles constructed at later time steps during the descent. In these figures, the stars represent the actual incoming measurements, and the solid line is the new wind profile estimate, while the dashed line represents the previous estimate. From these figures, it can be seen that the distance between the measurement affects the magnitude of change made in the wind estimate and that a measurement only affects the estimate of altitudes within the altitude interval through the C matrix.

Performance accuracy

Figure 5.7(a) shows estimated and true wind versus altitude throughout the entire descent. At 2,000 ft and 3,000 ft the aircraft flew level and the wind estimate and true wind therefore show a range of values for wind speeds.



(a) True wind and estimated wind throughout the en- (b) RMS of the wind speed estimation error and measurement error.

FIGURE 5-7: Wind estimation performance including mean and 95% confidence interval ($R_0=10$, $K_w=0.4$).

To verify the robustness of the estimation process, a bootstrap sample extracted from the simulation is used to calculate the mean and 95% confidence interval of the Root Mean Square (RMS) of the estimation error using 10 different noise realizations. For this combination of R_0 and K_w , the mean RMS of the estimation error is 1.35 KTS see Figure 5.7(b). For comparison, the mean RMS of the (simulated) measurement deviation is depicted on the right in the same figure and equals 1.94 KTS. As such, AWEA is effective in reducing the effects of measurement noise while employing measurements from surrounding aircraft to construct an estimated wind profile.

Kalman Filter Observation Model

According to Kalman filter theory, the accuracy of an estimate depends on the quality of the system model, the accuracy of the available measurements and the number of measurements. AWEA does not contain system dynamics, hence, the accuracy of the wind estimation depends on the measurements and actual prevailing wind. Therefore, it is hypothesized that the Kalman filter estimation error will decrease as more data become available.

Important parameters calculated in the Kalman filter (as described in Section 5-4) are the error covariance matrix P and Kalman gain K . The evolution of these parameters is shown in Figure 5-8. Shown in these figures are incoming wind observations from other aircraft flying at altitudes between 500–1500 ft.

Clearly seen in Figure 5.8(a) is the increasing value of the error covariance at $\approx 7 : 41 : 00$ hr when measurements are received farther away from the altitude of interest and

hence have a small coefficient in the C -matrix. Once a new and significant measurement is received ($\approx 7 : 46 : 00$), it is assigned a high weight and the uncertainty in the current estimated value drops as seen by the reduction of P . For a lower update rate of the Kalman filter, the P matrix would have increased less, assigning less weight to the new measurement. Hence, when using a lower update rate, the Q matrix should be adjusted accordingly, while the R matrix could include a time dependent factor similar to addition of distance information.

At certain moments during descent, the value of the Kalman gain is slightly negative. These negative values result from the applied observation model and altitude resolution. The used observation model relates altitude intervals through linear interpolation resulting in correlations in the prediction error covariance matrix. These, in turn, can result in negative values for the Kalman gain. Alternative observations models or altitude intervals could produce estimates without negative Kalman gain values, for instance by limiting the effect of distant measurements through truncating of coefficients in the C -matrix.

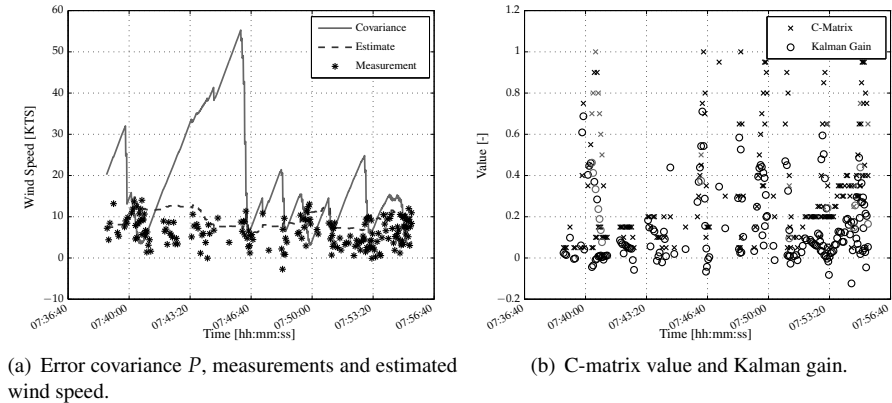


FIGURE 5-8: Kalman Filter parameters for observations at 1,000 ft.

Effect of distance information

Multiple simulations were run for varying values of R_0 and K_w to investigate the effect of both parameters on the performance of the AWEA algorithm. All conditions were simulated for 10 different Gaussian noise realizations, added to the wind measurements. The simulated values of R_0 were 0.1; 1; 5; 10; 50; 100; 200; and K_w was varied between 0 (all measurements have equal uncertainty) and 1 (full distance include) in steps of 0.1.

The performance of the algorithm is assessed by calculating the RMS wind estimation error at the current position. The RMS is calculated by determining the estimated value at every time step for which a true wind value is available and including this in the summation for the RMS value at that point.

Besides the current estimated RMS, the RMS value of an estimate (prediction) of the

winds at 1,000 ft along the trajectory is calculated by determining the current estimate for 1,000 ft and subtracting the actual value at 1,000 ft once the aircraft reaches this point.

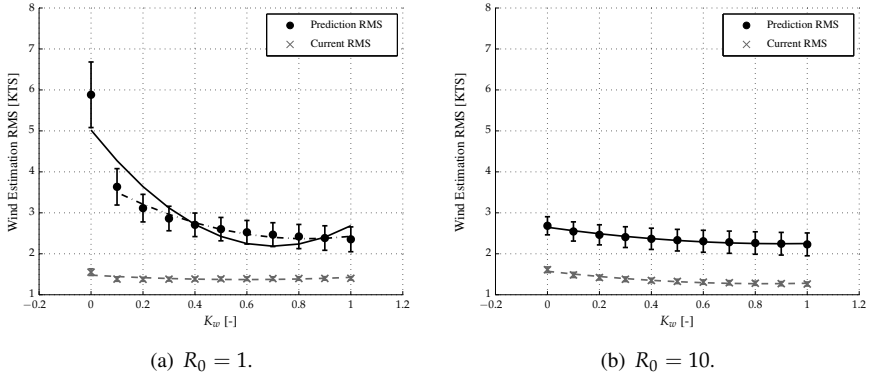


FIGURE 5-9: Mean and 95% confidence interval of RMS values for the current position (cross) and position along route (circle) including a quadratic fitted model.

Figure 5-9 shows that by increasing R_0 , the RMS of predicted estimates decrease while the RMS of the estimates at the current position increase slightly. This latter result was to be expected as the R matrix represents the uncertainty (covariance) in a measurement and hence the current estimate will primarily depend on the own measurement which will have increased uncertainty for larger values of R_0 . Alternatively, the reduced RMS values of the predicted estimates for larger values of R_0 show that the prediction benefits from increasing the uncertainty. This can be explained as the prediction is primarily based on measurements from other aircraft at that altitude and at different altitudes. As the wind is likely to change over time, increasing the modeled uncertainty thus makes sense.

Evident from these figures is that both RMS values benefit from introducing distance information into the R matrix. Moreover, increasing R_0 further leads to R_0 to be dominant and hence K_w has less effect on the found RMS values. Furthermore, the quadratic fitted model for $R_0 = 1$ shows that the RMS for $K_w = 0$ is an outlier and reduces the goodness of fit. Removing this value from the fitted model results in a better fit. This shows the importance of distance information for low values of R_0 and hence that the estimates benefit from assigning ‘uncertainty’ to an observation located farther away.

5-5-2 Case Study 2: Aircraft Spacing and Wind Estimation

A simulation study into aircraft spacing for approach, investigated the use of the AWEA algorithm to improve spacing between in-trail aircraft [9]. In this study, aircraft use Interval Management (IM) [39] and receive an ETA at the runway of an assigned lead aircraft while ATC instructs the aircraft to achieve a time spacing goal with the lead aircraft at the same runway. The own aircraft continuously adjusts its speed profile to achieve the spacing goal with respect to that lead aircraft.

This study uses NASA's Airborne Spacing for Terminal Arrivals (ASTAR) algorithm [40] to calculate speed adjustments to achieve the spacing goal using a 4D TP and speed-control law. AWEA is expected to improve the accuracy of the TP and consequently improve aircraft spacing accuracy. Five different implementations of wind estimation were compared of which four implementations used AWEA as seen in Table 5-1.

TABLE 5-1: Wind estimation implementations used in simulation study.

Name	Description
Charts	Wind estimation using wind charts
Ground 10	Ground-based AWEA algorithm with ADS-B broadcast rate of 10 seconds
Ground 30	Ground-based AWEA algorithm with ADS-B broadcast rate of 30 seconds
Air 10	Aircraft-based AWEA algorithm with ADS-B broadcast rate of 10 seconds
Air 30	Aircraft-based AWEA algorithm with ADS-B broadcast rate of 30 seconds

The wind charts implementation 'flattened' the simulated wind for each scenario into a single static wind profile at 4 altitude levels: ground level, 2,500, 5,000 and 10,000 ft. Wind estimates between these levels were obtained through linear interpolation.

The ground-based AWEA implementation (see Figure 5.3(b)) used broadcast wind measurements from aircraft within the own TMA to construct a single wind profile that represents the windfield in the entire TMA. As such, any dependency of the position of the measurements is removed and hence the R matrix is constant. In this implementation, the ground station broadcasts the latest estimated wind profile to an aircraft upon TMA entry. This profile is stored in the FMS and not updated with new measurements.

The aircraft-based implementation (see Figure 5.3(a)) works similarly except this implementation combines the received ground-based profile with measurements from other aircraft to continuously update the onboard profile. In these measurements, the positional information from the measurements is included in the construction of the R matrix, see Eq. (5-10).

Both AWEA implementations were evaluated twice using different measurement broadcast rates to investigate its effect on wind estimation. This means that aircraft broadcast measurements once every ten seconds or once every thirty seconds.

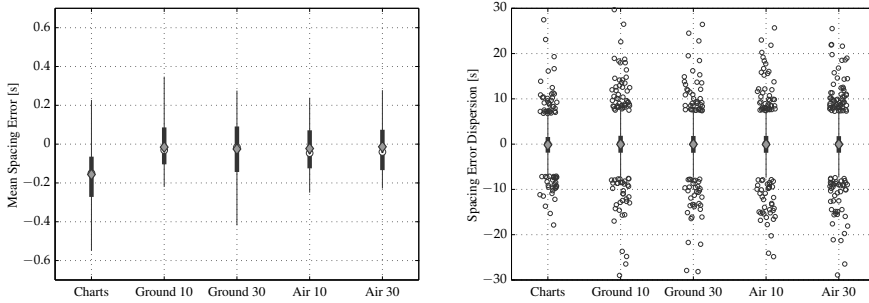
The simulated winds were constructed using actual AMDAR data [9]. Based upon this simulated windfield, all arriving aircraft sensed the current wind speed and direction including a measurement error ($\bar{X}_{V_W} = 0$ KTS, $\sigma_{V_W} = 0.7$ KTS; $\bar{X}_{\chi_W} = 0^\circ$, $\sigma_{\chi_W} = 2.4^\circ$).

Spacing performance

Besides the wind estimation implementations, various modifications to the spacing algorithm were evaluated in a within-subjects design which are not within the scope of this paper. Each scenario was repeated 50 times, using a different set of disturbances: *a*) timing at TMA entry; *b*) aircraft type arrival sequence; *c*) wind errors.

The mean spacing accuracy is the mean of the spacing error of all aircraft for a single scenario. Results of a one-way repeated measures Analysis of Variance (ANOVA) showed a significant main effect (Greenhouse-Geisser corrected, $\chi^2(9) = 116.173$, $p < 0.001$) on

the mean spacing accuracy ($F_{1,835,89.920} = 23.618, p < 0.001$). A Bonferroni corrected post-hoc analysis revealed that the AWEA implementations performed significantly better compared to using wind charts, see Figure 5.10(a). Analysis showed no significant differences between the AWEA implementations (see Figure 5.10(a) and Figure 5.10(b)).



(a) Mean spacing accuracy per scenario.

(b) Overall spacing accuracy.

FIGURE 5-10: Spacing accuracy for different wind estimation implementations (including mean and median).

Figure 5.11(a) shows the RMS error in estimating the wind along the trajectory. AWEA significantly reduces the RMS in estimating the wind. As normality was violated, a Friedman test was performed and confirmed this significant effect ($\chi^2_F(4) = 183.728, p < 0.001$). A post-hoc analysis, using a Wilcoxon Signed Rank test and a Bonferroni correction of 0.05/10, revealed that all implementations performed significantly different from another. These results show that using additional observations from airborne aircraft to update the onboard profile yields the smallest wind estimation error.

However, updating the wind profile also increased the mean number of speed changes additional to the nominal speed changes to fly the nominal profile as seen in Figure 5.11(b). As normality was violated, a Friedman test on these additional speed changes was used and showed a significant main effect ($\chi^2_F(4) = 94.910, p < 0.001$). The subsequent post-hoc Wilcoxon Signed Rank tests showed that the wind charts performed significantly different ($p < 0.001$) from the aircraft-based implementation while the wind charts showed no significant difference with the ground-based implementation ($p > 0.622$). Similarly, a significant difference between the ground-based and aircraft-based implementations was found. The broadcast rate, however, showed no significant influence ($p > 0.404$).

Relevance of Distance Information

To investigate the influence of distance information in the R matrix, Figure 5-12 shows wind profiles for a single aircraft during approach. These wind profiles show the wind at different altitudes during the descent from 10,000 ft to the runway. These profiles include the ‘true’ wind and the estimated winds using the ground-based AWEA, aircraft-based AWEA and a

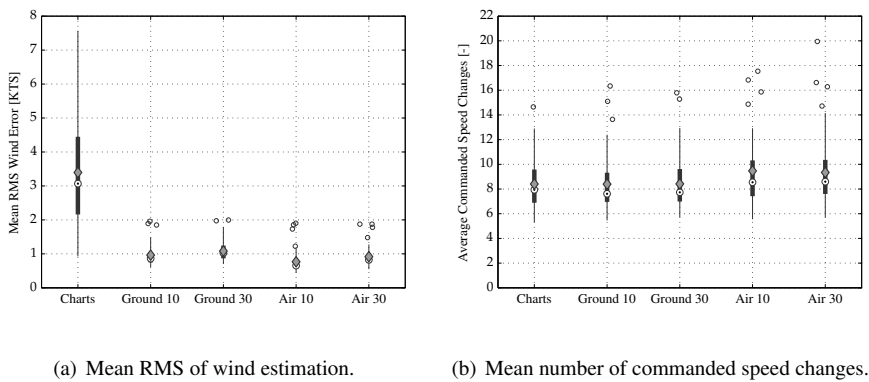


FIGURE 5-11: Spacing accuracy for different wind estimation implementations.

wind profile based on an aircraft-based AWEA using measurements from other aircraft but without distance information.

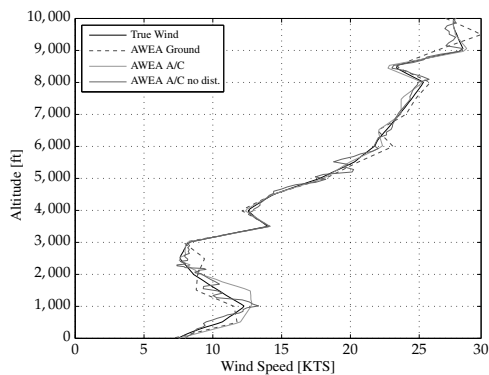
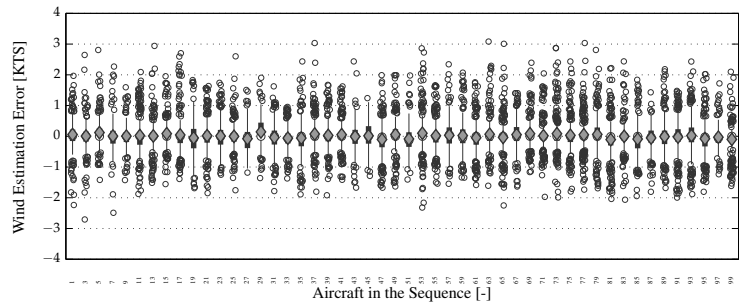


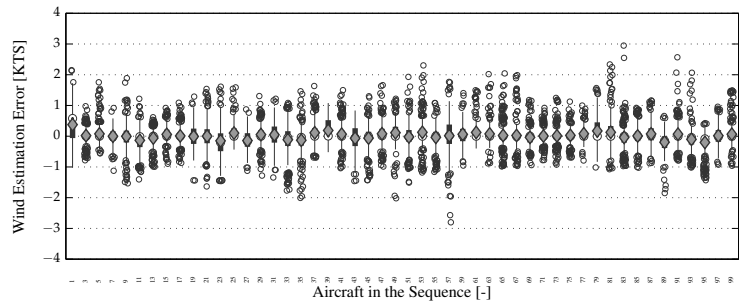
FIGURE 5-12: Different profile estimates and true wind for a single descending aircraft.

Figure 5-12 shows that the ground-based implementation provides a good estimate of the prevailing winds. However, the airborne-based AWEA often provides better results. Also shown is the influence of distance information as using this information provides additional smoothing since the ‘no distance’ implementation shows increased variations. This was to be expected as using the distance information assigns distant measurements with an increased uncertainty.

Finally, Figure 5-13 shows the wind estimation error throughout the arrival sequence for the ground-based and aircraft-based implementations. The results show only small differences but the aircraft-based implementation reduces the variation and outliers in the actual wind estimation best.



(a) Ground-based Algorithm.



(b) Airborne-based Algorithm.

FIGURE 5-13: Wind estimation error throughout the arrival sequence.

The results of this experiment showed statistically improved spacing performance, and limited in size, using AWEA compared to using wind charts using a simulated windfield. However, no significant difference between the types of AWEA implementation was observed.

5-6 Conclusions

An algorithm is proposed that estimates wind profiles using measurements of meteorological data from nearby aircraft. The algorithm has the benefit of producing high-fidelity, high-resolution and user-tailored wind profiles. Using actual wind observations from aircraft transponder data, the influence of distance on the quality of the estimation was evaluated and showed to reduce the estimation errors. Simulations showed that the algorithm was able to reduce measurement noise from 1.94 KTS to 1.35 KTS. Moreover, the estimated wind profiles can be used for predicting wind at locations farther along the own trajectory with minor errors. Airborne Wind Estimation Algorithm was also evaluated in a simulation study that investigated trajectory prediction and aircraft spacing in a varying windfield and shows that AWEA improves spacing performance. Today, the availability of actual meteorological data, through ADS-B data included in the ARV report is still limited. Once these reports become more widely available or through other systems such as SWIM, AWEA could be adapted and evaluated in a real-time environment onboard an aircraft. Future work should also investigate alternative observation models and investigate the use of an EKF to filter wind speed and direction simultaneously. Moreover, the state vector could be defined as a wind speed in the Earth reference frame and be applied to a 3D grid to obtain a windfield estimate.

Acknowledgments

The authors would like to thank dr. Siebren de Haan and Jan Sondij (both KNMI) for providing the wind observations used in this research. dr. Qiping Chu and dr. Christiaan Tiberius (both TU Delft) are acknowledged for their support on tuning the algorithm.

References

- [1] **R. A. Coppensbarger, R. W. Mead, and D. N. Sweet.** Field Evaluation of the Tailored Arrivals Concept for Datalink-Enabled Continuous Descent Approach. *Journal of Aircraft*, 46(4), 1200–1209, 2009. doi:10.2514/1.39795.
- [2] **J. E. Robinson and M. Kamgarpour.** Benefits of Continuous Descent Operations in High-Density Terminal Airspace Under Scheduling Constraints. In: *Proceedings of the 10th AIAA Aviation Technology, Integration, and Operations (ATIO) Conference, Fort Worth, Texas, September 13–15*, AIAA 2010-9115, pp. 1–21. American Institute of Aeronautics and Astronautics, 2010. doi:10.2514/6.2010-9115.

- [3] **J.-P. B. Clarke, J. Brooks, G. Nagle, A. Scacchioli, W. White, and S. R. Liu.** Optimized Profile Descent Arrivals at Los Angeles International Airport. *Journal of Aircraft*, 50(2), 360–369, 2013. doi:10.2514/1.C031529.
- [4] **P. M. A. De Jong, N. De Gelder, F. J. L. Bussink, R. P. M. Verhoeven, R. Kohrs, M. M. Van Paassen, and M. Mulder.** Time and Energy Management during Descent and Approach for Aircraft: A Batch-Simulation Study. *Journal of Aircraft*, 2013. Submitted for publication.
- [5] **P. M. A. De Jong, F. J. L. Bussink, R. P. M. Verhoeven, N. De Gelder, M. M. Van Paassen, and M. Mulder.** Time and Energy Management during Descent and Approach: A Human-in-the-Loop Study. *Journal of Aircraft*, 2013. Submitted for publication.
- [6] **J. K. Klooster, K. D. Wickman, and O. F. Bleeker.** 4D Trajectory and Time-of-Arrival Control to Enable Continuous Descent Arrivals. In: *Proceedings of the AIAA Guidance, Navigation and Control Conference and Exhibit, Honolulu, Hawaii, August 18–21*, AIAA 2008-7402, pp. 1–17. American Institute of Aeronautics and Astronautics, 2008. doi:10.2514/6.2008-7402.
- [7] **Y. Glina, S. Troxel, T. Reynolds, and M. McPartland.** Wind Information Requirements to Support Four Dimensional Trajectory-Based Operations. In: *Proceedings of the 12th AIAA Aviation Technology, Integration, and Operations (ATIO) Conference and 14th AIAA/ISSM, Indianapolis, Indiana, September 17–19*, AIAA 2012-5702, pp. 1–14. American Institute of Aeronautics and Astronautics, 2012. doi:10.2514/6.2012-5702.
- [8] **L. L. Stell.** Predictability of Top of Descent Location for Operational Idle-thrust Descents. In: *Proceedings of the 10th AIAA Aviation Technology, Integration, and Operations (ATIO) Conference, Fort Worth, Texas, September 13–15*, AIAA 2010-9116, pp. 1–12. American Institute of Aeronautics and Astronautics, 2010.
- [9] **F. J. L. Bussink, J. J. Van der Laan, and P. M. A. De Jong.** Combining Flight-deck Interval Management with Continuous Descent Approaches in high density traffic and realistic wind conditions. In: *Proceedings of the AIAA Guidance, Navigation and Control Conference, Minneapolis, Minnesota, August 13–16*, AIAA 2012-4523, pp. 1–25. American Institute of Aeronautics and Astronautics, 2012. doi:10.2514/6.2012-4523.
- [10] **R. E. Cole, S. Green, M. Jardin, B. E. Schwartz, and S. G. Benjamin.** Wind Prediction Accuracy for Air Traffic Management Decision Support Tools. In: *Proceedings of the 3rd USA/Europe Air Traffic Management Research and Development Seminar, Napoli, Italy, June 13–16*, pp. 1–9, 2000.
- [11] **S. M. Green, M. P. Grace, and D. H. Williams.** Flight Test Results: CTAS and FMS Cruise/Descent Trajectory Prediction Accuracy. In: *Proceedings of the 3rd USA/Europe Air Traffic Management Research and Development Seminar, Napoli, Italy, June 13–16*, pp. 1–11, 2000.

- [12] **J. Wat, J. Follet, R. Mead, J. Brown, R. Kok, F. Dijkstra, and J. Vermeij.** In Service Demonstration of Advanced Arrival Techniques at Schiphol Airport. In: *Proceedings of the 6th AIAA Aviation Technology, Integration, and Operations Conference (ATIO)*, Wichita, Kansas, September 25–27, AIAA 2006-7753, pp. 1–20. American Institute of Aeronautics and Astronautics, 2006.
- [13] **N. T. Ho and J.-P. B. Clarke.** Methodology for Optimizing Parameters of Noise-Abatement Approach Procedures. *Journal of Aircraft*, 44(4), 1168–1176, 2007. doi:10.2514/1.22292.
- [14] **L. Ren and J.-P. B. Clarke.** Flight-Test Evaluation of the Tool for Analysis of Separation and Throughput. *Journal of Aircraft*, 45(1), 323–332, 2008. doi:10.2514/1.30198.
- [15] **J. Bronsvoort, G. McDonald, R. Potts, and E. Gutt.** Enhanced Descent Wind Forecast for Aircraft: Facilitation of Continuous Descent Arrivals with Improved Efficiency and Predictability by the use of Tailored Descent Wind Forecasts. In: *Proceedings of the 9th USA/Europe Air Traffic Management Research and Development Seminar*, Berlin, Germany, June 14–17, pp. 1–10, 2011.
- [16] **C. N. Hewitt and A. V. Jackson.** *Handbook of atmospheric science, principles and applications*. Blackwell, 2003.
- [17] **M. Durham.** inFlight optimization Services offers Airlines more Fuel-efficient en-route operations. *AERO Magazine*, 42(Quarter 2), 21–23, 2011.
- [18] **AVTECH Sweden AB.** Aventus NowCast: Great fuel savings by accurate wind information. Product sheet, 2012.
- [19] **N. Bienert and H. Fricke.** Real-time Wind Uplinks for Prediction of the Arrival Time and Optimization of the Descent Profile. In: *Proceedings of the 3rd ENRI International Workshop on ATM/CNS*, Tokyo, Japan, February 19–22, EN-045, pp. 1–6. ENRI, 2013.
- [20] **S. Mondoloni.** A Multiple-Scale Model of Wind-Prediction Uncertainty and Application to Trajectory Prediction. In: *Proceedings of the 6th AIAA Aviation Technology, Integration, and Operations Conference (ATIO)*, Wichita, Kansas, September 25–27, AIAA 2006-7807, pp. 1–14. American Institute of Aeronautics and Astronautics, 2006.
- [21] **D. Delahaye, S. Puechmorel, and P. Vacher.** Windfield Estimation by Radar Track Kalman Filtering and Vector Spline Extrapolation. In: *Proceedings of the 22nd Digital Avionics Systems Conference*, Indianapolis, Indiana, October 12–16, vol. 1, pp. 5.E.2–1–5.E.2–11. IEEE/AIAA, 2003. doi:10.1109/DASC.2003.1245869.
- [22] **A. M. P. De Leege, M. Mulder, and M. M. Van Paassen.** Using Automatic Dependent Surveillance-Broadcast for Meteorological Monitoring. *Journal of Aircraft*, 50(21), 249–261, 2013. doi:10.2514/1.55833.

- [23] **J. L. De Prins, K. F. M. Schippers, M. Mulder, M. M. Van Paassen, A. C. In 't Veld, and J.-P. B. Clarke.** Enhanced Self-Spacing Algorithm for Three-Degree Decelerating Approaches. *Journal of Guidance, Control and Dynamics*, 30(2), 576–590, 2007. doi:10.2514/1.24542.
- [24] **W. F. De Gaay Fortman, M. M. Van Paassen, M. Mulder, A. C. In 't Veld, and J.-P. B. Clarke.** Implementing Time-Based Spacing for Decelerating Approaches. *Journal of Aircraft*, 44(1), 106–118, 2007. doi:10.2514/1.22253.
- [25] **A. C. In 't Veld, P. M. A. De Jong, M. M. Van Paassen, and M. Mulder.** Real-time Wind Profile Estimation using Airborne Sensors. In: *Proceedings of the AIAA Guidance, Navigation and Control Conference, Portland, Oregon, August 8–11*, AIAA 2011-6662, pp. 1–15. American Institute of Aeronautics and Astronautics, 2011. doi:10.2514/6.2011-6662.
- [26] **W. A. Mair.** The Effect of a Wind Gradient on the Rate of Climb of an Aircraft. A.R.C. Technical Report Reports and Memoranda No. 2953, Cambridge university Aeronautics Laboratory, 1954.
- [27] **G. J. J. Ruijgrok.** *Elements of Airplane Performance*. Delft University Press, 1996.
- [28] **EUROCAE.** *Minimum Operational Performance Standards for 1090 MHz Extended Squitter Automatic Dependent Surveillance – Broadcast (ADS-B) and Traffic Information Services – Broadcast (TIS-B) - ED-102A*. EUROCAE, 92240 Malakoff, France, 2012. Appendix V.3.2.
- [29] **Airbus.** *Flight Crew Operations Manual (Vol. 4)*, rev. 14 edn., 2002. 4.04.25.
- [30] **R. Walter.** *The Aviation Handbook*, chap. 15, Flight Management Systems. CRC Press LLC, 2000.
- [31] **D. J. Painting.** Aircraft Meteorological Data Relay (AMDAR) Reference Manual. Tech. Rep. WMO-No. 958, World Meteorological Organization, 2003.
- [32] **S. De Haan.** High-resolution wind and temperature observations from aircraft tracked by Mode-S air traffic control radar. *Journal of Geophysical Research: Atmospheres*, 116(D10111), 1–13, 2011. doi:10.1029/2010JD015264.
- [33] **S. De Haan, L. J. Bailey, and J. E. Können.** Quality assessment of Automatic Dependent Surveillance Contract (ADS-C) wind and temperature observation from commercial aircraft. *Atmospheric Measurement Techniques*, 6, 199–206, 2013. doi:doi:10.5194/amt-6-199-2013.
- [34] **ICAO.** *Procedures for Air Navigation Services - Air Traffic Management - Doc 4444 ATM/501*. International Civil Aviation Organization, Montreal, Canada, 15 edn., 2007.

- [35] **ICAO**. *Annex 3 to the Convention on International Civil Aviation - Meteorological Service for International Air Navigation*. International Civil Aviation Organization, Montreal, Canada, 2010.
- [36] **SESAR**. European ATM Master Plan. Tech. Rep. Edition 2, EUROCONTROL, 2012. SESAR JU & SESAR Work Package C and Partners.
- [37] **R. E. Kalman**. A New Approach to Linear Filtering and Prediction Problems. *Transaction of the ASME – Journal of Basic Engineering*, 82(Series D), 35–45, 1960.
- [38] **N. M. Zoumakis** and **A. G. Kelessis**. Methodology for Bulk Approximation of the Wind Profile Power-Law Exponent under Stable Stratification. *Boundary-Layer Meteorology*, 55(1-2), 199–203, 1990.
- [39] **EUROCAE**. *Safety, Performance and Interoperability Requirements Document for Airborne Spacing - Flight Deck Interval Management (ASPA-FIM) - ED-195*. EUROCAE, 92240 Malakoff, France, 2011.
- [40] **B. Barmore**. Airborne Precision Spacing: A Trajectory-Based Approach to Improve Terminal Area Operations. In: *Proceedings of the 25th Digital Avionics Systems Conference, Portland, Oregon, October 15–19*, pp. 2.C.3–1–2.C.3–12. IEEE/AIAA, 2006. doi:10.1109/DASC.2006.313683.

DISCUSSION AND RECOMMENDATIONS

In this thesis, a new Continuous Descent Operations (CDO) concept was developed: Time and Energy Managed Operations (TEMO). A batch simulation study investigated TEMO's robustness and environmentally-friendliness. To investigate the human role within the TEMO concept, a human-in-the-loop experiment was conducted that evaluated three cockpit displays and affects of variations in human response. Moreover, a new algorithm that improves wind estimation onboard aircraft has been developed. In addition, all results have been integrated to evaluate the bigger picture. This chapter also reflects on the research performed and provides recommendations for further investigation. Since Clean Sky continues beyond this thesis, this chapter also provides an overview of future development of TEMO.

6-1 Discussion

Over the last decades, new research provided insight into the effects of aviation on our environment. When burning fuel to generate engine thrust, pollutant emissions such as Carbon Dioxide (CO_2) and Nitrogen Oxide (NO_x) are emitted which we now know contribute to global warming and forming of acid rain. In addition, global oil reserves are depleting, leading to increased oil prices. Finally, air traffic is growing extensively, causing more nuisance for residential areas close to airports. For these reasons, researchers investigated methods to improve aviation efficiency through optimized aircraft operations.

Today, Air Traffic Control (ATC) commands aircraft to fly level segments at lower altitudes for vertical spacing of arriving and departing aircraft. For this reason, aircraft have to descend rather early and use engine thrust to maintain speed during these segments. Furthermore, level segments result in a lower vertical profile and increased fuel burn as compared to flying level at higher altitudes. For these reasons, effort has been put in reducing low-altitude level segments and enable a continuous descent, referred to as Continuous Descent Operations (CDO). During current CDOs, ATC must add additional spacing buffers since predicting arrival time and spacing between aircraft flying CDOs is complicated as aircraft descend and decelerate at different rates. These additional spacing buffers result in increased aircraft inter-arrival times and reduces runway capacity. Therefore, CDOs are primarily used during hours of low traffic demand.

Researchers developed several concepts to improve predictability of aircraft trajectories during CDO descents. Controller support tools [1–5] have been used to support Air Traffic Controllers (ATCos) in determining sufficient spacing at Top of Descent (ToD) to enable efficient CDOs. Others looked at improving trajectory predictability through ground-based [6–9] or airborne [10–16] Trajectory Predictors (TPs). However, many of these new CDO concepts require additional thrust to correct deviations from the planned trajectory. Deviations from a planned trajectory occur due to inaccuracies in modeling of aircraft performance and uncertainties in estimating the parameters used in trajectory prediction, such as wind estimates along the descent trajectory. Therefore, to reduce the need for engine thrust or speedbrakes to correct deviations, a new method to correct deviations is explored that uses energy management to correct deviations.

In this thesis a new concept is investigated, named Time and Energy Managed Operations (TEMO), to perform CDO whilst adhering to time constraints to maintain runway capacity. TEMO uses energy management to create control authority and reduce the need for additional thrust or speedbrakes. Using energy management — in this context, the exchange of potential and kinetic energy — an aircraft could fly a different energy strategy resulting in a different trajectory. Only when energy management alone does not suffice, minimized amounts of additional thrust or speedbrakes are allowed to achieve all objectives. Solving multi-objective problems is a complex task for humans and hence automation is used to solve these problems using a novel TP and optimization algorithm that calculates accurate trajectories. The more accurate a predicted trajectory is, the less control action is required when aircraft deviate from this trajectory. Using similar reasoning, TEMO descents are flown using the autopilot to reduce deviations from control variations which simultaneously

maintains pilot workload at an acceptable level.

To address these issues, the research was divided into three parts: developing the algorithm and TP using energy management, supporting the human operator in working with the concept, and improving the wind estimates used in trajectory prediction. To reduce the thesis scope, this research considered a single aircraft performing a straight-in descent, to evaluate performance in terms of time and environmental impact using energy management. Within this scope, it is assumed that aircraft separation is achieved as long as all aircraft adhere to their assigned time constraint.

In this discussion, the research goal stated in Chapter 1 is discussed using the results of the experiments of Chapter 3, Chapter 4 and Chapter 5. First, the three cornerstones of this thesis; energy management (Chapters 2 and 3), flight deck automation (Chapter 4) in the TEMO concept and associated variations in pilot response, and improved accuracy of wind estimates (Chapter 5) are discussed. Second, the limitations of the research in this thesis will be identified to provide recommendations for further research.

6-1-1 Energy Principles

Energy management

Flying an environmentally-friendly descent whilst adhering to a time constraint is a difficult task and requires multiple objectives to be achieved simultaneously: First, the engines are set to a low thrust setting to reduce the amount of fuel used, gaseous pollutants emitted and noise generated. However, this reduces the control authority of the aircraft significantly as the aircraft's energy level from then on can only be controlled through drag devices and elevator. When only one aircraft is considered, this does not necessarily impose issues as the aircraft can fly its own optimal trajectory. Second, to allow multiple aircraft to fly environmentally-friendly descents whilst maintaining safety, spacing between these aircraft and departing aircraft is mandated. Spacing can be achieved through time-management using time constraints. These time constraints, however, impose limitations on the optimal environmentally-friendly trajectory of the aircraft as it reduces control space. Combined with the reduced control authority of a low thrust setting, this formulation often results in a near-optimal trajectory in terms of environmental impact as objectives could be mutually exclusive. Compared to current day descents, however, these near-optimal descents are still likely to reduce overall environmental impact of aircraft flights.

The results from the batch simulation study, discussed in Chapter 3, showed that strategic replanning is successful in finding energy-neutral trajectories using energy management only. The realm of possible time constraints, however, is limited to a maximum range of 16 seconds and depends highly on the accuracy of the estimated winds. Moreover, the results showed that for certain conditions along the planned trajectory, the algorithm could not find an updated energy-neutral trajectory to correct deviations. By allowing minimized amounts of thrust or speedbrakes, however, the algorithm was able to calculate valid trajectories. Nonetheless, due to limiting operational constraints, wind estimation errors or time constraints, an energy-optimal solution was often not found when the aircraft was close to

the Initial Approach Fix (IAF) (13%) or during the deceleration phase after entering the Terminal Maneuvering Area (TMA) (21%). In these cases, a new replan was successful slightly later when these constraints were no longer active.

The algorithm consumed the available replan time window to find energy-neutral trajectories in the batch study. However, the remaining time window for sustained deviations proved to be too small when a wind estimation error was present. For this reason, the time window was removed from the revised algorithm to allow sufficient room for deviations.

Nominal scenarios without additional errors, such as time, energy and wind estimation errors, were compared with current conventional step-down descents. The results showed that flying a TEMO descent reduces environmental impact of aircraft as the amount of fuel used ($\approx 15\%$) and gaseous pollutants ($\approx 40\%$) emitted have decreased and showed smaller dimensions ($\approx 25\%$) of noise footprints. When errors were introduced, the environmental metrics were primarily affected by wind estimation errors as these errors result in a different flight duration and trajectory. Moreover, the other introduced errors (time and energy) were only active on a single basis and hence affected the trajectory 'less' than a constantly active wind estimation error. As expected, arriving early and headwind scenarios resulted in increased fuel use, gaseous emissions and larger noise contour areas due to the use of additional thrust to correct these errors.

The definition of energy used by TEMO uses altitude and True Airspeed (TAS). This trajectory could be flown using control laws [17, 18] that fly these trajectories accurately but require thrust and/or speedbrakes to do so. For this reason, TEMO only commands an Calibrated Airspeed (CAS) profile and allows deviations from the altitude profile. This approach assures that the aircraft is always within safe operating speeds (provided that the optimal control problem in the algorithm is safely formulated). When flying this CAS profile, energy deviations primarily result in altitude deviations and consequently TAS deviations which lead to time deviations. These time deviations could have been avoided by commanding a TAS or groundspeed profile [13]. This, however, is different from current practice where aircraft typically fly using Indicated Airspeed (IAS) — in this thesis assumed equal to CAS — profiles [19]. Moreover, time deviations that result from these altitude deviations were assumed to be small enough not to trigger a replan, or result in large and frequent tactical controller actuation to adhere to the strict Required Time Performance (RTP) of 2 seconds. The batch study showed that this assumption was valid since during the nominal simulations deviations remained within the predefined boundaries. Hence, the combination of speed deviations due to altitude deviations and modeling errors was sufficiently small.

Correcting deviations through replanning

The TEMO concept defines two implementations that use energy management to correct deviations from the planned trajectory: strategic and tactical replanning. Strategic replanning calculates optimal trajectories that are flown using Speed-on-Elevator (SOE) to fly a speed profile such that speed deviations result in altitude deviations through energy management. Furthermore, strategic replanning does not act instantaneously when deviations are detected but allows deviations to evolve in time such that these deviations could dissipate due to coun-

teracting disturbances. Full tactical replanning, however, cannot be flown without active use of engine thrust or speedbrakes. For this reason, a hybrid implementation combines tactical replanning using a control-law for correcting time deviations with strategic replanning for correcting energy deviations. In this implementation, a strategic replan is initiated when speed control actions and sustained deviations result in excessive energy deviations or when ATC issues a new time constraint. This new trajectory could potentially require minimized amount of thrust or speedbrakes to correct these deviations.

Since the tactical controller continuously minimizes time deviations without knowledge of the trajectory ahead of the aircraft, it was presumed that these control actions might not necessarily be optimal with respect to the environmental goals of TEMO. On the other hand, the strategic replan algorithm determines the optimal location of adding thrust or speedbrakes. The comparison between these methods, however, showed no significant difference in environmental impact. Using strategic replanning, a continuous wind estimation error caused significant deviations from the predicted trajectory and resulted in multiple replans. These replans were primarily caused by time deviations in excess of the allowable time boundary, while energy deviations only caused replans if no time constraint was active. However, in some situations the algorithm could not find a new trajectory, and the aircraft remained flying the current trajectory without correcting the deviation, due to strict operational constraints defined in the optimal control problem. The hybrid implementation reduces the time deviations effectively and used less replans to correct energy deviations. However, further research is required to investigate proper values for the energy boundaries to provide a more gradual transition towards the glideslope.

The initial algorithm, developed in General Pseudospectral Optimal Control Software (GPOPS), used a time window in the definition of Controlled-Time of Arrivals (CTAs). This allows the algorithm to deviate from the exact CTA in cases where this deviation could result in a more environmentally-friendly approach. The time window was smaller than the active RTP to provide room for deviations during descent towards the IAF. However, the results from the batch study showed that the difference between the RTP and time window was too small to assure that aircraft pass the IAF within the allowed RTP. For this reason, the revised algorithm did not include a time window at CTA constraint points to allow sufficient space for trajectory deviations.

In retrospect, it is questionable why energy and time deviations were defined for the glideslope segment while no replanning takes place during this segment. It would have been better to define boundaries up to the glideslope, and set the boundary values at this location strict such that deviations are small while commencing on the open-loop glideslope. Alternatively, closed-loop control should be made possible while on the glideslope, as discussed in Section 6-2.

Commanding energy during energy-optimal trajectories

The algorithm commands segments of thrust or speedbrake use when energy-management alone does not suffice to obtain a valid trajectory. The algorithm calculates the exact amount of thrust or drag required to alter the energy rate along segments of the trajectory. It uses

modeling of aircraft and engine dynamics to convert these parameters to throttle input and speedbrake deflection. In both simulations, the used modeling in the aircraft was equal to the models used in the simulation, hence, the corresponding inputs were accurate.

In real-life such accurate models are not available and it is doubtful whether required amounts of thrust and drag can be converted to proper throttle and speedbrake deflection inputs. Despite some sort of conversion between thrust and throttle, engine performance often differs per engine on a single aircraft. Hence, in spite of the correct input (throttle), the resulting output could not match the required thrust. Hence, some sort of closed-loop control is required to assure that the engine does not introduce additional deviations.

The auto-throttle system typically uses a control-loop that determines thrust variations required to fly a specific commanded speed, using parameters such as engine pressure ratio of engine fan speed, to control the aircraft speed. Moreover, no accurate inflight measurements of actual thrust are available on commercial aircraft and hence cannot be used in a control system. Therefore, another derived parameter is required to control thrust input for improved accuracy during execution of a TEMO descent. Since thrust or speedbrakes are used to control energy, an obvious control-law would be the Total Energy Control System (TECS) [17, 18] that controls both speed and vertical path and speed. However, research is required on integration of the TECS and the tactical controller.

6-1-2 Flight Deck Automation

Trajectory prediction and modeling errors

The TEMO optimization algorithm uses a TP to calculate trajectories. This algorithm is fully automated to employ computational power and enable repetitive and consistent results. The accuracy of these trajectories depends on the accuracy of models and dynamics used by the TP and any modeling error inherent to aircraft trajectory prediction will result in deviations from the planned trajectory. If an aircraft was a closed system, meaning exact modeling of the aircraft and disturbances is possible [20], full automation of the flight deck would be evident. Unfortunately, aircraft operate in the real world where external factors, such as wind (as seen in Chapter 5), and internal factors such as aircraft modeling, sensor noise and aircraft weight, cause disturbances that are unknown upon flight planning. Hence, an aircraft is considered an open system due to fast and often unpredictable interactions with a dynamic environment. For this reason, aircraft systems are probabilistic and exact modeling of what we actually know about the aircraft is impossible [21, Chapter 4] and the question remains, how accurate should one model the environment within a TP to obtain sufficient trajectory accuracy. Knowing that we cannot model the environment and aircraft exactly, modeling errors will result in deviations from the planned trajectory. Therefore, a full strategic solution is likely unable to achieve the desired time accuracy of 2 seconds at the runway threshold. Hence, using strategic replanning this RTP value should be increased to create a buffer such that both time and environmental objectives of TEMO descents can be achieved.

In both experiments, different aircraft simulation models and corresponding aircraft dy-

namics were used. An important difference in modeling between these studies is the inclusion of aircraft weight in the initial TP while the revised version did not include aircraft weight to reduce calculation times. Another mass assumption in the simulations is that the Flight Management System (FMS), upon calculating trajectories, knows the aircraft mass exactly. A test simulation showed that an initial mass error of 1% — a typical value for the accuracy of weight and balance systems [22–24] — can be flown using one single replan to correct this mass estimation error. This mass error resulted in an altitude deviation and consequently an energy deviation due to a deviation of both potential and kinetic energy as CAS is commanded. During the human-in-the-loop study of Chapter 4, variable mass and fuel flow were no longer modeled resulting in a mass estimation error (less than 1%). This error did not result in any replans.

Another modeling error resides in the TP due to the lack of transitions between flight phases (Table 2-1). This means that the aircraft should perform instantaneous attitude changes to minimize deviations between flown trajectory and planned trajectory. Other transitions that are not modeled in the TP are flaps and gear extension times and engine spool-up. This results in the planned trajectory being based upon instantaneously varying aircraft dynamics, such as thrust, drag and lift, while in reality the aircraft slowly transitions towards new thrust, lift and drag forces as flaps and gear are extended and engines spool up or down. In the simulations of this research, the total modeling errors were rather small and often canceled out, and hence did not exceed the allowed boundaries.

Based on the experience gained during algorithm development, implementing more complex modeling in the TP to increase the accuracy of planned trajectories, is likely to increase calculation times even further. However, lower calculation times would be better as the accuracy of a calculated trajectory also depends on the initial position of the planned trajectory. This initial position is predicted using simple extrapolation techniques based upon the current trajectory and sustained deviations. To reduce the extrapolation error, the replan calculation times should be as small as possible. In the batch study, the initial position was predicted 30 seconds ahead of the own aircraft while for the piloted experiment, the position was predicted only 20 seconds ahead of the current position. Although this is a significant improvement, the question remains how far ahead can the initial position be located in a more dynamic environment such that the initial position is sufficiently accurate. Moreover, what happens when the initial position deviates too much such that the aircraft does not pass through this point due control actions from the tactical controller or disturbances. Hence, even though we could strive towards increased complex modeling in the TP, which will not benefit trajectory calculation time, the prediction of the initial position of a replan will always result in (slight) deviations.

Pilot support information

To support pilots during TEMO operations, three Human-Machine Interface (HMI) variants were developed that each differ in level of information provided. These displays ranged from a rather basic display similar to today's display but with additional cues for selecting flaps and gear, to a display that included a configuration timer and Time and Energy Indi-

cator (TEI). These displays were designed to support the pilot in selecting configurations to reduce deviations from the planned trajectory and to improve automation awareness on the TEMO algorithm, its goals and possible corrective solutions.

The majority of pilots that participated in the human-in-the-loop experiment, discussed in Chapter 4, responded that they prefer the second HMI variant as this display provides pilots with all required information to set configurations accurately. The objective results obtained from this experiment showed that none of the displays significantly affected time performance. The configuration timer, however, resulted in less delay variation when selecting configurations. As such, the most basic display proved to be sufficient to inform pilots during a TEMO descent and reduce the effects of variations in pilot response.

The TEI, available in the third variant and designed to improve observability and directability [25], was only required by a third of all pilots as the limited deviations shown in this experiment does not warrant the addition of an additional indicator in the cockpit displays. Some pilots also responded that they fully trust the TEMO algorithm to find valid trajectories and inform pilots only during exceptions and hence do not require additional information in support of TEMO. This argument warrants the question whether the provided information is sufficient in case of an (extreme) exception. This holds specifically when the exception causes the automated system to stop operating (rejected trajectory) and requires the pilot to take control of the aircraft. In these cases, pilots shall negotiate with ATC on how to proceed the descent as a different time constraint could be assigned that can be met. Alternatively, ATC could resort to tactical intervention by assigning speed, altitude and heading instructions.

Although only a few pilots responded that they require the TEI, the limited variability of deviations and omission of exceptions in the executed experiment does not provide a proper basis to discard the TEI as a required display element for TEMO descents. Pilots indeed responded that they could use the TEI in a more dynamic environment, for instance due to turbulence or changing winds. Moreover, the TEI could prove useful when TEMO uses hybrid replanning. In this scenario, the TEI provides information about the current situation such that pilots can anticipate corresponding speed changes controlled by the tactical controller. Since these actions result in energy deviations, the TEI also shows when these actions will result in a replan to correct this error.

Pilots found the requirement to set configurations accurately rather stringent but manageable and opted to use an aural cue to inform them of upcoming configuration changes as the timer required too much attention during countdown. The pilots also responded that they did not like that TEMO cannot correct deviations while on the glideslope as they have no opportunity to correct deviations they could have introduced themselves when they selected configuration too early or late. Therefore, they suggested to use configurations to correct deviations in an environmentally-friendly fashion as they often do during today's approaches.

Variations in pilot response

The results of the piloted simulation study showed that the required time accuracy of 2 seconds at the runway threshold was sometimes exceeded with the pilot in the loop. However, simulations flown with a zero-delay response model also showed time performance close to the boundaries of the RTP. Hence, the variations in pilot response were minimal and added only slight additional time deviations to the total deviation at the runway threshold. The configuration timer was successful in reducing the variance of selection delay but did not affect time performance at the runway.

The rather large time deviations found for the automated descents resulted from deviations while descending down the glideslope during which no replanning is active and the aircraft thus performs an open-loop final descent. Although disturbances were limited in this experiment, the transition towards the glideslope resulted in time deviations as potential energy was exchanged for kinetic energy due to an energy deviation that resulted from modeling errors in the algorithm. Therefore, it is expected that enabling replanning during this final phase will increase time accuracy at the runway. Since on the glideslope the vertical trajectory is fixed, energy exchange is no longer possible such that other (tactical) methods are required to correct deviations. Strategic replanning proved difficult during this phase due to the imposed constraints and limited distance towards the runway. Therefore, tactical use of thrust and speedbrakes could be used which will negatively affect environmental impact during a phase where the aircraft is rather close to ground level. Hence, a more environmentally-friendly approach would be the use of flap-scheduling as demonstrated in the Three-Degree Decelerating Approach (TDDA) [26–31] and Advanced Continuous Descent Approach (ACDA) [32]. This latter approach is similar to what pilots suggested as discussed previously.

Although these tactical systems could reduce time deviations at the runway, it is uncertain whether in real-life with more disturbances the 2 seconds RTP at the runway can be achieved. For example, during the last segment of flight before touchdown and after passing the stabilization altitude at 1,000 ft, replanning is no longer allowed as the aircraft should perform a stabilized approach [33]. During this 3 NM segment, a wind disturbance of only 3 KTS will result in a time deviation in excess of the desired 2 seconds, see the derivation of time deviation in Appendix A. This could be minimized by using a closed-loop system such as Airbus' Ground Speed mini system for wind shear protection [34, Section 1.22.30].

Rejected trajectories

The definition of the TEMO nominal trajectory, the imposed time constraints, the definition of the optimal control problem and sustained deviations, sometimes resulted in infeasible solutions or extensive calculation times. Moreover, the used software packages cannot guarantee that found solutions correspond to the global optimal solution but only guarantee that a solution is a local optimum [35]. Through redefining of phases and tuning of parameters and aircraft dynamics, many invalid solutions had been solved. From this process, it became clear that the TEMO algorithm cannot guarantee to find *a* solution, or *any* solution within a predefined and reasonable time interval. Unfortunately, the optimization software cannot

‘return’ the problematic constraint, or dynamics causing the infeasible solution, such that this constraint could be removed or relaxed by either the TEMO algorithm or the pilot during flight. Not finding solutions does not impose a safety concern since the aircraft remains flying the previous trajectory and can always revert to other flying modes. For spacing and sequencing, however, this does impose a problem as aircraft not finding valid trajectories require either new constraints or revert to a conventional descent which impacts the entire arrival sequence and may affect airport capacity. Furthermore, certification of the TEMO system might prove difficult due to TEMO’s current robustness.

Automating speedbrake control

The TEMO algorithm calculates trajectories of thrust and speedbrakes when needed to fulfill all requirements. These trajectories are continuous functions [35] flown by the auto-throttle and auto-speedbrakes systems, respectively. However, an auto-speedbrakes system is currently not available although certain aircraft systems show similarities [36, 37]. Using the pilot to accurately control speedbrake deflection by following a commanded deflection indication will result in trajectory deviations and increased workload. Therefore, either an auto-speedbrake function should be available, however, it is unlikely that a auto-speedbrake system suitable for TEMO will be available in 2018¹. Alternatively, the speedbrake trajectories should be discontinuous [38] to select full deflection or no deflection, often referred to as ‘bang-bang’ control. Pilots responded that they need the auto-speedbrake system to reduce workload and appreciate its functional similarity with an auto-thrust system. However, they questioned how the use of (auto-)speedbrakes affects passenger comfort.

6-1-3 Wind Estimation

A major contributor of external disturbances that cause the aircraft to deviate from a planned trajectory is the prevailing wind. Using accurate wind estimates during trajectory prediction will reduce trajectory deviations. For this reason, the Airborne Wind Estimation Algorithm (AWEA) algorithm was developed that constructs profiles of estimated winds along the own trajectory, using wind observations from other aircraft in its vicinity. These observations contain measurement errors which are reduced by the algorithm using a Kalman filter (KF). The KF intelligently uses the distance between the location of an observation and the own trajectory to account for variations in wind between that location and the own trajectory.

Results from simulations, using actual meteorological data and noise realizations, showed that AWEA reduces the noise Root Mean Square (RMS) error effectively from 1.94 KTS to only 1.35 KTS using observations from other nearby aircraft. Moreover, the constructed profiles provide increased spatial and temporal resolution as compared to state-of-the-art wind forecast data. Including distance information proved beneficial for reducing the estimation error. Unfortunately, current FMS systems only provide a limited resolution of altitude levels for which wind data can be entered. However, Airbus already increased the number of available wind forecast levels from four to ten for use in the Initial 4D project [39].

¹Chapter 1 stated that 2018 was targeted as the time of implementation of the new CDO concept.

Hence, the aircraft industry is already moving towards increasing the wind resolution in the TP.

AWEA was also evaluated in a simulation study investigating aircraft spacing using Aircraft Surveillance Applications System Flight-deck Interval Management (ASPA-FIM). Compared to a low resolution wind-chart solution, AWEA reduced the instantaneous wind estimation RMS error from 3.5 KTS to below 1.0 KTS. Due to this reduction and the increased spatial and temporal resolution of wind estimation data, the mean spacing error was significantly reduced.

AWEA was foreseen for use onboard aircraft but can also be used by a ground station to derive wind profile estimates for an entire area. This could be done by assuming that the wind at a particular altitude is equal for the entire area [40] or by using the distance information contained in measurements and defining a grid of locations within this area to construct a 3D grid wind estimate. For every application for which AWEA is used, one should tune all parameters, such as the altitude interval, observation model and measurement noise covariance matrix that serve its needs best. For instance, during aircraft descent one could employ a dynamic state variable that discards altitudes above the own trajectory since these altitudes are of less interest.

AWEA has not been implemented in TEMO yet and hence AWEA's effect on reducing trajectory deviations is unknown at this stage. The current AWEA algorithm requires adjustments before implementation in TEMO as TEMO does not fly a fixed vertical trajectory as currently assumed by AWEA. Therefore, AWEA should define a 3D grid along the lateral TEMO trajectory such that wind estimates for various altitudes along the trajectory are known upon trajectory prediction. This will increase the state vector of the AWEA algorithm which is not foreseen to be detrimental on AWEA calculation performance. However, using a 3D wind grid in TEMO trajectory prediction will increase the number of parameters in the optimization problem which leads to increased calculation times.

6-2 Recommendations

6-2-1 Realism

The experiments performed in this thesis only used straight-in aircraft trajectories and as such no turn dynamics were included. As an aircraft's drag increases in a turn due to the increase in lift, the effect of turns should be thoroughly investigated. Moreover, the modeling of these (fixed-radius) turns is likely to introduce additional modeling errors in the TP due to the aircraft transitioning from straight to banked flight and vice versa. This effect is similar to the omission of transitions between TEMO flight phases in the algorithm and instantaneous modeling of configuration changes, engine spooling and speedbrake deflection. To reduce deviations due to omitting transitions between flight phases, the flight-path angle should be defined as a state variable as opposed to a control variable. On the other hand, switch functions [41] can be used to model instantaneous transitions. However, both improvements are likely to increase calculation times and complexity. The transition of

speedbrakes and turn dynamics are part of new development phase of the TEMO algorithm in the FASTOP project [42].

Only in the batch study was wind used in the simulations, while the human-in-the-loop experiment assumed no wind conditions. However, this windfield was constant in velocity and direction and thus more realistic windfields should be evaluated. This also allows an evaluation of the assumption that deviations can dissolve due to changing winds. Including the AWEA algorithm into TEMO will reduce wind estimation errors and hence reduce replans and deviations due to wind. However, in real-life the availability of meteorological data from other aircraft is still limited and not specifically mandated in aviation regulations. Once regulations are amended, airlines should be encouraged to broadcast meteorological observations for the benefit of other aircraft and ATC for trajectory prediction.

Moving towards increased realism sensor errors will introduce deviations due to inaccuracies in measurement of for example, aircraft attitude, position, mass and velocity. Thus, deviations are likely to increase even further such that descending on a nominal trajectory without time updates and minimal wind estimation errors can still require multiple replans to do so. For this reason, it is recommended to use hybrid replanning such that any deviation is corrected and time performance (and hence, spacing and capacity) is assured. Resulting energy errors are corrected using strategic replanning such that new trajectories are optimized with respect to thrust and speedbrake use.

To avoid excessive speedbrake use and possible negative effects on passenger comfort, one could consider defining a nominal trajectory that uses near-idle thrust, similar to Continuous Descent Approach for Maximum Predictability (CDA-MP) [13, 43]. This way, thrust can be reduced to decrease energy while speedbrakes are only used when the thrust reduction does not suffice to reduce energy. The effects on environmental impact, in terms of fuel use and (aerodynamic noise) should be carefully investigated before continuing along this development path.

6-2-2 Capacity

The research in this thesis considered only a single aircraft (type) performing a descent using an (absolute) CTA and RTP. Hence, an obvious improvement is evaluating TEMO for other types of aircraft. The nominal speed profile depends on the aircraft type and hence these differences will affect TEMO time performance. Using mixed-aircraft types, a simulation study should evaluate runway capacity and spacing and separation between aircraft. This study should also compare capacity and separation for absolute time-management and relative time-management using Interval Management (IM) [44, 45].

IM could also increase time robustness of the arrival flow to wind estimation errors as all aircraft flying the same trajectory are likely to be affected equally by the prevailing wind. This holds in particular for the final descent down the glideslope where the aircraft has limited control space. Even though aircraft in the arrival stream will deviate from their absolute time of arrivals, the relative spacing interval between these aircraft remains nearly unchanged [46].

Implementation of IM will require adjustments to the TEMO algorithm as the time de-

viation is currently calculated as the difference between actual time and planned time at the current location. However, using IM introduces an additional time deviation in the form of a variable Estimated-Time of Arrival (ETA) of the lead aircraft.

Currently, the own ETA at the constrained waypoint is assumed to be equal to the the planned time of arrival plus the current time deviation. For IM operations, this calculation should be changed to the difference between the own ETA and the ETA of the lead aircraft and spacing goal. Moreover, the own ETA should be determined using a deterministic TP and the latest available wind data for optimal predictability. This implementation could prove to be beneficial when using strategic replanning as it potentially reduces the number of replans as the ETA predictor could use the latest available wind estimates which could result in the current time deviation being resolved due to changing winds later during descent and hence no or minimal ETA error. However, what would be the ETA update rate and achievable accuracy? This new implementation could also prove problematic when a tactical controller is used as a low update rate introduces a delay in controller actuation. Therefore, new research should investigate whether TEMO should correct the current deviation or the expected deviation at a point located ahead of the aircraft.

The TEMO concept, and the experiments in this thesis, aimed at using low values for the RTP as small variations in arrival time will increase runway throughput [44]. However, the results of the batch simulation study that used part of the RTP in the planning time window showed that increasing the planning window will increase the energy-neutral control space. For this reason, the capacity study should evaluate environmental impact and runway capacity for different values of the RTP. A small RTP will increase runway capacity but reduces the control space of energy-neutral trajectories. Hence, it should be evaluated at what environmental cost is a certain runway capacity number achieved. This study will enable a trade-off between capacity and environmental-friendliness.

Conceptually, only a single CTA was active at a time to allow ATC to assign the next CTA at a later stage for fine-tuning of the final arrival sequence. This, however, might not be the most environmentally-friendly solution of assigning CTAs as the algorithm cannot use thrust or speedbrakes before entering the TMA to satisfy a time constraint in the TMA. Furthermore, actions prior to TMA entry could limit the possible achievable CTA's at the runway threshold. This could be counteracted by using both CTA's simultaneously during strategic replanning. However, the question rises whether this is operationally acceptable since the CTA at the runway should be assigned to the aircraft prior to ToD.

6-2-3 Environmental Impact

The TEMO optimization algorithm optimizes the trajectory by minimizing throttle and speedbrake controls as it is assumed that reducing thrust and speedbrakes reduces fuel use, gaseous emission and noise contour levels. This assumption is primarily based on simple (linear) relations between throttle and speedbrakes and the environmental metrics. Ideally, one would optimize with respect to fuel consumption, gaseous emission and noise levels using accurate modeling of these metrics. The TEMO cost function could be adjusted to include fuel-flow, based on accurate engine dynamics and gaseous emission [47] and noise

levels [48] using environmental models [49]. These environmental models, however, are also based on gross assumptions and for instance do not directly include aircraft configuration or speedbrake deflections. Hence, optimizing with respect to these metrics would allow TEMO to freely use speedbrakes while these aerodynamics devices are known to contribute to airframe noise [50].

6-2-4 New Concept

Based upon the results of this thesis and the experience gathered during development, a revised version of the TEMO concept is proposed. To minimize time deviations, a tactical controller is required such that assigned time constraints are satisfied. Resulting energy deviations are corrected using replans such that the combined TEMO system uses hybrid replanning. The TEI is still displayed on the flight deck as it allows pilots to quickly infer time and energy deviations and support pilots in anticipating possible tactical controller actions and energy replans. Tactical speed control actions are displayed on the Primary Flight Display (PFD) speed-tape in a similar fashion as employed by Airbus in the Initial-4D project [39]. This design presents the current commanded speed to achieve an assigned CTA and the minimum and maximum allowable commanded speeds, or in other words, the controller boundaries. Since the tactical controller minimizes time deviations, the planning time window can be reduced to match the RTP. A larger planning window will increase the energy-neutral control space of the TEMO planning algorithm.

AWEA should be integrated into TEMO by using groundspeed in the definition of energy. AWEA calculates wind and temperature estimates at altitude intervals along the lateral path to minimize wind estimation and groundspeed deviations during strategic replanning which will minimize time and energy deviations. The wind and temperature information can also be used to improve ETA prediction at the time constrained waypoint.

Energy deviations before intercepting the glideslope are minimized through improved estimates of wind along the trajectory while the energy boundaries should be further restricted to reduce the allowable energy deviation margin during descent. These energy boundaries are defined up to glideslope intercept since energy exchange is no longer possible on the glideslope. For this reason, TEMO switches from SOE control to Path-on-Elevator (POE) control and uses flaps and gear deployment to alter the deceleration profile to minimize deviations. Energy deviations are no longer monitored as the aircraft's vertical path is restricted to the glideslope while the speed profile is constrained by operational constraints. A flap-scheduling algorithm calculates the locations of flap and gear selection to correct deviations while respecting these operational constraints. In case this flap-scheduling does not suffice, full tactical control using engines or speedbrakes should be used to correct deviations.

6-3 Future Work

Development of TEMO continuous after finishing beyond this thesis to 2015, when Clean Sky is expected to complete. Throughout the course of the research described in this thesis, TEMO successfully passed several Technology Readiness Level (TRL) reviews [51]. TRL level 3 was passed in January 2012 while level 4 was passed in December 2012. The next step in development is partly done by a third-party in the FASTOP [42] project which aims at including turn dynamics, wind dynamics and discrete speedbrake control in the TEMO algorithm and TP whilst optimizing for calculation speed. This updated algorithm will be used in a new pilot-in-the-loop experiment during the summer of 2014 performed on National Aerospace Laboratory (NLR)'s GRACE full-motion simulator. The results of this new experiment will be used to pass the TRL level 5 review. The experiment will be performed using a Cessna Citation II aircraft model and the developed HMI variant will be adapted accordingly. The transition to a new aircraft type will be done for two reasons. First, it shows that TEMO can be applied to different aircraft types. Second, the simulator study serves as a dry-run for actual flight-tests in 2015 using TU Delft/NLR's Cessna Citation II aircraft.

References

- [1] **L. Ren** and **J.-P. B. Clarke**. Flight-Test Evaluation of the Tool for Analysis of Separation and Throughput. *Journal of Aircraft*, 45(1), 323–332, 2008. doi:10.2514/1.30198.
- [2] **M. Tielrooij**, **A. C. in 't Veld**, **M. M. van Paassen**, and **M. Mulder**. Development of a Time-Space Diagram to Assist ATC in Monitoring Continuous Descent Approaches. In: **M. Mulder**, ed., *Air Traffic Control*, pp. 135–147. InTech, Rijeka, Croatia, 2010. ISBN 978-953-307-103-9. doi:10.5772/9845.
- [3] **A. M. P. De Leege**, **A. C. In 't Veld**, **M. Mulder**, and **M. M. Van Paassen**. A Time-Space Diagram as Controller Support Tool for Closed Path Continuous Descent Operations. In: *Proceedings of the AIAA Guidance, Navigation and Control Conference, Portland, Oregon, August 8–11*, AIAA 2011-6220, pp. 1–29. American Institute of Aeronautics and Astronautics, 2011. doi:10.2514/6.2011-6215.
- [4] **A. Van der Eijk**, **C. Borst**, **A. C. In 't Veld**, **M. M. Van Paassen**, and **M. Mulder**. Assisting Air Traffic Controllers in Planning and Monitoring Continuous-Descent Approaches. *Journal of Aircraft*, 49(5), 1376–1390, 2012. doi:10.2514/1.C031686.
- [5] **J.-P. B. Clarke**, **J. Brooks**, **G. Nagle**, **A. Scacchioli**, **W. White**, and **S. R. Liu**. Optimized Profile Descent Arrivals at Los Angeles International Airport. *Journal of Aircraft*, 50(2), 360–369, 2013. doi:10.2514/1.C031529.
- [6] **R. A. Coppengbarger**, **R. Lanier**, **D. N. Sweet**, and **S. Dorsky**. Design and Development of the En Route Descent Advisor (EDA) for Conflict-Free Arrival Metering.

- In: *Proceedings of the AIAA Guidance, Navigation, and Control Conference and Exhibit, Providence, Rhode Island, August 16–19*, AIAA 2004-4875, pp. 1–19. American Institute of Aeronautics and Astronautics, 2004. doi:10.2514/6.2004-4875.
- [7] **R. A. Coppenbarger, R. W. Mead, and D. N. Sweet.** Field Evaluation of the Tailored Arrivals Concept for Datalink-Enabled Continuous Descent Approach. *Journal of Aircraft*, 46(4), 1200–1209, 2009. doi:10.2514/1.39795.
 - [8] **T. Miquel, H. Manzoni, F. Legrand, D. Martin, and M. Millischer.** 4D Green Approach Trajectory: Illustrative Assessment On Toulouse Approach. In: *Proceedings of the AIAA Guidance, Navigation, and Control Conference, Toronto, Ontario, Canada, August 2–5*, AIAA 2010-8456, pp. 1–15. American Institute of Aeronautics and Astronautics, 2010. doi:10.2514/6.2010-8456.
 - [9] **M. Kaiser, M. Schultz, and H. Fricke.** Automated 4D Descent Path Optimization using the Enhanced Trajectory Prediction Model (ETPM). In: *Proceedings of the 5th International Conference on Research in Air Transportation — ICRAT 2012, Berkeley, California, May 22–25*, pp. 1–8, 2012.
 - [10] **D. H. Williams, R. M. Oseguera-Lohr, and E. T. Lewis.** Design and Testing of a Low Noise Flight Guidance Concept. Technical Memorandum NASA/TM-2004-213516, National Aeronautics and Space Administration, Langley Research Center, Hampton, Virginia 23681-2199, 2004.
 - [11] **R. M. Oseguera-Lohr, D. H. Williams, and E. T. Lewis.** Crew Procedures for Continuous Descent Arrivals Using Conventional Guidance. Technical Memorandum NASA/TM-2007-214538, National Aeronautics and Space Administration, Langley Research Center, Hampton, Virginia 23681-2199, 2007.
 - [12] **J. K. Klooster, K. D. Wickman, and O. F. Bleeker.** 4D Trajectory and Time-of-Arrival Control to Enable Continuous Descent Arrivals. In: *Proceedings of the AIAA Guidance, Navigation and Control Conference and Exhibit, Honolulu, Hawaii, August 18–21*, AIAA 2008-7402, pp. 1–17. American Institute of Aeronautics and Astronautics, 2008. doi:10.2514/6.2008-7402.
 - [13] **D. Garrido-López, L. D’Alto, and R. Gomez Ledesma.** A Novel Four-Dimensional Guidance for Continuous Descent Approaches. In: *Proceedings of the 28th Digital Avionics Systems Conference, Orlando, Florida, October 23–29*, pp. 6.E.1–1–6.E.1–11. IEEE/AIAA, 2009. doi:10.1109/DASC.2009.5347433.
 - [14] **J. L. De Prins and R. Gomez Ledesma.** Towards Time-based Continuous Descent Operations with Mixed 4D FMS Equipage. In: *Proceedings of the 11th AIAA Aviation Technology, Integration, and Operations (ATIO) Conference, Virginia Beach, Virginia, September 20–22*, AIAA 2011-7018, pp. 1–18. American Institute of Aeronautics and Astronautics, 2011. doi:10.2514/6.2011-7018.

- [15] **D. H. Williams, R. M. Oseguera-Lohr, and E. T. Lewis.** Energy Navigation: Simulation Evaluation and Benefit Analysis. Technical Publication NASA/TP-2011-217167, National Aeronautics and Space Administration, Langley Research Center, Hampton, Virginia 23681-2199, 2011.
- [16] **S. G. Park and J.-P. B. Clarke.** Vertical Trajectory Optimization for Continuous Descent Arrival Procedure. In: *Proceedings of the AIAA Guidance, Navigation and Control Conference, Minneapolis, Minnesota, August 13–16*, AIAA 2012-4757, pp. 1–19. American Institute of Aeronautics and Astronautics, 2012. doi:10.2514/6.2012-4757.
- [17] **A. A. Lambregts.** Integrated System Design for Flight and Propulsion Control Using Total Energy Principles. In: *Proceedings of the AIAA Aircraft Design, Systems and Technology Meeting, Fort Worth, Texas, October 17–19*, AIAA-83-2561, pp. 1–12. American Institute of Aeronautics and Astronautics, 1983.
- [18] **A. A. Lambregts.** Vertical Flight Path and Speed Control Autopilot Design Using Total Energy Principles. In: *Proceedings of the Guidance and Control Conference, Gatlinburg, Tennessee, August 15–17*, vol. A83-41659 19-63, pp. 559–569. Boeing Commercial Airplane Company, Seattle, Washington 98124, 1983.
- [19] **Jeppesen Sanderson.** *Instrument Commercial Manual.* Guided Flight Discovery. Jeppesen Sanderson, Englewood, Colorado, 2002.
- [20] **K. J. Vicente and J. Rasmussen.** Ecological Interface Design: Theoretical Foundations. *IEEE Transactions on Systems, Man, and Cybernetics*, 22(4), 589–606, 1992. doi:10.1109/21.156574.
- [21] **T. B. Sheridan.** *Telerobotics, Automation, and Human Supervisory Control.* MIT Press, Cambridge, Massachusetts, 1992.
- [22] **R. Tarroux.** Weight & Balance System. In: **D. Dempster**, ed., *FAST - Airbus Technical Digest*, 6. Airbus Industrie, Engineering & Product Support Directorates, 1985.
- [23] **U. Kehlenbeck.** AIRBUS A340 Weight and Balance System. In: *Proceedings of the 58th SAWE Annual Conference, San Jose, California, May 24–26*, 2450. Society of Applied Weight Engineering, 1999.
- [24] **M. Idan, G. Iosilevskii, and S. Nazarov.** In-Flight Weight and Balance Identification using Neural Networks. *Journal of Aircraft*, 41(1), 137–143, 2004. doi:10.2514/1.592.
- [25] **K. Christoffersen and D. D. Woods.** How to Make Automated Teams Team Players. In: **E. Salas**, ed., *Advances in Human Performance and Cognitive Engineering Research*, vol. 2, pp. 1–12. JAI Press/Elsevier, 2002.
- [26] **A. C. In 't Veld and J.-P. B. Clarke.** Trajectory Prediction for Self Separation during Decelerating Approaches in a DATA-LINK Environment. In: *Proceedings of the 2nd AIAA Aircraft Technology, Integration, and Operations (ATIO) 2002 Technical Forum*,

Los Angeles, California, October 1–3, AIAA 2002-5887, pp. 1–6. American Institute of Aeronautics and Astronautics, 2002.

- [27] **J. L. De Prins, K. F. M. Schippers, M. Mulder, M. M. Van Paassen, A. C. In 't Veld, and J.-P. B. Clarke.** Enhanced Self-Spacing Algorithm for Three-Degree Decelerating Approaches. *Journal of Guidance, Control and Dynamics*, 30(2), 576–590, 2007. doi:10.2514/1.24542.
- [28] **W. F. De Gaay Fortman, M. M. Van Paassen, M. Mulder, A. C. In 't Veld, and J.-P. B. Clarke.** Implementing Time-Based Spacing for Decelerating Approaches. *Journal of Aircraft*, 44(1), 106–118, 2007. doi:10.2514/1.22253.
- [29] **A. M. P. De Leege, A. C. In 't Veld, M. Mulder, and M. M. Van Paassen.** Three-Degree Decelerating Approaches in High Density Arrival Streams. *Journal of Aircraft*, 46(5), 1681–1691, 2009. doi:10.2514/1.42420.
- [30] **A. C. In 't Veld, M. Mulder, M. M. Van Paassen, and J.-P. B. Clarke.** Pilot Support Interface for Three-Degree Decelerating Approach Procedures. *The International Journal of Aviation Psychology*, Volume 19, Issue 3, 287–308, 2009. doi:10.1080/10508410902983938.
- [31] **P. M. A. De Jong, A. C. In 't Veld, A. M. P. De Leege, M. M. Van Paassen, and M. Mulder.** Control Space Analysis of Three-Degree Decelerating Approaches at Amsterdam Airport Schiphol. In: *Proceedings of the AIAA Guidance, Navigation and Control Conference, Toronto, Ontario Canada, August 2–5*, AIAA 2010-8454, pp. 1–20. American Institute of Aeronautics and Astronautics, 2010. doi:10.2514/6.2010-8454.
- [32] **M. F. Koeslag.** Advanced Continuous Descent Approaches. Tech. Rep. NLR-TR-2001-359, Faculty of Aerospace Engineering, Delft University of Technology and National Aerospace Laboratory NLR, 2001.
- [33] **ICAO.** *Procedures for Air Navigation Services - Aircraft Operations - Volume II, Construction of Visual and Instrument Flight Procedures - Doc 8168, OPS/611*. International Civil Aviation Organization, Montreal, Canada, 2006.
- [34] **Airbus.** *Flight Crew Operations Manual (Vol. 1)*, rev. 34 edn., 2002. 1.22.30.
- [35] **V. M. Becerra.** *PSOPT Optimal Control Solver User Manual*, 2011. Release 3.
- [36] **S. Vèque.** A318 - Steep Approach Operation. Presentation at OLM FBW 2006, Toulouse, France, 2006.
- [37] **P. Smith.** Date with the Eight. *Flight International*, 182(5370), 26–35, 2012.
- [38] **I. M. Ross and F. Fahroo.** Pseudospectral Knotting Methods for Solving Optimal Control Problems. *Journal of Guidance, Control and Dynamics*, 27(3), 397–405, 2004. doi:10.2514/1.3426.

- [39] **P. Pellerin**. SESAR JU - Initial 4D “On Time”. Presentation at ATC Global 2012, Amsterdam, The Netherlands, 2012.
- [40] **A. M. P. De Leege, M. Mulder, and M. M. Van Paassen**. Using Automatic Dependent Surveillance-Broadcast for Meteorological Monitoring. *Journal of Aircraft*, 50(21), 249–261, 2013. doi:10.2514/1.55833.
- [41] **S. Hartjes, H. G. Visser, and S. J. Hebly**. Optimization of RNAV Noise and Emission Abatement Departure Procedures. *The Aeronautical Journal*, 114(1162), 2010.
- [42] **X. Prats, I. Bas, and S. Vilardaga**. FASTOP D1.1 Problem Definition. Deliverable FASTOP D1.1, GTD, Barcelona, Spain, 2013. WP3.3-Technology Studies and Concept Validation, System for Green Operations ITD.
- [43] **D. Garrido-López, R. Gomez Ledesma, G. R. Gershzohn, and S. Moore**. Analysis of Aircraft Descent Predictability: Implications for Continuous Four-Dimensional Navigation. In: *Proceedings of the AIAA Guidance, Navigation and Control Conference, Portland, Oregon, August 8–11*, AIAA 2011-6217, pp. 1–18. American Institute of Aeronautics and Astronautics, 2011. doi:10.2514/6.2011-6217.
- [44] **T. S. Abbot**. Speed Control Law for Precision Terminal Area In-Trail Self Spacing. Technical Memorandum NASA/TM-2002-211742, National Aeronautics and Space Administration, Langley Research Center, Hampton, Virginia 23681-2199, 2002.
- [45] **T. S. Abbot**. A Brief History of Airborne Self-Spacing Concepts. Contractor Report NASA/CR-2009-215695, National Aeronautics and Space Administration, Langley Research Center, Hampton, Virginia 23681-2199, 2009.
- [46] **V. E. Houston and B. Barmore**. An Exploratory Study of Runway Arrival Procedures: Time-Based Arrival and Self-Spacing. In: *Proceedings of the 9th AIAA Aviation Technology, Integration, and Operations Conference (ATIO), Hilton Head, South Carolina, September 21–23*, AIAA 2009-7005, pp. 1–14. American Institute of Aeronautics and Astronautics, 2009.
- [47] **R. L. Martin, C. A. Oncina, and J. P. Zeeben**. A simplified method for estimating aircraft engine emissions. In: **S. L. Baughcum, T. G. Tritz, S. C. Henderson, and D. C. Pickett**, eds., *Scheduled Civil Aircraft Emission Inventories for 1992: Database Development and Analysis - NASA Contractor Report 4700, April 1996*, pp. D1–D11. National Aeronautics and Space Administration, 1995. Reported as “Boeing Method 2” fuel flow methodology description in appendix D.
- [48] Standard Method of Computing Noise Contours around Civil Airports. Tech. Rep. Document 29, ECAC/CEAC, 2005. 3rd Edition, Volume 1.
- [49] **M. J. G. Spierings**. *Optimizing Tailored Arrival Trajectories for Noise Abatement*. Unpublished MSc. Thesis, Faculty of Aerospace Engineering, Delft University of Technology, 2012.

- [50] **G. J. J. Ruijgrok.** *Elements of Aviation Acoustics*. Delft University Press, P.O. Box 98 2600 MG Delft, The Netherlands, 2004.
- [51] **Assistant Secretary of Defense for Research and Engineering.** Technology Readiness Assessment (TRA) Guidance. Tech. rep., Department of Defence, 2011.

CONCLUSIONS

The question that started this research was whether a new Continuous Descent Operations (CDO) procedure could be developed that used energy principles and time management to reduce environmental impact of aircraft during descent.

The developed concept in this thesis, named Time and Energy Managed Operations (TEMO) enables aircraft to fly CDOs whilst adhering to time constraints for spacing. TEMO uses energy principles to find new trajectories when disturbances cause the aircraft to deviate from the planned trajectory. Simulations show that TEMO reduces fuel use, emitted pollutants, and noise footprints, compared to current conventional step-down descents. Moreover, TEMO's energy-neutral — no additional thrust or speedbrake use — time control space is in the order of 8–16 seconds while this control space can be further extended by allowing minimized amounts of thrust or speedbrakes.

In order to fly calculated trajectories as accurate as possible, the descents are flown using the autopilot. Human-Machine Interfaces (HMIs) were developed to support pilots in operating the aircraft during a TEMO descent and to perform accurate and timely manual actions as required by the TEMO trajectory. Pilots responded that they appreciate the TEMO concept and procedures, but rather dislike the strict requirement of accurately performing manual actions. For this reason, several enhancements have been proposed to alleviate this restriction.

To improve the accuracy of predicted trajectories, Airborne Wind Estimation Algorithm (AWEA) — a wind estimation algorithm — was developed which uses wind observations from other nearby aircraft to construct an estimate of the wind profile along the own trajectory. This wind profile can be used during trajectory prediction to improve groundspeed and vertical trajectory prediction. This new algorithm showed capable of reducing wind Root Mean Square (RMS) errors from 1.94 KTS to 1.35 KTS using observations from other aircraft. The AWEA constructed wind profiles also improved airborne spacing when these trajectories are used during Estimated-Time of Arrival (ETA) predictions.

ENERGY EQUATIONS AND THE DYNAMICS OF FLIGHT

Throughout the years of work on this thesis, various equations of motion and dynamic equations related to aircraft energy have been used. This appendix discusses many of these equations and provides a detailed explanation of their respective derivations.

A-1 Reference Frames

In this thesis, multiple frames of reference have been used to establish equations of motion. These reference frames are discussed in the next sub-sections. For more extensive information, the reader is referred to the lecture notes of Flight Dynamics [1].

A-1-1 Earth-centered Inertial Reference Frame

The first reference frame is the Earth-centered inertial reference frame \mathcal{F}_I as shown in Figure A-1. It is a right-handed orthogonal axis-system with its origin in the center of gravity of the Earth. The Z_I -axis is directed upwards along the Earth's spin axis. The X_I -axis passes through the equator at the vernal equinox, which is located at the intersection of the ecliptic and equator [1]. Finally, the Y_I -axis is directed perpendicular to the $X_I Z_I$ -plane.

A-1-2 Earth-centered, Earth-fixed Reference Frame

The Earth-centered, Earth-fixed reference frame, \mathcal{F}_C , is similar to the Earth-centered inertial reference frame \mathcal{F}_I with the exception that the X_C -axis passes through the Greenwich meridian instead of the vernal equinox.. As such, this right-handed reference frame rotates along the Z_C -axis — along the Earth's spin-axis — with the angular velocity of the Earth, Ω . This reference frame is shown in Figure A-2.

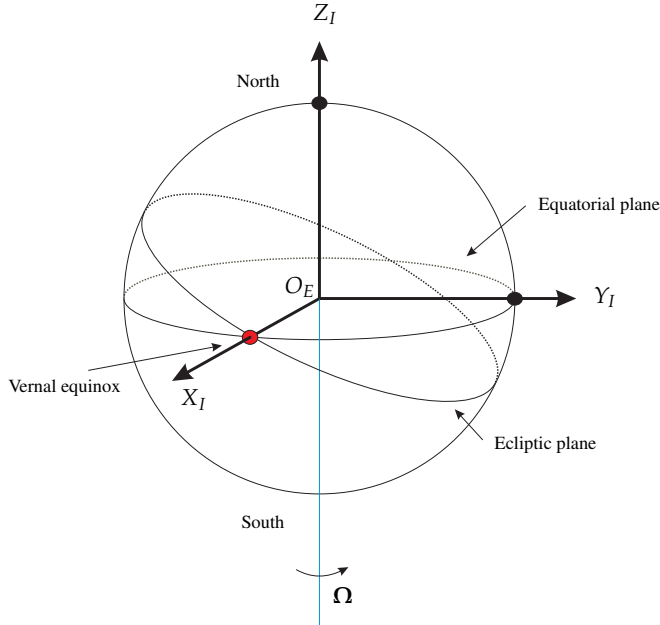


FIGURE A-1: Earth-centered inertial reference frame for spherical earth (used with permission from [1]).

A-1-3 Vehicle-carried Normal Earth Reference Frame

The vehicle-carried normal Earth reference frame, \mathcal{F}_E , has its origin in the aircraft's center of gravity and is denoted by the subscript E . The reference frame is fixed to the aircraft and moves along with it. This reference frame is parallel to the Earth's surface approximated by the Earth geoid. The X_E and Y_E -axes are tangent to the Earth's surface and X_E is directed North from this point and Y_E is directed East. The Z_E -axis is directed downwards towards the center of the Earth when the Earth is considered as a perfect sphere.

Figure A-3 shows the vehicle-carried normal Earth reference frame with respect to the Earth-centered inertial frame, \mathcal{F}_I .

A-1-4 Aerodynamic Reference Frame

The aerodynamic reference frame, \mathcal{F}_a , or flight-path reference frame is denoted by the subscript a . The origin of the reference frame lies in the center of gravity of the aircraft relative to the undisturbed air. The X_a -axis is in the direction of the aircraft's true airspeed, \mathbf{V}_a . The Z_a -axis lies in the symmetry plane of the aircraft and is positive downwards. To complete the right-handed axis system, Y_a is positive in starboard direction, see Figure A-4.

Figure A-4 shows the angles, α_a and β_a between the aerodynamic reference frame and the body-fixed reference frame, \mathcal{F}_b , denoted b [1]. Note that the aerodynamic reference frame is relative to air and not to ground.

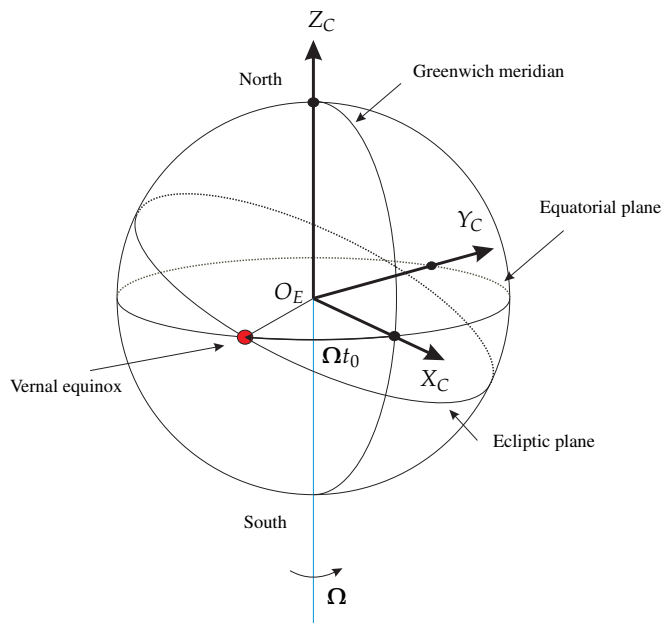


FIGURE A-2: Earth-centered, Earth-fixed reference frame for spherical earth (used with permission from [1]).

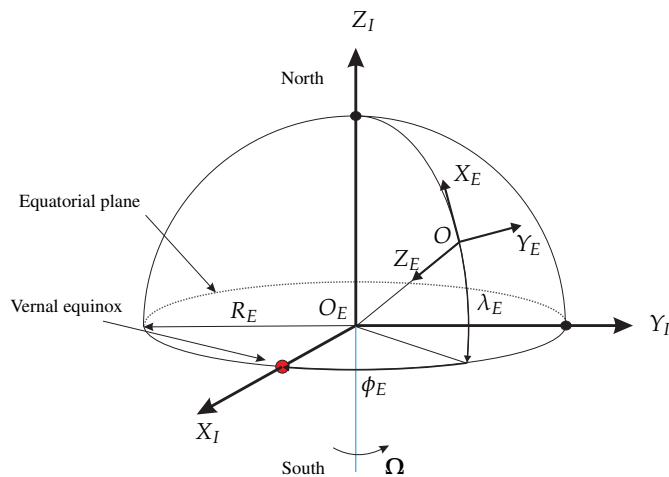


FIGURE A-3: Vehicle-carried normal earth reference frame for spherical earth (used with permission from [1]).

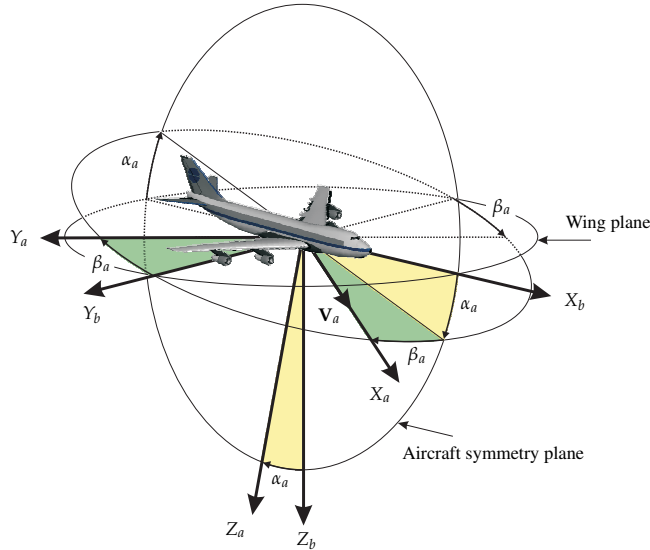


FIGURE A-4: Aerodynamic reference frame in relation to body-fixed reference frame (used with permission from [1]).

A-1-5 Kinematic Reference Frame

The kinematic reference frame, \mathcal{F}_k , is related to the kinematic velocity of the aircraft, \mathbf{V}_k . The component parallel to the Earth's surface is known as the ground velocity. The kinematic reference frame is similar to the aerodynamic reference frame with the main difference that the X_k -axis points in the direction of the kinematic velocity. This velocity is defined as the derivative of the aircraft's center of gravity relative to the vehicle carried normal Earth reference frame and as such accounts for wind.

The kinematic velocity equals the aerodynamic velocity accounting for wind. This relation between aerodynamic, kinematic and wind velocity is:

$$\mathbf{V}_k = \mathbf{V}_a + \mathbf{V}_w$$

A-1

When no wind is present the aerodynamic and kinematic velocity are equal and consequently the reference frames are equal as well.

A-2 Kinematics of a Point-Mass

Figure A-5 shows an aircraft descending through a horizontal windfield.

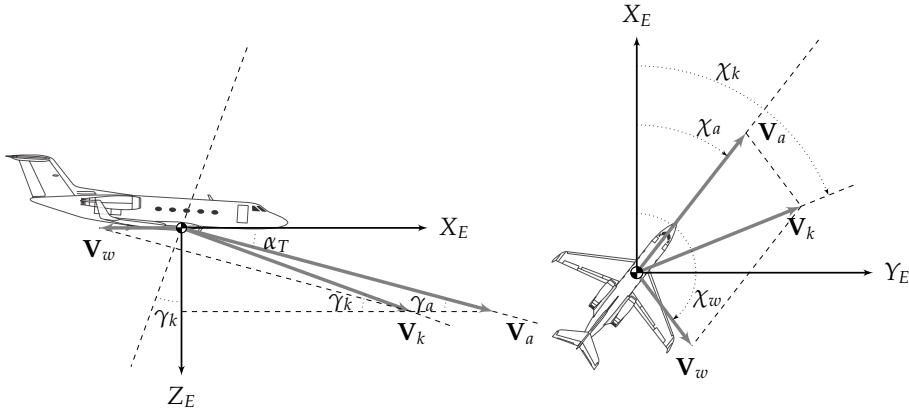


FIGURE A-5: Kinematic view of the aircraft.

From Figure A-5, the following relations are obtained:

$$\dot{X}_E = V_a \cos \gamma_a \cos \chi_a + V_w \cos \chi_w = V_k \cos \gamma_k \cos \chi_k \quad \text{A-2}$$

$$\dot{Y}_E = V_a \cos \gamma_a \sin \chi_a + V_w \sin \chi_w = V_k \cos \gamma_k \sin \chi_k \quad \text{A-3}$$

$$\dot{Z}_E = V_a \sin \gamma_a = V_k \sin \gamma_k \quad \text{A-4}$$

In which, χ_a is the aerodynamic heading angle, χ_w the wind heading angle and χ_k the kinematic heading angle; and, γ_a is the aerodynamic flight path angle and γ_k the kinematic flight path angle.

The latter equation of Eq. (A-4) can be rewritten to:

$$V_k = V_a \frac{\sin \gamma_a}{\sin \gamma_k} \quad \text{A-5}$$

Combining Eq. (A-2), Eq. (A-3) with Eq. (A-5) yields:

$$V_a \cos \gamma_a \cos \chi_a + V_w \cos \chi_w = V_a \frac{\sin \gamma_a}{\sin \gamma_k} \cos \gamma_k \cos \chi_k \quad \text{A-6}$$

$$V_a \cos \gamma_a \sin \chi_a + V_w \sin \chi_w = V_a \frac{\sin \gamma_a}{\sin \gamma_k} \cos \gamma_k \sin \chi_k \quad \text{A-7}$$

Reordering yields:

$$V_a \left(\frac{\sin \gamma_a \cos \chi_k}{\tan \gamma_k} - \cos \gamma_a \cos \chi_a \right) = V_w \cos \chi_w \quad \text{A-8}$$

$$V_a \left(\frac{\sin \gamma_a \sin \chi_k}{\tan \gamma_k} - \cos \gamma_a \sin \chi_a \right) = V_w \sin \chi_w \quad \text{A-9}$$

Multiplying Eq. (A-8) with $\sin \chi_k$ and Eq. (A-9) with $\cos \chi_k$ respectively and subtracting the resulting equations yields:

$$\sin \chi_a \cos \chi_k - \cos \chi_a \sin \chi_k = \frac{1}{\cos \gamma_a} \frac{V_w}{V_a} [\cos \chi_w \sin \chi_k + \sin \chi_w \cos \chi_k] \quad \text{A-10}$$

Rearranging, and using the subtraction theorem of trigonometry yields:

$$\sin(\chi_a - \chi_k) = \frac{V_w}{V_a} \frac{1}{\cos \gamma_a} \sin(\chi_k - \chi_w) \quad \text{A-11}$$

Solving for χ_a :

$$\chi_a = \chi_k + \arcsin \left[\frac{V_w}{V_a} \frac{1}{\cos \gamma_a} \sin(\chi_k - \chi_w) \right] \quad \text{A-12}$$

Further simplification can be achieved by using the following assumptions:

$$\begin{aligned} \gamma_a &\ll 1 \\ \sin \gamma_a &\approx \gamma_a \\ \cos \gamma_a &\approx 1 \end{aligned} \quad \text{A-13}$$

This reduces Eq. (A-12) to:

$$\chi_a = \chi_k + \arcsin \left[\frac{V_w}{V_a} \sin(\chi_k - \chi_w) \right] \quad \text{A-14}$$

By rewriting Eq. (A-8), γ_a is obtained:

$$\gamma_a = \arcsin \left(\frac{\tan \gamma_k}{\cos \chi_k} \left[\frac{V_w}{V_a} \cos \chi_w + \cos \gamma_a \cos \chi_a \right] \right) \quad \text{A-15}$$

Using the assumptions of Eq. (A-13), the final result is obtained:

$$\gamma_a = \left(\frac{\tan \gamma_k}{\cos \chi_k} \left[\frac{V_w}{V_a} \cos \chi_w + \cos \chi_a \right] \right) \quad \text{A-16}$$

The different aerodynamic and kinematic flight-path angle profiles for Time and Energy Managed Operations (TEMO) strategic and hybrid replanning descent and a 5 KTS tailwind are shown in Figure A-6. The figures shows the Speed-on-Elevator (SOE) control of the tactical controller for the hybrid solution as the aircraft pitches up to reduce airspeed and hence groundspeed due to the wrongly estimated tailwind. A TEMO descent flies a kinematic flight-path while on the Instrument Landing System (ILS) and hence the hybrid descent has to pitch down to intercept the glideslope as it arrives at an higher altitude due to tactical SOE control.

Also shown in this figure is the planned aerodynamic flight-path angle profile, calculated prior to Top of Descent (ToD) that discards wind information. Clearly seen is that the aerodynamic flight-path angle is larger than the kinematic flight-path angle due to this tailwind.

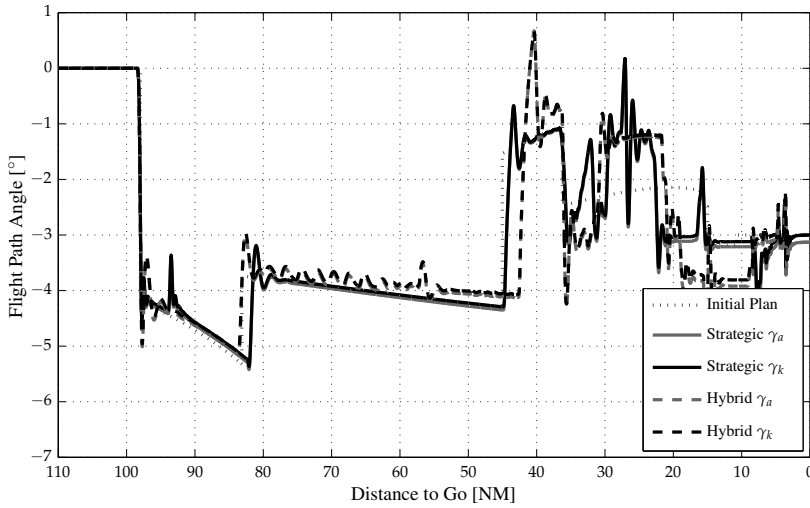


FIGURE A-6: Differences in flight-path angles due to 5 KTS tailwind.

A-3 Equations of Motion of a Point-Mass

Figure A-7 shows the forces acting on the aircraft modeled as a point-mass.

The equations of motion in a constant windfield expressed in the aerodynamic reference frame, \mathcal{F}_a , are:

$$\Sigma F_{X_a} = T \cos \alpha_T - D - mg \sin \gamma_a \quad \text{A-17}$$

$$\Sigma F_{Y_a} = L \sin \mu_a \quad \text{A-18}$$

$$\Sigma F_{Z_a} = -T \sin \alpha_T - L \cos \mu_a + mg \cos \gamma_a \quad \text{A-19}$$

In these equations, the flight-path angle is negative since the aircraft is descending.

Using the assumption that the angle between the velocity vector and engine thrust is small ($\alpha_T \approx 0$) yields simplified expressions:

$$\Sigma F_{X_a} = T - D - mg \sin \gamma_a \quad \text{A-20}$$

$$\Sigma F_{Y_a} = L \sin \mu_a \quad \text{A-21}$$

$$\Sigma F_{Z_a} = -L \cos \mu_a + mg \cos \gamma_a \quad \text{A-22}$$

To derive the equations of motion in the kinematic reference frame, \mathcal{F}_k , the transformation matrix $\mathbb{T}_{a \rightarrow k}$ is required [1, 2]:

$$\mathbb{T}_{a \rightarrow k} = \begin{bmatrix} \cos(\beta_w) \cos(\alpha_w) & -\sin(\beta_w) & -\cos(\beta_w) \sin(\alpha_w) \\ \sin(\beta_w) \cos(\alpha_w) & \cos(\beta_w) & -\sin(\beta_w) \sin(\alpha_w) \\ \sin(\alpha_w) & 0 & \cos(\alpha_w) \end{bmatrix} \quad \text{A-23}$$

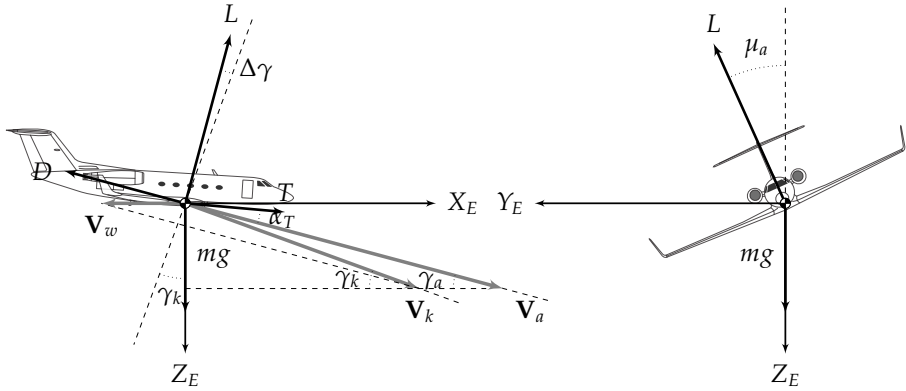


FIGURE A-7: Forces acting on the aircraft.

The transformation matrix is a function of three angles: *a*) the wind angle of roll, which is the rotation about the X_a -axis between \mathbf{V}_a and \mathbf{V}_k ; *b*) the wind angle of side-slip, β_w , which is the rotation angle about the $Z_{a'}$ -axis between \mathbf{V}_a and \mathbf{V}_k ; *c*) the wind angle of attack, α_w , which is the rotation angle about the $Y_{a''} = Y_k$ -axis between \mathbf{V}_a and \mathbf{V}_k . For simplification the angle of roll is neglected in Eq. (A-23). The remaining wind angles are shown in Figure A-8.

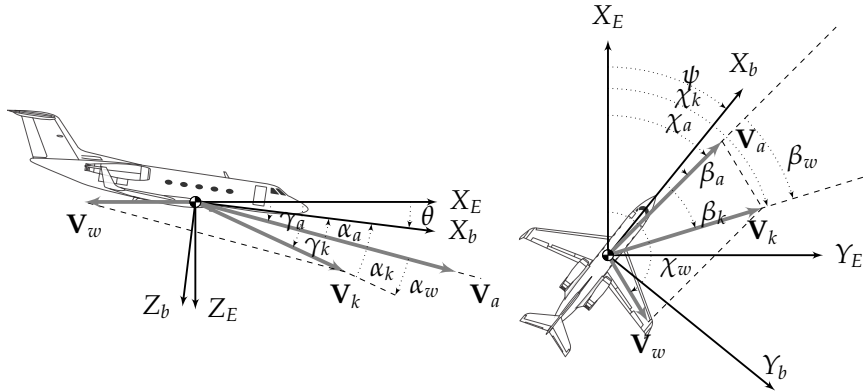


FIGURE A-8: Kinematic view of the aircraft including wind.

From Figure A-8, the following relations can be found:

$$\theta = \gamma_k + \alpha_k = \gamma_a + \alpha_a \quad \text{A-24}$$

$$\psi = \chi_k - \beta_k = \chi_a - \beta_a \quad \text{A-25}$$

Moreover, the kinematic angles of attack and side-slip can be written as a function of

the wind angles:

$$\alpha_k = \alpha_a - \alpha_w \quad \text{A-26}$$

$$\beta_k = \beta_a + \beta_w \quad \text{A-27}$$

Combining these equations results in expressions for the wind angle of attack and wind side-slip angle (often referred to as *drift angle*):

$$\alpha_w = \gamma_k - \gamma_a \quad \text{A-28}$$

$$\beta_w = \chi_k - \chi_a \quad \text{A-29}$$

The TEMO algorithm and Trajectory Predictor (TP) do not include turns or wind in the equations of motion of Eqs. (A-20,A-21,A-22) and are expressed in \mathcal{F}_a :

$$T - D - mg \sin \gamma_a = m\dot{V}_a \quad \text{A-30}$$

$$-L + mg \cos \gamma_a = mV_a\dot{\gamma}_a \quad \text{A-31}$$

Eq. (A-31) can be rewritten to calculate C_L :

$$C_L = \frac{mg \cos \gamma_a - mV_a\dot{\gamma}_a}{\frac{1}{2}\rho V_a^2 S} \quad \text{A-32}$$

For simplification of trajectory prediction, the TP assumes that $\dot{\gamma}_a \approx 0$. This yield:

$$C_L = \frac{mg \cos \gamma_a}{\frac{1}{2}\rho V_a^2 S} \quad \text{A-33}$$

The drag coefficient, C_D , is calculated using profile drag and induced drag:

$$C_D = C_{D_0}^{config} + \frac{C_L^2}{\pi A e_{config}} \quad \text{A-34}$$

A-4 The Energy Equations of Motion

When one considers the energy state of a system, another concept, *work*, comes into consideration as *energy* is defined as the possibility to do *work* and these two concepts are closely related.

Work is defined as a force applied to an object causing movement of said object. As such, work is only performed when an object, or system, is non-stationary relatively to a point of reference (or reference frame). Mathematically, work is defined as:

$$W = \int_{x(t_1)}^{x(t_2)} \mathbf{F} \cdot d\mathbf{x} \quad \text{A-35}$$

In this integral, W is the work performed by the external force F along the trajectory defined by the vector x .

An aircraft descending or climbing through the air, experiences work done by the gravitational force. This work is referred to as gravitational *potential* energy, ‘stored’ in the aircraft resulting from the gravitational force to keep the aircraft at a height h above an arbitrary reference location:

$$W = \int_{x(t_1)}^{x(t_2)} \mathbf{F}_g \cdot d\mathbf{x} = \int_{x(t_1)}^{x(t_2)} mg \, dx = mg \int_{x(t_1)}^{x(t_2)} dx = mgh \quad \text{A-36}$$

In this equation, g is the gravitational acceleration, h the height above the reference location, and m is the aircraft mass. Both parameters are assumed to be constant in order for the third part of Eq. (A-36) to hold. At higher altitudes from the Earth’s surface than typical commercial aircraft fly, g can no longer be assumed constant.

When considering the aircraft as a system, an aircraft can be approximated as a simple point-mass as shown in the previous sections. Using the force equations from Section A-3, the resultant force of the *non-potential* forces acting on the aircraft, i.e., thrust (T), lift (L) and drag (D) causes the aircraft to move. The total work done to bring the aircraft from rest to a velocity, V , is referred to as *kinetic* energy:

$$W = \int_{x(t_1)}^{x(t_2)} \mathbf{F}_r \cdot d\mathbf{x} \quad \text{A-37}$$

Using $\mathbf{V} = \frac{d\mathbf{x}}{dt}$ and assuming constant mass, this can be rewritten to:

$$\begin{aligned} W &= \int_{t_1}^{t_2} \mathbf{F}_r \cdot \mathbf{V} \, dt = \int_{t_1}^{t_2} m \mathbf{a}_r \cdot \mathbf{V} \, dt = \int_{t_1}^{t_2} m V \frac{dV}{dt} \, dt = \\ &= m \int_{t_1}^{t_2} V \, dV = \frac{1}{2} m \left(V(t_2)^2 - V(t_1)^2 \right) \end{aligned} \quad \text{A-38}$$

In this equation, the acceleration, a , is the resulting acceleration acting along the direction of the velocity, V . Eq. (A-38) is often referred to as the *work-energy* theorem, and states that the total work done by all forces acting on a system, as it moves from point $A = x(t_1)$ to point $B = x(t_2)$, is equal to the change in kinetic energy of the system from point A to point B .

Now, the *law of conservation of energy* states that the total amount of energy in a closed system remains constant over time. This means that energy can change its form and/or location within the system. For instance, aircraft engines change chemical energy stored in fuel to kinetic energy by generating thrust. Mathematically, total energy is defined as,

$$E_{tot} = E_{pot} + E_{kin} = mgh + \frac{1}{2} mV^2 \quad \text{A-39}$$

where E_{pot} is the potential energy and E_{kin} the kinetic energy.

By dividing Eq. (A-39) by the aircraft weight, mg , the specific energy [3, 4] is obtained:

$$E_{tot_s} = h + \frac{V^2}{2g} \quad \text{A-40}$$

Since specific energy has units of length and is directly related to height h , it is often referred to as energy height [3, 4].

The TEMO algorithm calculates specific energy profiles of trajectories such that deviations from this profile can be monitored and corrected when required. Since the TEMO algorithm does not use wind information and uses the aerodynamic reference frame, the aircraft's specific energy is expressed using true airspeed:

$$E_{tot_s} = h + \frac{V_a^2}{2g} \quad \text{A-41}$$

A-4-1 Energy Rate

The energy rate is obtained by differentiating Eq. (A-39):

$$\dot{E}_{tot} = mg\dot{h} + mV_a\dot{V}_a \quad \text{A-42}$$

Rewriting Eq. (A-30) and inserting into Eq. (A-42):

$$\dot{E}_{tot} = mgV_a \sin \gamma_a + mV_a \left(\frac{T - D - mg \sin \gamma_a}{m} \right) \quad \text{A-43}$$

$$= V_a (T - D) \quad \text{A-44}$$

Eq. (A-44) shows that the aircraft can change the energy rate, and hence the energy state, through thrust and drag. The engines add energy to the aircraft while aerodynamic forces, in the form of drag, dissipate energy from the aircraft.

A-4-2 Energy Rate Demand

The energy rate demand, \hat{E} is defined as the ratio between *commanded* energy rate and the *maximum* energy rate. When flying a descent the maximum energy rate, neglecting early flap selections, is achieved when the engines are set to idle and will be negative. The commanded energy rate depends on the flight trajectory through the commanded flight-path angle and commanded speed:

$$\dot{E}_{com} = mg\dot{h} + mV_a\dot{V}_a \quad \text{A-45}$$

$$= mgV_a \sin \gamma_a + mV_a\dot{V}_a \quad \text{A-46}$$

$$= WV_a \left(\sin \gamma_a + \frac{\dot{V}_a}{g} \right) \quad \text{A-47}$$

In which $W = mg$.

The energy rate demand is thus:

$$\hat{E} = \frac{WV_c \left(\sin \gamma_c + \frac{\dot{V}_a}{g} \right)}{V_a (T_{idle} - D)} \quad \text{A-48}$$

Assuming that the commanded speed equals the actual airspeed, the equation can be further simplified to:

$$\hat{E} = \frac{W \left(\sin \gamma_a + \frac{\dot{V}_a}{g} \right)}{(T_{idle} - D)} \quad \text{A-49}$$

A trajectory that has an energy rate demand of 1 is a full idle descent as described by Eq. (A-49). During a decelerating descent, the commanded energy rate will be negative as well and, therefore, the energy rate demand cannot exceed 1 since the commanded energy rate cannot exceed the maximum achievable energy rate. On the other hand, values below 1 of the energy rate demand means that the commanded profile prescribed less energy dissipation than the maximum achievable rate. Since commanded speed was assumed equal to the actual flown speed and control of drag devices was ignored, the aircraft used additional thrust to fly the trajectory.

A-4-3 Energy Share Factor

The *energy share factor* [5], k , is defined by:

$$k \triangleq \frac{\dot{h}}{\dot{E}_{tot_s}} \quad \text{A-50}$$

Expansion yields,

$$\begin{aligned} k &= \frac{\frac{dh}{dt}}{\frac{dh}{dt} + \frac{V_a}{g} \frac{dV_a}{dt}} \\ &= \frac{1}{1 + \frac{V_a}{g} \frac{dV_a}{dt} \frac{dt}{dh}} \\ k &= \frac{1}{1 + \frac{V_a}{g} \frac{dV_a}{dh}} \end{aligned} \quad \text{A-51}$$

Three interesting cases can be distinguished,

$$\begin{aligned} k = 0 &\longrightarrow \dot{h} = 0 \quad \rightarrow \quad \dot{E}_{tot_s} = \frac{V_a \dot{V}_a}{g} \\ k = 1 &\longrightarrow \dot{h} = \dot{E}_{tot_s} \\ k = \infty &\longrightarrow \dot{E}_{tot_s} = 0 \rightarrow \quad \dot{h} = -\frac{V_a \dot{V}_a}{g} \end{aligned} \quad \text{A-52}$$

A-4-4 Definition of Energy Error

The planned energy height (or specific energy, see Eq. (A-40)) is defined as:

$$h_{ep} = h_p + \frac{V_{ap}^2}{2g} \quad \text{A-53}$$

Now assume, that our actual energy deviates from the planned specific energy which results from a different altitude and/or true airspeed. This actual, but erroneous, specific energy is defined as:

$$h_{ef} = h_f + \frac{V_{af}^2}{2g} \quad \text{A-54}$$

Now, the energy error, f , between the actual and planned specific energy is:

$$f = h_{ef} - h_{ep} \quad \text{A-55}$$

Hence,

$$h_f + \frac{V_{af}^2}{2g} - h_p - \frac{V_{ap}^2}{2g} = f \quad \text{A-56}$$

The new true airspeed V_{af} is found as:

$$V_{af} = \sqrt{2g \left([h_p - h_f] + f \right) + V_{ap}^2} \quad \text{A-57}$$

And conversely, the new altitude h_f is found as:

$$h_f = h_p + f + \frac{V_{ap}^2 - V_{af}^2}{2g} \quad \text{A-58}$$

The (specific) energy error, f , in terms of potential and kinetic energy is given by:

$$f = h_p - h_f + \frac{2V_{af}V_{\Delta} - V_{\Delta}^2}{2g} \quad \text{A-59}$$

Where,

$$V_{\Delta} = V_{ap} - V_{af} \quad \text{A-60}$$

A-5 The Influence of a Vertical Wind Gradient on the Equations of Motion

In this section, it is assumed that the aircraft flies along a straight descent path in a horizontal, time and altitude dependent windfield. The wind acts along the longitudinal motion of the aircraft such that $\chi_k = \chi_a = \chi_w$, see Figure A-5. In this scenario, the aircraft's path is defined by:

$$V_{X_E} = V_a \cos \gamma_a - V_w = V_k \cos \gamma_k \quad \text{A-61}$$

$$V_{Z_E} = V_a \sin \gamma_a = V_k \sin \gamma_k \quad \text{A-62}$$

While the windfield can be defined as:

$$V_w \triangleq V_w(X_E, h, t) \quad \text{A-63}$$

In this definition, X_E is the aircraft's position along the straight flight-path, h the aircraft altitude and t is time.

The partial derivatives of this windfield are:

$$\dot{V}_w = \frac{\partial V_w}{\partial X_E} \dot{X}_E + \frac{\partial V_w}{\partial h} \dot{h} + \frac{\partial V_w}{\partial t} \quad \text{A-64}$$

For simplification, it is assumed that wind is constant irrespective of the aircraft position and time and thus only depends on altitude. Since the aircraft descends, the change of wind over time only depends on altitude. This yields the following expression for the windfield:

$$\dot{V}_w = \frac{\partial V_w}{\partial h} \dot{h} = \frac{dV_w}{dt} \quad \text{A-65}$$

Differentiate with respect to time:

$$\frac{dV_{X_E}}{dt} = \frac{dV_a}{dt} \cos \gamma_a - V_a \sin \gamma_a \frac{d\gamma_a}{dt} - \frac{dV_w}{dt} \quad \text{A-66}$$

$$\frac{dV_{Z_E}}{dt} = \frac{dV_a}{dt} \sin \gamma_a + V_a \cos \gamma_a \frac{d\gamma_a}{dt} \quad \text{A-67}$$

Transform to aerodynamic reference frame, \mathcal{F}_a :

$$\frac{dV_{X_a}}{dt} = \frac{dV_{X_E}}{dt} \cos \gamma_a + \frac{dV_{Z_E}}{dt} \sin \gamma_a \quad \text{A-68}$$

$$\frac{dV_{Z_a}}{dt} = -\frac{dV_{X_E}}{dt} \sin \gamma_a + \frac{dV_{Z_E}}{dt} \cos \gamma_a \quad \text{A-69}$$

Inserting Eq. (A-67) into the previous equations, yields:

$$\frac{dV_{X_a}}{dt} = \frac{dV_a}{dt} \cos^2 \gamma_a - V_a \sin \gamma_a \cos \gamma_a \frac{d\gamma_a}{dt} - \frac{dV_w}{dt} \cos \gamma_a + \frac{dV_a}{dt} \sin^2 \gamma_a + \quad \text{A-70}$$

$$V_a \cos \gamma_a \sin \gamma_a \frac{d\gamma_a}{dt} \quad \text{A-71}$$

$$\frac{dV_{Z_a}}{dt} = -\frac{dV_a}{dt} \cos \gamma_a \sin \gamma_a + V_a \sin^2 \gamma_a \frac{d\gamma_a}{dt} + \frac{dV_w}{dt} \sin \gamma_a + \frac{dV_a}{dt} \sin \gamma_a \cos \gamma_a + \quad \text{A-72}$$

$$V_a \cos^2 \gamma_a \frac{d\gamma_a}{dt} \quad \text{A-73}$$

This can be simplified to obtain the following equations:

$$\frac{dV_{X_a}}{dt} = \frac{dV_a}{dt} - \frac{dV_w}{dt} \cos \gamma_a \quad \text{A-74}$$

$$\frac{dV_{Z_a}}{dt} = V_a \frac{d\gamma_a}{dt} + \frac{dV_w}{dt} \sin \gamma_a \quad \text{A-75}$$

Wind Gradient and Energy Rate Demand Using the result of Eq. (A-74), the energy rate demand in a windfield as described by Eq. (A-65) can be derived.

The equation of motion along X_a is given by:

$$\frac{W}{g} \ddot{X}_a = T - D - mg \sin \gamma_a \quad \text{A-76}$$

With,

$$\ddot{X}_a = \frac{d^2 X_a}{dt^2} = \frac{dV_{X_a}}{dt}, \quad \text{A-77}$$

the previous equation can be written as:

$$\frac{W}{g} \left(\frac{dV_a}{dt} - \frac{dV_w}{dt} \cos \gamma_a \right) = T - D - W \sin \gamma_a \quad \text{A-78}$$

$$\frac{W}{g} \left(\frac{dV_a}{dt} - \frac{dV_w}{dt} \cos \gamma_a \right) = T - D - \frac{W}{V_a} \frac{dh}{dX_a} \left(\frac{dV_a}{dt} - \frac{dV_w}{dt} \cos \gamma_a \right) \quad \text{A-79}$$

$$\frac{W}{g} \left(\frac{dV_a}{dt} - \frac{dV_w}{dt} \cos \gamma_a \right) \left(1 + \frac{g}{V_a} \frac{dh}{dX_a} \right) = T - D \quad \text{A-80}$$

This latter equation is obtained by using:

$$\frac{dh}{dt} = V_a \sin \gamma_a \quad \text{A-81}$$

This equation can be rewritten to:

$$\frac{dh}{dX_a} \frac{dX_a}{dt} = V_a \sin \gamma_a \quad \text{A-82}$$

$$\sin \gamma_a = \frac{1}{V_a} \frac{dh}{dX_a} \left(\frac{dV_a}{dt} - \frac{dV_w}{dt} \cos \gamma_a \right) \quad \text{A-83}$$

The energy rate demand is thus:

$$\hat{E} = \frac{\frac{W}{g} \left(\frac{dV_a}{dt} - \frac{dV_w}{dt} \cos \gamma_a \right) \left(1 + \frac{g}{V_a} \frac{dh}{dX_a} \right)}{T - D} \quad \text{A-84}$$

$$= \frac{\frac{W}{g} \left(\frac{dV_a}{dt} - \frac{dV_w}{dt} \cos \gamma_a + g \sin \gamma_a \right)}{T - D} \quad \text{A-85}$$

The energy rate demand expressed in the aerodynamic reference frame is thus affected by a wind gradient $\frac{dV_w}{dt}$.

A-6 Time Deviation Resulting from a Speed Deviation

The planned time of arrival, t_p , over a planned ground-distance x_p is given by:

$$t_p = \int_{x_p} \frac{1}{V_{g_p}(t)} dx \quad \text{A-86}$$

Assuming that speed is constant yields:

$$t_p = \frac{x_p}{V_{g_p}} \quad \text{A-87}$$

Assume that our planned speed is offset by a deviation in value of ΔV , this will result in a different time of arrival, t_f , over the same distance, x_p during which the deviation is present:

$$t_f = \frac{x_p}{V_{g_f}} \quad \text{A-88}$$

Since $V_{g_f} = V_{g_p} + \Delta V$, the time deviation, Δt is given by:

$$\begin{aligned}\Delta t = t_f - t_p &= \frac{x_p}{V_{g_p} + \Delta V} - \frac{x_p}{V_{g_p}} \\ &= \frac{x_p V_{g_p} - x_p (V_{g_p} + \Delta V)}{V_{g_p} (V_{g_p} + \Delta V)} \\ &= \frac{x_p (V_{g_p} - V_{g_p} - \Delta V)}{V_{g_p}^2 + V_{g_p} \Delta V} \\ &= -\frac{x_p \Delta V}{V_{g_p}^2 + V_{g_p} \Delta V}\end{aligned}$$

A-90

References

- [1] **J. A. Mulder, W. H. J. J. Van Staveren, J. C. Van der Vaart, E. De Weerd, A. C. In 't Veld, and E. Mooij.** *Flight Dynamics*. Lecture notes, Faculty of Aerospace Engineering, Delft University of Technology, 2013.
- [2] **P. M. A. De Jong.** *Control Space Analysis of Noise Abatement Procedures: A Case Study at Amsterdam Airport Schiphol*. Unpublished MSc. Thesis, Faculty of Aerospace Engineering, Delft University of Technology, 2009.
- [3] **G. J. J. Ruijgrok.** *Elements of Airplane Performance*. Delft University Press, 1996.
- [4] **M. Asselin.** *An Introduction to Aircraft Performance*. AIAA Educational Series. American Institute of Aeronautics and Astronautics, Reston, Virginia, 1997.
- [5] **S. Gillet, A. Nuic, and V. Mouillet.** Enhancement in Realism of ATC Simulations by Improving Aircraft Behaviour Models. In: *Proceedings of the 29th Digital Avionics Systems Conference, Salt Lake City, Utah, October 3–7*, pp. 2.D.4–1–2.D.4–13. IEEE/AIAA, 2010. doi:10.1109/DASC.2010.5655482.

B

TEMO HMI VARIANTS

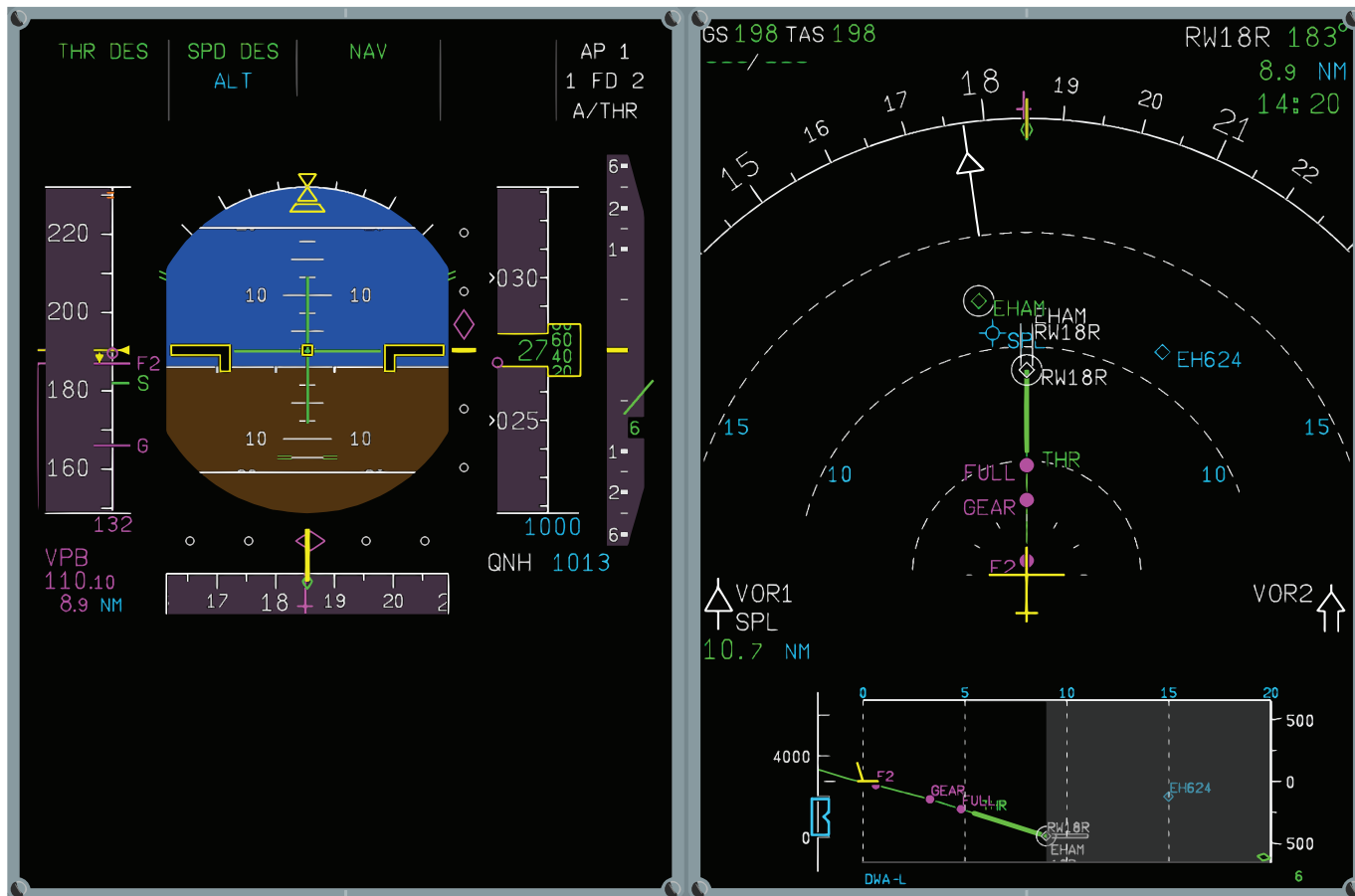


FIGURE B-1: HMI Variant 1

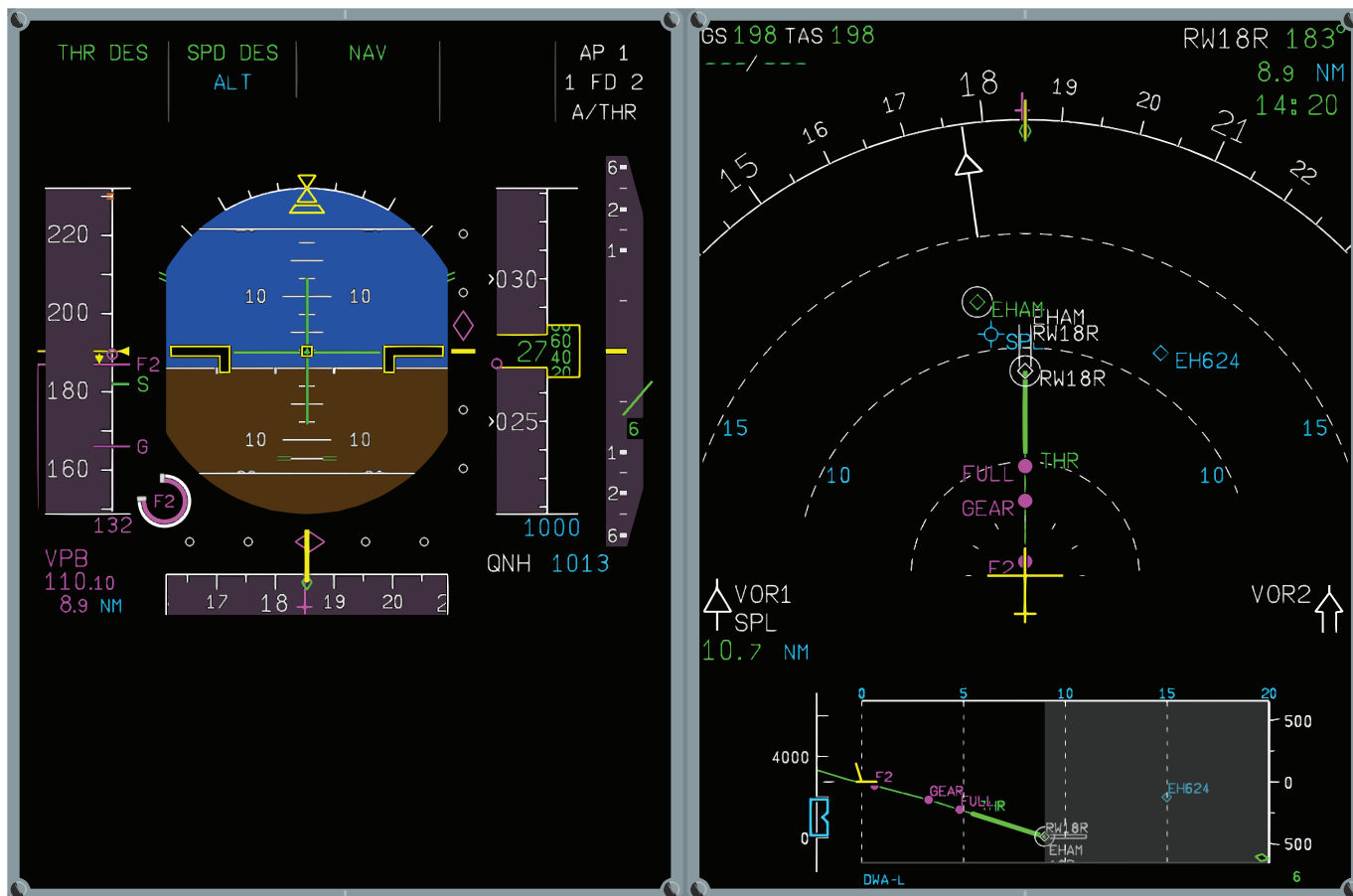


FIGURE B-2: HMI Variant 2

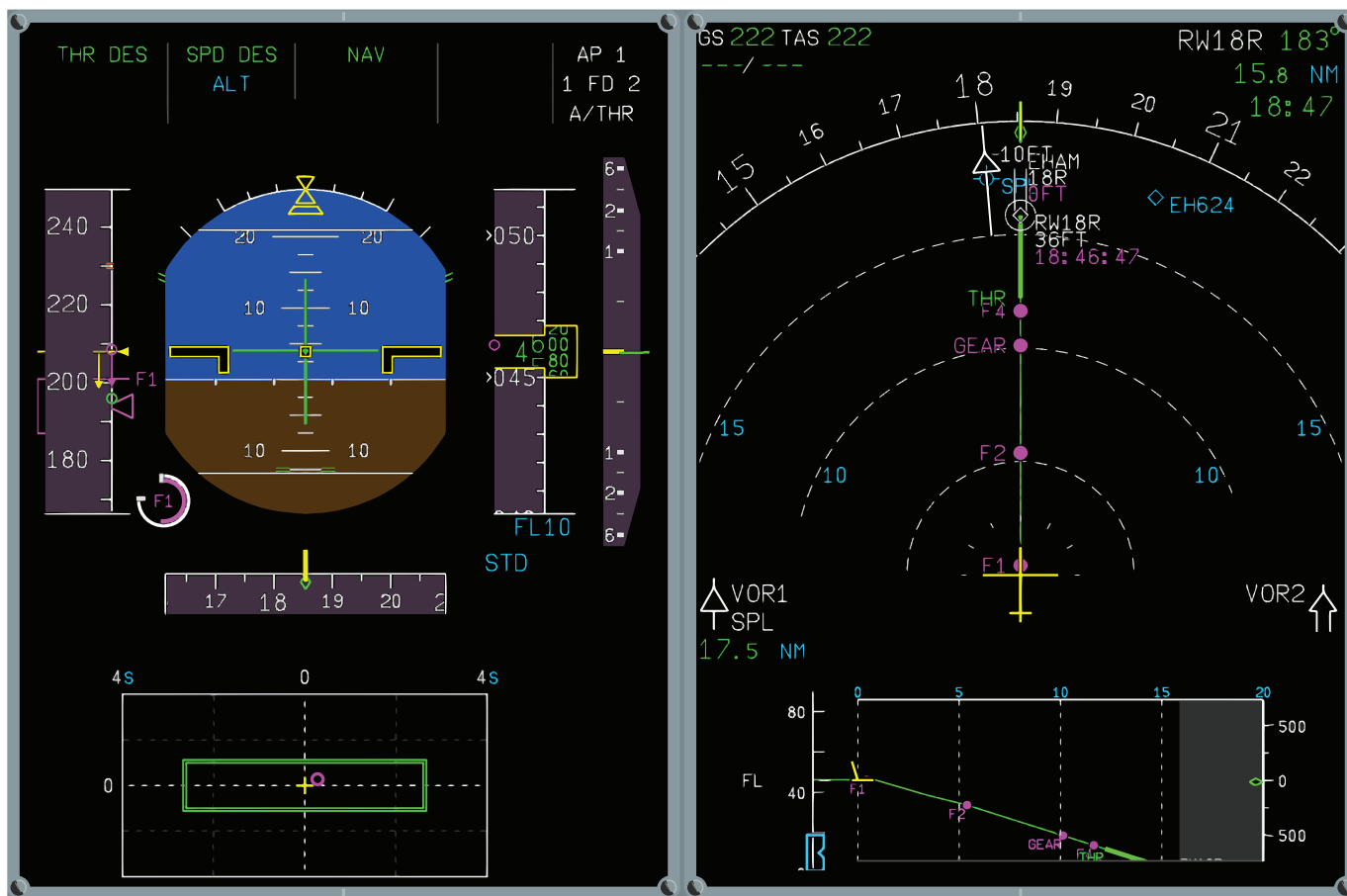


FIGURE B-3: HMI Variant 3

ANSWERS TO POST-EXPERIMENT QUESTIONNAIRE

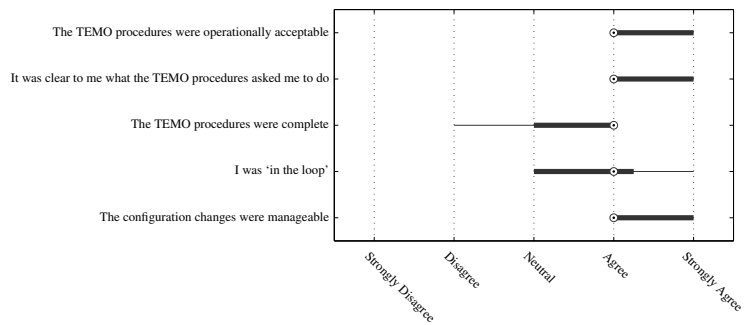


FIGURE C-1: Answers regarding Time and Energy Managed Operations (TEMO) procedures ($N = 8^1$).

¹One pilot did not answer all five questions and has been omitted in the analysis of these questions.

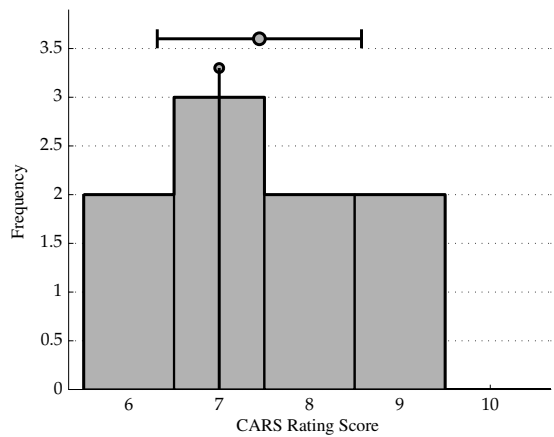


FIGURE C-2: Overall Controller Acceptance Rating Scale (CARS) rating scores ($N = 9$).

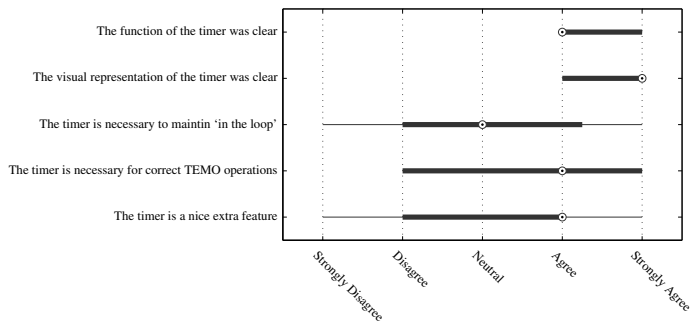


FIGURE C-3: Answers to questions related to the configuration timer on the PFD ($N = 9$)

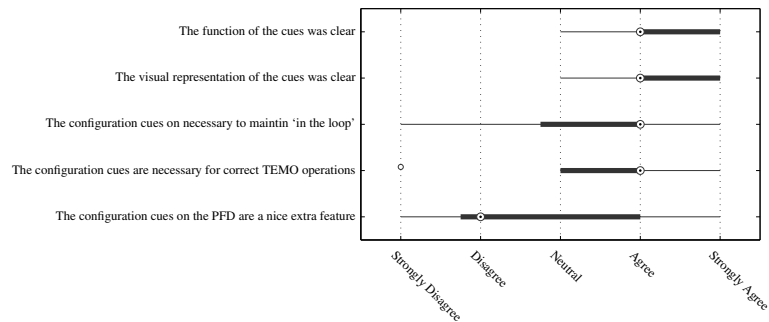


FIGURE C-4: Response to questions related to the flap and gear cues on the PFD speed-tape ($N = 9$)

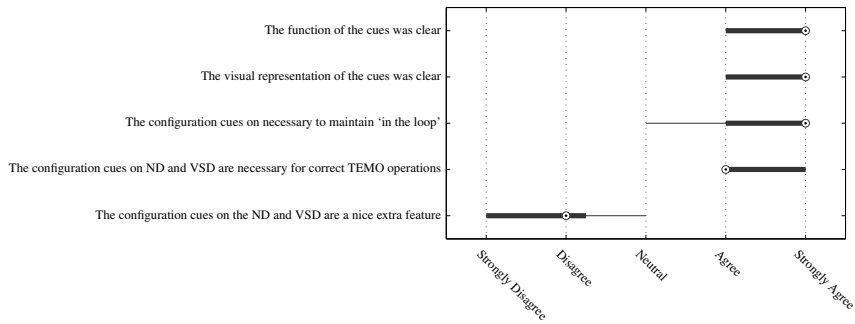


FIGURE C-5: Response to questions related to the flap and gear cues on the ND and VSD ($N = 9$)

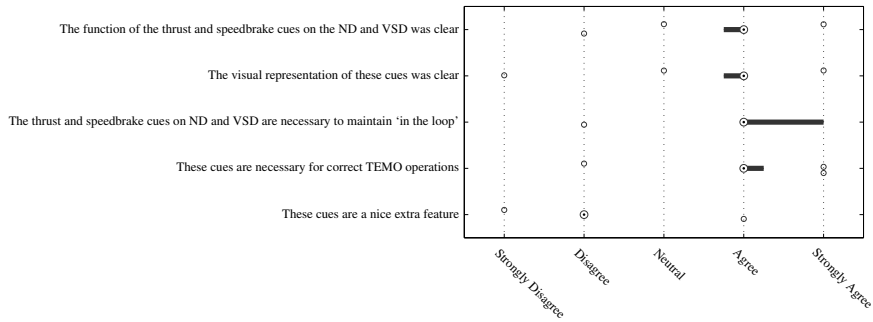


FIGURE C-6: Response to questions related to the thrust and speedbrake cues on the ND and VSD ($N = 9$)

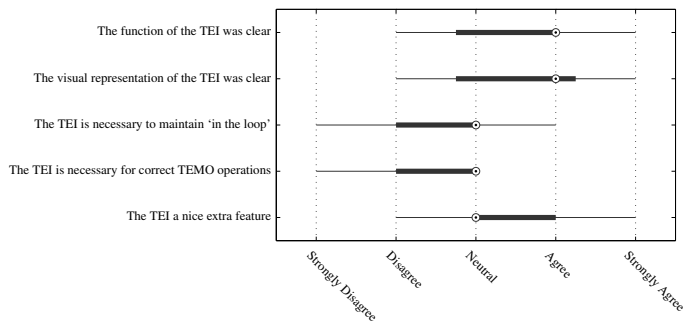


FIGURE C-7: Response to questions related to the TEI ($N = 9$)

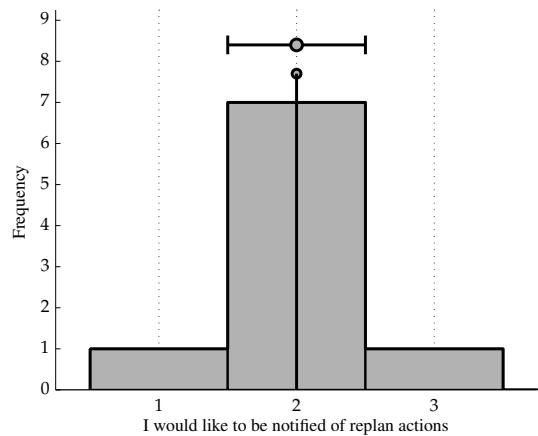


FIGURE C-8: Pilots response to re-plan notifications ($N = 9$)

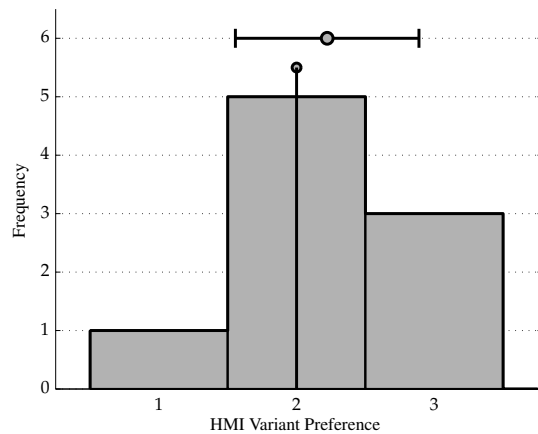


FIGURE C-9: HMI variant Preference ($N = 9$).

D

RSME RATING SCALE

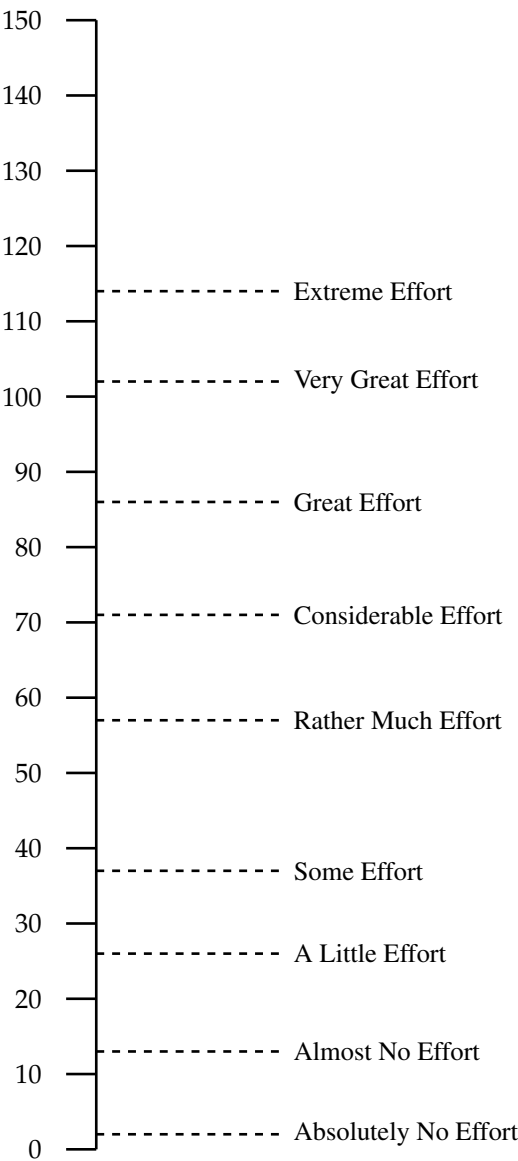


FIGURE D-1: Rating Scale Mental Effort.

E

CARS RATING SCALE

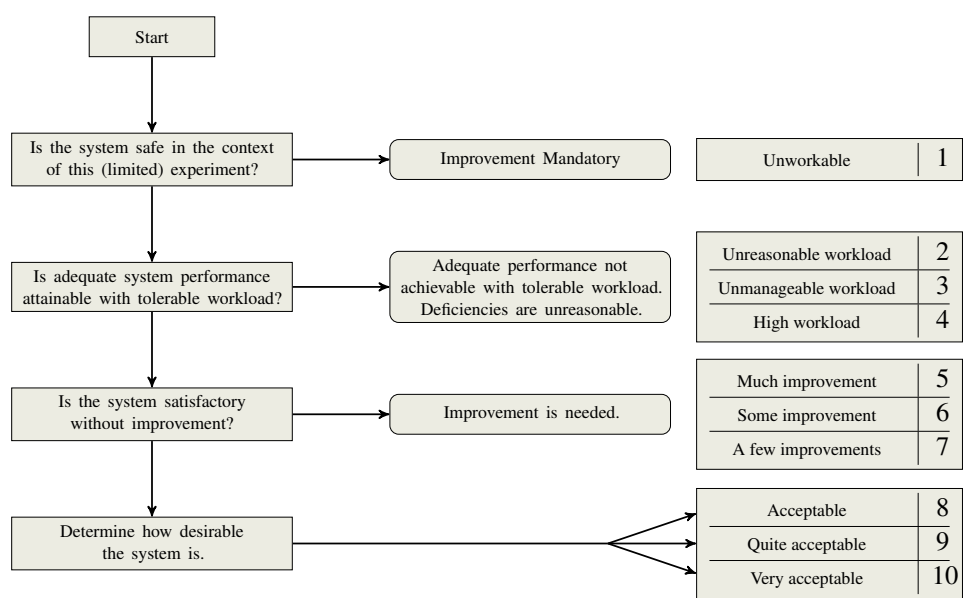


FIGURE E-1: Modified Controller Acceptance Rating Scale.

ABBREVIATIONS

ACARS	Aircraft Communication and Reporting System 123
ACAS	Aircraft Collision Avoidance System 11
ACDA	Advanced Continuous Descent Approach 5, 155
ADC	Air Data Computer 122, 123
ADS	Automatic Dependent Surveillance 123–125
ADS-B	Automatic Dependent Surveillance - Broadcast 35, 36, 46, 120, 124, 125, 137, 141
ADS-C	Automatic Dependent Surveillance - Contract 124, 125, 127
AIP	Aeronautical Information Publication 2
AMAN	Arrival Manager 14
AMDAR	Aircraft Meteorological Data Relay 123, 124, 137
ANOVA	Analysis of Variance 106–108, 137
ANSP	Air Navigation Service Provider 2
APERO	Avionics Prototyping Environment for Research and Operations 99, 103
ARV	Air Referenced Velocity 124, 141
ASPA-FIM	Aircraft Surveillance Applications System Flight-deck Interval Management 157
ASTAR	Airborne Spacing for Terminal Arrivals 137
ATC	Air Traffic Control v, 3–6, 8, 10, 14, 30–33, 35, 36, 39, 42, 46–48, 54, 55, 57, 59, 62, 66, 91–94, 103, 114, 126, 127, 136, 148, 151, 154, 158, 159, 207
ATCo	Air Traffic Controller 2–4, 8, 54, 148
ATIS	Automatic Terminal Information Service 13, 120
ATM	Air Traffic Management 4
ATS	Air Transportation System 54, 90, 120

AWEA	Airborne Wind Estimation Algorithm viii, 119–121, 125–128, 132–139, 141, 156–158, 160, 167, 210, 211
BDS	Comm-B Data Selector 124
BM2	Boeing Method 2 66
BRTE	Boeing Research and Technology Europe 6, 46
CARS	Controller Acceptance Rating Scale 103, 109, 192
CAS	Calibrated Airspeed 15, 33, 97, 150, 153
CDA	Continuous Descent Approach 99
CDA-MP	Continuous Descent Approach for Maximum Predictability 6, 46, 158
CDO	Continuous Descent Operations v, vi, 2–8, 10, 11, 13, 14, 16, 29–31, 35, 37, 54, 55, 57, 89–91, 93, 120, 147, 148, 156, 167, 207
CDU	Control and Display Unit 46, 47, 93, 96, 98, 101, 105
CFIT	Controlled Flight into Terrain 11
CO₂	Carbon Dioxide 66, 68, 69, 74, 79, 80, 148
CPDLC	Controller Pilot Data Link Communications 103
CTA	Controlled-Time of Arrival 31, 35–37, 41, 42, 45–49, 57, 58, 61–65, 74, 78, 79, 92, 93, 98, 99, 101, 102, 104–106, 109, 111–113, 151, 158–160
CTI	Controlled-Time Interval 46, 49, 58
DAP	Downlink Aircraft Parameters 124
DCDU	Data Communications Display Unit 101
DLR	German Aerospace Center 4, 47, 59, 213
EAS	Equivalent Airspeed 15
EID	Ecological Interface Design 95
EKF	Extended Kalman Filter 125, 141
ENAV	Energy Navigation 6
ETA	Estimated-Time of Arrival 3, 12, 13, 35–37, 46–48, 93, 94, 96, 101, 122, 136, 159, 160, 167
ETS	Emission Trading Scheme 1
FANS	Future Aircraft Navigation System 6
FAS	Final Approach Speed 34, 38, 41, 48, 58, 94, 104
FCU	Flight Control Unit 47, 48, 93, 101
FE	Flight Engineer 11
FMA	Flight Mode Annunciator 48, 98
FMS	Flight Management System 3–7, 11, 13, 35, 37, 38, 43, 46–48, 57, 58, 90, 93, 95, 98, 102, 103, 111, 113, 120, 122–124, 126, 127, 137, 153, 156
GPOPS	General Pseudospectral Optimal Control Software 39, 41–44, 46, 62, 151
GPS	Global Positioning System 122
HMI	Human-Machine Interface vii, 12, 16, 89–91, 94–98, 101–110, 113, 114, 153, 154, 161, 167, 214

IAF	Initial Approach Fix vi, vii, 14, 35–37, 41, 45–48, 58, 61, 64–67, 70–72, 74–76, 78–83, 90, 93, 102, 104, 105, 110, 150, 151, 209
IAS	Indicated Airspeed 15, 150
ICAO	International Civil Aviation Organization 1
ILS	Instrument Landing System 5, 34, 38, 48, 58, 66, 67, 91, 96, 97, 174, 209
IM	Interval Management 31, 36, 57, 82, 136, 158, 159
IRU	Inertial Reference Unit 122
ISA	International Standard Atmosphere 64, 103
ITD	Integrated Technology Demonstrator 4
KF	Kalman filter viii, 125, 126, 128, 129, 134, 135, 156
KNMI	Royal Netherlands Meteorological Institute 16, 132
LA	Instantaneous A-weighted Noise Level 68
LA_{MAX}	Maximum A-weighted Noise Level 66
LNAV	Lateral Navigation 103
LNG	Low Noise Guidance 6
MLW	Maximum Landing Weight 45, 102
Mode-S EHS	Mode-S Enhanced Surveillance 124, 132
Mode-S ELS	Mode-S Elementary Surveillance 123, 124
Mode-S ES	Mode-S Extended Squitter 124
NAP	Noise Abatement Procedure 2
ND	Navigation Display 97, 98, 110
NLP	Nonlinear Program 42
NLR	National Aerospace Laboratory 4, 161, 213, 215
NO_x	Nitrogen Oxide vii, 66, 68, 69, 74, 79, 80, 90, 104, 112, 113, 148
NOAA	National Oceanic and Atmospheric Administration 123
OPD	Optimum Profile Descent 6, 120
PBO	Performance-based Operations 4
PF	Pilot Flying 99
PFD	Primary Flight Display 48, 97, 110, 160
PNF	Pilot Not Flying 99
POE	Path-on-Elevator 5, 42, 65, 72, 160
RMS	Root Mean Square viii, 120, 134–136, 138, 156, 157, 167, 210
RNAV	Area Navigation 126
RNP	Required Navigation Performance 36, 124
RSME	Rating Scale Mental Effort 103, 104, 108, 109
RTA	Required Time of Arrival 4, 35, 36, 46–48, 93, 96
RTP	Required Time Performance vi, vii, 31, 36, 37, 41, 47, 48, 57, 58, 62, 70, 72, 74, 76, 79–82, 92, 93, 95, 96, 103, 104, 106, 114, 150–152, 155, 158–160
SEL	Sound Exposure Level vi, 66–68, 74, 78, 81, 83, 104, 112, 208
SESAR	Single European Sky ATM Research 4, 14, 36, 58, 95
SGO	System for Green Operations 4, 14

SOE	Speed-on-Elevator 6, 7, 30, 37, 42, 46, 47, 55, 56, 59, 65, 72, 79–81, 92, 110, 150, 160, 174
SOP	Standard Operating Procedure 99
SSR	Secondary Surveillance Radar 123
STAR	Standard Arrival Route 6, 47, 93
SV	State Vector 124
SWIM	System Wide Information Management 14, 124, 141
TA	Tailored Arrivals 6, 120
TAS	True Airspeed 15, 33, 76, 122, 124, 150
TASAT	Tool for Analysis of Separation and Throughput 3
TAWS	Terrain Awareness and Warning System 11
TBO	Trajectory-based Operations 4
TbO	Time-based Operations 3, 4
TDDA	Three-Degree Decelerating Approach 5, 55, 155, 215
TECS	Total Energy Control System 152
TEI	Time and Energy Indicator 98, 110, 113, 153, 154, 160
TEMO	Time and Energy Managed Operations v–viii, 8, 10–12, 14–16, 29–39, 41–49, 53–59, 62–68, 70, 74, 79, 81–83, 89–99, 101–106, 109, 111, 113, 114, 120, 147–161, 167, 174, 177, 179, 191, 207–211, 213, 214
TMA	Terminal Maneuvering Area vii, 6, 8, 36, 37, 41, 42, 45, 48, 58, 62, 93, 111, 125–127, 132, 137, 150, 159, 209
ToD	Top of Descent 3, 5, 7, 8, 14, 15, 30, 33, 35, 37, 44, 48, 54, 55, 58, 63–67, 70, 72, 74, 78, 80, 82, 91, 93, 94, 102, 105–107, 110–112, 120, 148, 159, 174
TP	Trajectory Predictor vi, vii, 2–4, 6, 8, 10, 11, 13, 14, 31, 55, 91, 93, 120, 137, 148, 149, 152, 153, 157, 159, 161, 177
TRL	Technology Readiness Level 161
TSD	Time Space Diagram 3
UAT	Universal Access Transceiver 124
VDL	VHF Data Link 124
VNAV	Vertical Navigation 5, 6, 12, 103
VSD	Vertical Situation Display 97–99, 110
WMO	World Meteorological Organization 123

SYMBOLS

a	Acceleration
d	Horizontal distance between measurement and own trajectory
e	Innovation
g	Gravitational acceleration
h	Reference altitude
h	Altitude
k	Energy share factor
m	Mass
p	Wind power-law exponent
R_E	Radius of the Earth
t	Time
Δt	Time deviation
Δt	Planning time window
$u(t)_{\widehat{N1}}$	Fan speed control
$u(t)_{SB}$	Speedbrake control
$u(t)_{THR}$	Throttle control
v	Measurement noise
w	Process noise
x	State vector
\hat{x}	Estimated state vector
y	Observation vector
f_f	Fuel Flow
A	Aspect ratio
C_D	Drag-coefficient
$C_{D_0}^{config}$	Profile drag-coefficient for an aircraft configuration
C_L	Lift-coefficient

e_{config}	Oswald efficiency number
$\tilde{N}1$	Normalized engine fan speed
$N1$	Engine fan speed
$E_{\epsilon_{GS}}$	Energy deviation at the glideslope intercept
$t_{\epsilon_{RWY}}$	Time deviation at the runway
A	State transition matrix
C	Measurement matrix
D	Drag
\hat{E}	Energy rate demand
E_{kin}	Kinetic energy
E_{pot}	Potential energy
E_{tot}	Total energy
\dot{E}_{tot}	Total energy rate
F	Force
f	Energy error
t_f	Offset time of arrival
t_p	Planned time of arrival
\mathcal{F}_a	Aerodynamic reference frame
\mathcal{F}_b	Body-fixed reference frame
\mathcal{F}_C	Earth-centered, Earth-fixed reference frame
\mathcal{F}_E	Vehicle-carried normal Earth-fixed reference frame
\mathbf{F}_g	Gravitational force
\mathcal{F}_I	Inertial reference frame
\mathcal{F}_k	Kinematic reference frame
\mathbf{F}_r	Resultant force
h_f	Offset altitude
h_p	Planned altitude
K	Kalman gain matrix
K_{SB}	Speedbrake control scaling parameter
K_{THR}	Throttle control scaling parameter
K_w	Distance scaling parameter for measurement
L	Lift
O	Origin
O_E	Earth origin
P	Prediction error covariance matrix
Q	Process noise covariance matrix
R	Measurement noise covariance matrix
S	Planform area
S	Innovation covariance matrix
T	Thrust
V	Velocity
V_0	Airbus green dot speed

V_{af}	Offset airspeed up to arrival
V_{ap}	Planned airspeed up to arrival
V_{APP}	Airbus final approach speed
V_F	Airbus F(laps) speed
V_{F1}	Flaps 1 speed
V_{F2}	Flaps 2 speed
V_{F3}	Flaps 3 speed
V_{F4}	Flaps 4 speed
V_{FAS}	Airbus final approach speed
V_G	Gear speed
V_{gf}	Offset groundspeed up to arrival
V_{gp}	Planned groundspeed up to arrival
V_{LOC}	Localizer intercept speed
V_{LOC}^+	Maximum localizer intercept speed
V_{LOC}^-	Minimum localizer intercept speed
V_S	Airbus S(lats) speed
\mathbf{V}_a	True airspeed vector
\mathbf{V}_g	Ground speed vector
\mathbf{V}_k	Kinematic airspeed vector
\mathbf{V}_w	Wind speed vector
V_{w_0}	Wind speed at reference height h_0
V_w	Wind speed
W	Work
X_a	X-coordinate in aerodynamic reference frame
X_b	X-coordinate in aircraft body reference frame
X_C	X-coordinate in Earth-centered reference frame
X_E	X-coordinate in vehicle-carried normal Earth reference frame
X_I	X-coordinate in inertial reference frame
X_k	X-coordinate in kinematic reference frame
x_p	Distance to point of arrival
Y_a	Y-coordinate in aerodynamic reference frame
Y_b	Y-coordinate in aircraft body reference frame
Y_C	Y-coordinate in Earth-centered reference frame
Y_E	Y-coordinate in vehicle-carried normal Earth reference frame
Y_I	Y-coordinate in inertial reference frame
Y_k	Y-coordinate in kinematic reference frame
Z_a	Z-coordinate in aerodynamic reference frame
Z_b	Z-coordinate in aircraft body reference frame
Z_C	Z-coordinate in Earth-centered reference frame
Z_E	Z-coordinate in vehicle-carried normal Earth reference frame
Z_I	Z-coordinate in inertial reference frame
Z_k	Z-coordinate in kinematic reference frame

α_a	Aerodynamic angle of attack
α_k	Kinematic angle of attack
α_T	Thrust angle of attack
α_w	Wind angle of attack
β_a	Aerodynamic side-slip angle
β_k	Kinematic side-slip angle
β_w	Wind side-slip angle
γ_a	Aerodynamic flight-path angle
γ_k	Kinematic flight-path angle
λ_E	Latitude
μ_a	Aerodynamic angle of roll
ϕ_E	Longitude
ψ	Angle of yaw
ρ	Density of air
τ_{F1}	Flaps 1 selection delay
τ_{F2}	Flaps 2 selection delay
τ_{F4}	Flaps 4 selection delay
τ_G	Gear selection delay
θ	Angle of pitch
Ω	Angular velocity of the Earth
χ_a	Aerodynamic heading angle
χ_k	Kinematic heading angle (track angle)
χ_w	Wind heading angle

SAMENVATTING

Gebruik van Energie Principes voor Glijvluchten tijdens de Daling

Paul M. A. de Jong

Tijdens de huidige vliegtuigen dalingen, commandeert Air Traffic Control (ATC) vliegtuigen te dalen naar specifieke hoogtes en windrichtingen om vliegtuig van elkaar te separeren. Indien het vliegtuig wordt opgedragen om een tussenliggende hoogte vast te houden, is motor stuwkracht nodig om de snelheid te behouden. Dit resulteert in extra brandstof verbruik, productie van emissies en geluidshinder. Door deze horizontale segmenten te vermijden kan brandstofverbruik, geluidshinder en emissies worden verminderd en kan een vliegtuig de daling uitvoeren gebruikmakend van een efficiëntere motorstand, namelijk stationair. In dit geval zal het vliegtuig een continue daling afleggen, dit wordt ook wel Continuous Descent Operations (CDO) genoemd. Een CDO verhoogt tegelijkertijd ook het hoogteprofiel, wat resulteert in het verminderen van het geluidsniveaus op de grond.

Hedendaags worden CDOs al operationeel gebruikt op diverse grote luchthavens, zoals Amsterdam Schiphol en London Heathrow. Vanwege moeilijkheden bij het voorspellen van het vliegtuigtraject en het tijdstip van aankomst van vliegtuigen die een CDO uitvoeren, moet ATC extra separatie buffers toevoegen om zich te verzekeren dat vliegtuigen voldoende afstand onderling bewaren. Deze extra buffer resulteert in een verminderde luchthavencapaciteit, waardoor het gebruik van CDOs beperkt wordt tot de uren van een lage capaciteitsvraag. Verschillende onderzoekers hebben diverse nieuwe CDO concepten onderzocht met als doel om de voorspelbaarheid van CDOs te verbeteren om zo de capaciteit van luchthavens tijdens CDOs te verbeteren. Veel van deze concepten vereisen echter extra stuwkracht om afwijkingen te corrigeren die plaatsvinden gedurende de daling. Daarom is in dit onderzoek een nieuw CDO concept ontwikkeld, genaamd Time and Energy Managed

Operations (TEMO), wat het mogelijk maakt om een vliegtuig een nauwkeurige 4D daling te laten vliegen met een stationaire motorstand door gebruik te maken van energie principes.

TEMO gebruikt de principes van energie om afwijkingen van het geplande traject te corrigeren (herplannen). TEMO doet dit zonder gebruik te maken van extra stuwkracht of remkleppen en kan tegelijkertijd een tijdlimiet respecteren voor het behouden van voldoende afstand en ordenen van de aankomende vliegtuigstroom. Het concept maakt gebruik van een optimalisatie algoritme om stuwkracht en remkleppen te minimaliseren en een nauwkeurig traject te berekenen. Het algoritme maakt gebruik van energiemangement en corrigeert afwijkingen door kinetische en potentiële energie uit te wisselen met behulp van het hoogte-roer. Afwijkingen worden gecorrigeerd door strategische herplanning, wanneer een vooraf bepaalde grens overschreden wordt, of door tactische herplanning, welke onmiddellijk afwijkingen corrigeert als deze opgemerkt worden. Om de nauwkeurigheid van de uitgevoerde daling te verbeteren en aanvaardbare werkbelasting te behouden wordt een TEMO daling gevlogen met behulp van de automatische piloot en de auto-thrust systemen. Echter worden de vleugelkleppen en het instellen van de automatische piloot nog steeds uitgevoerd door de piloot zelf.

Het TEMO concept is gevalideerd voor verschillende omstandigheden om zo te verifiëren of TEMO dalingen gevlogen kunnen worden en of hoe het concept omgaat met verschillende verstoringen. Een studie heeft daarom onderzocht of de milieubelasting wordt verminderd en daarnaast de verschillende herplannings methoden met elkaar vergeleken. Verschillende verstoringen werden kunstmatig geïntroduceerd om te evalueren in hoeverre energiemangement fouten voldoende kan corrigeren en in welke situaties extra stuwkracht of remkleppen vereist zijn. Ook moest de rol van de menselijke piloot binnen het TEMO concept worden geëvalueerd. De menselijke piloot introduceert extra onzekerheden die van invloed zijn op de gevlogen daling. Een andere onzekerheid tijdens de daling is wind welke de nauwkeurigheid van het gevlogen traject sterk beïnvloed. De vraag is dus of verbeterde wind schatting tijdens het voorspellen van het traject de uiteindelijke nauwkeurigheid verbeterd. Dit proefschrift licht deze onderwerpen toe en probeert de vragen te beantwoorden.

Een eerste experiment betrof een fast-time batch simulatie uitgevoerd in MATLAB en gericht op het identificeren van de milieuvoordelen en het vermogen van TEMO om afwijkingen te corrigeren met behulp van strategisch herplannen. Afwijkingen zijn het resultaat van modelleringsfouten in de traject voorspeller en algoritme om traject voorspelling te vereenvoudigen en versnellen. Uit een vergelijking van referentie scenario's tussen TEMO en stapsgewijze dalingen bleek dat TEMO de 65 dB en 75 dB Sound Exposure Level (SEL) contour oppervlakken verminderd met respectievelijk 20% en 13%. Bovendien is een vermindering van brandstofverbruik bereikt van tussen de 11% en 20% gedurende de daling. Wanneer men het brandstofverbruik per vluchttijd beschouwt, is de totale vermindering iets verlaagd tot waarden tussen 9% en 16%. Gasemissies zijn effectief verminderd met ongeveer 33-47%. Uit deze vergelijking bleek ook dat zonder extra verstoringen er geen herplanning nodig was om afwijkingen, die het gevolg zijn van modelleringsfouten, te corrigeren.

Vervolgens werden dalingen gesimuleerd met kunstmatig geïntroduceerde tijd, energie en windschattingsfouten. Deze studie richtte zich op het evalueren van strategische herplan-

nen onder dergelijke fouten. Zonder gebruik te maken van extra stuwkracht om afwijkingen te corrigeren werd een tijdvenster van 8–16 seconden bereikt met behulp van energiemana- gement. Het werkelijke tijdvenster is afhankelijk van de windinschattingsfout die invloed heeft op de waarden van het tijdvenster. Door minimale hoeveelheden van stuwkracht en remkleppen toe te staan was TEMO in staat om 30 seconden eerder en later dan gepland aan te komen. In sommige extreme scenario's werd de tijdafwijking op de Initial Approach Fix (IAF) van 5 seconden echter overschreden. Deze grotere tijdafwijkingen waren voorname- lijk het gevolg van windinschattingsfouten die een negatieve invloed hebben op de tijd en energie prestaties tijdens de daling. Deze voortdurende wind verstoring resulteerde in het meerdere malen herplannen van het traject om tijd en energie afwijkingen te corrigeren.

Dit experiment vergeleek ook resultaten van dalingen gevlogen met strategische herplan- nen en dalingen gevlogen met behulp van hybride herplannen onder windcondities. Deze hybride herplanning gebruikte een 4D-snelheidsregelaar om continu (tactisch) tijdafwijking- en te corrigeren en gebruikte strategische herplannen voordat de Terminal Maneuvering Area (TMA) werd binnen gevlogen om energie afwijkingen te corrigeren. De resultaten van deze vergelijking toonden aan dat de 4D-snelheidsregelaar effectief tijdafwijkingen minima- liseert met minimale kosten voor brandstofverbruik en de geluidsbelasting, zelfs wanneer een wind inschattingsfout werd geïntroduceerd. De tactische besturing is erg efficiënt in het corrigeren van afwijkingen die ontstaan door continue aanwezige verstoringen. Echter toonde hybride herplanning een grote energie afwijking tijdens het onderscheppen van de localizer. Deze fout werd automatisch gecorrigeerd met behulp van stuwkracht tijdens het onderscheppen van het Instrument Landing System (ILS) glijpad. Hierom moet hybride herplanning kleinere energie grenzen gebruiken zodat deze afwijking eerder gecorrigeerd wordt.

De TEMO fast-time simulaties gebruikten een piloot reactiemodel dat pilot-taken, zo- als het selecteren van de volgende configuratie, perfect en zonder vertraging uitvoerde. De vraag hoe variaties in pilot reactietijd op deze handmatige handelingen TEMO prestaties beïnvloeden was hiermee nog niet beantwoord. Met behulp van een real-time experiment, met piloten in de cockpit, werd getracht dit te beantwoorden. Ditzelfde experiment evalu- eerde ook welke cockpit informatie voldoende ondersteuning biedt om piloten nauwkeurige TEMO dalingen uit te laten voeren. Deze informatie werd getoond op de cockpit displays en de informatie was zo ontworpen om variaties in piloot reactie te minimaliseren. Drie cockpit displays werden ontworpen en ontwikkeld die verschilden in hoeveelheid nieuw weergege- ven ondersteunings informatie. De piloten gaven de voorkeur aan de variant die een timer bevatte en zo piloten ondersteunde tot nauwkeurige selectie van configuraties. De pilo- ten antwoordden dat hun werkdruk aanvaardbaar was en niet verhoogd. De nieuwe timer leidde echter niet tot significante verschillen in TEMO prestaties qua tijdafwijking op de landingsbaan. De timer verminderde wel de variantie in vertraging van het instellen van configuraties.

Ter vergelijking werden de met piloten gevlogen simulaties ook gesimuleerd met be- hulp van een nul-vertraging piloot reactiemodel om het effect van variaties te onderzoeken in pilot-respons op de milieu-impact en TEMO prestaties. Deze vergelijking toonde aan dat reactietijd weinig effect had op geluidscontouren en stikstofoxide uitstoot tijdens een

TEMO daling. Daarnaast was het verschil in tijdafwijking tussen menselijke en geautomatiseerde simulaties minimaal. Op basis hiervan kan men concluderen dat piloten voldoende geïnformeerd werden om hun handelingen tijdig uit te voeren. De vergelijking gaf ook aan dat zonder vertraging in het uitvoeren van handelingen het vliegtuig ook niet precies op tijd aankomt. Deze afwijking wordt veroorzaakt door vereenvoudigingen in het modelleren van de dynamische vergelijkingen van vliegtuigen in TEMO plannings algoritme en traject voorspeller. In het algemeen kwamen piloten te vroeg aan en dicht bij de grens van de vereiste tijd nauwkeurigheid. Dit leidt tot de vraag of een nauwkeurigheid van twee seconden wel haalbaar is in de realiteit. De autopilot en planning functies zullen verbeterd moeten worden om extra afwijkingen te kunnen compenseren, zodat het vliegtuig dezelfde tijd nauwkeurigheid kan behalen in minder gunstige wind omstandigheden.

Uit de analyse van de resultaten bleek dat de energie afwijking tijdens het onderschep-
pen van het glideslope signaal de aankomsttijd van de geautomatiseerde runs aanzienlijk beïnvloedt, terwijl voor de piloot simulaties dit effect iets kleiner is. Kortom, om op tijd aan te komen moet de energie afwijking bij het glideslope onderscheppingspunt worden vermindert en moet het mogelijk gemaakt worden om tijdens de glideslope daling correcties uit te voeren.

De resultaten van beide experimenten toonden aan dat TEMO gevoelig is voor verstoringen en modeleringsfouten. De batch studie toonde aan dat windschattingsfouten een grote bijdrage leveren aan de tijd en energie afwijkingen. Als deze windschattingsfout verkleind kan worden, zou het vliegtuig minder verstoringen moeten ondervinden gedurende een TEMO daling. Hedendaags gebruiken piloten voornamelijk grove en langzaam bijgewerkte windschattingen welke resulteren in een grove schatting van de heersende wind tijdens het voorspellen van het eigen traject. Om deze reden is een nieuw algoritme ontwikkeld die het mogelijk maakt om een real-time schatting van het heersende windprofiel te maken. Dit algoritme heet Airborne Wind Estimation Algorithm (AWEA) en verhoogt de temporele en ruimtelijke resolutie van windschattingen. AWEA gebruikt metingen van andere vliegtuigen in de omgeving om hoge resolutie windprofiel schattingen te construeren in real-time. Het algoritme gebruikt een Kalman filter om alle ontvangen metingen te relateren aan het eigen traject en meetruis te reduceren. De prestaties van het windschattingsalgoritme werden geëvalueerd met behulp van Mode-S afgeleide meteorologische gegevens van de luchthaven Schiphol. Met behulp van deze wind waarnemingen werd aangetoond dat AWEA de Root Mean Square (RMS) in de schattingsfout reduceerde tot 1.35 KTS ten opzichte van de waargenomen meetfout RMS van 1.94 KTS. Het relateren van andere metingen tot het eigen traject bleek ook bij te dragen tot het verbeteren van de windschattingen. In een afzonderlijk experiment werd AWEA gebruikt om nauwkeurige windschattingen te maken voor het eigen traject, zodat een betere separatie tussen vliegtuigen bereikt werd tijdens de nadering van het vliegveld.

De TEMO experimenten toonden veelbelovende resultaten met duidelijke voordelen voor het milieu terwijl het vliegtuig zich hield aan tijdsrestricties. Echter, op een aantal aspecten moet verder onderzoek verricht worden voordat TEMO in de realiteit getest kan worden. TEMO werd ontworpen voor het Airbus A320 vliegtuig en is alleen getest tijdens het vliegen van rechtlijnige naderingstrajecten. Daarnaast werd een omgeving gesimuleerd

met hierin maar een enkel vliegtuig. In de toekomst moet onderzocht worden of TEMO ook in andere vliegtuigtypes gebruikt kan worden. Verder zou onderzocht moeten worden hoe bochten in het naderingspad, variërende wind en turbulentie het TEMO traject beïnvloeden. AWEA moet worden geïntegreerd in TEMO om afwijkingen als gevolg van wind te verminderen. Vervolgens moet een experiment uitwijzen hoe luchthavencapaciteit, afstand tussen vliegtuigen en scheiding van vliegtuigen werkt tijdens TEMO dalingen. Om de tijdprestaties op de landingsbaan te verbeteren moet TEMO correcties kunnen uitvoeren op de glideslope omdat energiemangement niet mogelijk is tijdens de daling langs de glideslope. Gedurende dit segment kunnen afwijkingen gecorrigeerd worden met behulp van flap-scheduling, zodat de motor-stuwkracht beperkt blijft. Daarnaast zou gebruik gemaakt kunnen worden van een tactische component die stuwkracht en remkleppen gebruikt om tegelijkertijd tijd en energie afwijkingen te minimaliseren.

Het voorspellen van het vliegtuigtraject zal altijd modelleringsfouten bevatten omdat we de wereld niet expliciet en exact kunnen modelleren. Toekomstig werk zal zich moeten richten op het verder reduceren van deze fouten, omdat strategisch herplannen van het traject een open-lus systeem betreft. Hierdoor zullen modelleringsfouten altijd resulteren in afwijkingen van het geplande traject. Om de effecten van modelleringsfouten en onbekende verstoringen te minimaliseren, moet gebruik gemaakt worden van een gesloten-lus systeem dat actief deze fouten corrigeert. De hybride herplan methode bevat een gesloten-lus snelheidsregelaar en nieuw onderzoek zal moeten uitwijzen hoe hybride herplannen verbeterd kan worden en hoe de mens hiermee kan samenwerken.

ACKNOWLEDGEMENTS

During my internship at the Humans and Automation Laboratory of the Massachusetts Institute of Technology I decided to extend my stay in academia and pursue a Ph.D. degree. With Max' support, I became a Ph.D student in the Aerospace Software and Technologies Institute. I am Max enormously grateful for the opportunity he provided and for his support over the last six years. As many who pursued a Ph.D know, the four years of such a project comes with many ups and downs and Max was always there to keep me motivated and clearly show me the path towards the finish line. Rene, you so often have amazed me with your accurate, out-of-the-box but simple solutions to very complex problems. Thank you for allowing me to pick your brain every so often. Clark, thank you for being a great daily supervisor and the many laughs we had during our extensive discussions.

The research of this thesis was carried out within the European Clean Sky program and in close collaboration with the National Aerospace Laboratory (NLR) and German Aerospace Center (DLR). As of 2011, most of my hours were spent as a 'bijzonder medewerker' at NLR for which I have Rob to thank! This thesis would not have been possible without the hard work of Frank, Ronald, Nico, Adri and Wilfred. Frank, your ideas of what TEMO should become made TEMO to what it is today. Ronald, your great mathematical mind made TEMO possible and thank you for the many late nights you spend on improving the algorithms. Nico, your operational experience and vast knowledge proved extremely useful as you always kept track of the global big picture and straighten me out when I was lost in the little details. Wilfred and Adri, thank you both for your hard work on managing our work package and TU Delft and NLR interests. I enjoyed our many meetings all across Europe! I also want to thank, Jaap, Michiel and Bart for their work spent on making the TEMO simulations possible in APERO. Roy, Arjan and the others, thanks for the great discussions we had during our walks through Amsterdam! Ralf and Helge, thank for your contributions to TEMO.

A consortium of AVTECH AB, Use2Aces and Certifyer was established to support us during the development and execution of the human-in-the-loop experiment. I want to thank

Monique Heiligers, Gerard Temme, Wim Huson, Vincent Steinmetz, Jon Ertzgaard and Anders Palm for their work to make the experiment possible. Their experience and knowledge made every little iteration of the Human-Machine Interface (HMI) Variants better and improved my knowledge and ideas on cockpit and flight operations. I also want to thank Wim, Gerard, Vincent and Jon specifically for spending those countless hours in APERO with me.

Sander and Dries, who were not directly involved with TEMO, were always there to assist me when I had issues or questions regarding optimal control. Sander, thanks for all your help and the great times we had in Toulouse and Paris.

My thanks also goes out to all my colleagues at the Control and Simulation Division. I want to thank Jan in particular for being a great and fun roommate and your Belgian sense of humor. Herman, Daan and Rita, thank for the great office atmosphere in SIM 0.09. Joost, Coen, Erik-Jan, Pieter, Dennis and Peter, thanks for our weekly physical distraction in Pijnacker. I still remember the days (not that many) when I beat one of you during a game of squash! The places I visited with Erik-Jan during two road trips through the USA in 2010 and 2011 were beautiful. It still amazes me how much we have seen during one week across the USA! Hans and Xander, thanks for your ideas on TEMO and the great times we spend in the Citation. I would also like to thank Ping and Christiaan for the discussions we had on the application of the Kalman Filter to wind estimation.

Over the last four years, I worked closely with graduate students on their graduation projects. I greatly enjoyed working with Mark van den Hoven, Menno van Dijk, Richard Sopjes, Koen van Dijk, Hans van der Laan and Floris Freeman. Your enthusiasm and critical mindset helped a lot to form new ideas for my research.

My sincere gratitude goes out to all the pilots that participated in the human-in-the-loop experiment. You did not only spend a day and a half in a simulator but provided valuable feedback on TEMO too.

Arie and Else, my dear parents, thank you for your support during my many years in Delft. You raised me to what I am today and always encouraged me to study and chase my dreams!

After a year and a half in my Ph.D I met the most wonderful and loving person in my life: Renske. Even though my work agenda often conflicted with our own personal plans, you have been on my side all the way to the end. You are the silent force behind this thesis and without your pep-talks this thesis would not have been finished within four years. You changed my life and I look forward to the many great experiences we will encounter together!

CURRICULUM VITAE

Paul de Jong was born on September 11, 1984 in Arnhem. He attended secondary school (VWO N+T) at Olympus College in Arnhem which was successfully completed in 2002. That same year, he moved to Delft to study Civil Engineering at TU Delft. In January 2003, he shifted to Aerospace Engineering at the same university. He successfully obtained his Bachelor of Science in August of 2006. During his graduate studies, he interned in 2008 at the Humans and Automation Laboratory of the Massachusetts Institute of Technology, followed by a masters graduation project on an analysis of control space of the Three-Degree Decelerating Approach (TDDA). His masters thesis was successfully defended in August of 2009. Throughout his studies in Delft, he was actively involved in the VSV 'Leonardo da Vinci' Student Society by participating in several committees, such as, the Yearbook 2005, Bedrijven Informatie Team 2006 of De Delftse Bedrijvendagen and StudyTour 2007.

During his internship at MIT, Paul got interested in pursuing a doctorate degree which was made possible with the support of Professor Max Mulder. In August 2009, Paul started a Ph.D project at the Aerospace Software and Technologies Institute (ASTI) within the European Clean Sky program. Within Clean Sky, Paul represented the Faculty of Aerospace Engineering as project manager and performed research in close cooperation with NLR where he performed most of his research. Besides his research, Paul was active in many educational courses, such as supervision of graduate students, the undergraduate Design Synthesis Exercise and various graduate courses.

In September of 2013, Paul joined Sim-Industries in Sassenheim and is involved in the development of full-flight simulators as a software engineer.

List of Publications

- [1] **P. M. A. De Jong, A. C. In 't Veld, A. M. P. De Leege, M. M. Van Paassen, and M. Mulder.** Control Space Analysis of Continuous Descent Operations at Amsterdam

- Airport Schiphol. In: *Proceedings of the International Air Transport and Operations Symposium (ATOS 2010)*, Delft, The Netherlands, 14–15 April, 2010.
- [2] **P. M. A. De Jong, A. C. In 't Veld, A. M. P. De Leege, M. M. Van Paassen, and M. Mulder.** Control Space Analysis of Three-Degree Decelerating Approaches at Amsterdam Airport Schiphol. In: *Proceedings of the AIAA Guidance, Navigation and Control Conference, Toronto, Ontario Canada, August 2–5*, AIAA 2010-8454, pp. 1–20. American Institute of Aeronautics and Astronautics, 2010. doi:10.2514/6.2010-8454.
 - [3] **M. C. L. Van den Hoven, P. M. A. De Jong, C. Borst, M. Mulder, and M. M. Van Paassen.** Investigation of Energy Management during Approach - Evaluating the Total Energy-Based Perspective Flight-Path Display. In: *Proceedings of the AIAA Guidance, Navigation and Control Conference, Toronto, Ontario Canada, August 2–5*, AIAA 2010-8401, pp. 1–20. American Institute of Aeronautics and Astronautics, 2010. doi:10.2514/6.2010-8401.
 - [4] **J. W. Crandall, M. L. Cummings, M. Della Penna, and P. M. A. De Jong.** Computing the Effects of Operator Attention Allocation in Human Control of Multiple Robots. *IEEE Transactions on Systems, Man and Cybernetics, Part A: Systems and Humans*, 41(3), 385–397, 2011. doi:10.1109/TSMCA.2010.2084082.
 - [5] **P. M. A. De Jong, K. De Vos, C. Borst, M. M. Van Paassen, and M. Mulder.** Time-based Spacing for 4D Approaches using Speed-Profiles. In: *Proceedings of the AIAA Guidance, Navigation and Control Conference, Portland, Oregon, August 8–11*, AIAA 2011-6215, pp. 1–14. American Institute of Aeronautics and Astronautics, 2011. doi:10.2514/6.2011-6215.
 - [6] **A. C. In 't Veld, P. M. A. De Jong, M. M. Van Paassen, and M. Mulder.** Real-time Wind Profile Estimation using Airborne Sensors. In: *Proceedings of the AIAA Guidance, Navigation and Control Conference, Portland, Oregon, August 8–11*, AIAA 2011-6662, pp. 1–15. American Institute of Aeronautics and Astronautics, 2011. doi:10.2514/6.2011-6662.
 - [7] **R. Sopjes, P. M. A. De Jong, C. Borst, M. M. Van Paassen, and M. Mulder.** Continuous Descent Approaches with Variable Flight-Path Angles under Time Constraints. In: *Proceedings of the AIAA Guidance, Navigation and Control Conference, Portland, Oregon, August 8–11*, AIAA 2011-6219, pp. 1–20. American Institute of Aeronautics and Astronautics, 2011. doi:10.2514/6.2011-6219.
 - [8] **P. M. A. De Jong, N. De Gelder, R. P. M. Verhoeven, F. J. L. Bussink, A. P. L. A. Marsman, and M. Mulder.** Aircraft Noise and Emission Reduction through Time and Energy Management during Descent and Approach. In: **D. Collin**, ed., *Proceedings of the Aircraft Noise and Emission Reduction Symposium (ANERS) 2011, Marseille, France, October 25–27*, pp. 1–8. Association Aéronautique et Astronautique de France (3AF) and the American Institute of Aeronautics and Astronautics (AIAA), 2011.

- [9] **P. M. A. De Jong, F. J. L. Bussink, N. De Gelder, R. P. M. Verhoeven, and M. Mulder.** Time and Energy Management during Descent and Approach for Aircraft. In: **D. Young and S. Saunders-Hodge**, eds., *Proceedings of the 5th International Conference on Research in Air Transportation — ICRAT 2012, Berkeley, California, May 22–25*, pp. 1–6. FAA and EUROCONTROL, 2012.
- [10] **F. J. L. Bussink, J. J. Van der Laan, and P. M. A. De Jong.** Combining Flight-deck Interval Management with Continuous Descent Approaches in high density traffic and realistic wind conditions. In: *Proceedings of the AIAA Guidance, Navigation and Control Conference, Minneapolis, Minnesota, August 13–16*, AIAA 2012-4523, pp. 1–25. American Institute of Aeronautics and Astronautics, 2012. doi:10.2514/6.2012-4523.
- [11] **P. M. A. De Jong, N. De Gelder, F. J. L. Bussink, R. P. M. Verhoeven, R. Kohrs, M. M. Van Paassen, and M. Mulder.** Time and Energy Management during Descent and Approach for Aircraft: A Batch-Simulation Study. *Journal of Aircraft*, 2013. Submitted for publication.
- [12] **P. M. A. De Jong, F. J. L. Bussink, R. P. M. Verhoeven, N. De Gelder, M. M. Van Paassen, and M. Mulder.** Time and Energy Management during Descent and Approach: A Human-in-the-Loop Study. *Journal of Aircraft*, 2013. Submitted for publication.
- [13] **P. M. A. De Jong, J. J. Van der Laan, A. C. In 't Veld, M. M. Van Paassen, and M. Mulder.** Wind Profile Estimation using Airborne Sensors. *Journal of Aircraft*, pp. 1–18, 2013. Submitted for publication.
- [14] **P. M. A. De Jong, N. De Gelder, F. J. L. Bussink, R. P. M. Verhoeven, and M. Mulder.** Time And Energy Management During Descent: Human vs. Automated Response. In: *Proceedings of the 32th Digital Avionics Systems Conference, Syracuse, New York, October 6–10*, pp. 1–10. IEEE/AIAA, 2013.

Today, air traffic controllers use speed and altitude instructions to separate approaching and departing air traffic. As a result, aircraft fly a level segment for an extended period of time, burning fuel and generating noise and gaseous emissions. For this reason, Continuous Descent Operations (CDO) have been developed such that aircraft perform a near-idle descent from cruise level to the airport. However, various CDO concepts reduce airport runway capacity due to problems with the predictability of the aircraft's trajectory during a CDO, due to disturbances such as variations in pilot response, aircraft dynamics and wind. The research described in this thesis developed a new CDO concept that aims at maintaining runway capacity using time constraints and energy management.

This new concept, named Time and Energy Managed Operations (TEMO), was investigated using a fast-time, batch simulation study and compared with today's conventional step-down descents. A second experiment investigated procedures and the human role within TEMO. Finally, a new wind estimation algorithm was developed to improve trajectory accuracy using high resolution wind estimates. On-time performance proved accurate whilst the environmental impact was significantly reduced.

